warwick.ac.uk/lib-publications

Geosynthetic-Reinforced and Unreinforced Soil Slopes Subject to Cracks and Seismic Action: Stability Assessment and Engineered Slopes

By

Akram Hasan Abd (BSc, MSc)

A thesis submitted in partial fulfilment of the requirements for the degree of Doctor of Philosophy in Engineering.

University of Warwick, School of Engineering

July 2017

List of Contents

List of Figures

x

List of Tables

Acknowledgements

The completion of this work was made possible by a great many people, all of whom I will forever be indebted to.

First and foremost, to my supervisors, Professor Stefano Utili and Professor Toby Mottram.

I owe a particular debt of gratitude to my main supervisor Stefano for inspiring me to carry out a research on a subject of my interest. Stefano had been generous with his time and guidance, despite having to contend with the numerous academic duties especially when he moved to another institution taking me with him.

Many thanks also to my second supervisor Toby for his endless support and encouragement especially at the last year of my PhD study time.

I am particularly grateful to my wife Hadeel for her patience, encouragement and support.

I am also greatly indebted to my parents, my brothers and sisters for their encouragement especially my brothers, Dr Qais and Ibraheem for their endless support.

In addition, I would like to thank my colleagues Chrysoula Voulgari, and Weigao Wu, for their invaluable discussions throughout my PhD life.

Finally, I would like to appreciate the support of the Higher Committee of Education Development (HCED) in Iraq, which covered my tuition fees and living allowance.

Declaration

This thesis is submitted to the University of Warwick in support of my application for the degree of Doctor of Philosophy. It has been composed by myself and has not been submitted in any previous application for any degree. The work presented (including data generated and data analysis) was carried out by the author.

Parts of this thesis have been published by the author:

- **Abd, A. H.**, Utili S., 2017. "Design of geosynthetic-reinforced slopes in cohesive backfills"*Geotextiles & Geomembranes*, doi.org/10.1016/j.geotexmem.2017.08.004.

- **Abd, A. H.**, Utili S., 2017. "Geosynthetic-reinforced slopes in cohesive soils subject to seismic action" *Procedia Engineering*, *189*, pp.898-907.

- Utili S., **Abd, A. H.**, 2016. "On the stability of fissured slopes subject to seismic action" *International Journal for Numerical and Analytical Methods in Geomechanics*. Vol. 40, issue 5, pp. 785-806. DOI: 10.1002/nag.2498.

- **Abd, A. H.**, Utili S., 2016. "Geosynthetic layout optimization for reinforced slopes subject to cracks". *In Landslides and Engineered Slopes. Experience, Theory and Practice: Proceedings of the 12th International Symposium on Landslides* (Napoli, Italy, 12-19 June 2016) (p. 295). CRC Press.

- **Abd, A. H.**, 2015. "Earthquake-induced displacement of cohesive-frictional soil slopes subject to cracks" *IOP Conf. Series: Earth and Environmental Science* 26 (012046). doi:10.1088/1755-1315/26/1/012046

- **Abd, A. H.**, 2015. "Seismic displacement of geosynthetic-reinforced soil slopes subject to cracks" *IOP Conf. Series: Earth and Environmental Science* 26 (012045). doi:10.1088/1755-1315/26/1/012045.

Abstract

The main purpose of this thesis is on one hand to enhance the current predictive capabilities of the stability of soil slopes and on the other hand, to improve the design practice to stabilise natural slopes showing signs of distress and make the design of engineered slopes more affordable. To achieve the first objective an analytical method achieved by the upper bound theorem of limit analysis and the pseudo-static approach is derived for the assessment of the stability of slopes manifesting vertical cracks and subject to seismic action. The method is validated by numerical limit analyses and displacement-based finite-element analyses with strength reduction technique. Employing this method slope stability charts to assess the stability factor for fissured slopes subject to both horizontal and vertical accelerations for any combination of c, ϕ, and slope inclination are produced.

   To achieve the second objective limit analysis was employed to derive a semi-analytical method to extend the applicability of current method to design the slope reinforcement for frictional backfills to cohesive frictional backfills. Design charts providing the amount of reinforcement needed as a function of cohesion, tensile strength, angle of shearing resistance and slope inclination are obtained. From the results, it emerges that accounting for the presence of cohesion allows significant savings to be made, and that cracks are often significantly detrimental to slope stability so they cannot be overlooked in the design calculations of the reinforcement. Also, a new numerical method to determine multi-linear profiles of optimal shapes for reinforced slopes in frictional backfills is presented. The method is based on the limit analysis upper bound method together with genetic algorithms and provides an

optimal profile for a prescribed average slope inclination, backfill strength properties and desired number of layers to be used. Several stability charts illustrating the savings on the required amount of reinforcement are provided for the benefit of designers.

Symbols

A: area of the failing part.

$A_1, A_2, ..., A_6$: areas utilised in the calculation of the external work.

c: soil cohesion

C: seismic displacement coefficient.

$\dot{D}$: total energy dissipation rate.

$\dot{D}_r$: energy dissipation rate within the reinforcement.

$\dot{D}_s$: energy dissipation rate within the soil

$d\dot{D}_r$: infinitesimal dissipated energy within reinforcement.

f_b: bond coefficient between the soil and geosynthetic-reinforcement.

f_d: function for the dissipated energy.

f_w: function to evaluate the external work rate done by the pore water pressure.

f_{PSh}: horizontal pseudo-static force.

f_{PSv}: vertical pseudo-static force.

$f_1, f_2, ..., f_6$: function for the external work rate done by the soil weight.

$f_{1v}, f_{2v}, ..., f_{6v}$: function for the external work rate done by the soil weight and vertical seismic load.

$f_{1h}, f_{2h}, ..., f_{6h}$: function for the external work rate done by the horizontal seismic acceleration.

g: gravitational acceleration.

g_1, g_2, g_3 and g_4 : function for the internal dissipated energy done by the soil and reinforcement along the log-spiral failure surface and along the crack.

G: weight of the failing part.

h : height of crack.

h_w : height of water within the crack measured from the tip of the crack.

h_i : height of the slope that may fail above the toe measured from the slope crest.

h_{min} : the crack depth that provides minimum stability factor $\gamma H / c$.

H: slope height.

H_{cr} : critical height of slope.

i: counter usually denotes *i*th layer of reinforcement but it could also denotes *i*th point on the slope profile.

j: number of reinforcement layers that pull-out.

K : generic average tensile strength of reinforcement.

K_h :horizontal seismic acceleration coefficient.

K_t :average tensile strength of a uniformly distributed reinforcement.

K_v : vertical seismic acceleration coefficient.

K_y : yield acceleration.

l : arm length of G.

L_c : part of the anchorage length of the reinforcement spared because of the crack see Figure 7.1.

L_e : effective length of reinforcement layers to resist pull-out failure.

L_s : part of the length of reinforcement to be saved using linearly decreasing length, see Figure 7.1.

L_r : total length of reinforcement layer.

l_1 and l_2 lengths defined in Figure 3.1.

m: number of points used to discretise the slope profile.

M: mass of the failing part.

n: number of reinforcement layers.

n' : number of reinforcement layers involved in the above the toe failure.

N : stability factor upper bound.

N_s : stability factor

$N\uparrow$: stability factor upper bound associated with upward vertical acceleration.

$N0$: stability factor upper bound associated with nil vertical acceleration

$N\downarrow$: stability factor upper bound associated with downward vertical acceleration.

r : generic radius for the log-spiral part.

r_u :dimensionless coefficient of pore pressure (see (Bishop & Morgenstern, 1960))

r_χ: reference radius of the log-spiral part.

r_ς : distance from centre of rotation for the log-spiral to the crack tip.

r_υ : distance from centre of rotation for the log-spiral to the slope toe.

S: spacing between consecutive layers of reinforcement.

T: tensile strength of a reinforcement layer.

t: dimensionless coefficient denoting tensile strength of soil.

$\dot{u}$: displacement rate along the log-spiral part.

$\dot{u}_c$: displacement rate along the crack.

w: width of discontinuity layer along the log-spiral part

$\dot{W}$: total external work rate.

$\dot{W}_{ext}$: rate of external work.

$\dot{W}_d$: rate of dissipated energy.

$\dot{W}_s$: external work rate made by the soil weight.

$\dot{W}_w$: external work rate made by the pore water pressure.

$\dot{W}_1, \dot{W}_2, \dot{W}_3, \ldots, \dot{W}_6$: external work rate for different regions.

x: horizontal distance measured from the slope toe.

x_1: horizontal distance measured from slope toe to the point at which the crack starts to affect the slope stability.

x_2: horizontal distance measured from slope toe at which the crack is no longer affecting the slope stability because it is far inward.

x_c: horizontal distance measured from the slope toe to the location of the critical crack.

x_i: horizontal distance measured from the slope toe to the location of the point i on the slope profile.

y: vertical distance measured from slope toe.

z_i: the depth of the reinforcement below the slope crest.

β: slope face inclination.

β': angle in which the length of reinforcement layers decreasing with depth.

γ: unit weight of soil.

δ : infinitesimal increment.

$\dot{\varepsilon}_x$: strain rate in the direction of reinforcement.

η: angle made by the crack with the reinforcement layer.

$\dot{\theta}$: angular velocity.

θ_i: angle related to the intersection of the failure surface with the i-layer.

θ : generic angle of the failure surface along the log-spiral part.

λ : the ratio between K_v and K_h

ξ : angle made between the ground velocity vector and the crack.

σ : normal stress.

σ_t : ground tensile strength

σ_t^{M-C} : uniaxial tensile strength consistent with Mohr Coulomb failure criterion

σ_c^{M-C} : uniaxial compressive strength consistent with Mohr Coulomb failure criterion

τ : shear stress

ϕ : angle of shearing resistance.

ψ : angle of dilatancy.

χ, υ, ζ : angles identifying log-spiral failure surface and crack position and depth.

Я : vector of plastic modes making a convex domain in the stress space.

$\dot{ю}$: plastic multiplier.

Abbreviations

2D: Two-dimensional.

3D: Three-dimensional.

FE: Finite element.

FELA: Finite element limit analysis.

FESR: Finite element strength reduction.

LA: Limit analysis.

LEM: Limit equilibrium method

LID: Linearly increasing distribution of reinforcement.

UD: Uniform distribution of reinforcement.

Chapter 1: Introduction

1.1 Background and motivation

The need for research on landslides cannot be overestimated. The increase in settlement density in hazardous regions and in the value of assets in those areas has caused the amount of financial damages that are due to natural catastrophes to rise continuously over the last 50 years. According to the claim statistics provided by (Munich_Re, 2012), in 2011 alone the economic losses due to geohazards (classified as landslides, earthquakes and floods in the report) amounted to 275,000 € million which is about 40 times as much as the total losses due to the 9/11 terrorist attack on the World Trade Centre in 2001. A slowing or reversal of the upward trend of the financial costs due to geohazards is not predicted by insurance experts unless fundamental improvements in the understanding and modelling of geohazards are achieved by the scientific community (Munich_Re, 2012).

In the last century, Europe has experienced the second highest number of fatalities and the highest economic losses caused by landslides compared to other continents: 16,000 people have lost their lives because of landslides (SafeLand, 2012). In the period 1998-2009, 70 major landslides claimed a total of 312 lives and damaged or destroyed an extensive amount of infrastructure, including roads and houses. Among the largest events in terms of fatalities and destruction caused were the debris flows in Sarno in 1998 (Italy), claiming 160 lives, and the mudslides in Messina in 2009 (Italy), killing 31 people (EEA, 2010). These major events represent only a glimpse of the real impact of landslides, as the enquiry carried out by Eurogeosurvey yielded a total of

712,089 recognised mass movements recorded in Europe since World War II (Eurogeosurvey, 2010). To give an idea of the expenditure on landslides for single European member states: Spain spends 170 € million per year (Schuster & Kockelman, 1996) and Italy spent approximately 146,000 € million between 1957 and 2000 as a result of damage caused by landslides and floods. On one hand better understanding of the physical mechanisms leading to the onset of slope failures are urgently needed. On the other hand, engineering measures to prevent slope failure need to become cheaper. Moreover, the need for a more affordable design for soil slopes is exacerbated by the progressive urbanisation taking place all over the world, which implies less space available for excavations of cutting and the construction of embankments leading to the use of steeper engineered slopes. The thesis works towards both objectives.

1.2   Aim and Objectives

The main aim of this thesis is to provide semi-analytical solutions for the stability of geosynthetic-reinforced and unreinforced soil slops accounting for the presence soil cohesion, cracks and/or seismic action. The first objective is to account for cracks in the seismic analysis of unreinforced soil slopes. The effect of the presence of cracks on both seismic stability (chapter 3) and seismic-induced displacement (chapter 6) are considered. The second objective is to make the design of geosynthetic reinforcement more affordable to stabilise slopes. This is addressed by 1) introducing for the first time a design method for cohesive backfills since until now the positive contribution of cohesion to slope stability has been neglected (chapter 4, 5, 6 and 7), 2) introducing

a mathematical framework for the calculation of non-straight profiles of optimal shape for slopes reinforced with geosynthetics and tiered walls (chapter 8).

1.3 Outline of the thesis

This thesis is divided into eight chapters, which are briefly illustrated in Figure 1.1 and summarised as follows:

In chapter 1 background and motivation to the thesis together with thesis aim, objectives and outline are illustrated. In chapter 2, a literature review of the numerical and analytical methods employed in the thesis together with an overview on previous works on the stability assessment for slopes exhibiting cracks, geosynthetic-reinforced cohesive slopes and reinforced slopes of non-straight profile is provided.

In chapter 3, an analytical method achieved by the upper bound theorem of limit analysis and the pseudo-static approach is derived for the assessment of the stability of slopes manifesting vertical cracks and subject to seismic action. The method is validated by numerical limit analyses and displacement-based finite-element analyses with strength reduction technique. Employing this method slope stability charts to assess the stability factor for fissured slopes subject to both horizontal and vertical accelerations for any combination of c, ϕ and slope inclination are produced. Charts of displacement coefficients as a function of the slope characteristics are also provided. For the first time the effect of the direction of the vertical acceleration on slope stability is systematically investigated.

In chapter 4, limit analysis was employed to derive a semi-analytical method to extend the applicability of current method to design the slope reinforcement for

frictional backfills to cohesive frictional backfills. Design charts providing the amount of reinforcement needed as a function of cohesion, tensile strength, angle of shearing resistance and slope inclination are obtained. From the results, it emerges that accounting for the presence of cohesion allows significant savings to be made, and that cracks are often significantly detrimental to slope stability so they cannot be overlooked in the design calculations of the reinforcement. In chapter 5, the semi-analytical method of chapter 4 is extended to design the reinforcement of cohesive backfills subject to seismic action.

In chapter 6, a new technique is proposed to estimate the horizontal displacement at the slope toe due to a given earthquake under some simplifying assumptions about the earthquake induced crack formation. Seismic-induced displacement are calculated by Newmark's method incorporating a time varying yield acceleration accounting for cracks generated in the slope by the seismic action taking place. In chapter 7, the effect of cracks on the design length and distribution of geosynthetic layers in reinforced slopes is investigated.

In chapter 8 a new numerical method to determine multi-linear profiles of optimal shapes for reinforced slopes in frictional backfills is presented. The method is based on the limit analysis upper bound method together with genetic algorithms and provides an optimal profile for a prescribed average slope inclination, backfill strength properties and desired number of layers to be used. Several stability charts illustrating the savings on the required amount of reinforcement are provided for the benefit of designers. In chapter 9, the main conclusions of the thesis and recommendations for future studies are provided.
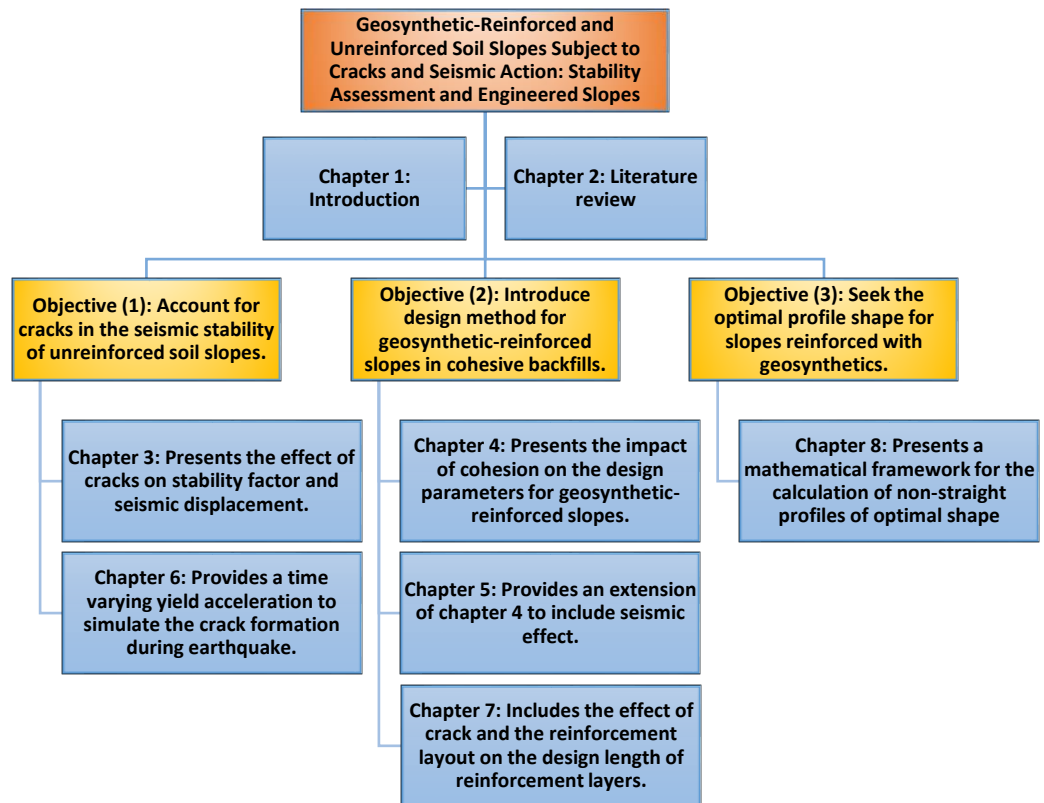
Figure 1.1 Research map showing how each objective is being addressed.

Chapter 2: Literature Review

2.1 Introduction

The first section of this chapter briefly reviews the numerical and analytical methods used for slope stability analysis. The second section summarises current knowledge on the influence of cracks on slope stability. The third one provides an overview on the use of cohesive backfills for reinforced slopes while the last one is an overview on the current literature on non-straight profiles for reinforced slopes.

2.2 Analytical and numerical methods for Slope Stability Analysis

There are several methods to study slope stability, and they can be categorised into three main groups: analytical, numerical and experimental. Given the content of the thesis, only analytical and numerical methods are reviewed herein.

2.2.1 Limit Equilibrium Methods

From a historical point of view, the first methods employed to analyse *slope stability* (and nowadays still the one most used in practice for the assessment of the stability of slopes) are the so-called limit equilibrium methods (LEM: (Fellenius, 1927)). Usually, they are used to assess the stability of a slope in terms of a factor of safety, which is then defined as the ratio of the shear strength of the soil over the actual shear stress along the failure surface. All limit equilibrium methods are based on subdividing the mass of potentially unstable ground to be analysed into (often) vertical slices of finite size (if the slices are not vertical they are sometimes called wedges), imposing the

equations of (global) equilibrium on each slice, and assuming reaction forces along the boundaries of the slices according to some physical assumptions concerning both the inter-slice forces (forces exchanged between slices) and the forces at the base of each slide which stem from the reaction offered by the ground underneath the failing mass and the water pressure. In some methods, some of the equations of equilibrium may not be satisfied and the methods are called non-rigorous; whereas if all the equations are satisfied the methods are called rigorous. These methods provide no information on the stress state inside the failing mass, the deformations or the displacements.

2.2.2   Limit Analysis

Limit analysis (LA) is a method that has been applied in many fields of engineering. One of them is slope stability. The limit analysis methods, kinematic (or upper bound) and static (or lower bound), are much more versatile than limit equilibrium methods and above all, supply solutions which are rigorously upper and lower bounds on the true collapse load. In the literature, lower bound solutions for *slope stability* problems are a few (Pastor, 1978) as the determination of a statically admissible stress field is rarely achievable. On the contrary, the determination of a kinematic admissible velocity field for homogeneous slopes allow the determination of analytical solutions. For this reason, the LA upper bound method has been extensively employed in the thesis and an in-depth treatment of its theoretical underpinning will be provided in the following section.

In this method, a failure mechanism has to be assumed as in the LEM, but with the additional constraint of being kinematically compatible. This means that the failure

mechanism has to satisfy equations imposing the constraint that the body can deform but remains a continuum at all times, *i.e.* if we consider two adjacent points with an infinitesimal distance between them, neither detachment nor penetration between them are allowed. Then an energy balance between the rate of external work done by the load applied on the failing mass and the rate of internal energy dissipation, *i.e.* the energy dissipated by the deforming soil, is imposed for all the potential failure mechanisms considered. The critical failure mechanism is identified as the mechanism giving rise to the minimum (lowest) stability number. The energy balance equation translates the well-known principle of virtual work. Both methods assume that the materials constituting the slope behave as an elasto-perfectly plastic body, *i.e.* they assume the validity of the normality rule according to which plastic deformations occur proportionally to the incremental stresses applied according to a so-called associate constitutive law. Considering a linear failure criterion like the Mohr-Coulomb criterion, it means that the so-called dilation angle is assumed equal to the angle of shearing resistance. However, real frictional-cohesive soils do not obey the normality rule. In fact, overconsolidated clays, cemented sands are usually characterised by a dilation angle smaller than the friction angle. Unfortunately, the limit theorems are not applicable to materials obeying a non-associated flow rule in all cases apart from translational failure (Drescher & Detournay, 1993), which is in general far less critical than rotational mechanisms. According to the limit analysis upper bound theorem (Chen, 1975), the collapse load for a material with a non-associated flow rule is smaller than those obtained for the same material when an associated flow rule is assumed. (Manzari & Nour, 2000) were the first to examine the effect of soil dilatancy on homogeneous slopes, performing nonlinear finite-element

analyses of slopes by the strength reduction technique. They showed that the stability

numbers obtained from limit analysis are not conservative (*i.e.* higher than the real

value) for soils exhibiting dilation angles smaller than friction angles. Recently,

(Crosta, Utili, De Blasio, & Castellanza, 2014) ran FEM analyses on straight

homogeneous $c - \phi$ slopes with both the associative flow rule as assumed in limit

analysis $\psi = \phi$ and with a dilation angle $\psi = \phi / 4$, typical for materials with little

dilatancy, for a range of slope inclinations of $20°$ to $30°$, with ϕ values ranging from

$8°$ to $28°$. It emerged that the influence of the dilation angle on the volume of the

sliding mass is negligible. This is due to the fact that the soil is little constrained from

a kinematic point of view in a slope (or in other words the level of confinement on the

material is small) whereas dilatancy may have a very important effect in case of high

confinement (*e.g.* tunnelling).

Considering a three-dimensional solid, a virtual rate of displacement, which

satisfies the following relations:

$$\dot{W}_{ext} = \int_V F_j \cdot \dot{u}_j dV + \int_{S_F} f_j \cdot \dot{u}_j dS > 0 \quad \text{and} \quad \dot{u}_i = 0 \quad \text{on} \quad S_u \tag{2.1}$$

$$\dot{\varepsilon}_{ij} = \frac{1}{2}\left(\dot{u}_{i,j} + \dot{u}_{j,i}\right) \tag{2.2}$$

$$\dot{\varepsilon}_{ij} = \frac{\partial \mathcal{A}}{\partial \sigma_{ij}} \dot{\imath o} \quad \text{and} \quad \dot{\imath o} \geq 0 \tag{2.3}$$

with $\dot{W}_{ext}$: external work rate, V and S_F are the loaded boundary volume and surface

respectively. $\dot{u}_j$: vector of the distributed forces, $\dot{\varepsilon}_{ij}$:strain rate in the kinematically

admissible velocity field, $\mathcal{A}$: vector of plastic modes making a convex domain in the

stress space, gives rise to a kinematically admissible act of motion, and $\dot{\imath o}$:plastic

multiplier. Assuming such an act of motion, the upper bound limit analysis theorem states that: *the loads determined by equating the rate at which the external forces do work*:

$$\dot{W}_{ext} = \int_V F_j \cdot \dot{u}_j dV + \int_{S_F} f_j \cdot \dot{u}_j dS \tag{2.4}$$

to the rate of internal dissipation:

$$\dot{W}_d = \int_V \sigma_{ij} \dot{\varepsilon}_{ij} dV \tag{2.5}$$

will be either higher than or equal to the actual limit load. Therefore, it can be inferred that the lowest load among all the loads relative to admissible failure mechanisms, determined by equating the rate of external work to the rate of energy dissipation, is the best approximation to the limit load. This load is an upper bound on the limit load.

In our problem, the only force present is the weight force (a body force) and no tractions are present on the solid boundary. Eq. (*2.3*) are satisfied since a *c-ϕ* soil type has been assumed. Further, the problem is two dimensional: equations (*2.4*) and (*2.5*) become:

$$\dot{W}_{ext} = \int_V F_j \cdot \dot{u}_j dV \to \int_A F_j \cdot \dot{u}_j dA \tag{2.6}$$

$$\dot{W}_d = \int_V \sigma_{ij} \dot{\varepsilon}_{ij} dV \to \int_A \sigma_{ij} \dot{\varepsilon}_{ij} dA \tag{2.7}$$

A further assumption about kinematics has been made: rigid body motions are considered. This means that strains only develop along a narrow separation layer (discontinuity surface) between a sliding rigid body and a fixed one (see Figure 2.1a) where all energy dissipation occurs. According to the assumptions made, the rate of energy dissipation is given by:

$$\dot{W}_d = \int_\Gamma (\sigma \dot{\varepsilon} + \tau \dot{\gamma}) dl \tag{2.8}$$

Strains develop according to an associated flow rule (see Figure 2.1b).
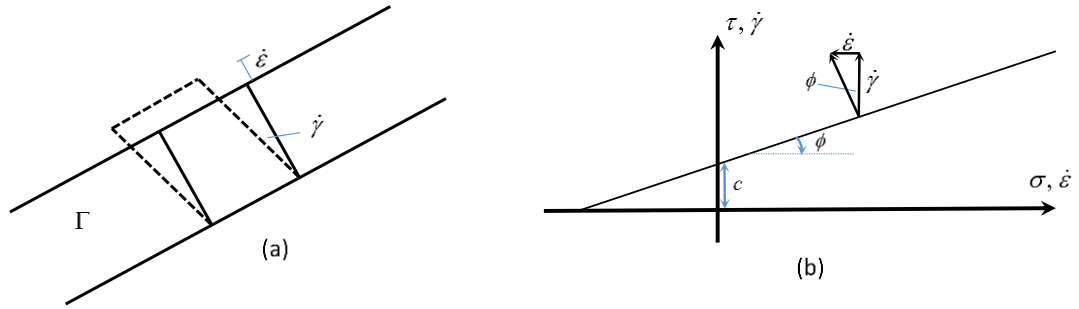
Figure 2.1 a) strains along the separation layer. b) stresses and strains according to the associated flow rule.

The slope self-weight is given by: $F = Mg = \rho g A$. Since the area A is proportional to the slope height H, the load is proportional to H as well. Finally, the energy balance equation:

$$\dot{W}_{ext} = \dot{W}_{d} \qquad (2.9)$$

makes it possible to determine a function by which the most critical mechanism can be determined. The minimum of this function gives an upper bound on the limit value. For slope stability problem, kinematically admissible mechanisms can be either translational in which rigid block are separated by velocity discontinuities or rotational in which the potential failing mass is assumed to rotate as a rigid body around the centre of rotation. This rotational failure mechanism is found to be log-spiral rather than circular unless $\phi = 0$ (Michalowski, 1998). Also, it is found to be more critical than the translational failure mechanism for both unreinforced slopes (Chen, 1975; Utili, 2013) and geosynthetic-reinforced soil slopes (Zhao, 1996).

Limit analysis has also been successfully utilised to seismically analyse soil slope incorporating pseudo-static approach (Chang, Chen, & Yao, 1984; Chen & Liu, 1990) as the upper bound to the horizontal seismic acceleration were sought. Consequently, this has led to estimate the earthquake-induced displacement in soil slopes based on Newmark's method (Newmark, 1965).

Finally, limit analysis method has been developed to overlap with finite element method creating what is known as Finite Element Limit Analysis (FELA) see for example (Anderheggen & Knöpfel, 1972; Makrodimopoulos & Martin, 2007; Sloan, 1989). FELA provides a combination between the bounding theorems and the discretization technique of finite element rendering a powerful approach to analyse soil slopes. In case of FELA upper bound, a finite element discretisation of the slope the velocity field is optimised to find the lowest upper bound and while in case of FELA lower bound the stress field is optimised to obtain the highest lower bound. Unlike traditional displacement based finite elements, each node of the finite elements used in limit analysis is unique to a given element. The FELA code Opt+umCE produced by University of Newcastle (Australia) was used in the thesis for validation of the analytical solution in chapter 3 and 4.

2.2.3 Finite element method

The displacement based finite element method (perhaps the most world-wide known method in engineering) has been used for slope stability analysis since 1975 (Zienkiewicz O.C., Humpheson C., & Lewis RW., 1975). Several books have been written about it, a few cornerstone textbooks are worth of mention:(Zienkiewicz & Taylor, 2005) and the several previous editions, and specifically dedicated

geotechnical engineering (D.M. Potts & Zdravkovic, 1999; David M. Potts & Zdravkovic, 2001). Unlike limit equilibrium method and limit analysis, any constitutive law can be considered, so there are no restrictions on the type of mechanical behaviour that can be considered for the soil/rock of the slope analysed. This is a continuum mechanics approach since the materials constituting the slope are assumed to be one continuum or several continua separated by known boundaries (*e.g.* between different strata of geomaterial) along which a mechanical law ruling the interaction has to be specified. The differential equations of classical solid mechanics are applied, *i.e.* equations imposing equilibrium on the stress field, equations imposing kinematic compatibility on the deformation or strain field, and constitutive equations imposing the law of material behaviour linking stresses to strains.

In order to find the potential failure surface, usually the so-called strength reduction technique is employed. First, a solution is found for the whole slope in its current stable state, and then the strength parameters of the slope are decreased by steps, with a new solution being sought after each step of strength decrease has been applied. After each step the slope suffers extra deformations, which typically tend to localise in a narrow band called a shear band that identifies the failure surface in the slope.

Finite element method with strength reduction technique analyses of slope stability have been run to validate results from semi-analytical solutions derived from LA (*e.g.* chapter 3 and 4). Obviously, validation by a numerical method is not as strong as a validation against experimental data. However, the fact that two independent methods provide results in agreement does constitute a form of validation.

2.3 Cracks in Slopes

Since the time of (Terzaghi, 1943), the presence of cracks has been recognised as an important factor affecting the stability of slopes made of cohesive soils (*e.g.* clayey soils) and/or rock. The presence of cracks poses significant challenges to the assessment of slope stability because they introduce one or a few discontinuities that may substantially reduce the stability of the slope. In the case of a small number of discontinuities, homogenisation techniques work badly because the slope behaviour tends to be heavily affected by the specific features of each discontinuity that therefore has to be considered explicitly in the stability analysis of the slope. This implies a significant extra computational effort for the numerical methods typically used in continuum mechanics (*e.g.* finite element (FE) method, finite difference method, etc.) that struggle to include discrete discontinuities. Furthermore, if a comprehensive parametric analysis is to be run to explore how slope stability is affected by the presence of cracks for a variety of geometrical and mechanical parameters of the slope, the computational effort required appears prohibitive. Hence, the appeal of an analytical solution is apparent.

Cracks can either exist prior to slope failure or they could form simultaneously as part of the failure mechanisms due to the tensile strength of the soil being exceeded (Michalowski, 2013). Usually when limit analysis is employed, the Mohr-Coulomb (M-C) function is adopted as failure criterion. But experimental evidence shows that the tensile f_t strength associated with the Mohr-Coulomb (M-C) criterion $f_t = c / \tan\phi$ is a significant overestimation of the true tensile strength (Bishop, Webb, & Lewin, 1965), here called σ_t, of most soils. To partially remedy this shortcoming

but still use the simple linear M-C criterion, a tensile cut off is commonly adopted. (Michalowski, 2013) instead proposed to modify the M-C criterion by adopting a non-linear function in the stress range where cracks are expected to form. This non-linear function is made by a stress circle defined as being tangent to the M-C linear function $\tau = c + \sigma \tan\phi$, and having the minor principal stress σ_3 equal to the soil tensile strength, $\sigma_3 = -\sigma_t$, with tensile stresses assumed negative according to the soil mechanics sign convention. (Michalowski, 2013) in his work, accounts for the non-linearity of soil shear strength in the stress range where cracks are expected to form.

2.4   Geosynthetic-Reinforced Cohesive Slopes

Since the 1980s, the use of geosynthetics with the aim of increasing the shear strength of cohesive soils has been investigated (Fourie & Fabian, 1987; T. S. Ingold, 1981; Terence S. Ingold & Miller, 1983; Hoe I. Ling & Tatsuoka, 1994). In the 1990's Zornberg and Mitchell in their review papers on cohesive backfills (Mitchell, 1995; J. G. Zornberg & Mitchell, 1994) state that the use of cohesive backfills has led to substantial savings in areas where granular materials are not locally available. More recently, substantial experimentation has been performed to investigate the behaviour of geotextile reinforced cohesive slopes (Hu, Zhang, Zhang, & Lee, 2010; R. Noorzad & Mirmoradi, 2010; Wang, Zhang, & Zhang, 2011). In particular non-woven geotextiles and geogrids of sufficient tensile strength have shown to be effective at increasing the strength of cohesive soils and providing effective drainage (*e.g.* (Reza Noorzad & Omidvar, 2010; Portelinha, Bueno, & Zornberg, 2013; Portelinha, Zornberg, & Pimentel, 2014; Sukmak et al., 2015). However, in the methods currently

available in the literature, reinforcements are still calculated assuming soils to be cohesionless (de Buhan, Mangiavacchi, Nova, Pellegrini, & Salençon, 1989; Richard A. Jewell, 1991; Dov Leshchinsky & Boedeker, 1989; D. Leshchinsky, Ling, & Hanks, 1995; Michalowski, 1997).

This conservative assumption is due to the fact that geosynthetics were initially conceived for cohesionless granular soils and that the first design guidelines published for geosynthetic reinforced earth structures disregard the beneficial effect of cohesion (*e.g.* (AASHTO, 2012; R. A. Jewell, 1996)). However, the recent edition of AASHTO LRFD *bridge design specifications* (AASHTO, 2012), allows for the inclusion of cohesion in the design of geo-reinforced slopes although unfortunately no formulae are provided for this purpose. The AASHTO revisit was prompted by the work of (Anderson, Geoffrey, Ignatius, & (Joe), 2008) which, for example, shows that an amount of cohesion as small as 10 kPa can reduce the thrust against an earth structure of up to 50-75% for typical design conditions. In light of these findings, (Vahedifard, Leshchinsky, Sehat, & Leshchinsky, 2014) have investigated the beneficial effect of cohesion on geosynthetic reinforced earth structures based on limit equilibrium concluding that '*the results clearly demonstrate the significant impact of cohesion on the K_{ae} value*' (K_{ae} being the design seismic active earth pressure coefficient). Unlike (Vahedifard et al., 2014), this study is concerned with the stability of geo-reinforced slopes in the absence of any retaining structure. One of the objectives of this study is to provide a method for the design of slope reinforcements where the effect of cohesion is accounted for that may feed into future new guidelines.

2.5 Non-straight optimal profiles for geo-reinforced slopes

Currently geosynthetic-reinforced slopes are designed according to a straight profile in elevation. However, in nature slope profiles exhibit all sorts of different shapes, ranging from concave to convex or partly convex and partly concave. The literature on the mechanical stability of non-straight slope profiles is very limited: presented slope stability analyses in axial symmetry based on the slip-line theory formulated by Sokolovskiĭ (1960). Hoek and Bray (1981) argued that concave slopes in rock are more stable than convex slopes but they did not produce any systematic investigation to underpin their claim.

With regard to geosynthetic reinforced slopes, recent research on multi-tiered reinforced walls seem to indicate that reinforced slopes of non-straight profile can be more stable than the traditional straight ones (Dov Leshchinsky & Han, 2004; Liu, Yang, & Ling, 2014; G.-Q. Yang, Liu, Zhou, & Xiong, 2014), but the geometric configuration considered are limited to a maximum of four walls (Stuedlein, Bailey, Lindquist, Sankey, & Neely, 2010) and more importantly the studies do not compare the mechanical performance of non-straight profiles with the performance of straight profiles of the same average inclination so no firm conclusions can be drawn. In case of unreinforced slopes instead, better performance of concave profiles over straight profiles of the same average inclination has been systematically proved by (Utili & Nova, 2007) for concave profiles of log-spiral shape for cohesive frictional geomaterials. Then, (Jeldes, Drumm, & Yoder, 2014; Vahedifard, Shahrokhabadi, & Leshchinsky, 2016b)) considered concave profiles whose shape is derived from Sokolovski's theory of slip-lines and (Vahedifard, Shahrokhabadi, & Leshchinsky,

2016a) concave circular profiles both showing superior properties to straight profiles in terms of mechanical stability. In (Vahedifard et al., 2016a) the performance of non-straight (circular) concave profiles is systematically compared to the performance of reinforced slopes of the same average inclination made of frictional backfills. They show that circular concave profiles are always better from a stability point of view and conclude that saving of up to 30% on the required tensile strength of the reinforcement can be achieved. Unlike previous studies in this thesis, the search for the optimal profile will not be restricted to a particular category of shapes, *i.e.* circular or log-spiral or from Sokolovski's slip lines, but any possible shape will be considered to achieve the most economical possible design.

Chapter 3: On the stability of fissured slopes subject to seismic action[1]

SUMMARY

A set of analytical solutions achieved by the upper bound theorem of limit analysis and the pseudo-static approach is presented for the assessment of the stability of homogeneous c, ϕ slopes manifesting vertical cracks and subject to seismic action. Rotational failure mechanisms are considered for slopes with cracks of both known or unknown depth and location. A validation exercise was carried out based on numerical limit analyses and displacement-based finite-element analyses with strength reduction technique. Charts providing the stability factor for fissured slopes subject to both horizontal and vertical accelerations for any combination of c, ϕ and slope inclination are provided. The effect of the direction of the vertical acceleration on slope stability is specifically analysed. Yield seismic coefficients are also provided. When the presence of cracks within the slope can be ascertained with reasonable confidence, maps showing the zones within the slope where they have no destabilising effect are provided. Finally, Newmark's method was employed to assess the effect of cracks on earthquake-induced displacements. To this end, displacement coefficients are

---

[1] This chapter has been published in *International Journal for Numerical and Analytical Methods in Geomechanics* (see Utili and Abd 2016).

provided in chart form as a function of the slope characteristics. Two examples of slopes subjected to known earthquakes are illustrated.

3.1 Introduction

The presence of cracks or fissures in slopes made of cohesive soils (*e.g.* clayey soils) and/or rock because of the development of tension for instance has long been recognised as an important factor affecting their stability since the time of Terzaghi (Terzaghi, 1943). The presence of cracks poses significant challenges to the assessment of slope stability because they introduce one or a few discontinuities that may substantially reduce the stability of the slope. In the case of a small number of discontinuities, homogenisation techniques work badly because the slope behaviour tends to be heavily affected by the specific features of each discontinuity that therefore has to be considered explicitly in the stability analysis of the slope. This implies a significant extra computational effort for the numerical methods typically used in continuum mechanics (*e.g.* finite element (FE) method, finite difference method, etc.) that struggle to include discrete discontinuities. Furthermore, if a comprehensive parametric analysis is to be run to explore how slope stability is affected by the presence of cracks for a variety of geometrical and mechanical parameters of the slope, the computational effort required appears prohibitive. Hence, the appeal of an analytical solution is apparent.

In the large body of literature on limit analysis applied to slopes subject to seismic excitation (*e.g.* (Cao & Zaman, 1999; Chang et al., 1984; Chen & Liu, 1990; Crespellani, Madiai, & Vannucchi, 1998; Gao et al., 2013; Loukidis, Bandini, & Salgado, 2003; X.-g. Yang & Chi, 2014; You & Michalowski, 1999)), there is no

provision to take into account the presence of cracks. In this chapter, an analytical method based on the upper bound theorem of limit analysis and on the so-called pseudo-static approach (Terzaghi, 1950) is presented for the assessment of the stability of uniform c, ϕ slopes manifesting vertical cracks and subject to seismic action. Three situations are considered in this chapter: i) the most unfavourable scenario of cracks present in the slope, (practitioners may assume such a scenario in the absence of reliable information on the presence of cracks); ii) slopes subject to cracks of known depth; iii) slopes subject to cracks of known location. With regard to the first problem, i), the assumption of the most unfavourable scenario reflects the fact that often neither the position nor the depth of a crack are known. In this case, all possible failure mechanisms involving any crack that may be present in the slope must be considered in the analysis. Assuming the terminology of Terzaghi (Terzaghi, 1943), Taylor (Taylor, 1948) and Chen (Chen, 1975), the 'stability factor' for a slope at impending failure is defined as $N_s = \gamma H_{cr} / c$, with γ being the ground unit weight, H_{cr} the critical slope height and c the ground cohesion (note that in some references the stability factor may be called stability number).

On the basis of the obtained solutions, charts of (least upper bound) stability factor versus inclination of the slope face, β, are presented in this chapter for all values of engineering interest of angle of shearing resistance, ϕ, and horizontal and vertical seismic coefficients, K_h and K_v respectively. These charts, together with the values reported in tabular form in the 'Supporting Information' (see Appendix A), can be used by practitioners to get an immediate estimate of the destabilising influence of the presence of cracks on the slope of interest for a wide range of prescribed seismic

action. However, if reliable information on the cracks existing in the slope is available, the conservative assumption of the most unfavourable scenario is no longer justified. In this eventuality, either the depths of the cracks (problem ii) or their locations (problem iii) can be prescribed reducing the number of potential failure mechanisms to be considered in the search for the least upper bound. With regard to crack depth, according to some lower bound analyses (*e.g.* (Antao, Guerra, Matos Fernandes, & Cardoso, 2008; R. Baker, 2003; Terzaghi, 1943)), it can be determined as a function of the tensile strength of the ground and its stress state. However, exceedance of the ground tensile strength is only one of the possible causes for the formation of cracks, because there is experimental evidence about cracks caused and/or deepened by processes such as the occurrence of differential settlements (Vanicek & Vanicek, 2008), desiccation (Dyer, Utili, & Zielinski, 2009; Konrad & Ayad, 1997; Tang, Cui, Tang, & Shi, 2009; Utili, Castellanza, Galli, & Sentenac, 2015) and freezing (Hales & Roering, 2007). In the large majority of cases, accurate estimates of crack depths are not available to the practitioner; therefore, the stability of a slope needs to be analysed for a range of possible crack depths rather than a single value. Accordingly, in this chapter, the yield horizontal acceleration is calculated for various prescribed crack depths.

Numerical simulations with other methods, namely FE limit analysis (numerical upper and lower bounds) and FE displacement based method with strength reduction technique, were run to validate the obtained results. A very good agreement in terms of both geometry of the predicted failure mechanism and yield seismic coefficient was found. Then, an analysis of the influence of the vertical seismic acceleration on slope stability is presented for both cases of intact and fissured slopes. Dimensionless charts

showing which case is more critical for the stability of slopes between no vertical acceleration, upward acceleration and downward acceleration are provided for any combination of β, ϕ and K_h. In addition, maps showing zones where cracks have no detrimental effect on slope stability are provided for various combinations of horizontal and vertical accelerations.

To this end, the locations of the cracks (problem iii) are prescribed in the search for the most unfavourable failure mechanism. These maps can be employed for two purposes: (i) in the case of earth structures prone to fissuring, as for instance flood defence embankments (Allsop W., 2007; Dyer et al., 2009; Environment_Agency, 2006; Utili et al., 2015), they may help inspection engineers to reduce significantly the extent of the zones to be inspected by excluding the zones where cracks have no detrimental effect on slope stability; (ii) when the presence of one or more cracks in a slope is known, the maps tell the geotechnical engineer whether the crack may be discarded from the stability analysis of the slope.

Finally, Newmark's approach (Newmark, 1965), also called 'block sliding procedure', was used to calculate seismic induced displacements. Horizontal yield accelerations were calculated for any combination of values of β, ϕ, λ and of the normalised cohesion, $c / \gamma H$, of engineering interest, having assumed the presence of the most unfavourable crack in the slope. In the analysis here presented, unlike Newmark's original formulation that assumes translational failure mechanisms, rotational mechanisms were used instead because they are more critical for the stability of slopes. Seismic displacement coefficients were calculated as a function of

slope characteristics (ϕ and β values). Finally, the influence of crack depth on earthquake-induced displacements was investigated.

3.2   Derivation of the analytical solution

The failure mechanisms assumed in our analysis are 2D single wedge rigid rotational mechanisms (see Figure 3.1). The failing wedge E-D-C-B rigidly rotates around point P with the ground lying on the right of the log-spiral D-C and of the vertical crack C-B remaining at rest. The equation of the log-spiral D-C is:

$$r = r_\chi \exp\left[\tan\phi\left(\theta - \chi\right)\right]$$ (3.1)

with r being the distance of a generic point of the spiral to its centre, θ being the angle formed by r with the horizontal axis, r_χ identifying the distance of point F of the spiral to its centre and χ being the angle made by segment P-F with the horizontal (see Figure 3.1). The upper bound is derived by imposing energy balance for the failing wedge E-D-C-B:

$$\dot{W}_d = \dot{W}_{ext}$$ (3.2)

where $\dot{W}_d$ and $\dot{W}_{ext}$ are the rate of dissipated energy and of external work respectively.

The calculation of $\dot{W}_d$ accounting for the energy dissipated along the log-spiral segment D-C is reported in (Utili, 2013). Note that in this formulation cracks are treated as no-tension non-cohesive perfectly smooth (no friction) interfaces, therefore no energy is ever dissipated along a crack and the angle η is $0° < \eta < 180°$.
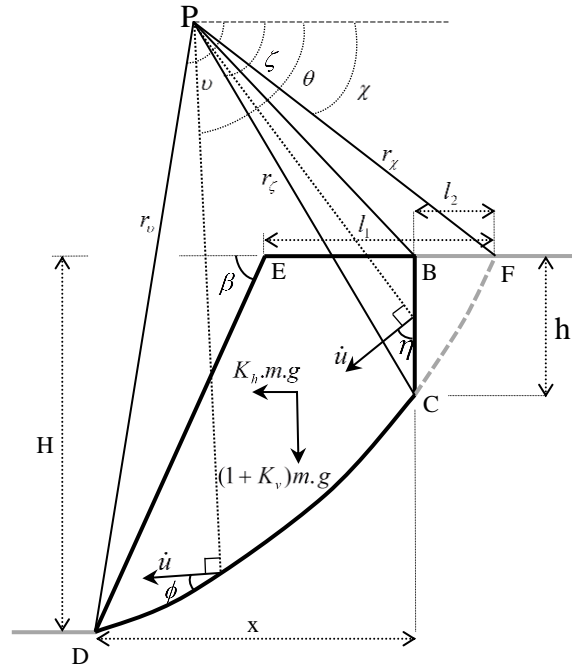
Figure 3.1 Failure mechanism. Note that $\eta \neq \phi$. The wedge of soil enclosed by black lines D-C (logarithmic spiral failure line), B-C (pre-existing crack), B-E (upper surface of the slope) and E-D (slope face) rotates around point P.

(Michalowski, 2013) has provided a limit analysis upper bound formulation for vertical cracks that form simultaneously with the onset of the failure mechanism in an intact slope. These cracks assumed to form due to the soil tensile strength being exceeded at the same time as the log-spiral surface D-C is formed due to the shear strength being exceeded. However, these cracks generated as part of the failure mechanism taking place are always less detrimental (critical) to slope stability than cracks pre-existing the formation of the slope failure mechanism, since they require energy to be dissipated for their formation which is not the case for pre-existing cracks (Michalowski, 2013). Therefore, in this chapter only the presence of (more critical) pre-existing cracks is considered.

The rate of external work for the sliding wedge E-B-C-D, $\dot{W}_{ext}$, is calculated as the work of block E-D-F minus the work of block B-C-F. The work of block E-D-F is calculated by algebraic summation of the work of blocks P-D-F, P-E-F and P-D-E (Chen, 1975). The work of block B-C-F is calculated by algebraic summation of the work of blocks P-C-F, P-B-F and P-C-B (Utili, 2013; Utili & Crosta, 2011; Utili & Nova, 2007). Note that here, in addition to the weight force, a horizontal pseudo-static force, $F_{PSh} = M.K_h.\text{g} = \gamma K_h A$, with g being the gravitational acceleration and M the mass of the wedge, and a vertical one, $F_{PSv} = M.K_v.\text{g} = \gamma K_v A$, are added to account for the seismic action (Chang et al., 1984; Chen & Liu, 1990).

The calculation of the expression $\dot{W}_{ext}$ for each block is provided in Appendix B. Substituting them into Eq. (*3.2*), the following is obtained:

$$c\dot{\theta}r_{\chi}^2 f_d = \dot{\theta}\gamma r_{\chi}^3 \begin{bmatrix} (1+K_v)(f_{1v} - f_{2v} - f_{3v} - f_{4v} + f_{5v} + f_{6v}) + \\ K_h(f_{1h} - f_{2h} - f_{3h} - f_{4h} + f_{5h} + f_{6h}) \end{bmatrix} \qquad (3.3)$$

with f_{1v}, f_{2v}, f_{3v}, …, f_{6h} are functions provided in Appendix B. Dividing all terms in Eq. (*3.3*) by $\dot{\theta}$ and r_{χ}^2, and rearranging, the stability factor, $\gamma H / c$, is obtained:

$$\begin{aligned} N &= \frac{\gamma H}{c} = f\left(\chi, \upsilon, \zeta, \phi, \beta, K_h, \lambda\right) \\ &= \frac{f_d\left[\exp\left[\tan\phi(\upsilon - \chi)\right]\sin\upsilon - \sin\chi\right]}{\begin{bmatrix}(1+\lambda K_h)(f_{1v} - f_{2v} - f_{3v} - f_{4v} + f_{5v} + f_{6v}) + \\ K_h(f_{1h} - f_{2h} - f_{3h} - f_{4h} + f_{5h} + f_{6h})\end{bmatrix}} \end{aligned} \qquad (3.4)$$

With $\lambda = K_v / K_h$ (consistently with Figure 3.1, the + sign indicates vertical downward acceleration, whereas the – sign indicates vertical upward acceleration). The global minimum of $f\left(\chi, \upsilon, \zeta, \phi, \beta, K_h, \lambda\right)$ over the three geometrical variables χ, υ, ζ

26

provides the least (best) upper bound on the stability factor having assumed that the most unfavourable crack for the slope is present. By solving Eq. (*3.3*) with respect to K_h instead, the upper bound on the yield seismic coefficient, K_y, is obtained:

$$
\begin{aligned}
K_y &= f_y\left(\chi, \upsilon, \zeta, \phi, \beta, c/\gamma H, \lambda\right) \\
&= \frac{(c/\gamma H) f_d\left[\exp\left[\tan\phi(\upsilon-\chi)\right]\sin\upsilon - \sin\chi\right] - \left(f_{1v}-f_{2v}-f_{3v}-f_{4v}+f_{5v}+f_{6v}\right)}{\lambda\left(f_{1v}-f_{2v}-f_{3v}-f_{4v}+f_{5v}+f_{6v}\right)+\left(f_{1h}-f_{2h}-f_{3h}-f_{4h}+f_{5h}+f_{6h}\right)}
\end{aligned}
\tag{3.5}
$$

The global minimum of $f_y\left(\chi, \upsilon, \zeta, \phi, \beta, c/\gamma H, \lambda\right)$ over the three geometrical variables χ, υ, ζ provides the least upper bound on K_y.

Note that unlike the case of intact slopes, failure mechanisms may in principle daylight on the slope face above the slope toe. So potential failure mechanisms passing above the toe were considered in the current analysis by discretising the slope face in several points and calculating the stability factor associated to each potential mechanism (see

Figure 3.2a). In all the cases considered here no potential mechanism passing above the slope toe turned out to be a critical failure mechanism. In the case of intact slopes with a low value of ϕ, (You & Michalowski, 1999) found that for high values of K_h, the failure mechanism passes below the slope toe (see

Figure 3.2b). The results reported here in this chapter include both types of failures. Failure mechanisms passing below the toe were found for slopes with low friction (*e.g.* $\phi = 20°$) and high $c/\gamma H$.

Figure 3.2 a) Potential failure mechanism passing above the slope toe (wedge E-R-N-M) and the one taking place (wedge E-D-C-B),(after Utili, 2013). b) Failure mechanism passing below the slope toe (wedge E-D-Q-C-B).

3.3   Stability factor
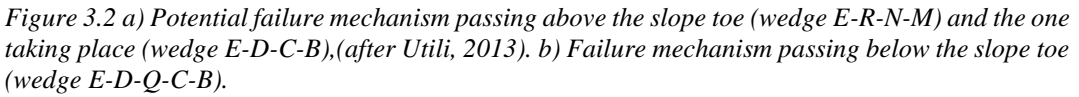
The global unconstrained minimization of $f\left(\chi,\upsilon,\zeta,\phi,\beta,K_h,\lambda\right)$ in Eq. (*3.4*) provides

the stability factor when the most unfavourable crack is present. The stability factors

obtained are plotted in Figure 3.3 against the inclination of the slope face, β, for $\phi =$

20°, 30° and 40°, with K_h ranging from 0.1 to 0.4, and for λ ranging from -1 to +1.

For sake of completeness, the largest range of λ reported in the literature (λ ranging

from -1 to +1) was chosen (see (Hoe I. Ling, Leshchinsky, & Mohri, 1997; Shukha &

Baker, 2008)). The four charts of Figure 3.3 are useful to practitioners in order to get

an immediate estimate, erring on the safe side, of the stability of a fissured slope

subject to seismic excitation when no data on either the depth or the position of the

existing cracks are known. For some combinations of the slope parameters, a

translational failure mechanism, indicated by grey lines in the figures, occurs instead

28

of the rotational one. Note that translational mechanisms are always particular cases of rotational ones, obtained when the radius of the spiral, r_χ approaches infinity.

A key question from a practitioner's viewpoint is how much the presence of cracks may affect slope stability and when they may be safely neglected in a stability analysis. The answer to this is provided in Figure 3.4, where the difference in percent between the obtained stability factors and the corresponding factors for a slope of the same characteristics but intact is plotted for all the parameter combinations of engineering interest. From the figure is apparent that the presence of cracks can cause substantial reduction of stability (up to 30%), with the reduction being more significant for steep slopes. This result is explained by the fact that steep slopes are subject to failure mechanisms that involve deeper cracks than gentle slopes. The depth, h_c and location, x_c of the crack associated to the failure mechanism found as a result of the analysis for various levels of K_h are plotted in Figure 3.5a and b respectively. The subscript 'c' stands for critical since the crack here considered is the most critical that may exist for the stability of the slope. From the figure emerges that h_c increases with K_h whatever the slope inclination. Also for $\beta \rightarrow 90°$, $x_c \rightarrow 0$ independently of the value of K_h.
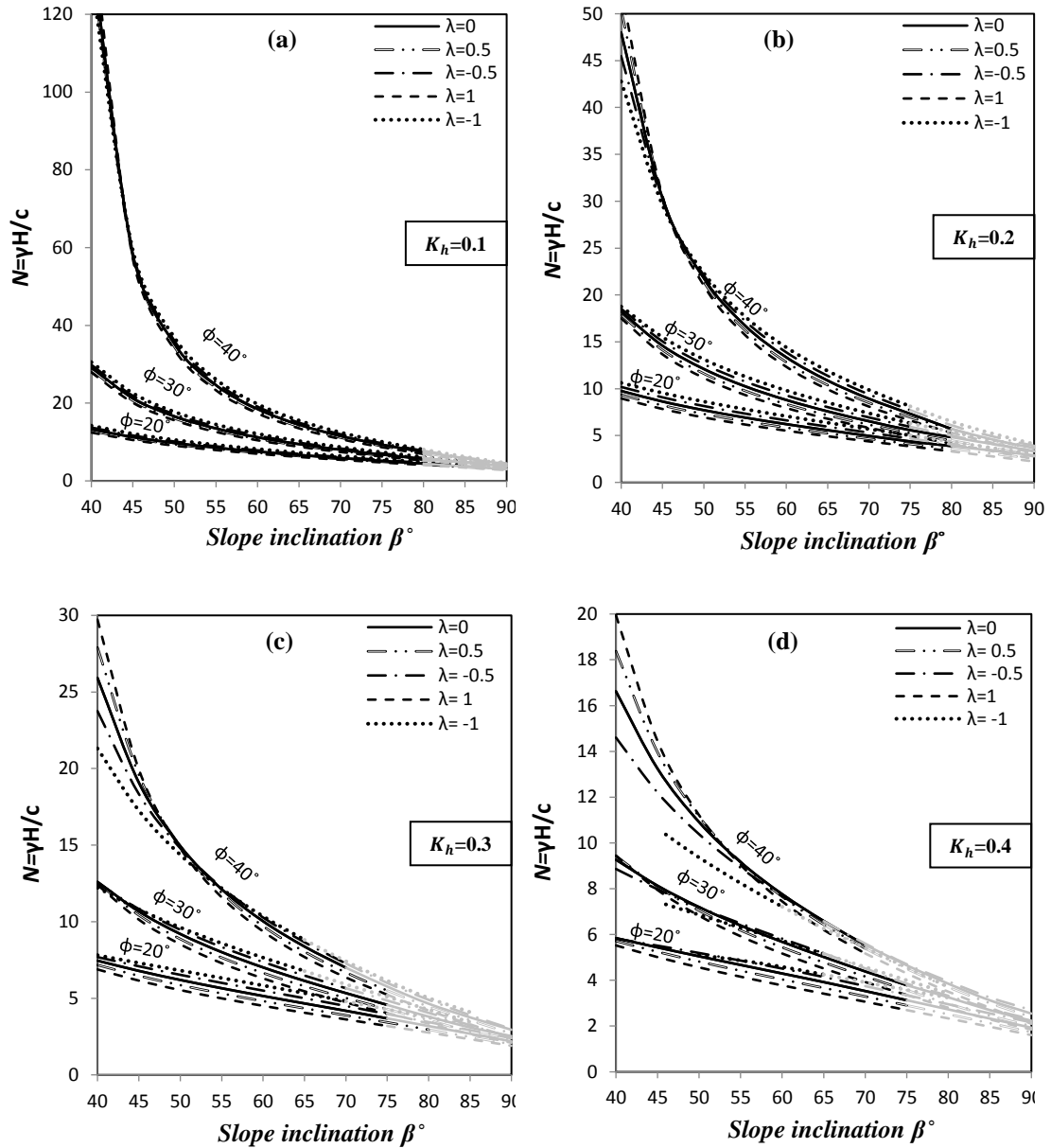
Figure 3.3 Stability factor against slope inclination for the most unfavourable crack scenario, i.e. the most critical mechanism among all the potential mechanisms involving cracks of any depth and location is sought, with $\lambda = K_v / K_h$. a) $K_h =0.1$;b) $K_h =0.2$; c) $K_h =0.3$

In Figure 3.5b, the horizontal distance of the crack from the slope crest, x_c is plotted against β. It turns out that the higher the intensity of the seismic excitation, the more xc shifts inwards. When $\beta \to 90°$, $x_c \to 0$ independently of the level of K_h with the failing wedge becoming an infinitesimal slice. As observed in (Utili, 2013) in the absence of seismic action, $\beta = 90°$ is a singular case with the failure mechanism

involving a vertical slice of infinitesimal width and of finite height H, translating away $r_\chi \to \infty$.

Finally comparing the curves plotted in Figure 3.4 for different levels of K_h, it can be inferred that the stronger the earthquake is, the larger the reduction of slope stability caused by the presence of cracks. On the other hand when β is close to ϕ and K_h is small, the reduction of N is less than 5%. Therefore, it can be concluded that the presence of cracks cannot be neglected except in the case of gentle slopes of high angle of shearing resistance subject to moderate earthquakes.

In previous limit analysis works accounting for the presence of a vertical pseudo-static acceleration, this is always assumed to be downward (*e.g.* (Chen & Liu, 1990; Hoe I. Ling et al., 1997)) implying that downward acceleration is always detrimental to slope stability whereas upward acceleration is beneficial or, at least less detrimental than the downward one. Here instead, it will be shown that both downward and upward directions can be detrimental (or beneficial) depending on the geometrical and mechanical characteristics of the slope. As shown in Figure 3.3, in general the stability factor, N, increases with the value of λ (with the lowest line being for $\lambda =+1$ and the highest one for $\lambda =-1$), so for low values of ϕ, downward vertical acceleration is detrimental to stability whereas upward acceleration is beneficial.
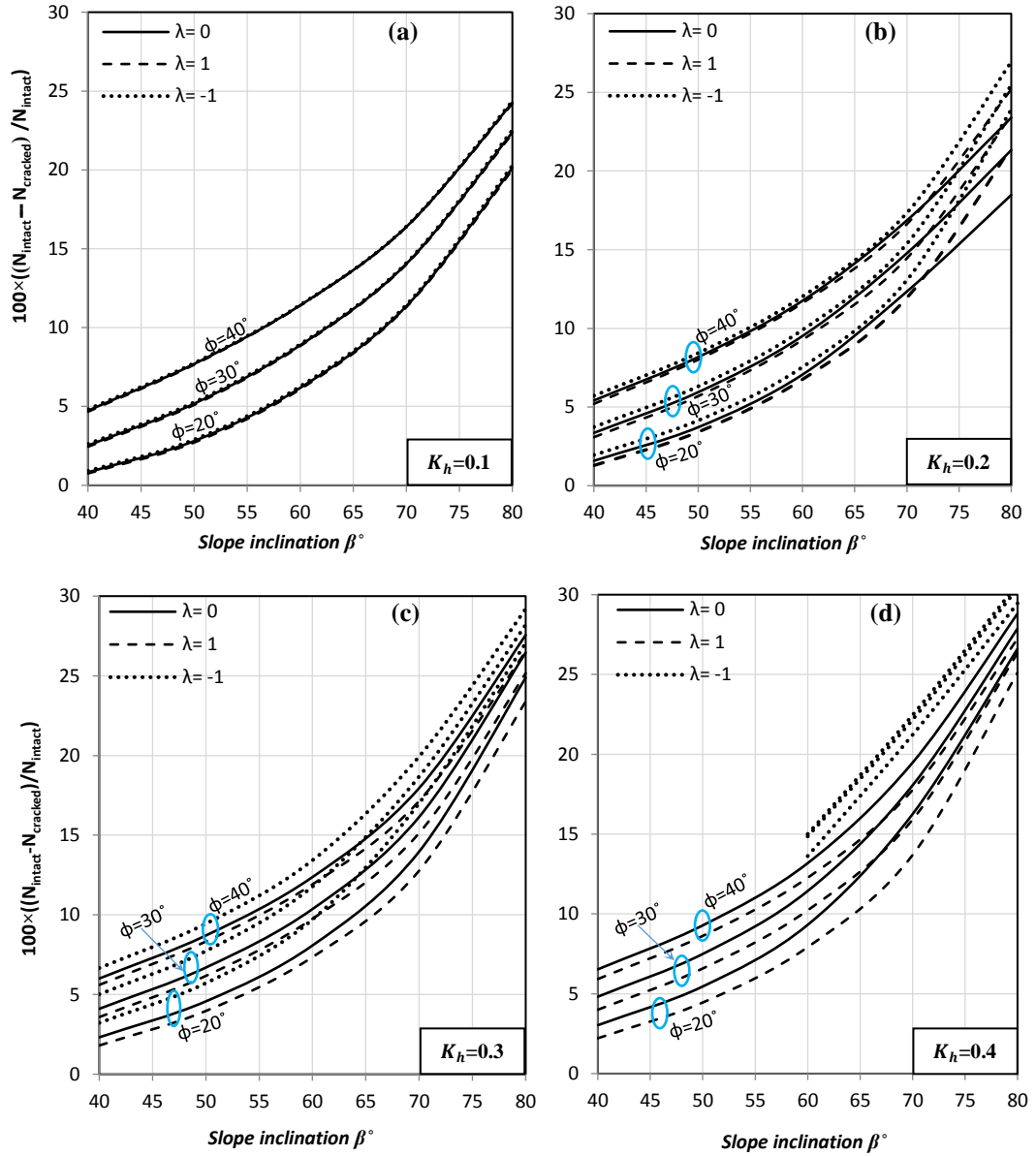
Figure 3.4 Reduction in percent of the stability factor due to the most unfavourable crack versus slope inclination, for various combinations of K_h, and λ.
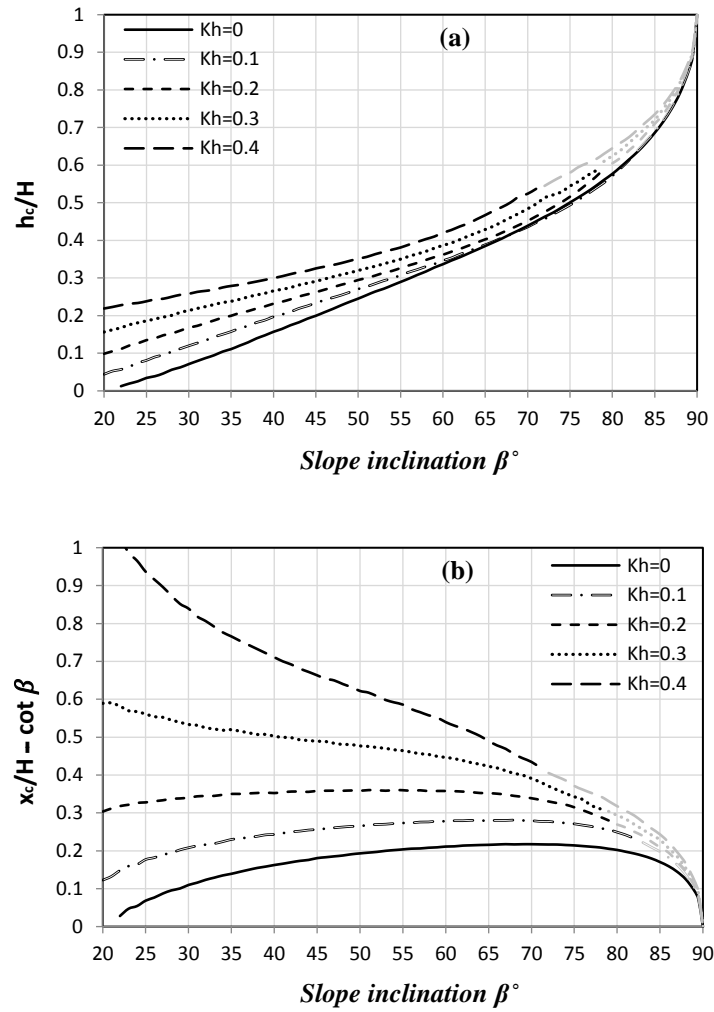
Figure 3.5 a) Depth of the most unfavourable crack versus slope inclination for various K_h with ϕ =20º and λ =0. b) Location of the most unfavourable crack, measured from the slope toe, versus slope inclination for various K_h with ϕ =20º and λ =0. Black curves indicate a rotational failure mechanism whilst grey curves indicate a translational failure mechanism.

This is in agreement with the assumption routinely made in the literature. However, examining the charts of Figure 3.3 more closely, there are several instances where curves for the same ϕ and K_h but different λ value intersect. For instance all the lines obtained for K_h =0.2 and ϕ =40° intersect at $\beta \approx 47°$ (see Figure 3.3b): on the right side of the intersection point, N decreases with λ increasing, but on the left side of the point, the trend is the opposite with N increasing for λ increasing. So on the left side of $\beta = 47°$, upward vertical acceleration is detrimental to slope stability

whereas downward acceleration is beneficial. This trend becomes increasingly more marked for higher K_h. The results here illustrated are in agreement with the analysis recently carried out by Shuka and Baker (Shukha & Baker, 2008) employing limit equilibrium on intact slopes; however, the results here illustrated were obtained for slopes subject to cracks and are based on the rigorous framework of limit analysis.

At high values of K_h (see chart 3c and 3d), there are several intersection points between the curves obtained for the same ϕ and K_h values rather than one. This makes it difficult to establish which case is more critical. To address this question, the maps of Figure 3.6 are provided. In the maps, four zones exist. In zone 1, the stability factor for vertical downward acceleration, $N_\downarrow$, is lower than the factor for the case of no vertical acceleration, N_0, that in turn is lower than the factor for the case of vertical upward acceleration, $N_\uparrow$. In zone 2 $N_\uparrow < N_\downarrow < N_0$, in zone 3 $N_\downarrow < N_\uparrow < N_0$ and in zone 4 $N_\downarrow < N_0 < N_\uparrow$. The four zones exist for intact slopes as well (see Figure 3.6b and d). Comparing the maps obtained for fissured slopes with the ones obtained for the corresponding intact slopes subject to the same λ values (*i.e.* Figure 3.6a with b and Figure 3.6c with d), it turns out that the presence of cracks makes zones 2 and 3 larger. Another observation can be made about the influence of the magnitude of K_v on the extent of those zones.
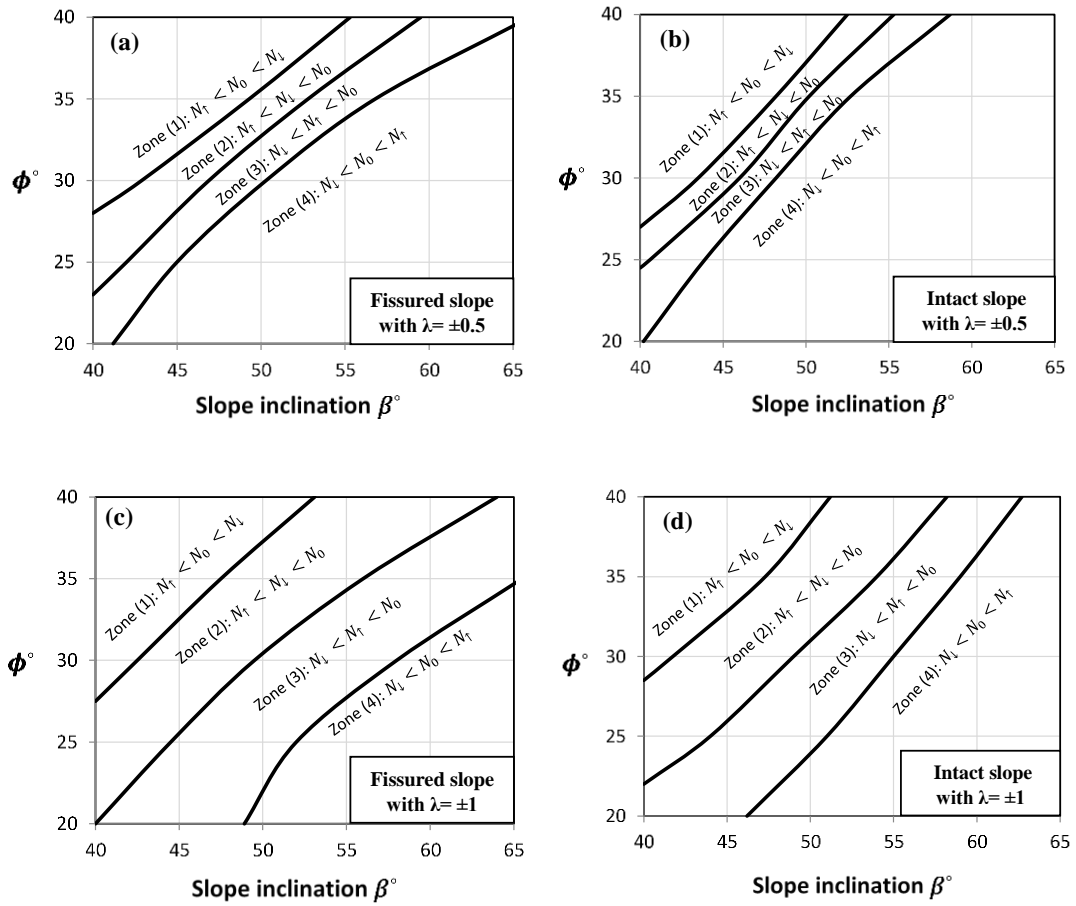
Figure 3.6 Charts illustrating which case is more critical for various combinations of ϕ and β with K_h =0.4. $N\uparrow$, N_0 and $N\downarrow$ represent the stability numbers $\gamma H / c$ calculated considering upward vertical acceleration, zero vertical acceleration and downward vertical acceleration respectively.

In Figure 3.7a, the boundary between the zone where $N_\uparrow < N_\downarrow$ and where $N_\downarrow < N_\uparrow$ is plotted for various levels of K_h and λ. This figure provides the key information needed by practitioners to decide whether to assume upward or downward vertical acceleration for the stability analysis of a given slope. For sake of completeness also the boundary between the zone where $N_0 < N_\downarrow$ and $N_\downarrow < N_0$ is plotted in Figure 3.7b and the boundary between the zone where $N_\uparrow < N_0$ and $N_0 < N_\uparrow$ in Figure 3.7c.
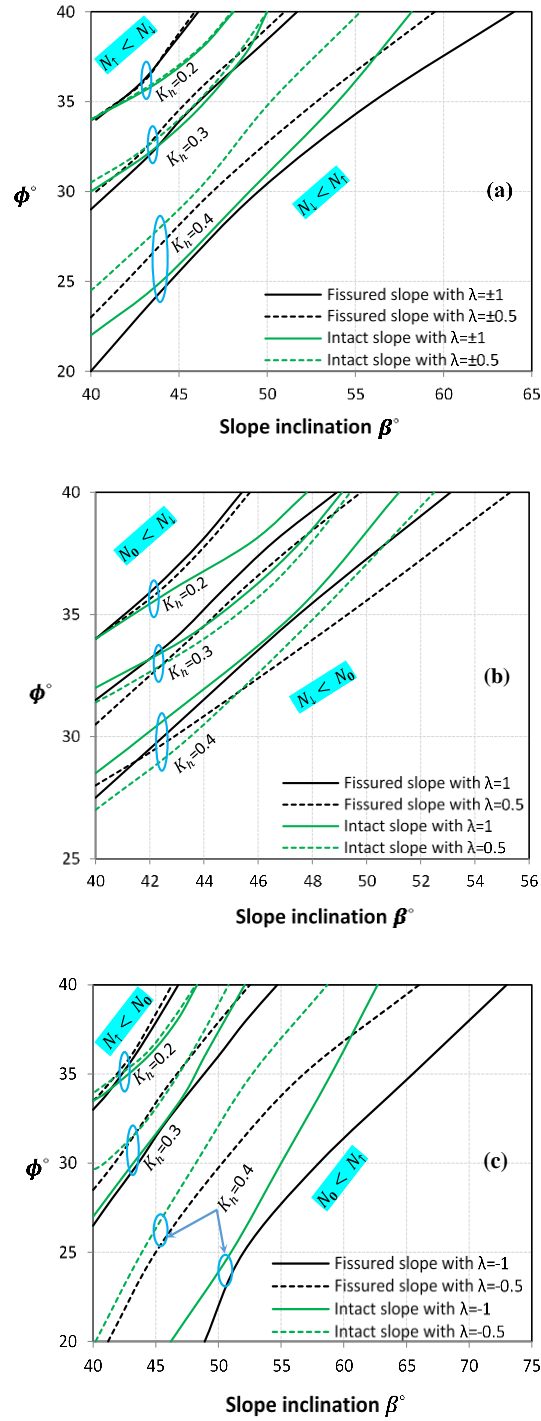
Figure 3.7 Black lines are for fissured slopes (most unfavourable crack scenario), green lines for intact slopes. Solid lines are for $\lambda = 1$, whilst dashed lines are for $\lambda = 0.5$: a) in the region above the lines, $N\uparrow < N\downarrow$; the opposite holds true in the region below; b) in the region above the lines, $N_0 < N\downarrow$; the opposite holds true in the region below; c) in the region above the lines, $N\uparrow < N_0$;the opposite holds true in the region below.

3.4 Yield acceleration

The yield (in some references also called critical) horizontal acceleration, $g.K_y$, is a key parameter informing practitioners of the level of seismic acceleration for which a given slope, stable under static conditions, becomes unstable. Also, it is needed to calculate earthquake induced permanent displacements via the Newmark's approach (Newmark, 1965).

The global minimum of $f_y(\chi,\upsilon,\zeta,\phi,\beta,c/\gamma H,\lambda)$ over the three geometrical variables χ,υ,ζ (see Eq.(*3.5*)) Provides the least upper bound on the yield seismic coefficient, K_y assuming that the most unfavourable crack for the slope is present. In Figure 3.8, the K_y values obtained are plotted for slopes of various characteristics β,ϕ, and $c/\gamma H$ together with the values of K_y obtained for intact slopes. In Figure 3.9 the difference in percent between the obtained yield seismic coefficients and the corresponding coefficients for a slope of the same characteristics but intact is plotted. It can be seen that the presence of cracks causes substantial reduction of the yield seismic coefficient, especially for steep slopes of low ϕ. This result is in agreement with the trend observed in Figure 3.4 for the reduction of the stability factor under a prescribed $g.K_h$. Figure 3.9 is useful to investigate the relative influence between the two strength parameters (c and ϕ) on the yield seismic coefficient. Looking at the charts for $\beta=60°$ and $\beta=75°$ (see Figure 3.9b and c respectively) it can be noticed that the reduction of K_y due to the presence of cracks becomes less significant for c increasing. However, in case of gentle slopes (see Figure 3.9a), there

is an inversion of the trend at $\phi=30°$: for slopes with $\phi>30°$ the reduction in K_y due

to the presence of cracks becomes more significant for c increasing.
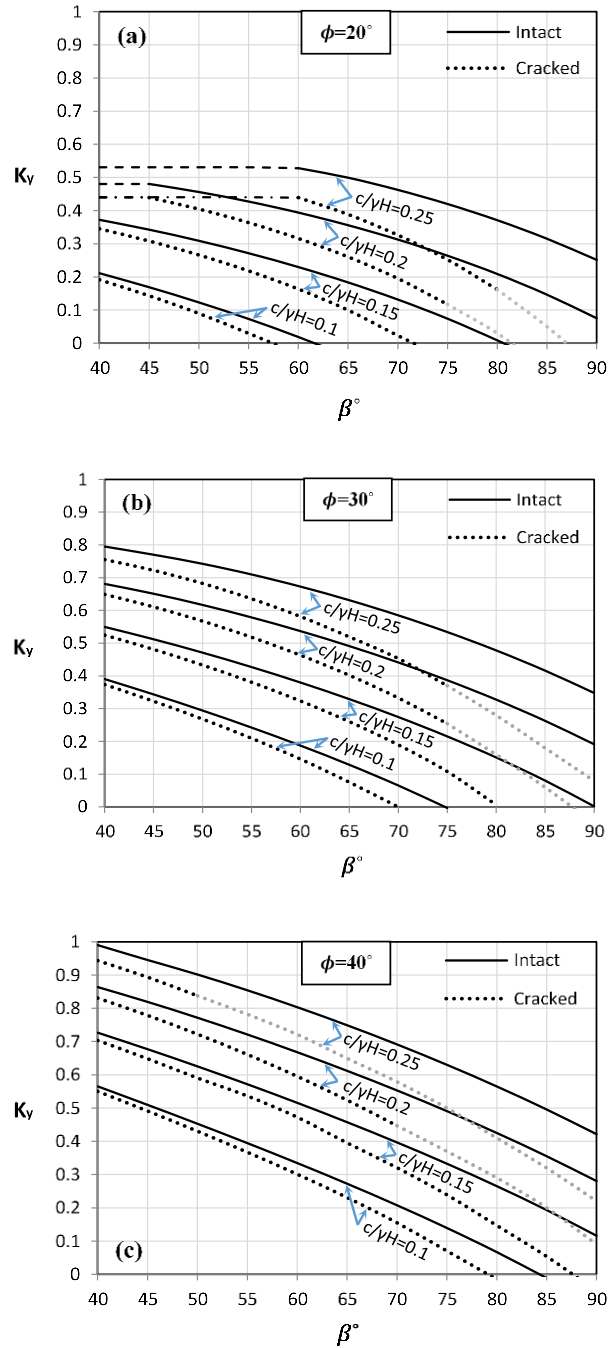
Figure 3.8 Coefficient of yield acceleration versus slope inclination for intact slopes (solid lines) and for fissured slopes for the most unfavourable crack scenario (dotted lines). Vertical acceleration is absent (λ =0): a)) ϕ =20º; b)) ϕ =30º; c)) ϕ =40º . Grey lines indicate a translational failure mechanism. Dashed and dashed-dotted lines indicate a below the slope toe mechanism occurring for intact and fissured slopes respectively.
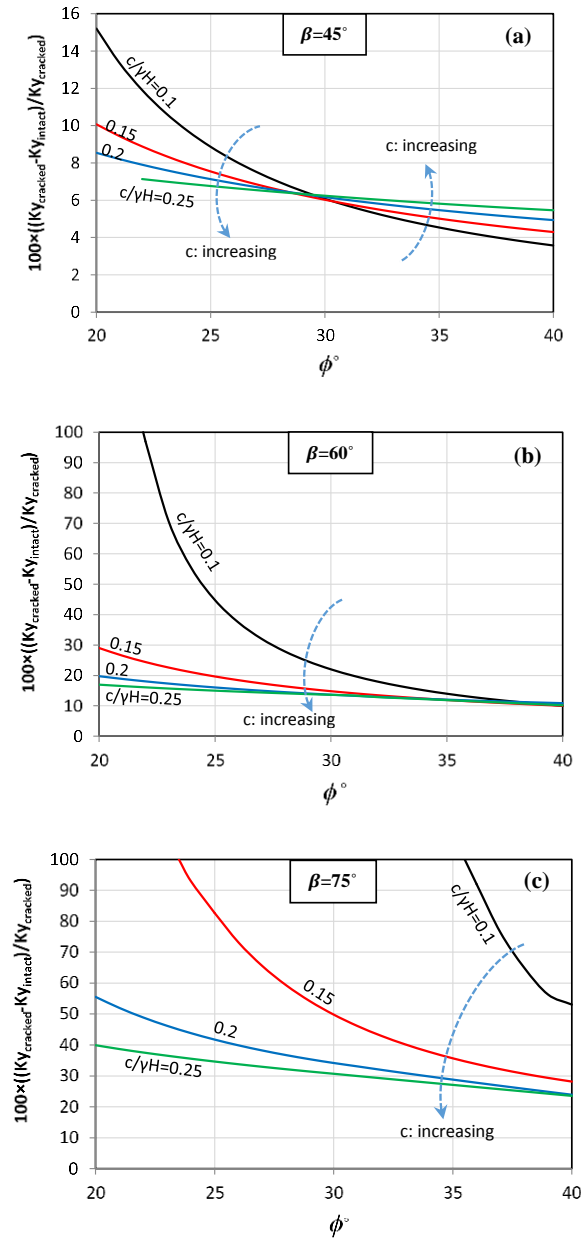
Figure 3.9 Percentage of reduction in the yield acceleration due to the presence of the most unfavourable crack for the stability of the slope with λ =0. a) β =45°, b) β =60°, and c) β =75°.

   As noted in the investigation of the stability factor under prescribed seismic excitation, assuming the presence of the most unfavourable crack can be overly conservative. When the maximum depth of cracks in a slope can be inferred by either a stress analysis or in-situ measurements, this information can be included in the

search for the least upper bound on K_y (problem ii) listed in the Introduction).

Mathematically, this is done by imposing the following constraint (Utili, 2013):

$$\exp\left[\tan\phi.\zeta\right]\sin = \left[\exp\left[\tan\phi.\chi\right]\sin\chi\left(1-\frac{h}{H}\right)+\frac{h}{H}\exp\left[\tan\phi.\upsilon\right]\sin\upsilon\right] \qquad (3.6)$$

into the maximisation of $f_y\left(\chi,\upsilon,\zeta,\phi,\beta,c/\gamma H,\lambda\right)$ in Eq.(*3.5*). In Figure 3.10, the

function $K_y^h\left(h\right)$ obtained from the maximisation of $f_y\left(\chi,\upsilon,\zeta,\phi,\beta,c/\gamma H,\lambda\right)$

constrained by Eq. (*3.6*), is plotted against the prescribed λ values for $\lambda=0$, $\lambda=0.5$

and $\lambda=1$. $K_y^h\left(h\right)$ gradually decreases for h increasing until a minimum at $h=h_{min}$ is

reached and then increases for h increasing (see the grey curves in Figure 3.10). Note

that the results represented by the grey curves are obtained assuming the log-spiral

failure surface C-D constrained to depart from the crack bottom end (see Eq. (*3.6*)).

When $h/H \rightarrow 1$, the function $K_y^h\left(h\right)$ tends to infinity because the volume of the

wedge E-B-C-D sliding away becomes infinitesimal. However, physics dictates that

the failure mechanism taking place may involve only one part of the total crack depth,

i.e. the log-spiral C-D may depart from the crack above its bottom end. This possibility

is not reflected by the mathematical function $K_y^h\left(h\right)$ since Eq. (*3.6*)constrains the

failure log-spiral C-D to depart from the crack bottom end. For $h > h_{min}$, the least upper

bound on the yield acceleration coefficient is provided by $K_y^h\left(h=h_{min}\right)$ which is

represented by black horizontal lines in Figure 3.10.

   Finally from Figure 3.10 emerges that for steep slopes (Figure 3.10d and e), the

presence of a vertical downward acceleration reduces the yield seismic coefficient

(hence it is detrimental to slope stability) whereas for gentle slopes with high ϕ

(Figure 3.10c) the opposite is true. This trend is in agreement with the results of the investigation, carried out in the previous section, on the influence of K_v on the stability factor for prescribed values of K_h.
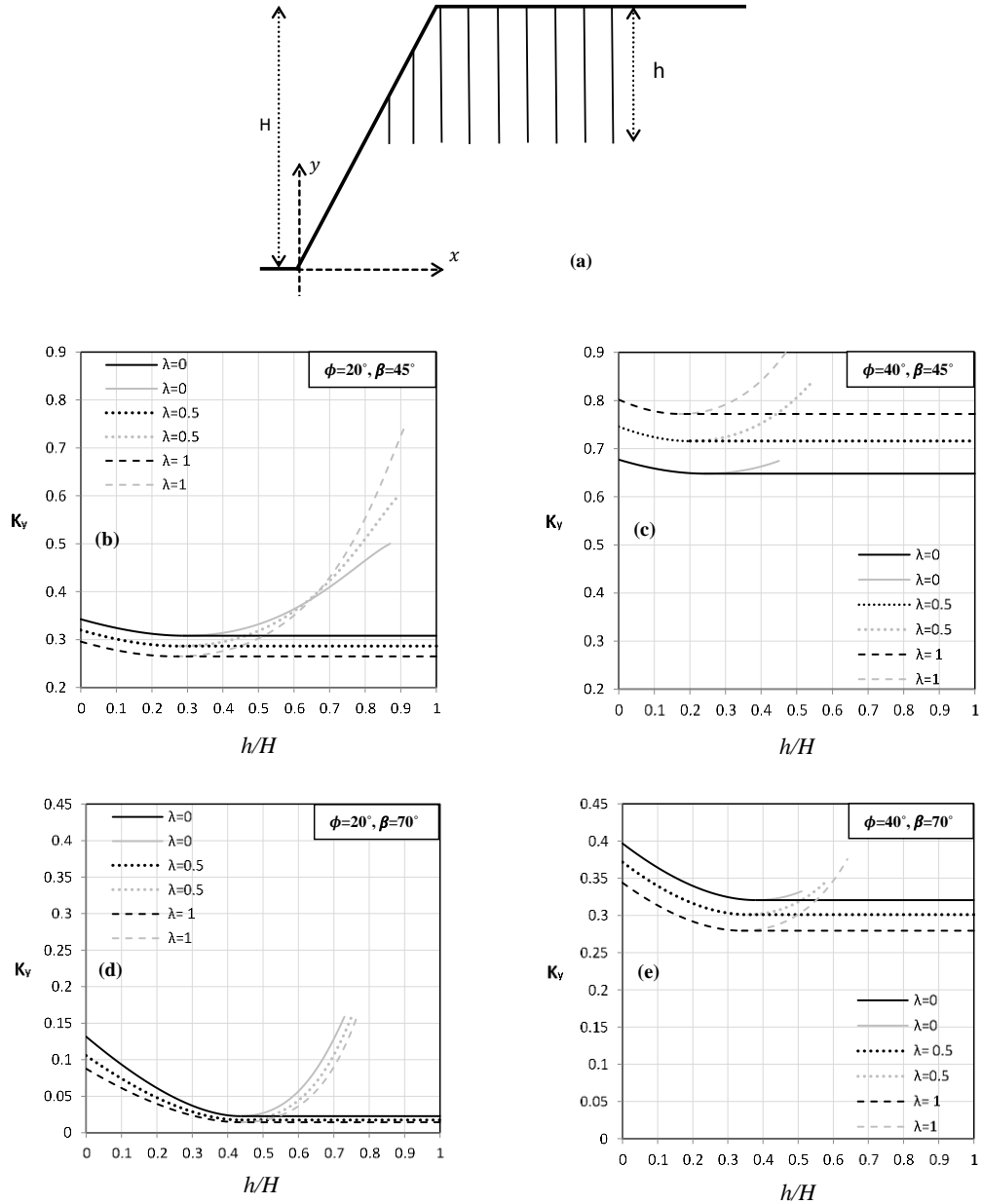
Figure 3.10 a) Visualisation of a slope subject to cracks of known depth but unspecified location. In figures b), c), d) and e) K_y is plotted against the prescribed crack depth for slopes of various β, ϕ and λ values with $c/\gamma H$ =0.15: b) ϕ =20º, β =45º; c) ϕ =40º, β =45º; d) ϕ =20º, β =70º; e) ϕ =40º, β =70º. The grey lines represent the mathematical function $K_y^h(h)$, whilst the black lines represent the yield seismic coefficient of the slope.

3.5 Validation

The validation exercise consisted of performing finite element (FE) displacement based analyses with strength reduction method assuming an associated flow rule ($\psi = \phi$) and FE upper and lower bound limit analyses to determine the yield seismic coefficient for a prescribed crack depth (problem ii in 'Introduction') and in the presence of the most unfavourable crack for the slope (problem i). The software package Opt+umCE (OptumG2, 2014) was used for this purpose since it allows running both types of analyses. Mesh dependency of the numerical results was checked by running simulations for different mesh sizes. The results here reported refer to simulations with a sufficient large number of elements (minimum of 8000 elements) and using mesh adaptivity so that mesh dependency is negligible. The boundaries dimensions were chosen such that they do not affect the calculations and normal fixities were applied for these boundaries. Triangular element of three stress node and one displacement node is used for the finite element lower bound analysis , triangular element with 3 stress node and 3 displacement node is used for the finite element upper bound analysis while 15- displacement node triangular Gauss element type is used for the finite element displacement based analysis. The crack is implemented as joints of negligible strength, *i.e.* no-tension non-cohesive perfectly smooth interface, consistent with LA assumptions. In Figure 3.11a, the yield seismic coefficient obtained for various values of prescribed crack depth is plotted. It can be noted that the current analytical LA upper bound is significantly lower (*i.e.* better) than the FE upper bound. Also the gap between the numerical upper and lower bounds remains within ±9%, for any value of prescribed crack depth (the largest gap being at high depths). These results are consistent with the findings of (Loukidis et al., 2003)

for intact slopes subject to seismic actions. Finally note that the analytical upper bounds here found are quite close to the numerical lower bounds so that true collapse values can be determined, by taking the average of the two bounds, with an accuracy of $\pm 3\%$.

In Figure 3.11b, the failure mechanism obtained from FE displacement based analyses with strength reduction technique and the mechanism obtained from our analytical upper bound are plotted for the case of h/H =0.1. A very good agreement is apparent. This implies that the failure mechanism assumed in the analyses presented in this chapter, rigid rotation of block E-B-C-D, is not only a kinematically admissible mechanism but it can also be considered a proxy of the true collapse mechanism. Therefore, the failure mechanisms determined in the presented analyses can be used to obtain an estimate of the volume of the failed material especially for the central part of a 3D landslide where plane strain conditions apply. For this reason, the areas of the failure mechanisms determined in this chapter are provided in the 'Supplementary material'. Furthermore, several numerical analyses in the last decade for both associated and non-associated geomaterials, via the finite difference method (Dawson, Roth, & Drescher, 1999), via the finite element method (Conte, Silvestri, & Troncone, 2010; Crosta et al., 2014; Loukidis et al., 2003; Zheng, Liu, & Li, 2005) and via the discrete element method (Utili & Nova, 2008) have shown that a log-spiral rigid rotational mechanism is a realistic failure mechanism for uniform c-ϕ intact slopes under static or seismic conditions. The validation exercise here presented extends this knowledge to slopes manifesting cracks.
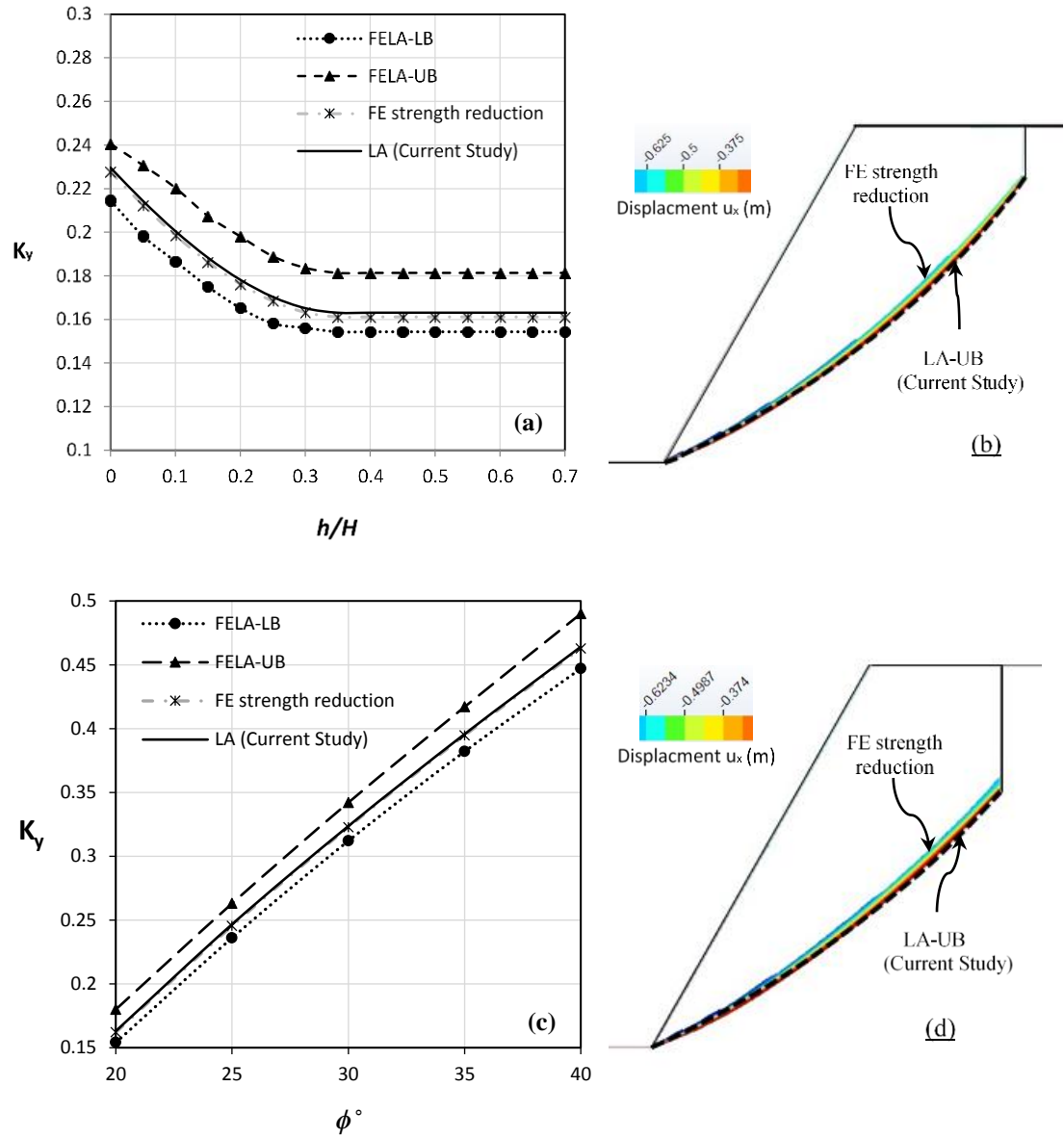
Figure 3.11 Comparison between the current analytical results and those obtained using finite element method (FE-limit analysis and FE- displacement-based method using strength reduction technique), $\beta = 60°$ and $\lambda = 0$. (a) & (b) refer to the case of a slope subject to cracks of any possible location with a prescribed depth of $h/H = 0.1$ for $\phi = 20°$. (c) & (d) refer to the same slope subject to the most unfavourable crack for its stability.

In Figure 3.11c, the yield seismic coefficient obtained for the case of the most unfavourable crack being present is plotted for various values of ϕ. To find the yield seismic coefficient associated to the most detrimental crack scenario by the finite

element method is not a straightforward exercise. In fact, in principle the depth and position of the most unfavourable (critical) crack may differ from the one determined by minimisation of $f_y(\chi, \upsilon, \zeta, \phi, \beta, c/\gamma H, \lambda)$ in Eq. (*3.5*). To find the critical crack, several analyses need to be run for the same slope, each analysis for a crack of a different prescribed depth and position. The crack associated to the mechanism giving rise to the minimum value of the yield seismic coefficient is the critical one. According to Figure 3.11d, the most unfavourable crack is slightly deeper but almost in the same location as the one determined by our analytical LA. Analogous results, not reported for sake of space, were obtained when the stability factor is sought rather than the yield seismic coefficient.

3.6   Extent of the slope zones unaffected by the presence of cracks

In (Utili, 2013), it is shown that the presence of cracks reduces the stability of a slope only if they are located in a region inside the slope, depicted in Figure 3.12a as extending between the horizontal coordinate x_1 and x_2. The effect of seismic acceleration on the extension of this zone is here investigated. The location of the crack needs to be prescribed by imposing the following constraint (Utili, 2013):

$$\exp[\tan\phi.\chi]\sin\chi = \frac{\begin{bmatrix} \exp[\tan\phi.\upsilon]\sin\upsilon + \\ \exp[\tan\phi.\upsilon]\cos\upsilon - \exp[\tan\phi.\zeta]\cos\zeta \end{bmatrix}}{x/H} \qquad (3.7)$$

into the minimisation of $f(\chi, \upsilon, \zeta, \phi, \beta, K_h, \lambda)$ in Eq. (*3.5*) (problem iii in 'Introduction'). Once the stability factors associated to failure mechanisms involving cracks of prescribed location, *x*, are found, *i.e.* the function *N(x)*, then the limits, x_1

and x_2, are determined as the values of x where $N(x) = N_{int}$ with N_{int} being the stability factor for the intact (un-cracked) slope. The obtained results are shown in Figure 3.12b, where the distance of the innermost limit of the 'unaffected' zone from the slope toe, x_2, is plotted for various levels of K_h. In the figure, slopes of various inclinations are considered for both cases of low and high ϕ (20° and 40° respectively). It can be observed that for a sufficiently high value of K_h, the curves relative to various slope inclinations (*e.g.* $\beta = 45°$; $\beta = 60°$; $\beta = 75°$) tend to intersect at a common point in all the cases analysed. This means that for a sufficiently high value of K_h, the extent of the zone where the presence of cracks affects slope stability is no longer a function of the slope inclination, but of ϕ and K_v solely. This result can be explained by looking at the geometry of the failure mechanisms taking place: for increasing K_h. The failing wedge involves an increasingly larger inward portion of slope especially along the horizontal direction, to the extent that both the area of the failing wedge (governing the amount of external work) and the length of the failure log-spiral (governing the amount of energy dissipated) become very little affected by the inclination of the slope face.

Moreover, the influence of K_v on the extent of the zone is important: comparing the curves for the case of no vertical acceleration ($\lambda = 0$) with the curves for the case of vertical acceleration present, $\lambda = \pm 1$ a marked difference between the trends can be observed. The direction of the vertical acceleration is also important: upward acceleration $\lambda = -1$ makes the zone where the presence of cracks affects slope stability larger (see the dotted lines in Figure 3.12b) whereas downward acceleration $\lambda = +1$ reduces the extent of the zone (see the dashed lines in Figure 3.12b). With

regard to ϕ, when friction is low (so cohesion tends to contribute more to the shear resistance against sliding) the zone where the presence of cracks affects slope stability is larger than when friction is high (so friction tends to contribute more to shear resistance against sliding).
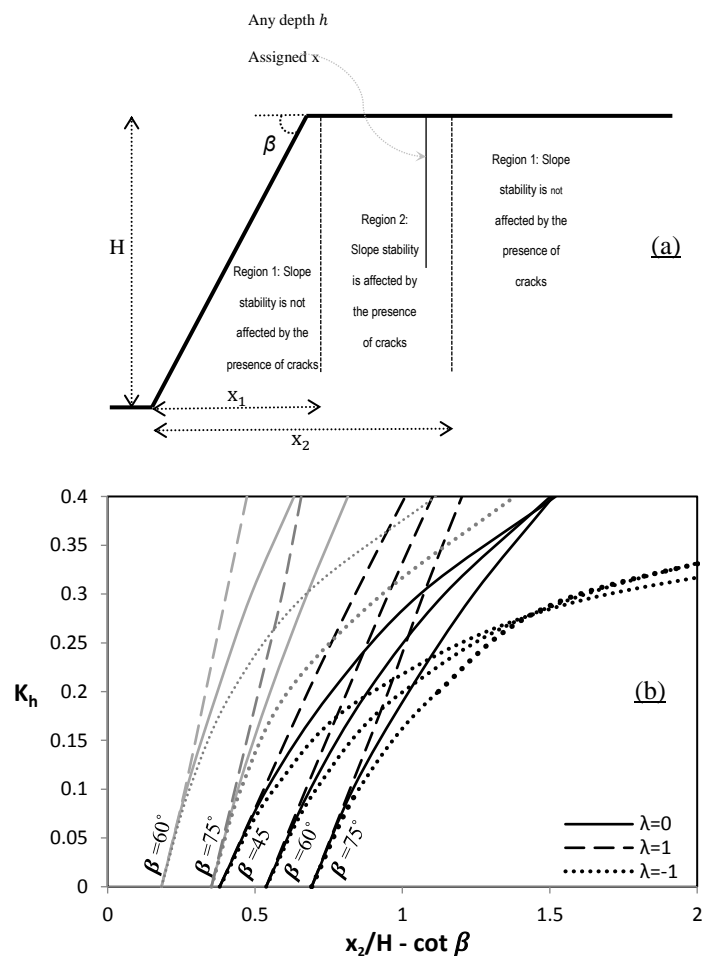
Figure 3.12 a) Illustration of the zones where cracks do and do not affect slope stability. b) The distance ($x_2 / H - \cot \beta$) is plotted against K_h for various values of λ and β. Black lines are for $\phi = 20^o$ and grey lines for $\phi = 40^o$.

3.7   Influence of cracks on earthquake induced displacements

The derivation of an analytical expression to calculate permanent seismic induced displacements for intact slopes, was carried out by (Chang et al., 1984) based on Newmark's method (Newmark, 1965). The presence of cracks makes the geometry of the failing wedge rotating away substantially different (see Figure 3.1) and, consequently, makes the analytical expression needed to calculate the induced displacements different too. Defining u_x, as the horizontal displacement of the slope toe, its rate can be calculated as (Chang et al., 1984):

$$\delta u_x = r_\upsilon \sin\upsilon\,\delta\theta = r_\upsilon \sin\upsilon \iint_{\delta t\ \delta t} \ddot{\theta} dt\ dt = C \iint_{\delta t\ \delta t} \left(K_i - K_y\right) g\ dt\ dt \tag{3.8}$$

with $\ddot{\theta}$ being the angular acceleration of the failing wedge and C a dimensionless coefficient relating the displacement of the slope toe to the integral of the recorded earthquake acceleration above $g.K_y$. K_i is the applied earthquake acceleration. The seismic induced displacements can be calculated from Eq. (*3.8*). Assuming the most unfavourable crack being present in the slope, the following expression for C is found (calculations given in Appendix C):

$$C = \frac{\gamma r_\chi^4 \left[\exp\left[\tan\phi(\upsilon-\chi)\right]\sin\upsilon\right] \left[\begin{array}{l}\lambda\left(f_{1v} - f_{2v} - f_{3v} - f_{4v} + f_{5v} + f_{6v}\right) + \\ \left(f_{1h} - f_{2h} - f_{3h} - f_{4h} + f_{5h} + f_{6h}\right)\end{array}\right]}{Gl^2} \tag{3.9}$$

According to Eq. (*3.9*), C depends on both the slope geometrical features and the ground strength parameters. *C* values are plotted in Figure 3.13 for various combinations of K_y, β and ϕ. It is convenient to plot *C* as a function of K_y, β and ϕ since K_y appears explicitly in the double integral in Eq. (*3.8*), *i.e.* out of the four

parameters $\gamma H / c$, β and ϕ, and K_y, only three are independent. In Figure 3.13, values of *C* calculated for intact slopes are reported as well for sake of comparison.

To assess the influence of the presence of cracks on seismic induced displacements an example is here considered. The records of two well-monitored earthquakes, the Northridge earthquake in 1994 (California, USA) and the Loma Prieta earthquake in 1989 (California, USA), whose features are provided in Table 3.1, are applied to a slope with $\phi=20°$, $c/\gamma H=0.1$, $\beta=55°$ and $\lambda=0$.

The horizontal displacement of the slope toe accumulating over time is plotted in Figure 3.14a whilst the final accumulated displacement is plotted against ϕ values in Figure 3.14b for both cases of intact slope and slope subjected to the most unfavourable (critical) crack. By comparing the two curves for the same given earthquake, it turns out that the presence of cracks increases the amount of displacement significantly: for instance, in the case of the Northridge earthquake, cracks make the total accumulated displacement 5 times larger than the displacement occurring if the slope is un-fissured. With regard to the influence of the angle of shearing resistance ϕ, it can be observed that the difference between displacements undergone in case of intact slope and in case of fissured slope is strongly affected by the value of ϕ with the difference decreasing for increasing ϕ and becoming negligible at high value of ϕ.
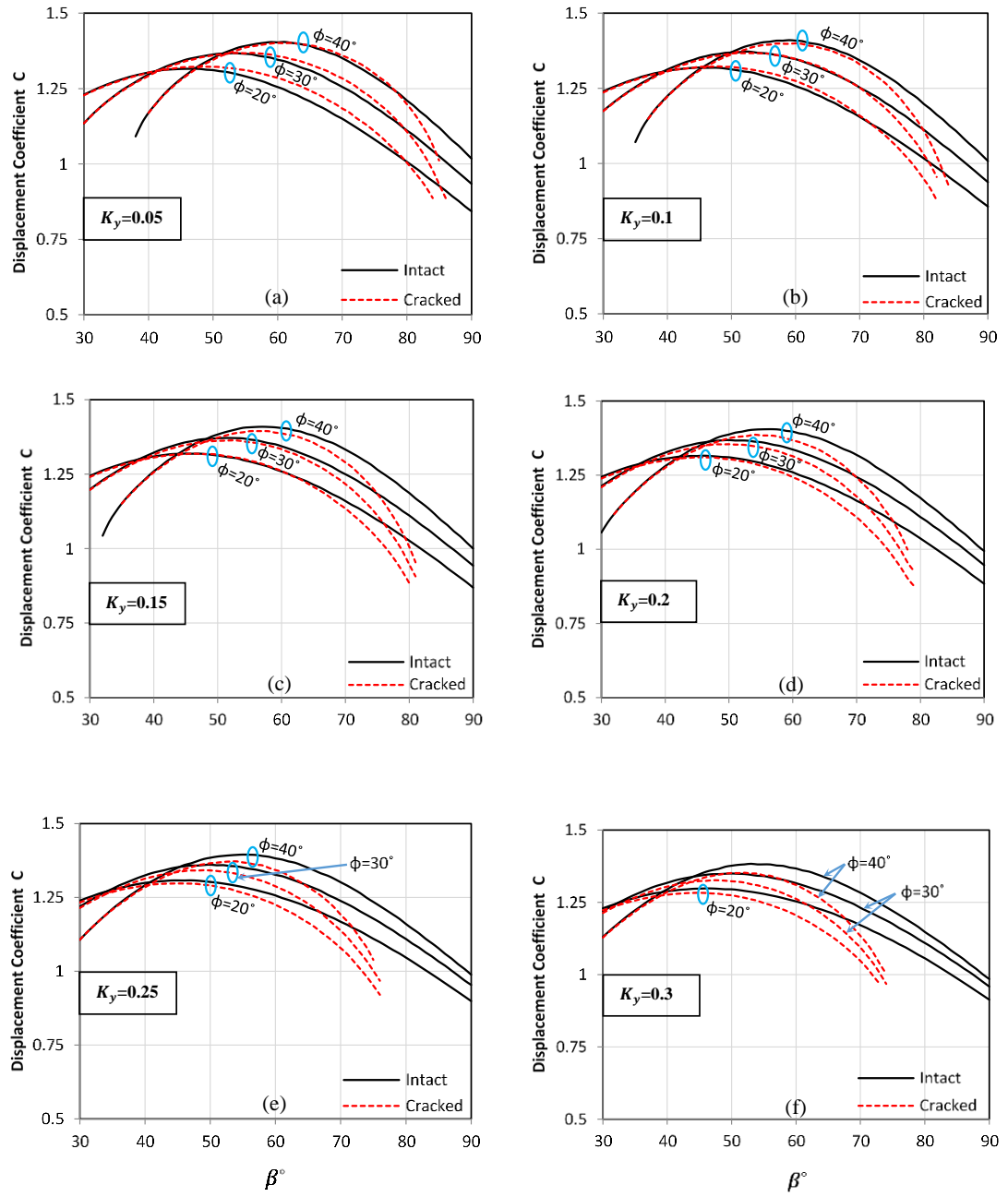
Figure 3.13 Seismic displacement coefficient versus slope inclination for intact slopes (solid lines) and for slopes subject to the most unfavourable crack (dashed lines) for various values of β, ϕ and K_y.
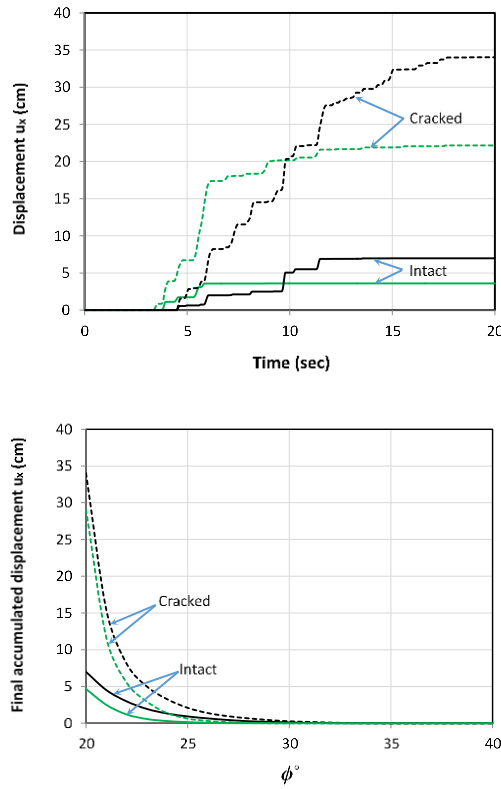
Figure 3.14 a) Horizontal displacement of the slope toe, u_x, versus time (ϕ =20º, β =55º, λ =0, and $c/\gamma H$ =0.1). b) Relationship between the final accumulated displacement u_x and the angle of shearing resistance (β =55º, λ =0, and $c/\gamma H$ =0.1). Black lines represent the displacements induced by the Northridge earthquake while green lines the displacements induced by the Loma Prieta earthquake. Solid lines refer to the case of intact slope whilst dashed lines to the case of slope subject to the most unfavourable crack.

Finally, the relationship between crack depth and final accumulated displacements was investigated by analysing an example case. Final accumulated displacements were calculated for various prescribed crack depths (*h*) assuming as input the accelerogram of the Northridge earthquake and for various level of vertical acceleration (Eq. (*3.5*), (*3.6*) and (*3.9*).

The final accumulated displacements are plotted in Figure 3.15 against h/H. From the figure a highly non-linear dependence of the displacements on crack depth is apparent implying that limiting the maximum crack depth (*e.g.* by using geosynthetics to increase the ground tensile strength) can have a substantial beneficial effect in

51

reducing displacements. Furthermore, Figure 3.15 is useful to investigate the influence of the vertical acceleration on accumulated displacements. In the case here considered, it turns out that the vertical acceleration has a significant influence with downward vertical acceleration being detrimental to slope stability and upward vertical acceleration being beneficial. However, according to the results reported in previous sections of this chapter, depending on the geometrical and mechanical features of the slope (*i.e.* the values of ϕ and β), the opposite may also be true.

Table 3.1 Main characteristics of the earthquakes considered in the example cases.

Earthquake	Northridge	Loma Prieta
Date	17/1/1994	9/2/1989
Station	24283 Moorpark - Fire Sta.	57476 Gilroy – Historic Bldg.
Magnitude	6.7	6.9
Direction	180º	180º
Peak accel. (g)	0.292	0.241
Epicentre distance (km)	23	28.1
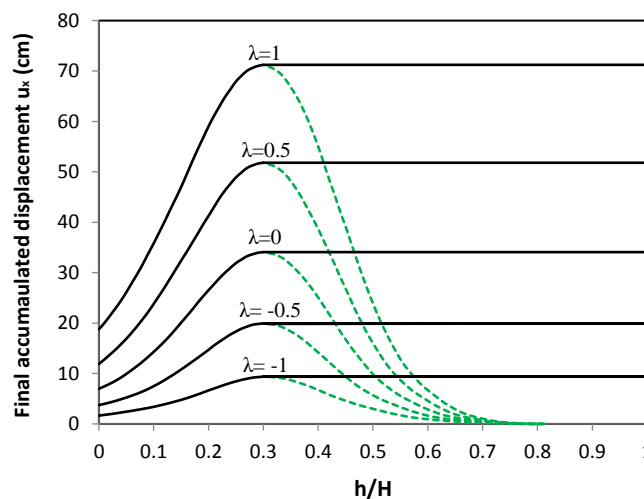
Figure 3.15 Horizontal final displacement at the slope toe versus normalised crack depth for a slope of given characteristic (ϕ =20º, β =55º and c / γH =0.1) subject to the Northridge earthquake for various values of λ .

3.8 Conclusions

A comprehensive parametric analysis was carried out to investigate the effect of seismic action on fissured slopes employing the upper bound limit analysis method together with the pseudo static approach. An analytical solution was derived assuming uniform c, ϕ slopes with vertical cracks of either known or unknown geometry. Charts providing the stability factor for fissured slopes subject to both horizontal and vertical accelerations and charts providing the slope yield acceleration for any combination of c, ϕ and slope face inclination were produced assuming the existence in the slope of the most unfavourable crack.

It was found that fissures may substantially reduce slope stability, *i.e.* lower both stability factor and yield acceleration up to 30% in comparison with the case of intact slope. The amount of reduction depends on both the geometrical characteristics of the slope and the ground strength parameters: the reduction is higher for steep slopes of low friction angle subject to high accelerations, whereas for gentle slopes of high ϕ subject to moderate earthquakes it is negligible. In addition, the effect of vertical seismic acceleration on slope stability was analysed for both cases of intact and fissured slopes. Maps showing which case is more critical for slope stability between no vertical acceleration, upward acceleration, and downward acceleration were provided for any combination of β, ϕ, and K_h.

Maps showing zones within the slope where cracks have no detrimental effect on its stability were provided for various combinations of horizontal and vertical acceleration. To produce the maps, the location of the cracks was prescribed in the search for the most critical failure mechanism. When the presence of one or more

cracks in a slope is known, the maps tell the geotechnical engineer whether the crack may be discarded from the stability analysis and may help inspection engineers to reduce significantly the extent of the zones in a slope or embankment to be inspected. Finally, Newmark's approach was employed to calculate seismic induced displacements. Horizontal yield accelerations were calculated for any combination of β, ϕ, and K_h of engineering interest, having assumed the most unfavourable crack for the stability of the slope to be present. Unlike Newmark's original formulation, rotational failure mechanisms, which are more critical than translational ones, were considered in the presented analysis. Seismic displacement coefficients were calculated as a function of the slope characteristics. Then, the relationship between crack depth and final accumulated displacements was investigated for an example slope subjected to the accelerograms of two past earthquakes. It emerges that the displacements induced for a fissured slope can be significantly larger, up to five times, than the case of intact slope depending on the slope characteristics.

Chapter 4: Geosynthetic-Reinforced Slopes in Cohesive Backfills[2]

SUMMARY

Currently, geosynthetics for reinforced slopes are calculated assuming the ground strength to be purely frictional, *i.e.* without any cohesion. However, accounting for the presence of even a modest amount of cohesion could allow the use of locally available cohesive soils as backfills to a greater extent and less overall reinforcement. But cohesive soils are subject to the formation of cracks that tend to reduce slope stability so their presence has to be accounted for in any slope stability assessment. Although many cracks may be present in a slope, the failure mechanism typically involves one crack only, which is the one that has the most adverse influence on the stability of the slope. In this chapter, limit analysis was employed to derive a semi-analytical method for uniform $c - \phi$ slopes that provides the amount of reinforcement needed as a function of cohesion, tensile strength, angle of shearing resistance and slope inclination. Design charts providing the value of the required reinforcement are plotted for both uniform and linearly increasing reinforcement distributions. From the results, it emerges that accounting for the presence of cohesion allows significant savings to

---

[2] This chapter has been published in *Geotextiles and Geomembranes*, (see Abd and Utili 2017a).

be made, and that cracks are often significantly detrimental to slope stability so they cannot be overlooked in the design calculations of the reinforcement.

4.1 Introduction

Since the 1980s, the use of geosynthetics with the aim of increasing the shear strength of cohesive soils has been investigated (Fourie & Fabian, 1987; T. S. Ingold, 1981; Terence S. Ingold & Miller, 1983; Hoe I. Ling & Tatsuoka, 1994). In the 1990's Zornberg and Mitchell in their review papers on cohesive backfills (Mitchell, 1995; J. G. Zornberg & Mitchell, 1994) state that the use of cohesive backfills has led to substantial savings in areas where granular materials are not locally available. More recently, substantial experimentation has been performed to investigate the behaviour of geotextile reinforced cohesive slopes (Hu et al., 2010; R. Noorzad & Mirmoradi, 2010; Wang et al., 2011). In particular non-woven geotextiles and geogrids of sufficient tensile strength have shown to be effective at increasing the strength of cohesive soils and providing effective drainage (*e.g.* (Reza Noorzad & Omidvar, 2010; Portelinha et al., 2013; Portelinha et al., 2014; Sukmak et al., 2015). However, in the methods currently available in the literature, reinforcements are still calculated assuming soils to be cohesionless (de Buhan et al., 1989; Richard A. Jewell, 1991; Dov Leshchinsky & Boedeker, 1989; D. Leshchinsky et al., 1995; Michalowski, 1997). This conservative assumption is due to the fact that geosynthetics were initially conceived for cohesionless granular soils and that the first design guidelines published for geosynthetic reinforced earth structures disregard the beneficial effect of cohesion (*e.g.* (AASHTO, 2012; R. A. Jewell, 1996)). However, the recent edition of AASHTO LRFD *bridge design specifications* (AASHTO, 2012), allows for the inclusion of

cohesion in the design of geo-reinforced slopes although unfortunately no formulae are provided for this purpose. The AASHTO revisit was prompted by the work of Anderson (Anderson et al., 2008) which, for example, shows that an amount of cohesion as small as 10 kPa can reduce the thrust against an earth structure of up to 50-75% for typical design conditions. In light of these findings, (Vahedifard et al., 2014) have investigated the beneficial effect of cohesion on geosynthetic reinforced earth structures based on limit equilibrium concluding that '*the results clearly demonstrate the significant impact of cohesion on the* K_{ae} *value*' (K_{ae} being the design seismic active earth pressure coefficient). Unlike (Vahedifard et al., 2014), this study is concerned with the stability of geo-reinforced slopes in the absence of any retaining structure. One of the objectives of this study is to provide a method for the design of slope reinforcements where the effect of cohesion is accounted for that may feed into future new guidelines.

In general, cohesive soils manifest limited, if not negligible, tensile strength so they are subject to the formation of cracks. The development of cracks in $c - \phi$ geo-reinforced slopes leading to slope instability has also been observed in post-earthquake deformations (*e.g.* (Hoe I. Ling, Leshchinsky, & Chou, 2001)) as well as in experiments in geotechnical centrifuge *e.g.* (Porbaha & Goodings, 1996). Moreover, (Rafael Baker, 1981; Michalowski, 2013; Utili, 2013) investigating unreinforced slopes conclude that when the presence of cracks is neglected, slope stability may be significantly overestimated. In this chapter, it will be shown that in order to safely design the geosynthetic-reinforcement of a slope accounting for the beneficial effect of cohesion. The possibility of the onset of a single crack forming as part of the slope

failure mechanism as well as the presence of multiple cracks generated over time by climate actions, *e.g.* cycles of drying − wetting (Dyer et al., 2009; Utili et al., 2015) and / or freezing − thawing (Hales & Roering, 2007), need to be accounted for.

In summary, this chapter will 1) provide an analytical approach to derive lower bounds to the required reinforcement for $c - \phi$ slopes; 2) quantitatively investigate the beneficial effect of cohesion on slope stability; 3) quantitatively investigate the influence of soil tensile strength and the presence of climate-induced cracks on the required level of reinforcement. In addition, the influence of water pore pressures will be investigated.

There are two main approaches to investigate the stability of geosynthetics-reinforced slopes: one where the local equations of equilibrium for an equivalent continuum formed by ground and reinforcement together are derived via homogenization techniques (*e.g.* (de Buhan et al., 1989; Sawicki, 1983)), called continuum approach by (Michalowski & Zhao, 1995). Another one, to be used here, where ground and geosynthetic-reinforcement are considered as two separate structural components, called structural approach (Michalowski & Zhao, 1995). Limit analysis (LA) can be used with both approaches. (Sawicki & Lesniewska, 1989; Sawicki & Leśniewska, 1991) employed the continuum approach together with the static (lower bound) method of LA to provide upper bounds on the required reinforcement for $c - \phi$ slopes using the slip line method. However, their solutions do not account for the presence of cracks, which may significantly reduce slope stability, so these bounds cannot be relied upon to design the reinforcement.

In this study the structural approach is employed together with the kinematic (upper bound) method of LA to obtain lower bounds on the required level of reinforcement extending the LA formulation of (Michalowski, 1997) for purely frictional slopes to cohesive frictional ($c - \phi$) geo-reinforced slopes. (Dov Leshchinsky & Reinschmidt, 1985) have already used the structural approach for $c - \phi$ slopes employing limit equilibrium, but for the case of a single reinforcement layer only and neglecting the presence of cracks.

Note that LA assumes a simplified constitutive behaviour for both ground and reinforcement, *i.e.* rigid – perfectly plastic, and the validity of the normality rule, *i.e.* associated plastic flow, which might not hold true for most soils. A comprehensive treatment of limit analysis assumptions and limitations and their implications for slope stability can be found in (Chen, 1975).

4.2   Formulation of the Problem

Geosynthetic-reinforced slopes are subject to three main possible failure modes: reinforcement rupture, pull out failure, and direct sliding. In this study, a rupture failure will be assumed in order to design the minimum amount of geosynthetic-reinforcement whereas a combined failure (rupture and pullout) will be assumed in order to calculate the required length of reinforcement.

Traction-free uniform $c - \phi$ slopes with an inclination angle β, ranging from 40° to 90° and reinforced with geosynthetics layers are here considered. A common choice for the distribution of reinforcement with depth is to employ reinforcement layers of equal strength laid at equal spacing or at a spacing decreasing linearly with depth. The

former case gives rise to a uniform distribution (UD) of tensile strength over depth (see Figure 4.1a) which can be determined as:

$$K_t = \frac{nT}{H} \tag{4.1}$$

with K_t being the average strength of reinforcement in the slope, n the number of reinforcement layers, T the strength of a single layer at yielding point and H the slope height. Note that the influence of the overburden stress on the strength of the geosynthetics has been neglected for sake of simplicity (Michalowski, 1997). The second case instead, gives rise to a linearly increasing distribution (LID) of strength over depth (see Figure 4.1b):

$$K = 2K_t \frac{(H - y)}{H} \tag{4.2}$$

with K representing the local reinforcement strength in the slope, and y the vertical upward coordinate departing from the slope toe (see Figure 4.2a). Note that there is plenty of evidence from field observations and experimental tests showing that the load distribution in the reinforcements for slopes under working stress conditions is non-linear (Allen & Bathurst, 2015; Viswanadham & Mahajan, 2007; K. H. Yang, Zornberg, Liu, & Lin, 2012; Jorge G. Zornberg & Arriaga, 2003) so neither a UD nor a LID. However, the assumption of UD or LID is consistent with the LA assumption of the geosynthetic-reinforced slope being at impending failure and of rigid – perfectly plastic behaviour for the materials of the system (ground and reinforcement) which possess infinite ductility. These two assumptions imply that the distribution of forces in the reinforcement must coincide with the distribution of reinforcement strength (Michalowski, 1997).
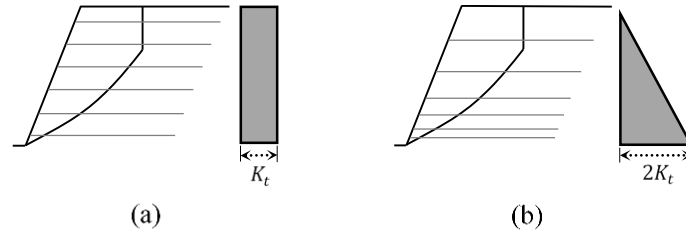
Figure 4.1 Geosynthetic-reinforcement layouts: (a) Uniform distribution, and (b) Linearly increasing distribution with depth.

Experimental tests in the centrifuge provide clear evidence that geosynthetic-reinforced slopes fail because of a rotational mechanism (Viswanadham & Mahajan, 2007; K. H. Yang et al., 2012; Jorge G. Zornberg, Sitar, & Mitchell, 1998) which is the mechanism here assumed: the block E-B-C-D rotating around point P whose location is yet to be determined (see Figure 4.2a). In this mechanism, all deformations occur along the log-spiral D-C whose mathematical expression is:

$$r = r_\chi \exp\left[\tan \phi \left(\theta - \chi \right) \right] \tag{4.3}$$

where θ and χ are the angles made by r and r_χ respectively with the horizontal axis, r is the distance between the spiral centre, point P, and a generic point on the log-spiral slip surface, and r_χ is the length of the chord P-F. The deformations undergone by the reinforcement layers along the log-spiral slip surface and along crack B-C are illustrated in Figure 4.2(b) and Figure 4.2(c) respectively. The analysis here performed is a two dimensional analysis, *i.e.* plane strain conditions are assumed. Recently (F. Zhang, Leshchinsky, Gao, & Leshchinsky, 2014) and (Gao, Yang, Zhang, & Leshchinsky, 2016) considered three dimensional failure mechanisms for reinforced slopes, the former employing limit equilibrium while the latter LA. Their analyses confirm that the most critical mechanisms are found for plane strain conditions.

Although from a physical viewpoint, the formation of cracks in cohesive slopes is due to the same ultimate mechanical cause, *i.e.* the presence of tensile stresses exceeding the ground tensile strength, here cracks will be grouped into two types according to the way they are dealt with by limit analysis. First type, climate induced multiple cracks existing in the slope prior to the formation of any failure mechanism, here termed 'pre-existing' cracks, and second type; cracks forming as part of a slope failure mechanism, here termed 'forming' cracks. A formation crack forms as part of a failure mechanism which is made of a log-spiral surface (D-C in Figure 4.2a) where soil fails in shear and of a crack (B-C in Figure 4.2a) where soil fails in tension.

Climate induced cracks need to be considered for reinforced slopes in regions subject to high annual temperature fluctuations, *e.g.* regions subject to a continental climate with rigid cold winters and arid summers as in central Asia and North America, whereas in regions with a temperate climate cracks are much less likely to occur. So in regions subject to high temperature fluctuations, the presence of climate induced cracks cannot be overlooked since these cracks can make the slope significantly less stable (Michalowski, 2013; Utili, 2013) while in regions with a temperate climate, the geo reinforced slope may be assumed to be intact. In both cases, the possibility of cracks forming as part of the failure mechanism will be accounted for.

(a)

(b)

(c)

Figure 4.2 (a) Rigid rotational failure mechanism in a reinforced slope with a crack (B-C). The mass of soil enclosed by (E-B-C-D) rotates clockwise around point P. (b) Rupture of the reinforcement layer across the slip surface (after (Zhao, 1996)). (c) Rupture of the layer across the vertical crack.
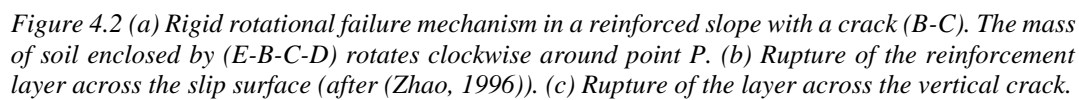
4.3 Derivation of the semi-analytical solution

According to the kinematic theorem of LA, the highest (best) lower bound to the required reinforcement can be derived from the following energy balance equation:

$$\dot{D} = \dot{W} \tag{4.4}$$

where $\dot{D}$ and $\dot{W}$ are the internal energy dissipation rate and the external work rate respectively. $\dot{D}$ is here calculated as follows:

$$\dot{D} = \dot{D}s_{(B-C)} + \dot{D}r_{(B-C)} + \dot{D}s_{(C-D)} + \dot{D}r_{(C-D)} \tag{4.5}$$

with $\dot{D}s_{(B-C)}$ and $\dot{D}r_{(B-C)}$ being the energy rates dissipated along B-C by ground and reinforcement respectively and $\dot{D}s_{(C-D)}$ and $\dot{D}r_{(C-D)}$ the energy rates dissipated along the log-spiral C-D (see Figure 4.2a) by ground and reinforcement respectively.

With regard to $\dot{D}s_{(B-C)}$, if the crack B-C is a pre-existing crack, no energy is dissipated by the ground since the crack is already formed hence $\dot{D}s_{(B-C)} = 0$; conversely if the crack B-C forms as part of the failure mechanism, energy is dissipated for the crack to form hence $\dot{D}s_{(B-C)} \neq 0$ with the value of $\dot{D}s_{(B-C)}$ to be calculated as a function of the ground tensile strength (Michalowski, 2013). Usually when limit analysis is employed, the Mohr-Coulomb (M-C) function is adopted as failure criterion. But experimental evidence shows that the tensile f_t strength associated with the Mohr-Coulomb (M-C) criterion $f_t = c / \tan \phi$ is a significant overestimation of the tensile strength (Bishop et al., 1965), here called σ_t, of most soils. To partially remedy this shortcoming but still use the simple linear M-C criterion, a tensile cut off is commonly

adopted. (Michalowski, 2013) instead proposed to modify the M-C criterion by adopting a non-linear function in the stress range where cracks are expected to form (see Figure 4.3). This non-linear function is made by a stress circle defined as being tangent to the M-C linear function $\tau = c + \sigma \tan \phi$, and having the minor principal stress σ_3 equal to the soil tensile strength, $\sigma_3 = -\sigma_t$, with tensile stresses assumed negative according to the soil mechanics sign convention. The adopted failure criterion, indicated by the solid curve in Figure 4.4, lends itself to simple LA calculations (see (Michalowski, 2013)) and on the other hand, accounts for the non-linearity of soil shear strength in the stress range where cracks are expected to form. The energy expended for the formation of a crack $\dot{D}s_{(B\text{-}C)}$ turns out to be (Michalowski, 2013):

$$\dot{D}s_{(B-C)} = \dot{\theta} r_\chi^2 \left(\frac{\sin \chi}{\tan \mu} \right)^2 \left(\frac{\sigma_c^{M-C}}{2} \int_\mu^\zeta \frac{1-\sin\theta}{\cos^3\theta} d\theta + \frac{\sigma_t}{1-\sin\phi} \int_\mu^\zeta \frac{\sin\theta - \sin\phi}{\cos^3\theta} d\theta \right) \qquad (4.6)$$

With μ being the angle made by the segment P-B with the horizontal (see Figure 4.2a), σ_c^{M-C} being the uniaxial compressive strength consistent with the M-C criterion (see Figure 4.3). The two surfaces of the formed crack B-C are considered no-tension non-cohesive perfectly smooth (no friction) surfaces, therefore the angle η between the velocity vector of the mass of soil sliding away and the crack surface is $0° < \eta < 180°$ (see B-C in Figure 4.2a).
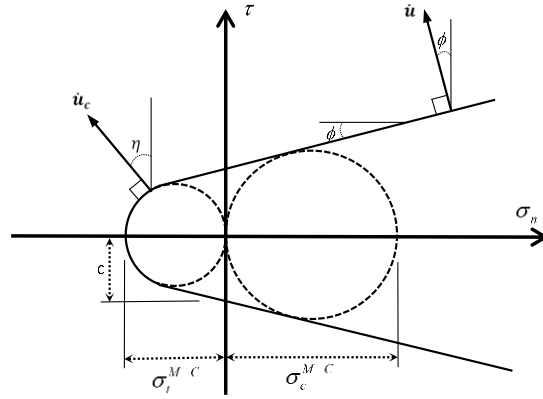
(a)
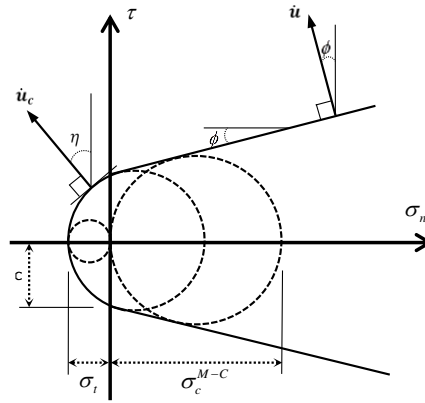
(b)
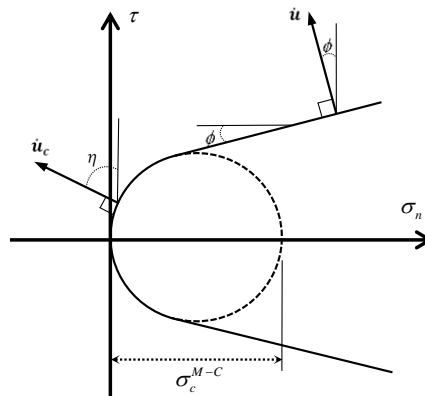
(c)

Figure 4.3 Modified Mohr-Coulomb failure envelope for: (a) soil with t=1; (b) soil with $0 \geq t \geq 1$; (c) soil with t=0 (i.e. tension cut-off), based on (Michalowski, 2013)

66
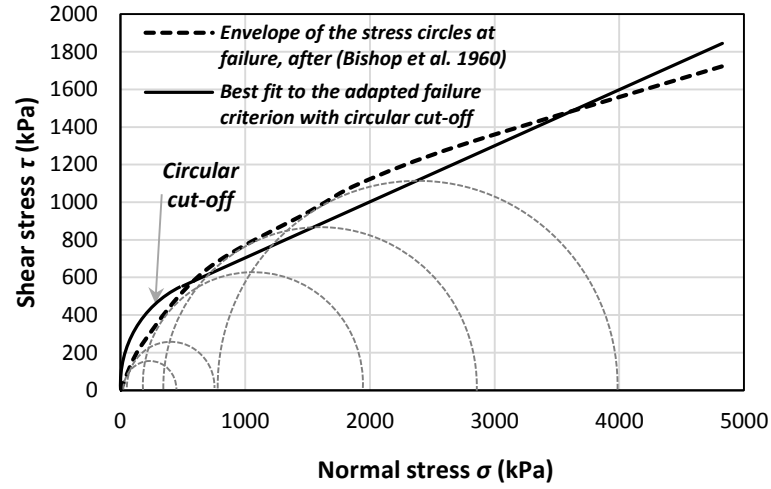
Figure 4.4 shear strength of London clay inferred from drained compressive triaxial tests: non-linear envelope (dashed curve) to the stress circles at failure (after (Bishop et al., 1965)); linear $c - \phi$ best fit with tension cut-off (solid curve).

It is convenient to introduce a dimensionless coefficient, *t*, defined as the ratio of the ground tensile strength, σ_t to be measured experimentally, f_t over the maximum unconfined tensile strength consistent with the M-C criterion, σ_t^{M-C} (see Figure 4.3):

$$t = \frac{\sigma_t}{\sigma_t^{M-C}} \tag{4.7}$$

It is straightforward to observe that $0 \leq t \leq 1$. Both σ_c^{M-C} and σ_t^{M-C} are uniquely related to *c* and ϕ :

$$\sigma_c^{M-C} = 2c\left(\frac{\cos\phi}{1-\sin\phi}\right) \tag{4.8}$$

$$\sigma_t^{M-C} = 2c\left(\frac{\cos\phi}{1+\sin\phi}\right) \tag{4.9}$$

The amount of cohesion and tensile strength that can be relied upon in the design of slopes made of soils depends on several factors that vary over time. To name a few:

the ground water content, the level of the phreatic line and presence of suction, the design lifespan for the reinforced slope since this has implications on the number of wetting–drying cycles and therefore the deterioration that the soil strength is likely to experience over time, etc. Moreover, lime or cement is often added to soils to provide a reliable amount of true cohesion. Several publications have been dedicated to choice of the shear strength parameters of clayey soils in the mechanics literature with the use of peak strength, residual strength, operational strength (D. M. Potts, Kovacevic, & Vaughan, 2009) and critical state strength advocated depending on the different geotechnical problem tackled. The choice of the strength parameters is outside the scope of this chapter. Here it is enough to recall that the designer must design the slope reinforcement considering the worst-case scenario for the slope in terms of soil strength and of hydraulic conditions that can occur over the entire lifetime of the slope and adopting caution.

It is key to note that even in case of soils possessing no true cohesion, *i.e.* exhibiting zero shear strength at zero confinement, their shear strength can still be suitably described by the failure criterion here adopted with $t = 0$ and $c \neq 0$ (see Figure 4.4). In this case, c is to be interpreted as an apparent cohesion with the strength envelope intercepting the τ axis at the origin. From a mathematical point of view, the presence of this apparent cohesion means that the straight part of the failure criterion is above the $\tau = \tan \phi$ line and therefore reinforcement can be saved. The lack of true cohesion (and of any tensile strength) for these soils will be reflected in the solution (and in the results obtained) by the onset of deep cracks.

Now substituting equations (*4.7*), (*4.8*), and (*4.9*) into Eq. (*4.6*), the following expression is obtained for the energy dissipated in the ground due to the formation of a crack:

$$\dot{D}s_{(B-C)} = c\dot{\theta}r_\chi^2 \left(\frac{\sin\chi}{\tan\mu}\right)^2 \left(\frac{\cos\phi}{1-\sin\phi}\int_\mu^\zeta \frac{1-\sin\theta}{\cos^3\theta}d\theta + \frac{2t\cos\phi}{1-\sin^2\phi}\int_\mu^\zeta \frac{\sin\theta-\sin\phi}{\cos^3\theta}d\theta\right)$$

$$= c\dot{\theta}r_\chi^2 g_1(\chi,\upsilon,\zeta,\phi,t)$$

(4.10)

The energy dissipated by the reinforcement along the crack is unaffected by the type of crack, 'pre-existing' or 'formation', and can be written here as:

$$\dot{D}r_{(B-C)} = \int_{B-C} K\dot{u}_c \sin\eta\, dh$$

(4.11)

where $\dot{u}_c$ represents the velocity vector along B-C (see Figure 4.2a) and *dh* an infinitesimal length of the crack. They can be expressed as:

$$\dot{u}_c = r_c\dot{\theta} = \left(\frac{r_\zeta\cos\zeta}{\cos\theta}\right)\dot{\theta}$$

(4.12)

$$dh = \frac{r_c\, d\theta}{\cos\theta}$$

(4.13)

with r_c being the distance between point P and a generic point along the crack. Substituting equations (*4.12*), and (*4.13*) into Eq. (*4.11*) and after integration, the following expression is obtained:

$$\dot{D}r_{(B-C)} = \frac{1}{2}K_t\dot{\theta}r_\chi^2 \left[\exp\left[2\tan\phi(\zeta-\chi)\right]\sin^2\zeta - \sin^2\chi\right]$$

$$= K_t\dot{\theta}r_\chi^2 g_2(\chi,\upsilon,\zeta,\phi)$$

(4.14)

The expression for the energy dissipated in the ground along the log-spiral part of the failure mechanism (log-spiral C-D in Figure 4.2a), $\dot{Ds}_{(C-D)}$, is provided by (Chen, 1975):

$$
\begin{aligned}
\dot{Ds}_{(C-D)} &= c\,\dot{\theta}r_\chi^2 \exp\left[2\tan\phi(\zeta-\chi)\right]\frac{\exp\left[2\tan\phi(\upsilon-\chi)\right]}{2\tan\phi} \\
&= c\,\dot{\theta}r_\chi^2 g_3(\chi,\upsilon,\zeta,\phi)
\end{aligned}
\tag{4.15}
$$

where $\dot{\theta}$ is the angular velocity of the sliding wedge, υ and ζ are the angles made by r_υ and r_ζ with the horizontal line respectively.

The energy dissipated by the reinforcement along the log-spiral part of the failure mechanism, $\dot{Dr}_{(C-D)}$, is calculated by integrating the product of the infinitesimal increment of reinforcement strain rate with the reinforcement tensile strength, T, averaged over the slope height. The infinitesimal increment is (Zhao, 1996):

$$
d\dot{D}_{r(C-D)} = \int_0^{w/\sin\eta} K\sin\xi\,\dot{\varepsilon}_x\,dx = K\sin\xi\,\dot{u}\cos(\xi-\phi)
\tag{4.16}
$$

with w being the width of the discontinuity band (see Figure 4.2b), ξ the angle made by the reinforcement layer with the discontinuity surface, $\dot{\varepsilon}_x$ the strain rate in the longitudinal direction of the reinforcement layer, and $\dot{u}$ the velocity vector of the sliding ground. For sake of space, calculations are here reported only for the case of UD of reinforcement (*i.e.* $K = K_t$), while calculations for LID reinforcements are reported in Appendix D. The energy dissipated by the reinforcement over the log-spiral part (C-D) is (Zhao, 1996):

$$\dot{Dr}_{(C-D)} = \int_{C-D} d\dot{Dr} = \int_{C-D} K_t \sin \xi \, \dot{u} \cos(\xi - \phi) \frac{r \, d\theta}{\cos \phi} \tag{4.17}$$

After integration, the following expression is obtained:

$$\dot{Dr}_{(C-D)} = \frac{1}{2} K_t \dot{\theta} r_\chi^2 \left(\exp\left[2 \tan \phi (\upsilon - \chi)\right] \sin^2 \upsilon - \exp\left[2 \tan \phi (\zeta - \chi)\right] \sin^2 \zeta \right)$$

$$= K_t \dot{\theta} r_\chi^2 g_4 (\chi, \upsilon, \zeta, \phi) \tag{4.18}$$

Note that the reinforcement layers lying above the centre of rotation P, are subject to compressive stresses and therefore buckling, hence they are discarded in the calculation of $\dot{Dr}$ (Michalowski, 1997).

From Eq. (*4.14*) and Eq. (*4.18*) it emerges that the energy dissipated by the reinforcement along the spiral part F-C for the case of intact (un-fissured) slope is the same as the energy dissipated by the reinforcement along the crack (B-C), *i.e.* $\dot{Dr}_{(F-C)} = \dot{Dr}_{(B-C)}$. This means that the energy dissipated by the reinforcement is not affected by the presence, or absence, of cracks.

External work ($\dot{W}$) is done by the weight of the sliding wedge E-D-C-B ($\dot{W}_s$) and any pore water pressure in the ground ($\dot{W}_w$): $\dot{W} = \dot{W}_s + \dot{W}_w$. The term $\dot{W}_s$ is here calculated as the work of block E-D-F minus the work of block B-C-F (Figure 4.2a). The work of block E-D-F and of block B-C-F are calculated by the algebraic summation of the work of blocks P-D-F, P-E-F and P-D-E (Chen, 1975) and of blocks P-C-F, P-B-F and P-C-B (Utili, 2013; Utili & Nova, 2007) respectively. So

$$\dot{W} = \dot{W}_1 - \dot{W}_2 - \dot{W}_3 - \left(\dot{W}_4 - \dot{W}_5 - \dot{W}_6\right) + \dot{W}_w$$

$$= \gamma \dot{\theta} r_x^3 \left(f_1 - f_2 - f_3 - f_4 + f_5 + f_6 + f_w\right)$$

(4.19)

The analytical expressions for f_1, f_2, f_3, f_4, f_5, and f_6 are given in Appendix B while for f_w see Appendix E. Note that here only static forces are considered for sake of simplicity. However, in case of seismic excitation, the formulation here presented can be straightforwardly extended to include seismic loads by adding the contribution of the seismic pseudo-static forces to the external work as shown in (Utili & Abd, 2016).

Substitution of the various energy rate contributions calculated into the energy balance equation (Eq. (*4.4*)), provides the objective function to be optimised to determine the required geosynthetic-reinforcement. Substituting Eq. (*4.5*) and Eq. (*4.9*) with their components into Eq. (*4.4*) and rearranging, K_t is determined as:

$$\frac{K_t}{\gamma H} = \frac{\left(f_1 - f_2 - f_3 - f_4 + f_5 + f_6 + f_w\right)}{\dfrac{H}{r_\chi}\left(g_2 + g_4\right)} - \frac{c}{\gamma H}\left(\frac{g_1 + g_3}{g_2 + g_4}\right)$$

$$= f\left(\chi, \upsilon, \zeta, \beta, \gamma_w / \gamma, \phi, c / \gamma H, t\right)$$

(4.20)

Eq. (*4.20*) provides an expression of general validity covering both types of cracks: pre-existing and forming cracks. In the following, first the case of geo-reinforced intact slope is treated followed by the case of slopes exhibiting cracks.

4.3.1   Intact slopes

The unconstrained maximisation of $f_{deep\ pre-existing}$ over the three geometrical variables χ, υ, ζ provides the least (best) lower bound on the required level of reinforcement,

$K_t / \gamma H$. The failure mechanism is identified by the values of χ, υ, ζ associated with the found least lower bound. Length and location of the crack, which forms as part of the failure mechanism, are found as a result of the maximisation. In Figure 4.5, the level of reinforcement required is plotted for various slope features. The results are commented in section4.4.

4.3.2   Slopes manifesting (pre-existing) cracks

As observed earlier on, several cracks may develop over time in a geosynthetic-reinforced slope due to climate actions. Among these cracks, the failure mechanism will always engage the one crack that has the most adverse effect on stability. There may also be the situation of the failure mechanism not engaging any existing crack. This can happen depending on the location and depth of the cracks. (Utili, 2013) analysing unreinforced slopes shows that only cracks in a (central) zone of the slope will be engaged by the slope failure mechanism. The worst-case scenario for the stability of the slope is found by setting $\dot{D}s_{(B-C)} = 0$ in Eq. (*4.20*), to reflect the fact that no energy is dissipated by crack formation:

$$
\frac{K_t}{\gamma H} = \frac{\left(f_1 - f_2 - f_3 - f_4 + f_5 + f_6 + f_w\right)}{\dfrac{H}{r_\chi}\left(g_2 + g_4\right)} - \frac{c}{\gamma H}\left(\frac{g_3}{g_2 + g_4}\right)
$$
$$
= f_{deep\ pre-existing}\left(\chi, \upsilon, \zeta, \beta, \gamma_w / \gamma, \phi, c / \gamma H\right)
$$

(4.21)

and minimising $f_{deep\ pre-existing}\left(\chi, \upsilon, \zeta, \beta, \gamma_w / \gamma, \phi, c / \gamma H\right)$ over the three angles χ, υ, ζ.

$f_{deep\ pre-existing}\left(\chi, \upsilon, \zeta, \beta, \gamma_w / \gamma, \phi, c / \gamma H\right)$ is   a   particular   case   of

$f\left(\chi, \upsilon, \zeta, \beta, \gamma_w / \gamma, \phi, c / \gamma H, t\right)$ in Eq. (*4.20*), and is independent of the ground tensile

strength. The values of χ, υ, ζ provide the geometry of the most adverse failure

mechanism for the slope with the angle ζ identifying the crack most adverse for the

stability of the slope. Among all the possible climate induced cracks, it is very unlikely

that the most adverse crack will be present, so in general the slope will need less

amount of reinforcement than the amount predicted by the maximisation of

$f_{deep\ pre-existing}\left(\chi, \upsilon, \zeta, \beta, \gamma_w / \gamma, \phi, c / \gamma H\right)$. However, assuming the existence of the most

adverse crack in the slope implies that the worst-case scenario in terms of climate-

induced cracks is assumed which can be a desirable choice for the designer of the

reinforcement especially when no long term monitoring of the reinforced slope is

planned. If the slope designer wishes to make a less conservative and more realistic

assumption on the climate induced cracks, an equality constraint prescribing either

depth or location of the cracks or both can be added into the search of the least lower

bound in Eq. (*4.21*). This type of constraints will also be used to prescribe values of

pre-existing crack depths in the section 'Pre-existing cracks deepened by the failure

process' to investigate the stability of slopes subject to 'shallow' pre-existing cracks.

In that section, it will also become clear why the function in Eq. (*4.21*) has been named

$f_{deep\ pre-existing}$.

4.3.3   Maximum depth of cracks

The maximum depth for a crack, which is part of a failure mechanism, has to be limited

due to the requirement that the new slope profile left after failure has occurred has to

be stable (the new vertical slope on the right of B-C in Figure 4.2). In theory cracks

deeper than this maximum depth may form, but if they become part of a slope failure

mechanism, the mechanism will engage them above their bottom tip so that the engaged crack depth will be less than or equal to the maximum depth. Lower and upper bounds obtained by LA to the maximum crack depth, h_{max}, were first proposed by (E. Spencer, 1967; Terzaghi, 1943) and (Michalowski, 2013; Eric Spencer, 1968) respectively. Here, to stay on the side of caution, an upper bound rather than a lower bound was prescribed. This in case of a dry crack takes the following expression h_{max} (Michalowski, 2013):

$$h_{max} = \frac{3.83c}{\gamma} \tan\left(\frac{\pi}{4} + \frac{\phi}{2}\right)$$

(4.22)
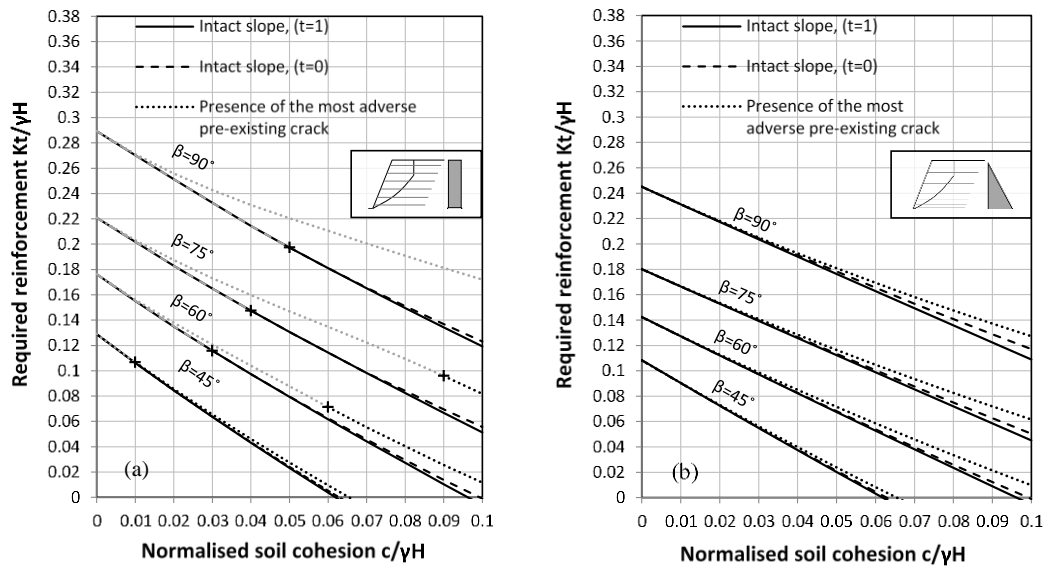
*Figure 4.5 Normalized required reinforcement versus normalised soil cohesion for a slope with $\phi = 20°$: (a) uniform distribution of reinforcement, (b) linearly increasing distribution. Grey lines indicate that the constraint of maximum crack depth is active, while black lines indicate the constraint is inactive. The mark + indicates the boundary between the two.*

4.3.4 Mechanisms passing above the slope toe

Failure mechanisms may in principle daylight on the slope face above the slope toe (Utili, 2013). So potential mechanisms passing above the toe were considered in our analysis for both types of reinforcement distribution by discretising the slope face in several points and calculating the stability factor associated to each potential mechanism. In all the cases considered no potential mechanism passing above the slope toe turned out to be a critical failure mechanism.

4.4 The minimum required reinforcement

The lower bounds on the required reinforcement expressed in dimensionless form, $K_t / \gamma H$, obtained by the maximisation of $f\left(\chi, \upsilon, \zeta, \phi, \beta, c / \gamma H, t, \gamma_w / \gamma\right)$ and of $f_{deep\ pre-existing}\left(\chi, \upsilon, \zeta, \phi, \beta, c / \gamma H, \gamma_w / \gamma\right)$ subject to the physical constraint of the crack depth not exceeding the maximum crack depth, are plotted in Figure 4.5 against an assigned level of soil cohesion for the case of intact slopes and of slopes manifesting pre-existing cracks respectively. The charts obtained for $\phi = 20°$ cover the whole spectrum of cohesive geomaterials ranging from *c*=0, for cohesion-less materials (*e.g.* a granular fill), to values of cohesion so high that no reinforcement is needed (where the lines intersect the horizontal axis). Note that at $c = 0$ all the three lines depart from the same point since in case of zero cohesion, no cracks can form and the obtained $K_t / \gamma H$ values coincide with the values already published in the literature for purely frictional fills as it can be expected (*e.g.* (Michalowski, 1997)). Grey lines indicate that the constraint on the maximum crack depth was active, whereas black lines indicate that the constraint was inactive.

From the charts emerges that the three lines tend to diverge for increasing cohesion. This trend can be explained by considering the term for the energy dissipated by the ground along the crack, $\dot{D}s_{(B-C)}$: the higher the value of cohesion, the higher is the influence of $\dot{D}s_{(B-C)}$ in the energy balance equation (see Eq.(*4.20*)) so the larger is the difference between the case of slopes subject to the most adverse pre-existing crack ($\dot{D}s_{(B-C)} = 0$) and of intact slopes subject to crack formation ($\dot{D}s_{(B-C)} \neq 0$). In the latter case, higher values of cohesion also imply a larger influence of the ground tensile strength on slope stability (see the lines for $t=1$ and $t=0$ in Figure 4.5) due to the

term $\dot{\theta}r_\chi^2 \left(\dfrac{\sin\chi}{\tan\mu} \right)^2 \dfrac{2t\cos\phi}{1-\sin^2\phi} \displaystyle\int_\mu^\zeta \dfrac{\sin\theta - \sin\phi}{\cos^3\theta} d\theta$ in the analytical expression of $\dot{D}s_{(B-C)}$

(see Eq. (*4.10*)). Slopes subject to the most adverse pre-existing crack require significant more reinforcement (because they are less stable) than intact slopes especially in case of steep slopes with a UD of reinforcement and low ϕ. Also note that whatever the crack scenario is, LID reinforcements are more effective (*i.e.* lower required overall reinforcement) than UDs of reinforcement because more reinforcement layers are concentrated in the lower part of the slope.

4.4.1 Numerical validation

The validation exercise undertaken entailed finite element displacement-based analyses with strength reduction technique (FESR), where the validity of the normality rule $\left(\phi = \psi\right)$ consistently with the theory of limit analysis was assumed and Finite Element Limit Analyses (FELA) of slopes of various inclinations reinforced with UD of reinforcement and subject to the presence of the most adverse pre-existing crack.

All the simulations in this validation were performed using the software package Opt+umCE (OptumG2, 2014). The location and depth of the most critical pre-existing cracks found by maximisation of Eq. (*4.20*) for various values of $c/\gamma H$ were given as input into both the FESR and FELA simulations. The pre-existing cracks were mimicked by joints of negligible strength, *i.e.* as no-tension non-cohesive perfectly smooth interfaces, consistent with LA assumptions. The geosynthetics were modelled using truss element with interface reduction factor equals to unity. The length of the reinforcement layers where chosen to be equal to slope height to avoid pull-out failure. Any mesh dependency of the obtained results was investigated by running the same simulation for different mesh sizes. The results reported here are from simulations performed with a sufficiently large number of elements, 8000 (see Figure 4.6a), so that mesh dependency is negligible. The dimensions of the boundaries were chosen such that they do not affect the calculations and normal fixities were applied for these boundaries. Triangular element of three stress node and one displacement node is used for the finite element lower bound analysis , triangular element with 3 stress node and 3 displacement node is used for the finite element upper bound analysis while 15-displacement node triangular Gauss element type is used for the finite element displacement based analysis.

The obtained values of $K_t/\gamma H$ are plotted in Figure 4.6b against $c/\gamma H$. It can be noted that the semi-analytical LA lower bounds found by maximisation of Eq. (*4.20*) are slightly better than the FELA upper bounds. This finding is consistent with previous literature (Loukidis et al., 2003; Utili & Abd, 2016) showing that the analytical upper bound found assuming a rigid rotational mechanism is lower (better)

than the FELA upper bound. Also the difference between the analytical upper bound and the FELA lower bounds is lower than 14% for any value of cohesion considered. Therefore, true collapse values can be determined by considering the average of the two bounds with an accuracy of $\pm$ 7%. Finally, the values of $K_t / \gamma H$ determined by FESR simulations are very close to the semi-analytical lower bounds. Therefore, the results of the validation exercise performed provide confidence to adopt the upper bounds determined by the semi-analytical method here presented as a design tool.

4.4.2   Charts for dry slopes

In Figure 4.7, four design charts have been produced where $K_t / \gamma H$ is plotted against slope inclinations ranging from 40° to 90° for various combinations of the shearing resistance angle, cohesion and tensile strength of engineering interest as well as the case of the most adverse pre-existing crack being present. Considering the case of intact slopes, it can be observed that for relatively low values of cohesion, $c / \gamma H = 0.05$, the tensile strength, t, possesses a negligible effect on the required reinforcement level. But for higher levels of cohesion ($c / \gamma H = 0.1$), the tensile strength becomes important: for instance for t=0, 0.2, and 0.5 an extra reinforcement amount of 32%, 15%, and 5% respectively is required over what needed in case of $t = 1$. Since a reliable determination of in situ soil tensile strength may be difficult to achieve, the charts in Figure 4.7 can be used to decide whether it is worth the investment. For instance, if the material exhibits a low cohesion, determining σ_t is not worthwhile since its value makes very little difference to the required reinforcement; vice-versa for soils exhibiting a high cohesion, proving some tensile

strength would allow making important savings on the reinforcement. Finally, it is observed that the beneficial influence of some tensile strength is larger in slopes of high ϕ and reinforced with a LID of reinforcement.
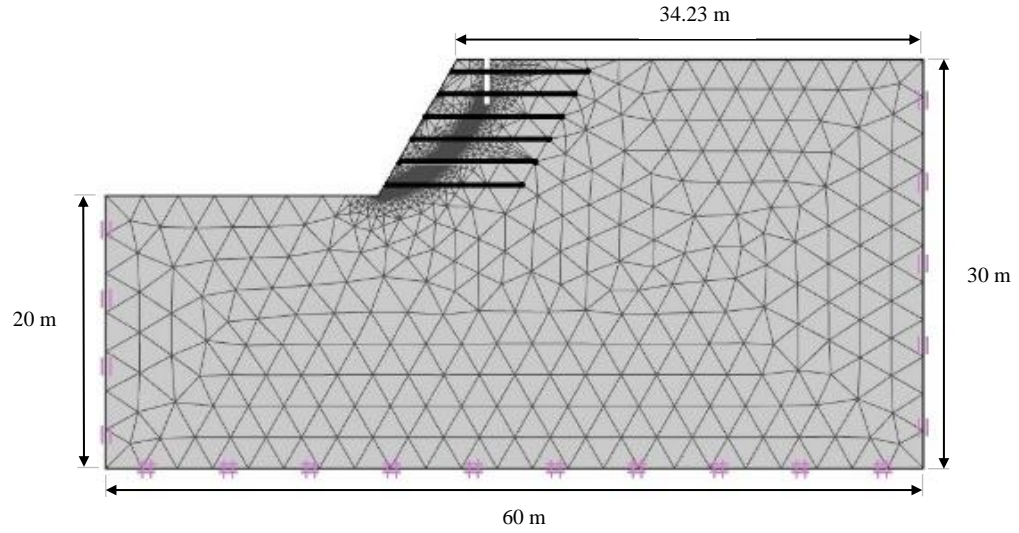

(a)
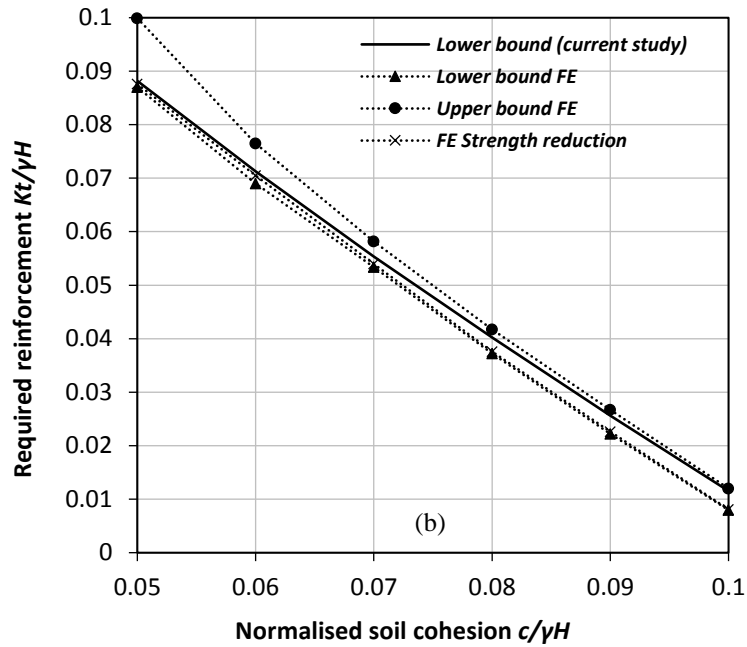
(b)

Figure 4.6 slope with a pre-existing crack employed for validation purposes ($\phi = 20°$, $\beta = 60°$ and uniform distribution of reinforcement). a) Illustration of the boundary conditions and mesh used in the software (OptumCE). The size of the crack is exaggerated for visualisation purposes b)

Comparison among the analytical upper bounds (current study) and those obtained using FE analyses.
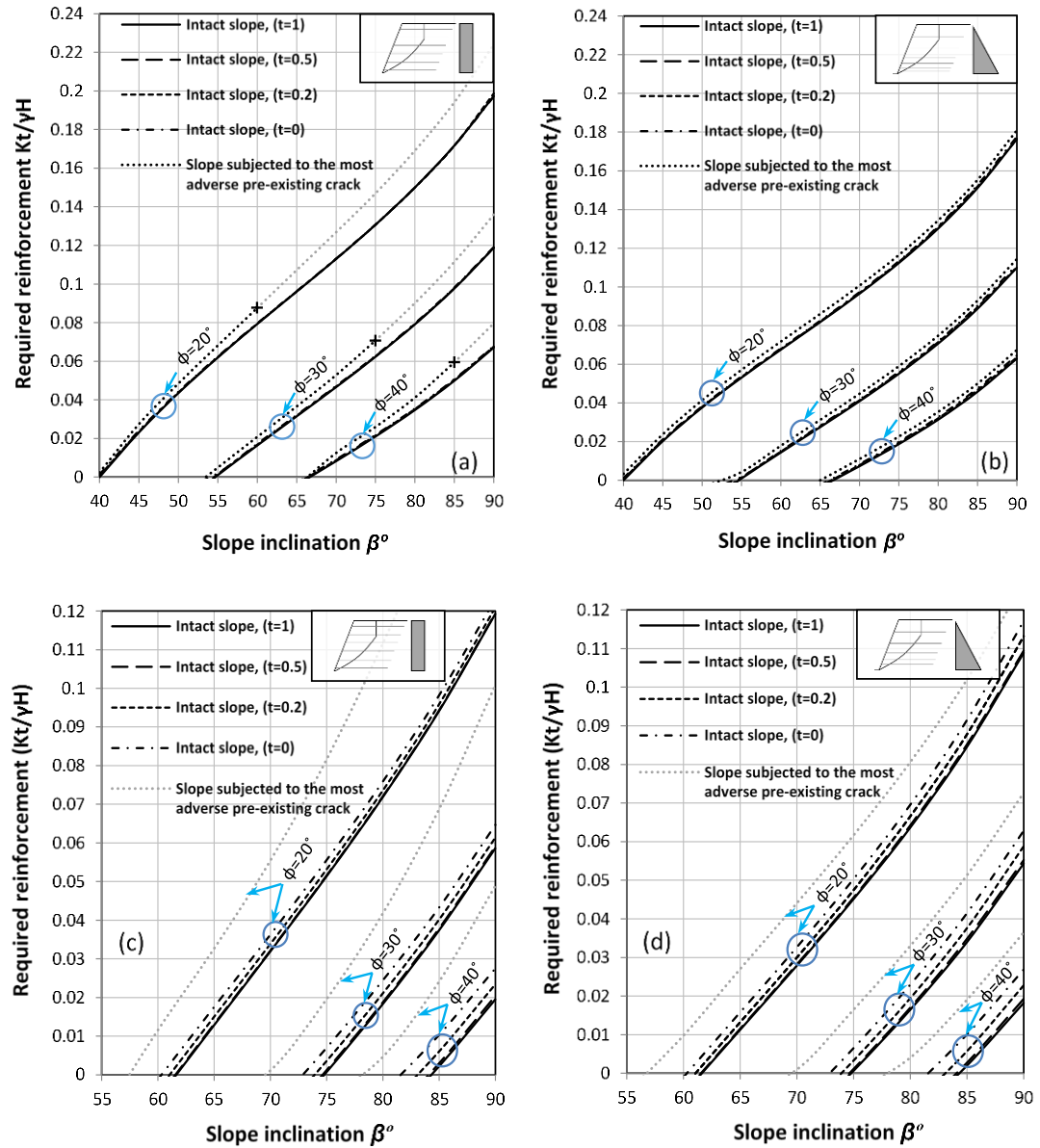
Figure 4.7 Required reinforcement for intact slopes subject to crack formation (limited tensile strength of t=0.5, t=0.2 and t=0) and cracked slopes. (a) & (b) are for $c/\gamma H = 0.05$ while (c) & (d) are for $c/\gamma H = 0.1$. Grey lines indicate that the constraint of maximum crack depth is active, while black lines indicate the constraint is inactive. The mark + indicates the boundary between the two.

Considering now the case of the most adverse pre-existing crack being present in the slope, from the figure it can be noted that $K_t / \gamma H$ becomes significantly larger for soils manifesting high values of cohesion and ϕ. To put this result in context, let us recall that this is a worst-case scenario to be assumed when no other information about climate-induced cracks is available and a conservative design is desired. If depth or location of the cracks can be ascertained, a less conservative estimate of the required reinforcement will be obtained by imposing a crack depth or location as an equality constraint to be added into the search for the minimum of

$$f_{\textit{deep dep pre-existing}} \left(\chi, \upsilon, \zeta, \phi, \beta, c / \gamma H, \gamma_w / \gamma \right).$$

4.4.3 Illustrative examples

To highlight quantitatively the beneficial effect that accounting for cohesion may have in the design of geosynthetic-reinforcements, two design examples are here provided.

Example (1): A slope of 8m height and 75° inclination in clayey ground to be stabilised employing geosynthetics. The soil exhibiting a shearing resistance angle of $\phi = 20°$, a modest cohesion of 7.5 kPa and unit weight of 18.5 kN/m³.

Example (2): Consider the realisation of a 5m high embankment of 45° inclination in a cohesive soil weighing 20 kN/m³ exhibiting a shearing resistance angle of $\phi = 20°$ and 5 kPa of apparent cohesion but no tensile strength in a continental climate (presence of pre-existing cracks). Results of the two examples are obtained from Figure 4.5 and listed in Table 4.1 Examples of the savings on the reinforcement that can be achieved by accounting for the presence of cohesion and tensile strength.. From

the table it emerges that accounting for cohesion without considering cracks or limited

tensile strength allows saving up to 82% and 81.3% on reinforcement for UD and LID

respectively. These two percentiles are 33.9% and 35.3% respectively when the worst

crack scenario is assumed.

Table 4.1 Examples of the savings on the reinforcement that can be achieved by accounting for the presence of cohesion and tensile strength.

Normalised cohesion	Uniform distribution				Linearly increasing distribution			
	Case (1) $c/\gamma H = 0$	Case (2) $c/\gamma H = 0.05$			Case (1) $c/\gamma H = 0$	Case (2) $c/\gamma H = 0.05$		
Soil tensile strength and crack scenario	-	*t=1*	*Tension cut-off (t=0)*	*Presence of crack**	-	*t=1*	*Tension cut-off (t=0)*	*Presence of crack**
Example 1, Required reinforcement $K_t/\gamma H$	0.2211	0.1307	0.1307	0.1460	0.1800	0.1123	0.1129	0.1163
Savings for Example 1= $\left(\dfrac{case(1) - case(2)}{case(1)}\right)$ $\times 100\%$	-	40.8%	40.8%	33.9%	-	37.6%	37.2%	35.3%
Example 2, Required reinforcement $K_t/\gamma H$	0.1288	0.0231	0.0241	0.0273	0.1084	0.0202	0.0210	0.0235
Savings for Example 2= $\left(\dfrac{case(1) - case(2)}{case(1)}\right)$ $\times 100\%$	-	82%	81.2%	78.8%	-	81.3%	80.6%	78.3%

* The most unfavourable crack scenario is assumed.

4.4.4 Influence of pore water pressure

The effect of various hydraulic conditions on the required level of reinforcement is

here analysed by employing the so called r_u method (Bishop & Morgenstern, 1960)

with r_u defined as: $r_u = u / \gamma z$ with u being the pore water pressure and z being the

overburden depth of the point on the slip surface below the soil surface. In this method,

a uniform value of r_u is assumed throughout the entire slope and an effective stress

analysis is carried out. This is an approximate method to account for the presence of

pore water pressure in partially saturated slopes, the higher the water table in the slope

and/or the excess pore pressure due to slow drainage in the ground and or geosynthetic-reinforcement, the higher the value of r_u. The depth of water within the crack is calculated to be consistent with the assumed value of r_u.

The maximum depth of crack was chosen consistently with the seepage scenario examined according to table 2 of (Michalowski, 2013). In Figure 4.8 values of $K_t / \gamma H$ are plotted against slope inclinations ranging from 40° to 90° for $r_u = 0$, 0.25 and 0.5. Looking at the charts two important observations can be made: the effect of the presence of cracks is higher in UD of reinforcements especially for steep slopes and the destabilising influence of pore water pressure is significantly higher in UDs of reinforcement than in LIDs. The reason for this is that in case of a LID, more reinforcement layers are laid in the lower part of the slope the pore water pressure is higher.
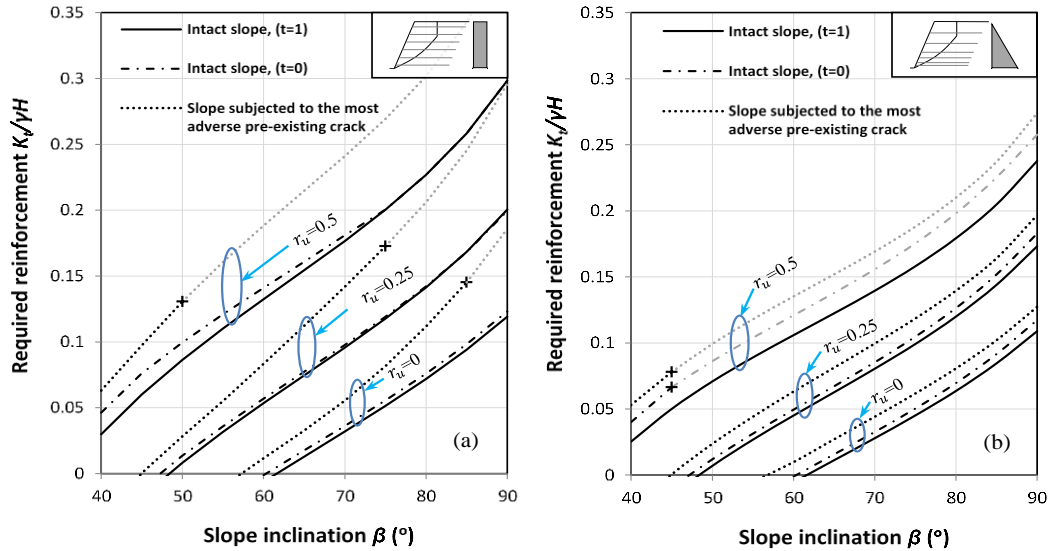
Figure 4.8 Required reinforcement for slopes (with $\phi = 20°$ and $c / \gamma H = 0.1$); (a) for uniform distribution of reinforcement and (b) for linearly increasing distribution. Grey lines indicate that the constraint of maximum crack depth is active, while black lines indicate the constraint is inactive. The mark + indicates the boundary between the two.

4.4.5   Shallow (pre-existing) cracks deepened by the failure process

In this section we consider the possibility of a failure mechanism entailing the extent

of a pre-existing crack underneath its bottom tip (point I in Figure 4.9a) as part of the

failure process. This implies that energy is dissipated underneath the crack tip, *i.e.*

$\dot{D}s_{(I-C)} \neq 0$. The maximisation of $f\left(\chi, \upsilon, \zeta, \phi, \beta, c/\gamma H, t, \gamma_w/\gamma\right)$ (see Eq. (*4.20*)) over

χ, υ, ζ constrained by the following additional equation prescribing the pre-existing

crack depth, $h_{pre-existing}$:

$$\exp\left(\tan\phi.\zeta\right)\sin\zeta = \begin{bmatrix} \exp\left(\tan\phi.\chi\right)\sin\chi\left(1 - \dfrac{h_{pre-existing}}{H}\right) + \\ \dfrac{h_{pre-existing}}{H}\exp\left(\tan\phi.\upsilon\right)\sin\upsilon \end{bmatrix} \qquad (4.23)$$

specifies the amount of reinforcement needed having assumed the presence in the

slope of the most adverse crack. The horizontal position of the crack engaged by the

failure mechanism is provided as a result of the optimisation process.

In Figure 4.9b, values of $K_t/\gamma H$ are plotted against the prescribed pre-existing crack

depth for different values of $c/\gamma H$. The red lines refer to failure mechanisms

involving further crack formation ($\dot{D}s_{(I-C)} \neq 0$), whereas the black lines refer to failure

mechanisms not involving further crack formation ($\dot{D}s_{(I-C)} = 0$ and $I \equiv C$). For

shallow pre-existing crack depths (small values of $h_{pre-existing}/H$) the red lines are

distinct from the black lines lying above them. This means that if crack formation due

to the exceedance of the tensile strength is accounted for in the calculations, the failure

mechanism is more critical than the failure mechanism found by disregarding it. So

the possibility of further crack formation cannot be overlooked and the reinforcement design should be based on the red lines. Instead at high values of $h_{pre-existing}/H$, red lines and black lines coincide, so the critical failure mechanism does not entail the deepening of pre-existing cracks which are therefore called deep cracks to indicate that no deepening occurs as result of the slope failure mechanism taking place. The boundary between shallow and deep pre-existing cracks can now be unambiguously identified as the point where the red and black lines no longer coincide (see the square symbols in Figure 4.9b).

Another important observation is about the fact that the required reinforcement increases with the depth of the pre-existing cracks, but only until a certain threshold value beyond which it remains constant (see the horizontal parts of the lines in Figure 4.9b). For values of $h_{pre-existing}/H$ smaller than the threshold, the log-spiral part of the failure mechanism (D-C) joins the pre-existing crack at its tip whereas for values larger than the threshold, the log-spiral part of the failure mechanism joins the pre-existing crack above its tip. Importantly observing Figure 4.9b, we can conclude that the most adverse situation for the stability of slopes subject to climate-induced cracks occurs for the failure mechanism found by the maximisation of the function $f_{deep\,pre-existing}\left(\chi,\upsilon,\zeta,\phi,\beta,c/\gamma H,\gamma_w/\gamma\right)$ in Eq. (*4.21*) which also provides the most adverse crack for the slope as a result of the maximisation. This failure mechanism does not entail any further crack formation.
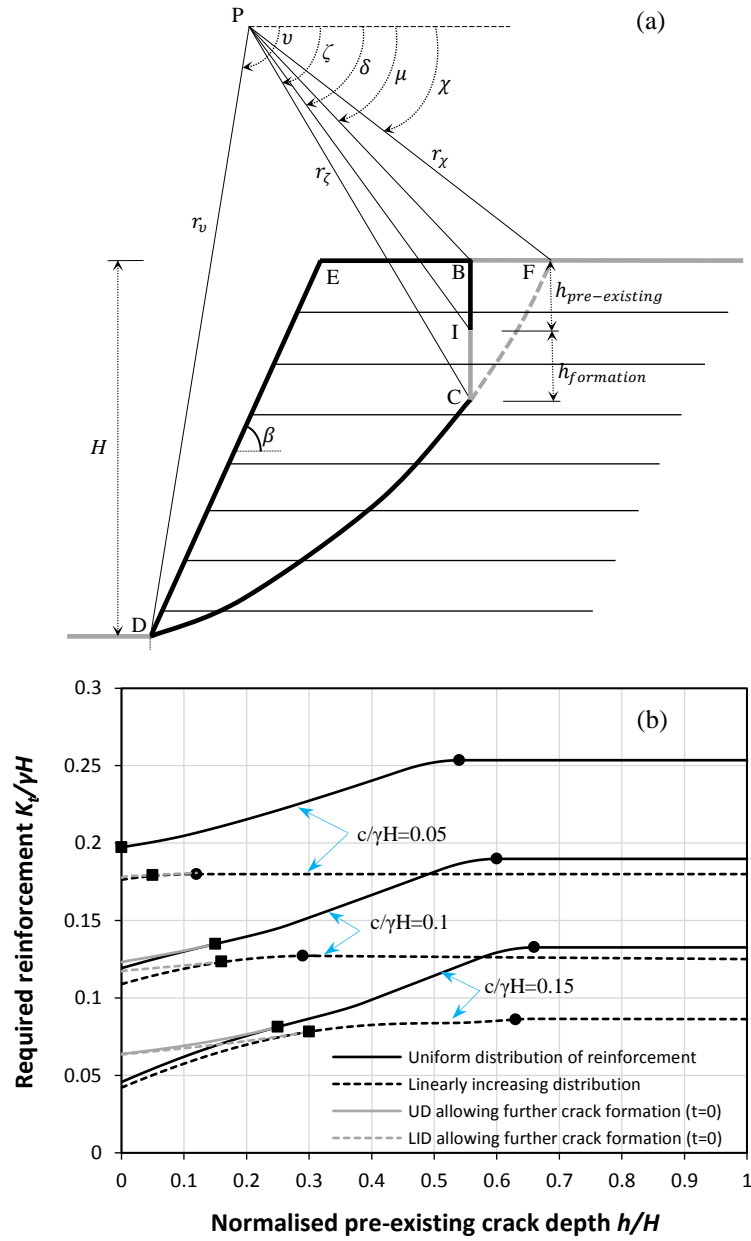
Figure 4.9 (a) Sketch of a failure mechanism involving the deepening of an existing crack. (b) Required reinforcement versus depth of existing cracks for $\beta = 90°$, $\phi = 20°$, $r_u = 0$ and both UD and LID. Grey lines refer to failure mechanisms involving further crack formation $\dot{D}s_{(I-C)} \neq 0$, whereas black lines refer to failure mechanisms not involving further crack formation $\dot{D}s_{(I-C)} = 0$.

4.5 Length of reinforcement

In this section, the way in which the design of the length of reinforcement layers is affected by the presence of cracks is investigated. To calculate the minimum length of the reinforcement layers, a combined failure mode consisting of pull-out in some layers and rupture (tensile failure) in others, needs to be considered. This means that all possible combinations involving: rupture in some layers, layer(s) that may bypassed by the failure surface and layer(s) being pull-out are covered. The normalised length of reinforcement, L_r / H, is calculated following the procedure set by (Michalowski, 1997) extended to the case of $c - \phi$ soil slopes and accounting for the presence of cracks. Assuming all layers are of the same length, it turns out to be:

$$\frac{L_r}{H} = \begin{bmatrix} \dfrac{L_{ei}}{H} - \left(\cos\upsilon + \sin\upsilon\cot\beta\right)\dfrac{r_\chi}{H}\exp[\tan\phi\left(\upsilon - \chi\right)] + \\[2mm] \left(\cos\theta_i + \sin\theta_i\cot\beta\right)\dfrac{r_\chi}{H}\exp\left[\tan\phi\left(\theta_i - \chi\right)\right] - \dfrac{L_{ci}}{H} \end{bmatrix} \tag{4.24}$$

with L_{ei} / H being the effective (or anchorage) length of reinforcement (see Figure 4.2a) yet to be calculated, θ_i being the angle related to the intersection between the failure surface and the layer *i*, and L_{ci} being part of the length of reinforcement as illustrated in Figure 4.2a.

Trigonometry dictates that for a reinforcement layer crossing the crack:

$$\frac{L_{ci}}{H} = \frac{r_\chi}{H}\exp\left[\tan\phi\left(\theta_i - \chi\right)\right]\cos\theta_i - \exp\left[\tan\phi\left(\zeta - \chi\right)\right]\cos\zeta \tag{4.25}$$

whereas for any reinforcement layer below the crack tip $L_{ci} = 0$. L_{ei} / H is determined from the following equation (Michalowski, 1997):

$$\frac{K_t}{\gamma H} = \frac{\left[\begin{array}{c} \left(\dfrac{r_\chi}{H}\right)^2 (f_1 - f_2 - f_3 - f_4 + f_5 + f_6 + f_w) - \left(\dfrac{r_\chi}{H}\right)\dfrac{c}{\gamma H}(g_1 + g_2) - \\[2em] 2f_b \tan\phi \displaystyle\sum_{i=1}^{j} \dfrac{z_i^*}{H}\dfrac{L_{ei}}{H}\left(\sin\chi + \dfrac{z_i}{r_\chi}\right) \end{array}\right]}{\dfrac{1}{n}\displaystyle\sum_{i=j+1}^{n}\left(\sin\chi + \dfrac{z_i}{r_\chi}\right)} \qquad (4.26)$$

with $K_t/\gamma H$ determined from the semi-analytical method expounded in the previous sections; j being the number of layers pulled out; z_i^* being the overburden depth of reinforcement layer i which for gentle slopes it can be less that the depth z_i of the reinforcement layer below the slope crest, f_b the bond coefficient between soil and reinforcement and n, the number of reinforcement layers.

An optimization procedure was carried out to find the maximum value of L_r over the variables (χ, υ, ζ) for an example slope with $n = 6$. f_b was taken as 0.6 according to the latest report from the U.S. Federal Highway Administration (Berg, Christopher, & Samtani, 2009). The results, presented in Figure 4.10, show that in case of the most adverse pre-existing crack being present the largest anchorage length is required and the higher the soil tensile strength the shorter the required reinforcement length (*i.e.* the case of $t = 1$ requires less anchorage length than $t = 0$). This is true for both reinforcement distributions considered. This finding is not surprising recalling from previous sections of the study the fact that the case of the most adverse pre-existing crack being present is the most critical one for slope stability and the higher the soil tensile strength is the less a slope is prone to tension cracking.
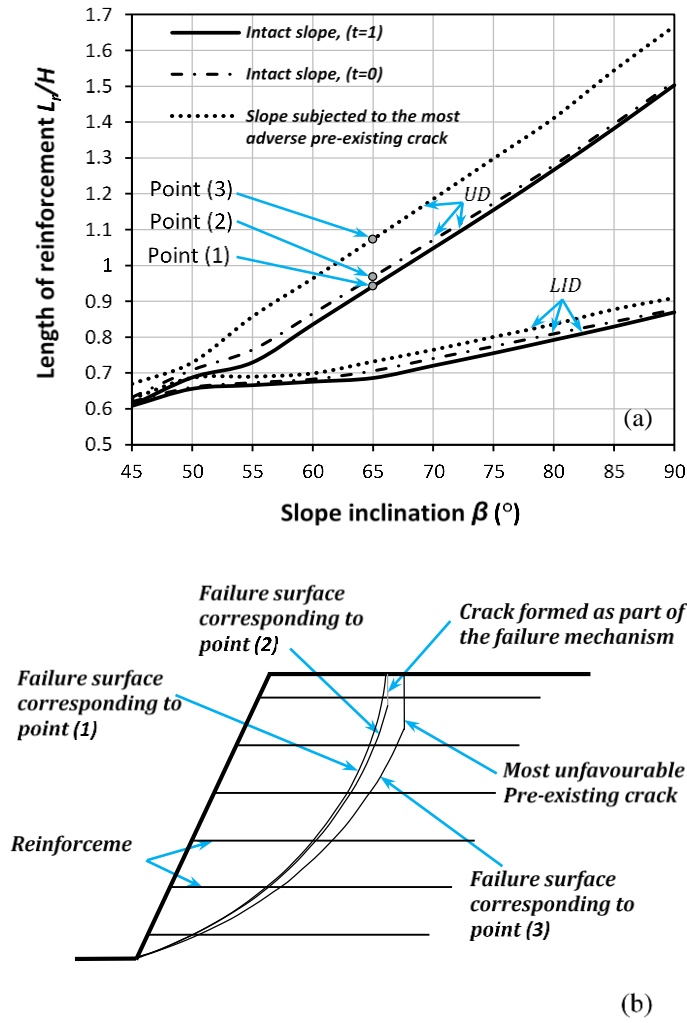
Figure 4.10 (a) Length of reinforcement versus slope inclination for a slope with $\phi = 20°$, $c/\gamma H = 0.05$ and $r_u = 0$. (b) Failure mechanisms for a slope with $\beta = 65°$ and uniform distribution of reinforcement: 1) case of intact slope not subject to crack formation (high tensile strength); 2) case of intact slope subject to crack formation (limited tensile strength); and 3) case of slope with a pre-existing crack.

4.6 Conclusions

A new semi-analytical method for the design of geosynthetic-reinforcement in cohesive backfills was presented. Since the presence of cohesion is accounted for, significant savings on the amount of reinforcement to be used can be made. The method, derived using the kinematic approach of limit analysis, provides the amount

of required reinforcement as a function of slope inclination and of three soil strength parameters: angle of shearing resistance, cohesion, and tensile strength. In addition, cracks are often significantly detrimental to slope stability so they cannot be overlooked in the design calculations of the reinforcement. Also the method takes into account the presence of cracks, which are a very common occurrence in cohesive soils. Cracks cannot be overlooked since may have a significant detrimental effect on the stability of the slopes. Lower bounds on the required level of reinforcement were determined and presented in the form of design charts. Various hydraulic scenarios were investigated as well. A formula is also provided to calculate reinforcement anchorage lengths.

In the chapter it is shown that 1) accounting for the presence of cohesion allows achieving a less conservative design so that significant savings on the overall level of reinforcement can be made. 2) there are several situations where the presence of cracks reduces significantly the stability of the reinforced slopes so that in general they cannot be neglected in the stability analysis performed to design the amount of reinforcement required. 3) there are situations where the tensile strength of the ground, which rules the depth of the tension cracks forming in the reinforced slope, has a significant influence on slope stability, for instance with high levels of cohesion and angle of shearing resistance.

A validation exercise was undertaken by means of both finite element lower bound analyses and finite element with strength-reduction technique analyses showing results very close to the ones obtained by the semi-analytical method here introduced. This provides confidence in the use of the method for design purposes.

Chapter 5: Geosynthetic-Reinforced Slopes in Cohesive Soils Subject to Seismic Action[3]

SUMMARY

Currently, geosynthetic reinforcements are calculated assuming the backfill purely frictional. However, accounting for the presence of even a modest amount of cohesion may allow using locally available cohesive backfills to a greater extent and less overall reinforcement. Unlike purely frictional backfills, cohesive soils present are subject to the formation of cracks that tend to reduce slope stability which therefore need to be properly accounted for in any slope stability assessment.

In the previous chapter, a semi-analytical method is derived for uniform $c - \phi$ slopes accounting for the presence of cracks that provides the amount of reinforcement needed as a function of soil cohesion, tensile strength, angle of shearing resistance and slope inclination employing the limit analysis upper bound method.

In this chapter, the formulation is extended to the seismic case, accounting for earthquake action by employing the pseudo-static approach. Ready to use design charts providing the value of the required reinforcement are plotted for both uniform and linearly increasing reinforcement distributions. From the results, it emerges that

---

[3] This chapter has been published in *Procedia Engineering*, see (Abd and Utili, 2017b)

accounting for the presence of cohesion allows significant savings to be made, but the presence of seismic action may require considerable additional reinforcement.

5.1 Introduction

The use of geosynthetics with the aim of increasing the shear strength of cohesive soils has been investigated by several authors (Fourie & Fabian, 1987; T. S. Ingold, 1981; Terence S. Ingold & Miller, 1983; Hoe I. Ling & Tatsuoka, 1994). Also, substantial experimentation has been performed during the last decade to investigate the behaviour of geotextile reinforced cohesive slopes (Hu et al., 2010; R. Noorzad & Mirmoradi, 2010; Wang et al., 2011). In particular non-woven geotextiles and geogrids of sufficient tensile strength have been proved to be effective at increasing the strength of cohesive soils (Reza Noorzad & Omidvar, 2010; Sukmak et al., 2015). However, in the methods currently available in the literature, reinforcements are still calculated assuming soils to be cohesionless (de Buhan et al., 1989; Richard A. Jewell, 1991; Michalowski, 1997). This conservative assumption is due to the fact that geosynthetics were initially conceived for cohesionless granular soils and that the first design guidelines published for geosynthetic reinforced earth structures disregard the beneficial effect of cohesion (*e.g.* (R. A. Jewell, 1996)). However, the recent edition of AASHTO LRFD *bridge design specifications* (AASHTO, 2012), allows for the inclusion of cohesion in the design of geo-reinforced slopes although unfortunately no formulae are provided for this purpose. However, (Anderson et al., 2008) show that an amount of cohesion as small as 10 kPa can reduce the thrust against an earth structure of up to 50-75% for typical design conditions.

Prompted by these findings (Abd & Utili, 2017a) derived a semi-analytical method for uniform $c - \phi$ slopes accounting for the presence of cracks that provides the amount of reinforcement needed as a function of soil cohesion, tensile strength, angle of shearing resistance and slope inclination employing the limit analysis upper bound method. In this chapter the formulation is extended to the seismic case, accounting for earthquake action by employing the so called pseudo-static approach (Terzaghi, 1950).

5.2   Problem formulation

There are two main approaches to investigate the stability of geosynthetics-reinforced slopes: one where the local equations of equilibrium for an equivalent continuum formed by ground and reinforcement together are derived via homogenization techniques (*e.g.* (de Buhan et al., 1989)), called continuum approach by (Michalowski & Zhao, 1995), and another one, to be used here, where ground and geosynthetic-reinforcement are considered as two separate structural components, called structural approach (Michalowski & Zhao, 1995). Limit analysis can be used with both approaches. In this chapter, the structural approach is employed together with the kinematic (upper bound) method of limit analysis to obtain lower bounds on the required strength of reinforcement.

Limit state analyses are based on considering mechanisms in which the material reaches the limit state and the collapse is imminent. Such mechanisms are then kinematically admissible only when the forces in the reinforcement layers reach their limit (equal to tensile strength or the pullout force). Therefore, the reinforcement force distribution coincides with the distribution of reinforcement strength (Michalowski,

1997). A common choice is to employ reinforcement layers of equal strength laid at equal spacing or at a spacing decreasing linearly with depth. The former case gives rise to a uniform load distribution (UD) while the second one to a load distribution increasing with depth (LID) (see Figure 4.1 in chapter 4). Another scenario is the adoption of reinforcements laid at equal spacing whose strength increases (linearly) with depth, which also gives rise to LID. Neglecting the (little) influence of the overburden stress on the strength of the geosynthetics for sake of simplicity (Michalowski, 1997) in case of UD, the reinforcement tensile strength, K, can be determined as:

$$K = K_t = \frac{nT}{H} \tag{5.1}$$

with n being the number of reinforcement layers, T the strength of a single layer at yielding point and H the slope height.

In case of a LID reinforcement instead:

$$K = 2K_t \frac{(H-y)}{H} \tag{5.2}$$

with y is the vertical upward coordinate departing from the slope toe.

Geosynthetics in reinforced slopes are subject to three main possible failure modes: reinforcement rupture, pull out failure, and direct sliding. In this chapter, a rupture failure will be assumed in order to design the amount of geosynthetic-reinforcement. Traction-free uniform $c - \phi$ slopes with an inclination angle β, ranging from 45° to 90° and reinforced with geosynthetic layers are here considered. Note that any surcharge loads could be accounted for by a slight extension of the formulation

presented. Following (Michalowski, 2013) , two types of cracks will be considered: cracks existing in the slope before the formation of any failure mechanism, here called pre-existing cracks, and cracks forming as part of the failure mechanism due to the exceedance of ground tensile strength, here called tension cracks. Cracks will be treated as no-tension non-cohesive perfectly smooth (no friction) interfaces; therefore the angle η between the velocity vector of the mass of soil sliding away and the crack surface is $0° \leq \eta \leq 180°$. The wedge E-B-C-D is assumed to rotate as a rigid body around point P whose location is yet to be determined. Experimental tests in the centrifuge provide clear evidence that this is the failure mechanism taking place in geosynthetic-reinforced slopes (Viswanadham & Mahajan, 2007; K. H. Yang et al., 2012; Jorge G. Zornberg et al., 1998). The log-spiral D-C is described by the following expression:

$$r = r_\chi \exp\left[\tan\phi\left(\theta - \chi\right)\right]$$
(5.3)

where θ and χ are the angles made by r and r_χ respectively with the horizontal axis, r is the distance between the spiral centre, point P, and a generic point on the log-spiral slip surface, and r_χ is the length of the chord P-F.

5.3   Derivation of the semi-analytical solution

According to the kinematic theorem of LA, the highest (best) lower bound to the required reinforcement can be derived from the following energy balance equation:

$$\dot{D} = \dot{W}$$
(5.4)

Where $\dot{D}$ and $\dot{W}$ are the internal energy dissipation rate and the external work rate respectively. $\dot{D}$ is here calculated as follows:

$$\dot{D} = \dot{D}s_{(B-C)} + \dot{D}r_{(B-C)} + \dot{D}s_{(C-D)} + \dot{D}r_{(C-D)} \tag{5.5}$$

with $\dot{D}s_{(B-C)}$ and $\dot{D}r_{(B-C)}$ being the energy rates dissipated along the crack by ground and reinforcement respectively and $\dot{D}s_{(C-D)}$ and $\dot{D}r_{(C-D)}$ the energy rates dissipated along the log-spiral part C-D (see Figure 5.1) by ground and reinforcement respectively. With regard to $\dot{D}s_{(B-C)}$: if the crack is pre-existing the formation of the failure mechanism, no energy is dissipated by the ground so $\dot{D}s_{(B-C)} = 0$; conversely if the (tension) crack opens up because the ground tensile strength is exceeded, energy is dissipated: $\dot{D}s_{(B-C)} \neq 0$ (Michalowski, 2013).
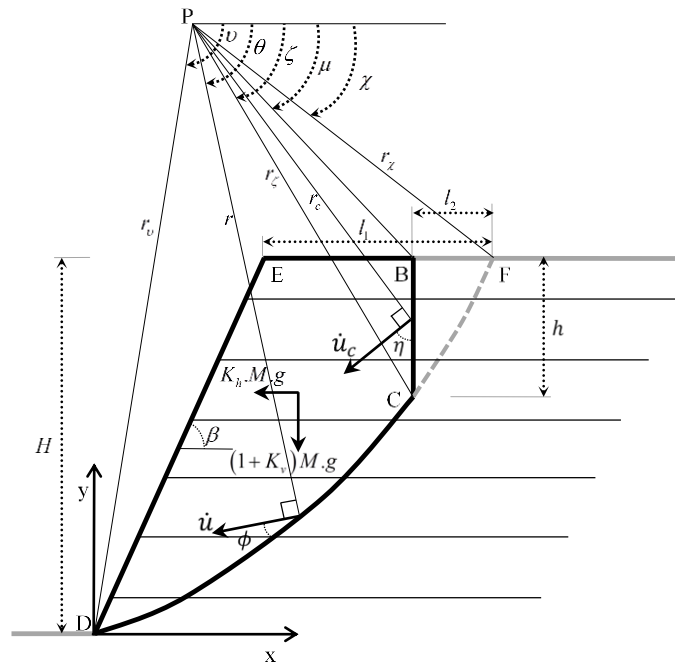
Figure 5.1 Rigid rotational failure mechanism in a reinforced slope subject to a crack (B-C). The mass of soil enclosed by (E-B-C-D) rotates clockwise around point P.

Considering tension cracks, it is known that the uniaxial tensile strength, predicted by the Mohr-Coulomb (M-C) failure criterion for cohesive soils, represents a significant overestimation of the real soil tensile strength. In fact, experimental evidence (*e.g.* (Bishop et al., 1965)) shows that a linear failure envelope is unsuitable to describe the tensile strength of cohesive soils because it is highly non-linear. To partially remedy this shortcoming yet using the linear M-C criterion, a tensile limit is commonly added. (Michalowski, 2013) proposed to limit the M-C envelope with the stress circle obtained from an unconfined uniaxial tensile strength test (see Figure 5.2). This composite failure criterion (circle plus M-C straight line) is sufficiently realistically non-linear in the tension zone and on the other hand lends itself to LA calculations. Accordingly, the energy expended for the formation of a tension crack, $\dot{D}s_{(B-C)}$ turns out to be (Michalowski, 2013):

$$\dot{D}s_{(B-C)} = \dot{\theta} r_\chi^2 \left(\frac{\sin \chi}{\tan \mu} \right)^2 \left(\frac{\sigma_c^{M-C}}{2} \int_\mu^\zeta \frac{1-\sin\theta}{\cos^3\theta} d\theta + \frac{\sigma_t}{1-\sin\phi} \int_\mu^\zeta \frac{\sin\theta-\sin\phi}{\cos^3\theta} d\theta \right) \qquad (5.6)$$

with μ being the angle made by the segment P-B with the horizontal (see Figure 5.1), σ_c^{M-C} being the uniaxial compressive strength consistent with the M-C criterion and σ_t the unconfined tensile strength as measured from laboratory experiments. It is convenient to introduce a dimensionless coefficient, t, defined as the ratio of the unconfined tensile strength measured in laboratory experiments, σ_t over the maximum unconfined tensile strength according to the M-C envelope, σ_t^{M-C} (see Figure 5.2a):

$$t = \frac{\sigma_t}{\sigma_t^{M-C}} \qquad (5.7)$$

It is straightforward to observe that $0 \leq t \leq 1$. Both σ_c^{M-C} and σ_t^{M-C} are related to c and ϕ:

$$\sigma_c^{M-C} = 2c\left(\frac{\cos\phi}{1-\sin\phi}\right) \tag{5.8}$$

$$\sigma_t^{M-C} = 2c\left(\frac{\cos\phi}{1+\sin\phi}\right) \tag{5.9}$$

Now substituting equations (5.7), (5.8), and (5.9) into Eq. (5.6), the following expression is obtained for the energy dissipated in the ground due to the formation of a tension crack:

$$\dot{D}s_{(B-C)} = c\dot{\theta}r_\chi^2\left(\frac{\sin\chi}{\tan\mu}\right)^2\left(\frac{\cos\phi}{1-\sin\phi}\int_\mu^\varsigma\frac{1-\sin\theta}{\cos^3\theta}d\theta + \frac{2t\cos\phi}{1-\sin^2\phi}\int_\mu^\varsigma\frac{\sin\theta-\sin\phi}{\cos^3\theta}d\theta\right)$$
$$= c\dot{\theta}r_\chi^2 g_3(\chi,\upsilon,\varsigma,\phi,t) \tag{5.10}$$

To calculate the energy dissipated by the reinforcement along the crack, it does not matter whether the crack is pre-existing or tension induced. The energy dissipated turns out to be (Abd & Utili, 2017a):

$$\dot{D}r_{(B-C)} = \frac{1}{2}K_t\dot{\theta}r_\chi^2\left[\exp\left[2\tan\phi(\varsigma-\chi)\right]\sin^2\varsigma - \sin^2\chi\right] = K_t\dot{\theta}r_\chi^2 g_4(\chi,\upsilon,\varsigma,\phi) \tag{5.11}$$

The expression for the energy dissipated in the ground along the log-spiral part of the failure mechanism (see log-spiral C-D in Figure 5.1), $\dot{D}s_{(C-D)}$, is provided by (Chen, 1975):

$$\dot{D}s_{(C-D)} = c\dot{\theta}r_\chi^2\exp\left[2\tan\phi(\varsigma-\chi)\right]\frac{\exp\left[2\tan\phi(\upsilon-\chi)\right]}{2\tan\phi} = c\dot{\theta}r_\chi^2 g_1(\chi,\upsilon,\varsigma,\phi) \tag{5.12}$$

where $\dot{\theta}$ is the angular velocity of the sliding wedge, υ and ζ are the angles made by r_υ and r_ζ with the horizontal line respectively.

The energy dissipated by the reinforcement over the log-spiral part of the failure mechanism (C-D) is calculated by integrating the product of the infinitesimal increment of reinforcement strain rate with the reinforcement tensile strength, *T*, averaged over the slope height. The following expression is obtained (Zhao, 1996):

$$\dot{Dr}_{(C-D)} = \frac{1}{2}K_t\dot{\theta}r_\chi^2\left(\exp\left[2\tan\phi(\upsilon-\chi)\right]\sin^2\upsilon - \exp\left[2\tan\phi(\zeta-\chi)\right]\sin^2\zeta\right)$$
$$= K_t\dot{\theta}r_\chi^2 g_2\left(\chi,\upsilon,\zeta,\phi\right)$$

(5.13)
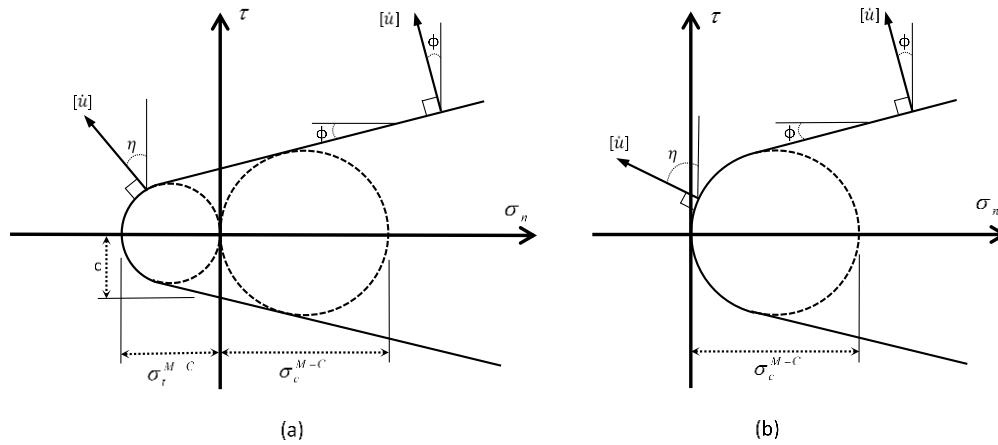
Figure 5.2 Modified Mohr-Coulomb failure envelope for: (a) soil of full unconfined tensile strength;
(b) soil of zero tensile strength (tension cut-off), based on (Michalowski, 2013).

Note that the reinforcement layers lying above the centre of rotation P, are subject to compressive stresses and therefore buckling, hence they are discarded in the calculation of $\dot{D}_r$ (Michalowski, 1997).

The rate of external work for the sliding wedge E-B-C-D, $\dot{W}_{ext}$, is calculated as the work of block E-D-F minus the work of block B-C-F. The work of block E-D-F is

calculated by algebraic summation of the work of blocks P-D-F, P-E-F and P-D-E (Chen, 1975). The work of block B-C-F is calculated by algebraic summation of the work of blocks P-C-F, P-B-F and P-C-B (Utili, 2013; Utili & Nova, 2007). To account for the seismic action, in addition to the weight force, a horizontal pseudo-static force, $F_{PSh} = M.K_h.g = \gamma.K_h.A$, with M being the mass of the wedge, K_h the coefficient of horizontal seismic acceleration and g the gravitational acceleration, and a vertical one, $F_{PSh} = M.K_v.g = \gamma.K_v.A$, with K_v being the coefficient of vertical seismic acceleration need to be considered (Chang et al., 1984). The calculation of the expression $\dot{W}_{ext}$ for each block is provided in (Utili & Abd, 2016). Here the final expression is recalled:

$$\dot{W}_{ext} = \dot{\theta}\gamma r_\chi^3 \begin{bmatrix} (1+K_v)(f_{1v} - f_{2v} - f_{3v} - f_{4v} + f_{5v} + f_{6v}) + \\ K_h(f_{1h} - f_{2h} - f_{3h} - f_{4h} + f_{5h} + f_{6h}) \end{bmatrix} \tag{5.14}$$

with $f_{1v}, f_{2v},...,f_{6v}$ and $f_{1h}, f_{2h},...,f_{6h}$ accounting for the external work done by the vertical and horizontal forces respectively. Their expression is given in Appendix B.

Substitution of the various energy rate contributions calculated into the energy balance equation (Eq. (*5.4*)), provides the objective function to be optimised to design the geosynthetic-reinforcement. Substituting Eq. (*5.5*) and Eq. (*5.14*) with their components into Eq. (*5.4*) and rearranging, leads to determine K_t :

$$\frac{K_t}{\gamma H} = \frac{\begin{bmatrix} (1+K_v)(f_{1v} - f_{2v} - f_{3v} - f_{4v} + f_{5v} + f_{6v}) + \\ K_h(f_{1h} - f_{2h} - f_{3h} - f_{4h} + f_{5h} + f_{6h}) \end{bmatrix}}{\dfrac{H}{r_\chi}(g_3 + g_4)} - \frac{c}{\gamma H}\left(\frac{g_1 + g_2}{g_3 + g_4}\right) \tag{5.15}$$

$$= f(\chi, \upsilon, \zeta, \beta, \phi, c/\gamma H, t, K_h, K_v)$$

Note that $f\left(\chi,\upsilon,\zeta,\beta,\phi,c/\gamma H,t,K_h,K_v\right)$, depends on three ground parameters: angle of shearing resistance, ϕ, cohesion, c, and tensile strength, t.

5.4 Reinforcement Design

The lower bounds on the required reinforcement expressed in dimensionless form, $K_t/\gamma H$, obtained by the maximisation of $f\left(\chi,\upsilon,\zeta,\beta,\phi,c/\gamma H,t,K_h,K_v\right)$ subject to the physical constraint of the crack depth not exceeding the maximum crack depth, are plotted in Figure 5.3 against an assigned level of soil cohesion for the case of initially intact slopes subject to tension crack formation and slopes with deep pre-existing cracks respectively. The constraint on the maximum crack depth stems from the fact that crack depth is limited because for a crack to exist, its faces need to be a stable slope in itself (see B-C in Figure 5.1). Lower and upper bounds on the maximum depth admissible for a stable vertical crack were calculated by (Terzaghi, 1943) and (Michalowski, 2013) using the static and kinematic methods of limit analysis respectively. In the search of the failure mechanism, the following upper bound to the maximum crack depth, h_{max} is prescribed:

$$h_{max} = \frac{3.83c}{\gamma}\tan\left(\frac{\pi}{4}+\frac{\phi}{2}\right) \tag{5.16}$$

Note that assuming an upper (rather than a lower) bound on the maximum crack depth is a conservative assumption. The charts in Figure 5.3 obtained for $\phi = 20°$ cover the whole spectrum of cohesive geomaterials ranging from $c = 0$, for cohesion-less materials, *e.g.* a granular fill, to values of cohesion so high that reinforcement is not needed (where the lines intersect the horizontal axis). Although the general

formulation here provided covers the case of both vertical and horizontal accelerations, all design charts here presented were obtained assuming no vertical acceleration ($K_v = 0$) for sake of simplicity. Note that at $c = 0$ all the three lines depart from the same point since in case of zero cohesion, no cracks can form. The three lines, dotted line for the case of pre-existing cracks being present, dashed lines for intact slopes undergo crack formation and solid lines for intact slopessubject to but do not undergo crack formation, these three lines tend to diverge for increasing cohesion. This is because at higher values of cohesion, the influence of $\dot{D}s_{(B-C)}$ in the energy balance equation (see Eq. (*5.4*)) is larger, which in turn makes the difference between the case of slopes subject to pre-existing crack ($\dot{D}s_{(B-C)} = 0$) and of initially intact slopes subject to the formation of tension cracks ($\dot{D}s_{(B-C)} \neq 0$) larger. In the latter case, higher values of cohesion also imply a larger influence of the ground tensile strength on slope stability (see the lines for $t=1$ and $t=0$ in Figure 5.3).

From the charts emerges that seismic action affects gentler slopes to a much greater extent than steep slopes so that even for high levels of cohesions the reinforcement required for stability tend be significantly higher. For instance considering the case of a slope with $\beta = 45°$ with a modest amount of cohesion, $c/\gamma H = 0.05$, the reinforcement required in the static case is $K_t/\gamma H = 0.02$ but in the presence of a seismic action of $K_h = 0.3$, $K_t/\gamma H = 0.21$ so ten times higher.
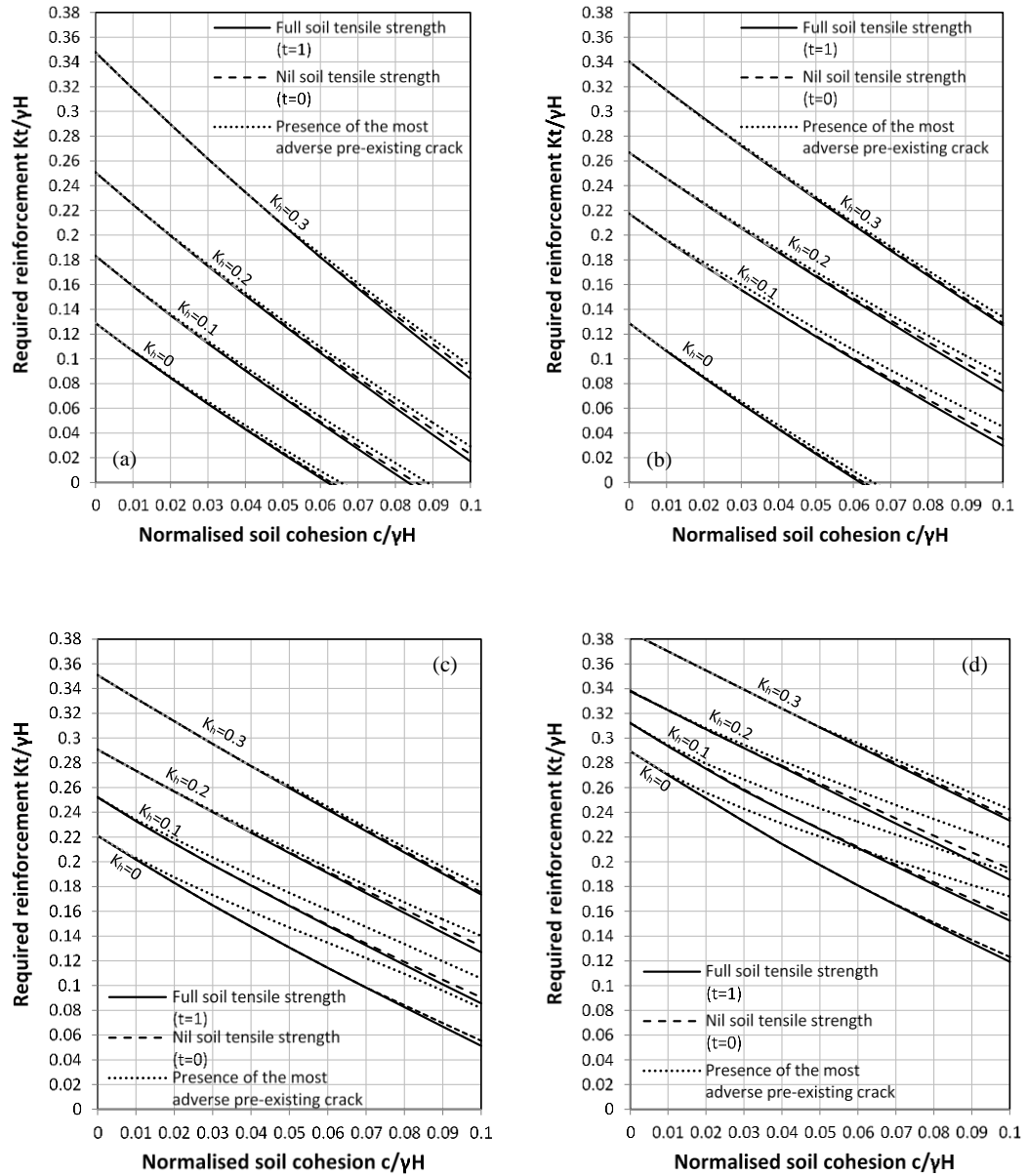
Figure 5.3 Normalized required reinforcement versus normalised soil cohesion for a slope with $\phi = 20°$ and uniform distribution of reinforcement: (a) for $\beta = 45°$, (b) for $\beta = 60°$, (c) for $\beta = 75°$, and (d) for $\beta = 90°$.

Another aspect emerging from the charts is the effect of the presence of pre-existing cracks. Looking at Figure 5.3d, emerges that the seismic action tends to reduce the influence of pre-existing cracks on the stability of the slopes, since the distance of the curve for the case of pre-existing crack (dotted line) and the one for intact slope subject

to crack formation (dashed line) and intact slope not subject to the formation of cracks (solid line) tend to become closer with increasing seismic intensity. The interpretation proposed here for this finding is that seismic action makes the slope less stable overall (so more reinforcement is required overall) but also the higher the intensity of the seismic action the higher its contribution to slope instability in comparison with the instability due to the presence of cracks. Therefore, the performance of slopes subject to strong earthquakes tends to be dominated by the intensity of the seismic acceleration rather than the presence or absence of cracks.

In Figure 5.4 the design charts are provided for the case of LID reinforcement. The general trend of the lines is similar to the case of UD reinforcement. However, comparing Figure 5.3 with Figure 5.4, it can be seen that LID reinforced slopes is more vulnerable to cracks than UD reinforced slopes and it is more clear for high seismic intensities, so it can be concluded that the presence of cracks has higher detrimental impact on LID reinforced slopes than on UD reinforced ones especially when subjected to seismic action.
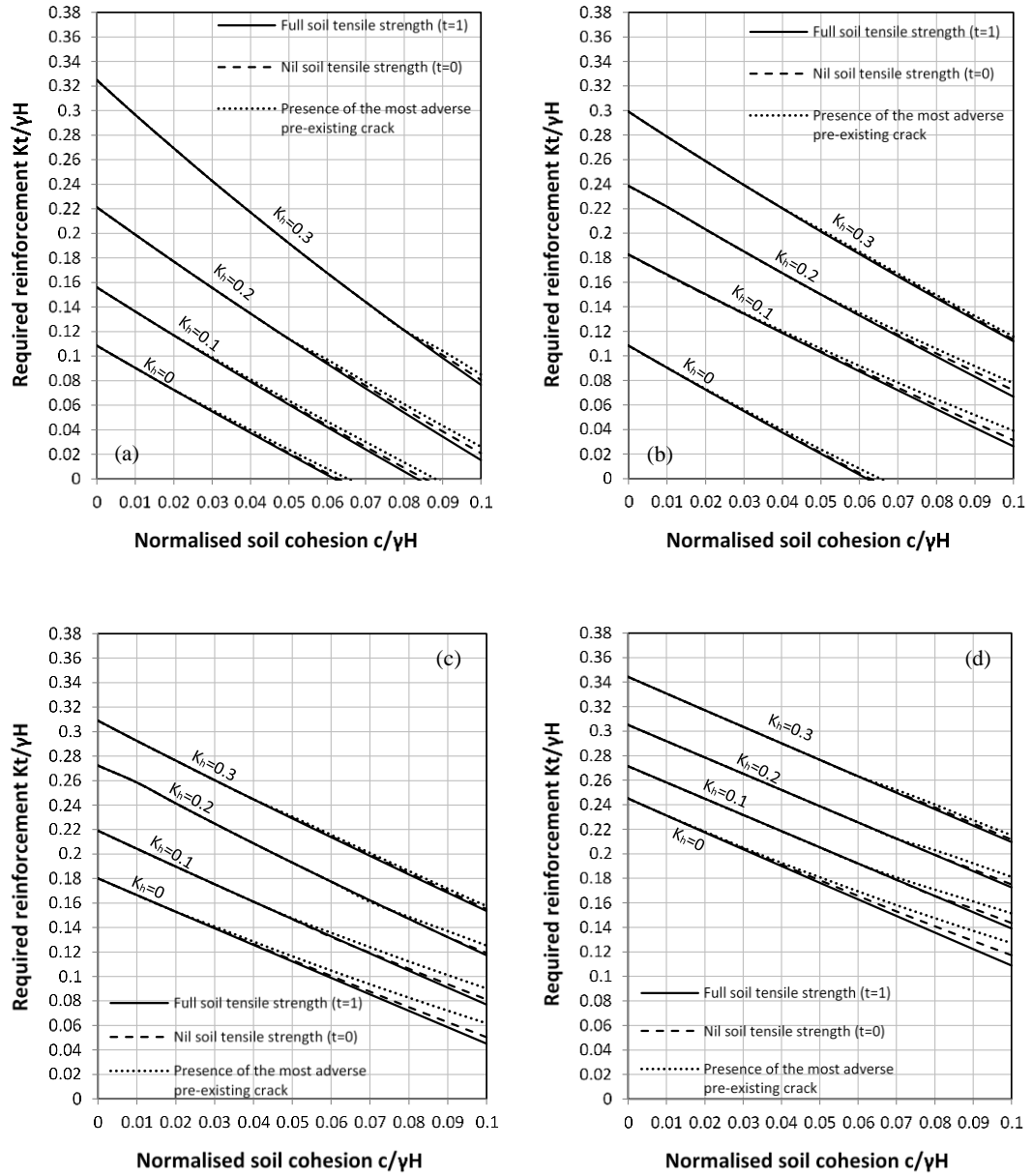
Figure 5.4 Normalized required reinforcement versus normalised soil cohesion for a slope with $\phi = 20°$ and linearly increasing distribution of reinforcement: (a) for $\beta = 45°$, (b) for $\beta = 60°$, (c) for $\beta = 75°$, and (d) for $\beta = 90°$.

5.5   Conclusions

A semi-analytical method for the design of geosynthetic-reinforcement in uniform *c-ϕ* slopes subject to seismic action was presented. The method accounts for the presence of cracks which are a very common occurrence in cohesive soils and may have a significant detrimental effect on the stability of slopes. Design charts were presented which provide lower bounds on the required level of geosynthetic reinforcement as a function of slope inclination, soil strength parameters (angle of shearing resistance, cohesion, and tensile strength) and level of seismic pseudostatic acceleration.

The main findings emerging from the design charts are that i) seismic action affects gentler slopes to a much greater extent than steep slopes so that even for high levels of cohesions the reinforcement required for stability may be significantly higher. ii) seismic action tends to reduce the influence of pre-existing cracks on slope stability since the performance of slopes subject to strong earthquakes tends to be dominated by the intensity of the seismic acceleration rather than the presence or absence of cracks . iii) The presence of cracks has higher detrimental impact on LID reinforced slopes than on UD reinforced ones especially when subjected to seismic action.

Chapter 6: Earthquake-Induced Displacement of Soil Slopes Subject to Cracks[4]

SUMARRY

The upper bound theorem of limit analysis together with Newmark's method are employed to evaluate the displacement of both unreinforced and geosynthetic-reinforced soil slopes subject to cracks. The pseudo static approach has been routinely used in the literature to estimate the seismic displacement of soil slopes. However, the effect of cracks on the slope displacement has yet to be tackled. In this chapter, a new technique is proposed to estimate the horizontal displacement at the slope toe due to a given earthquake postulating rough estimation of real time crack formation. Rotational failure mechanisms for intact slopes exhibiting the formation of cracks as part of the failure process and pre-existing cracks were considered. On the basis of Newmark's method, the seismic-induced displacement is calculated by incorporating a stepwise yield acceleration corresponding to the cracks occurring in the slope. Results of the proposed technique can reasonably bridge the gap between the conservatism of assuming the slopes subject to the most detrimental cracks, and the overestimation of slope stability resulted from the neglect of crack formation. Two examples illustrating

---

[4] This chapter consists of two papers have been published in *IOP Conf. Series: Earth and Environmental Science*, see (Abd 2015a &b).

the procedure for a given earthquake is presented. Also, charts providing the values needed to calculate the stepwise yield accelerations are proposed.

6.1 Introduction

Cracks can be found in soil slopes and embankments due to tensile stresses such as seismic action or external static loading, and/or due to desiccation and cycles of wetting and drying. Pre-existing cracks can cause significant reduction in the stability of soil slopes (Rafael Baker, 1981; Nadukuru & Michalowski, 2013; Utili, 2013), especially if these slopes are subjected to seismic action (Utili et al., 2015). The presence of a vertical crack can reduce the safety factor of the slope depending mainly on its location and depth. Not only form potential part of the slip surface, cracks can also be an easy flow channel for rainfall water, which reduces the soil strength and exerts a lateral stress, inducing the failure when the crack is filled with water.

   As a stabilizing material, geosynthetics have been used successfully and effectively during the last thirty years (Ausilio, Conte, & Dente, 2000; Michalowski, 1998). However, cracks can cause significant reduction in the stability of unreinforced soil slopes (Rafael Baker, 1981; Utili, 2013), especially if these slopes are subjected to seismic action (Utili & Abd, 2016). Pre-existing cracks can be detrimental for geosynthetically-reinforced slopes (Abd & Utili, 2017a). The presence of a vertical crack can reduce the safety factor of the slope depending mainly on its location and depth. The presence of cracks form not only potential parts of the slip surface, but also they form easy flow channels for rainfall water which reduces the soil strength and exerts a lateral stress inducing the failure when these cracks are filled with water.

Cracks can be found in soil slopes and embankments due to tensile stresses such as seismic action or external static loading, and/or due to desiccation and cycles of wetting and drying.

Methods for assessing the seismic stability of slopes have been developed during the last century. The Mononobe-Okabe methods are one of the first published works that address the stability of retaining walls and dams during earthquake incorporating dynamic earth pressure (Mononobe, 1929; Okabe, 1924). Thereafter, several limit equilibrium methods were developed for this purpose (*e.g.* (Janbu, 1954; Little & Price, 1958; Morgenstern & Price, 1965)) which remain the most commonly used by practitioners.

More recently, numerical methods for continuum mechanics, such as the finite element method with strength reduction technique (*e.g.* (Conte et al., 2010; Dawson et al., 1999)) have provided the capability to reliably detect the onset of failure in slopes according to the approach of continuum mechanics. However, if cracks are present, a continuum approach no longer works since the onset of instability is ruled by the behaviour of single fractures. In this case, the Discrete Element Method can nowadays be employed for 3D analyses of slopes with cracks (Boon, Houlsby, & Utili, 2014). Recent algorithmic advances in terms of contact detection algorithms (Boon, Houlsby, & Utili, 2012, 2013) have substantially reduced the runtime of these analyses. However, when little information on the presence of cracks is available, extensive parametric analyses requiring large computational times are necessary. In this case, an analytical approach is very desirable so that numerical analyses would be run only for the case(s) identified by the analytical approach as the most critical.

Newmark's analytical method (Newmark, 1965) is popular among practitioners where a pseudo-static force is used instead of the dynamic excitation to calculate earthquake-induced displacements. The analytical solution for earthquake-induced displacements undergone by intact slopes subject to a rotational failure mechanism is presented by (Chang et al., 1984). One of the main limitations of using Newmark's method to estimate slope displacement is the neglect of the earthquake induced degradation of the soil strength, *i.e.* it assumes a constant yield acceleration throughout the analysis (Jibson, 2011). In this chapter, however, earthquake induced crack occurrence and the consequent reduction of yield acceleration are accounted for. Seismic induced displacements are calculated based on a stepwise time varying yield acceleration.

6.2   Formulation of the Problem

The kinematic approach of limit analysis is used to calculate the least upper bound on the yield (critical) coefficient of acceleration K_y for a given uniform c-ϕ slope. The yield acceleration can be defined as the minimum level of horizontal acceleration (vertical acceleration being proportional to the horizontal acceleration) that brings the slope to the verge of failure (*i.e.* safety factor =1). According to Newmark's method (Newmark, 1965), slope displacements start to accumulate whenever the seismic induced acceleration exceeds the yield acceleration. Then, displacements occurring during the earthquake can be obtained by double integrating the differences between the applied accelerations and the yield one during the time intervals when the ground velocity is larger than zero.

Pre-existing cracks, *i.e.* cracks existing in the slope before any seismic excitation occurs, can significantly reduce the yield acceleration for a given slope, depending on their locations and depths (Utili et al., 2015). Here, an initially intact slope subject to the formation of tension cracks as a result of the earthquake is considered. In this case, the cracks are formed as part of the failure process at the first time the slope yield acceleration is exceeded. Then, in order to calculate the slope displacements generated by the earthquake, a new yield acceleration, accounting for the presence of the cracks formed the first time the yield acceleration of the intact slope was exceeded, needs to be calculated for all the subsequent steps. Four cases are considered in this chapter:

   I.   Slopes made of rocks / cohesive soils of unlimited tensile strength, hence not subject to tension cracks.

  II.   Slopes made of rocks / cohesive soils of limited tensile strength.

 III.   Slopes made of rocks / cohesive soils of zero tensile strength.

 IV.   Slopes subject to the most unfavourable crack from a stability point of view pre-existing the onset of the earthquake.

The procedure for calculating the stepwise time varying yield acceleration is outlined as follows:

   1.   Determine the yield acceleration for an initially intact slope subject to the formation of tension cracks $K_{y(c)}^1$. Vertical tension cracks are formed as part of the occurring failure mechanism since energy is needed to form any crack (Michalowski, 2013). Therefore, the yield acceleration of a slope subject to the formation of tension cracks is lower than the yield acceleration of a slope of

sufficient tensile strength to resist crack formation $K^{\text{int}}_{y(c)}$, *i.e.* $K^1_{y(c)} \leq K^{\text{int}}_{y(c)}$. This acceleration is used to calculate the displacements at the first time that the seismic acceleration exceeds the yield acceleration $K^1_{y(c)}$.

2. Determine the yield acceleration for the same slope but accounting for the presence of the crack generated in step 1, treated now as a pre-existing crack (*i.e.* the crack is already present so that no energy is dissipated for crack formation). This new value of yield acceleration, $K^2_{y(c)}$ is used to calculate the displacements in all subsequent steps.

3. Determine the accumulated wedge displacement D_i with respect to the ground surface, at each time step (*i*) when the seismic acceleration exceeds $K^2_{y(c)}$.

4. Calculate the dimensionless coefficient *C* that relates the displacement of the slope toe to the integral of the earthquake acceleration record above the level of yield acceleration.

5. Determine the accumulated horizontal displacement at the slope toe D_{xi}, where $D_{xi} = C \times D_i$, and then the total horizontal displacement D_t is to be found.

It should be noted that, although several tension cracks at different locations in the slope may form during an earthquake, only the crack which has the worst detrimental effect on slope stability needs to be considered in the calculation. According to the kinematic approach of limit analysis, the failure mechanism taking place is the most critical mechanism for the stability of the slope among all the kinematically feasible mechanisms.

6.3 Calculations of the Yield Acceleration

The upper bound theorem of limit analysis is employed here to calculate the yield acceleration for both intact and cracked slopes. The analytical expressions for the calculation of the external work done by soil masses sliding along composite log-spiral failure surfaces, which requires the use of fictitious wedges bordered by a log-spiral, were first presented in (Utili, 2005; Utili & Nova, 2008) for the case of slopes with horizontal upper part subject to a sequence of landslides, and for more general case of slopes with an inclined upper part, see (Utili & Crosta, 2011). Note that these calculations apply to slopes made of bonded granulates (Jiang, Zhu, Liu, & Utili, 2014; Utili & Crosta, 2011) as well. In (Utili & Nova, 2007), the calculation of the work done by a wedge enclosed by two log-spirals was first presented. The analytical solution is derived here for the case of a horizontal upper slope surface and vertical pre-existing cracks from the upper slope (see Figure 6.1). However, the solution can be straightforwardly extended to the case of a non-horizontal upper slope and that of cracks departing from the slope face, such an extension is reported in (Utili, 2013).
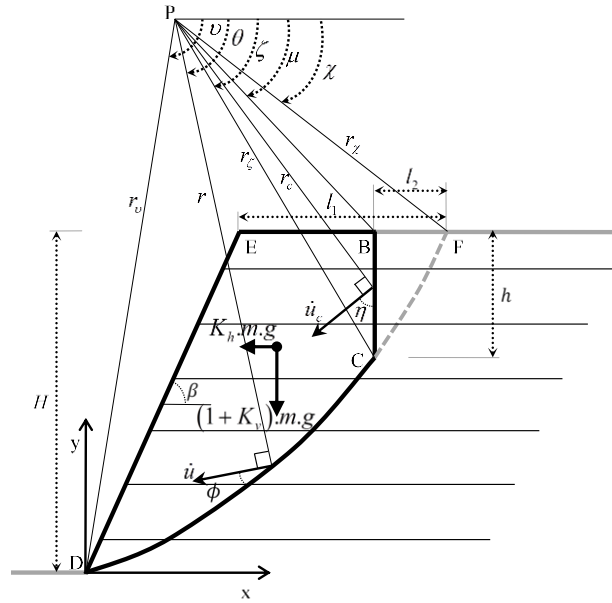
(a)

Figure 6.1 Failure mechanism. Note that $\eta \neq \phi$. The wedge of soil enclosed by black lines D-C (logarithmic spiral failure line), B-C (pre-existing crack), B-E (upper surface of the slope) and E-D (slope face) rotates around point P.

According to the upper bound theorem of limit analysis, the failing wedge E-D-C-B rotates rigidly and log-spirally around the centre of rotation P, as yet undefined, with the ground lying on the right of the log-spiral piece D-C and of the vertical crack C-B remaining at rest. The equation of log-spiral D-C is:

$$r = r_\chi \exp\left[\tan\phi(\theta - \chi)\right] \tag{6.1}$$

with r being the distance of a generic point of the spiral to its centre, ϕ being the angle of shearing resistance, r_χ identifying the distance of point F of the spiral to its centre, and χ, υ being the angles made by segment P-F and segment P-D with the horizontal, respectively (see Figure 6.1).

For reinforced soil slopes, two different distributions of reinforcement will be considered, namely uniform distribution (UD) and linearly increasing distribution with

115

depth (LID), both illustrated in Figure 6.2. Let us introduce the dimensionless variable K_t as the average tensile strength of reinforcement per unit height of the slope. K_t is a function of the tensile strength of the reinforcement layer per unit width, *T*, and of the spacing between reinforcement layers, *S*, and can be written as:

$$K_t = \frac{nT}{H} \tag{6.2}$$

the two cases of reinforcement distributions have been analysed by assigning the corresponding value of *K*, for uniform distribution (UD):

$$K = K_t \tag{6.3}$$

and for linearly increasing distribution (LID):

$$K = 2K_t \frac{\exp[\tan\phi(\theta - \chi)]\sin\theta - \sin\chi}{\exp[\tan\phi(\upsilon - \chi)]\sin\upsilon - \sin\chi} \tag{6.4}$$

where θ, χ and υ are the angles made by r (or r_c), r_χ and r_υ respectively with a reference axis, (see Figure 6.1), r is the distance between point P and any point on the log-spiral slip surface, r_c is the distance between point P and any point on the crack, r_χ and r_υ are the lengths of the chords P-F and P-D respectively, and ϕ is the angle of shearing resistance of the soil.

(a)   (b)
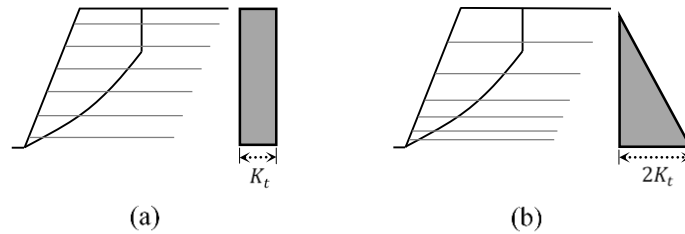
Figure 6.2 Geosynthetic-reinforcement layouts. (a) Uniformly distribution (UD), and (b) Linearly increasing distribution (LID).

The upper bound on the yield acceleration K_y will be derived imposing energy balance for the failing wedge E-D-C-B:

$$\dot{D} = \dot{W} \tag{6.5}$$

where $\dot{D}$ and $\dot{W}$ are the rate of dissipated energy and of external work respectively. In this chapter $\dot{D}$ has four terms as follow:

$$\dot{D} = \dot{Ds}_{C-D} + \dot{Ds}_{B-C} + \dot{Dr}_{C-D} + \dot{Dr}_{B-C} \tag{6.6}$$

where $\dot{Ds}_{C-D}$ and $\dot{Ds}_{B-C}$ are the rates of dissipated energy within the soil along the log-spiral segment (D-C) and along the crack (B-C) respectively. While $\dot{Dr}_{C-D}$ and $\dot{Dr}_{B-C}$ are the rates of dissipated energy within the geosynthetic reinforcement along the log-spiral segment (D-C) and the crack (B-C) respectively. The energy dissipated within the soil, $\dot{Ds}_{C-D}$, along the log-spiral segment (D-C) is (Utili, 2013):

$$\dot{Ds}_{C-D} = c\dot{\theta}r_\chi^2 \exp\left[2\tan\phi(\zeta - \chi)\right]\frac{\exp\left[2\tan\phi(\upsilon - \zeta)\right] - 1}{2\tan\phi}$$

$$\dot{Ds}_{C-D} = c\dot{\theta}r_\chi^2 f_{C-D}(\chi, \upsilon, \zeta, \phi) \tag{6.7}$$

the dissipated energy within the soil $\dot{Ds}_{B-C}$ along the crack can be written as:

$$\dot{Ds}_{(B-C)} = \dot{\theta}r_\chi^2\left(\frac{\sin\chi}{\tan\mu}\right)^2\left(\frac{\sigma_c^{M-C}}{2}\int_\mu^\zeta\frac{1-\sin\theta}{\cos^3\theta}d\theta + \frac{\sigma_t}{1-\sin\phi}\int_\mu^\zeta\frac{\sin\theta - \sin\phi}{\cos^3\theta}d\theta\right) \tag{6.8}$$

with μ: angle made by the segment P-B with the horizontal (see Figure 6.1), σ_c^{M-C} and σ_t^{M-C} being the uniaxial compressive and tensile strength consistent with the M-C criterion respectively, see Figure 5.2 in the previous chapter. According to the Mohr-Coulomb failure criteria, they can be expressed as:

$$\sigma_c^{M-C} = 2c\left(\frac{\cos\phi}{1-\sin\phi}\right) \tag{6.9}$$

$$\sigma_t^{M-C} = 2c\left(\frac{\cos\phi}{1+\sin\phi}\right) \tag{6.10}$$

It is convenient to introduce a dimensionless coefficient, t, defined as the ratio of the

ground tensile strength, σ_t to be measured experimentally, f_t over the maximum

unconfined tensile strength consistent with the M-C criterion, σ_t^{M-C}

$$t = \frac{\sigma_t}{\sigma_t^{M-C}} \tag{6.11}$$

It is straightforward to observe that $0 \le t \le 1$. Now substituting Eq. (*6.9*) and Eq. (*6.10*)

into Eq. (*6.8*), the following expression is obtained:

$$\dot{D}s_{B-C} = c\dot{\theta}r_\chi^2\left(\frac{\sin\chi}{\tan\theta_c}\right)^2\left[\frac{\cos\phi}{1-\sin\phi}\int_{\theta_c}^{\zeta}\frac{1-\sin\theta}{\cos^3\theta}\,d\theta + \frac{2t\cos\phi}{1-\sin^2\phi}\int_{\theta_c}^{\zeta}\frac{\sin\theta-\sin\phi}{\cos^3\theta}\,d\theta\right]$$

$$\dot{D}s_{B-C} = c\dot{\theta}r_\chi^2 f_{B-C}\left(\chi,\upsilon,\zeta,\phi,t\right) \tag{6.12}$$

the third term of the dissipated energy is the one that occurs within the geosynthetic

reinforcement along the log-spiral part, $\dot{D}r_{(C-D)}$. This can be calculated by integrating

the product of the infinitesimal increment of strain rate undergone by the

reinforcement and the tensile strength of the reinforcement T averaged over the

spacing S between consecutive layers of reinforcement (Michalowski and Zhao,

1995). For sake of space, the calculations are herein reported for uniform distribution

(UD) of reinforcement (*i.e. $K=K_t$*) only:

$$dr = \int\limits_{0}^{t/\sin\xi} K\sin\xi\,\dot{\varepsilon}_{x}\,dx = K\sin\xi\,\dot{u}\cos(\xi-\phi) \tag{6.13}$$

with $\dot{\varepsilon}_{x}$: strain rate in the direction of reinforcement, t : thickness of the discontinuity layer, and ξ : angle made by the reinforcement layer with discontinuity surface, which can be written as:

$$\xi = \frac{\pi}{2} - \theta + \phi \tag{6.14}$$

now, by integrating Eq. (*6.13*) over the log-spiral part (C-D),

$$\dot{D}r_{(C\text{-}D)} = \int\limits_{C\text{-}D} K\sin\xi\,\dot{u}\cos(\xi-\phi)\frac{r\,d\theta}{\cos\phi} \tag{6.15}$$

after substituting and simplifying, the following expression is obtained:

$$\dot{D}r_{(C\text{-}D)} = r_{\chi}^{2}\dot{\theta}\int\limits_{\zeta}^{\upsilon} K\left(\begin{array}{l}\exp[2\tan\phi(\theta-\chi)]\sin\theta\cos\theta\,+\\ \sin^{2}\theta\tan\phi\exp[2\tan\phi(\theta-\chi)]\end{array}\right)d\theta \tag{6.16}$$

for uniform distribution of reinforcement (UD), $K = K_{t}$, then:

$$\dot{D}r_{(C\text{-}D)} = K_{t}r_{\chi}^{2}\dot{\theta}\frac{1}{2}\Big[\exp[2\tan\phi(\upsilon-\chi)]\sin^{2}\upsilon - \exp[2\tan\phi(\zeta-\chi)]\sin^{2}\zeta\Big] \tag{6.17}$$

$$\dot{D}r_{(C\text{-}D)} = K_{t}r_{\chi}^{2}\dot{\theta}g_{2}(\chi,\upsilon,\zeta,\phi)$$

the dissipated energy by the reinforcement along the crack B-C has been reported by (Abd & Utili, 2017a). An analytical formula similar to that one presented by (Michalowski, 1997) to calculate the energy dissipated along the log-spiral part C-D is employed. Note that here the angle made by the velocity vector of the ground mass slipping away and the crack, η is different from the soil friction angle, ϕ (see

Figure 6.1). Now using Eq. (*6.15*), but with vertical crack (*i.e.* $\xi = \dfrac{\pi}{2}$) the following expression can be obtained:

$$\dot{D}r_{(B\text{-}C)} = \int_{B\text{-}C} K\,\dot{u}_c \sin\eta\,dh \tag{6.18}$$

With

$$\dot{u}_c = r_c\dot{\theta} = \left(\frac{r_\zeta \cos\zeta}{\cos\theta}\right)\dot{\theta} \tag{6.19}$$

$$dh = \frac{r_c\,d\theta}{\cos\theta} \tag{6.20}$$

with $\dot{u}_c$ the velocity vector along the crack B-C, r_c the distance between point P and any point along the crack B-C, then,

$$\dot{D}r_{(B\text{-}C)} = \dot{\theta}\int_{\mu}^{\zeta} K r_c \sin\theta \frac{r_c\,d\theta}{\cos\theta} \tag{6.21}$$

with μ is the angle made by the line P-B and a horizontal reference.

$$\dot{D}r_{(B\text{-}C)} = r_\chi^2\dot{\theta}\exp\left[2\tan\phi(\zeta - \chi)\right]\cos^2\zeta\int_{\mu}^{\zeta} K \frac{\sin\theta}{\cos^3\theta}\,d\theta \tag{6.22}$$

for uniform distribution of reinforcement (UD), $K = K_t$, then, integration leads to

$$\dot{D}r_{(B\text{-}C)} = K_t r_\chi^2\dot{\theta}\frac{1}{2}\left(\exp\left[2\tan\phi(\zeta - \chi)\right]\sin^2\zeta - \sin^2\chi\right)$$

$$\dot{D}r_{(B\text{-}C)} = K_t r_\chi^2\dot{\theta}\,g_3(\chi,\upsilon,\zeta,\phi) \tag{6.23}$$

The rate of external work for the sliding wedge E-B-C-D, (*i.e.* $\dot{W}$), will be calculated as the work of block E-D-F minus the work of block B-C-F. The work of block E-D-F will be calculated by algebraic summation of the work of blocks P-D-F, P-E-F and

P-D-E (Chen, 1975) that are here called $\dot{W}_1$, $\dot{W}_2$ and $\dot{W}_3$ respectively. The work of

block B-C-F will be calculated by algebraic summation of the work of blocks P-C-F,

P-B-F and P-C-B that are here called $\dot{W}_4$, $\dot{W}_5$ and $\dot{W}_6$ respectively. So, $\dot{W}$ can be

calculated from the following summation:

$$\dot{W} = \dot{W}_1 - \dot{W}_2 - \dot{W}_3 - \left(\dot{W}_4 - \dot{W}_5 - \dot{W}_6\right) = \dot{W}_1 - \dot{W}_2 - \dot{W}_3 - \dot{W}_4 + \dot{W}_5 + \dot{W}_6 \qquad (6.24)$$

In (Utili, 2013), the expressions for $\dot{W}_1$, $\dot{W}_2$, ..., etc. are derived for each block by

calculation of the vectorial product of the displacement rate, u, of the block (see

Figure 6.1) times its weight force. Here instead, in addition to the weight force, a

horizontal pseudo-static force, $F_h = MK_h g = \gamma K_h A$, with g being the gravitational

acceleration and M the mass of the wedge, and a vertical one, $F_v = MK_v g = \gamma K_v A$, are

added to account for seismic action. For sake of space, only the final expressions are

reported here:

$$\dot{W}_1 = \dot{\theta} \gamma r_\chi^3 \left[\left(1 + k_v\right) f_{1v}\left(\chi, \upsilon, \phi\right) + k_h f_{1h}\left(\chi, \upsilon, \phi\right)\right]$$

$$= \dot{\theta} \gamma r_\chi^3 \begin{bmatrix} \left(1 + K_v\right) \dfrac{\exp\left[3\tan\phi\left(\upsilon - \chi\right)\right]\left(3\tan\phi\cos\upsilon + \sin\upsilon\right) - 3\tan\phi\cos\chi - \sin\chi}{3\left(1 + 9\tan\phi^2\right)} + \\[2em] K_h \dfrac{\exp\left[3\tan\phi\left(\upsilon - \chi\right)\right]\left(3\tan\phi\sin\upsilon - \cos\upsilon\right) - 3\tan\phi\sin\chi + \cos\chi}{3\left(1 + 9\tan\phi^2\right)} \end{bmatrix} \qquad (6.25)$$

with $\dot{\theta}$ being the rate of angular displacement of the failing, wedge E-B-C-D. For

block P-E-F instead:

$$\dot{W}_2 = \dot{\theta} \gamma r_\chi^3 \left[\left(1 + K_v\right) f_{2v}\left(\chi, \upsilon, \phi\right) + K_h f_{2h}\left(\chi, \upsilon, \phi\right)\right]$$

$$= \dot{\theta} \gamma r_\chi^3 \left[\left(1 + K_v\right) \frac{L_1}{6r_\chi} \sin\chi \left(2\cos\chi - \frac{L_1}{r_\chi}\right) + K_h \frac{L_1}{3r_\chi} \sin^2\chi\right] \qquad (6.26)$$

for block P-D-E:

$$\dot{W}_3 = \dot{\theta}\gamma r_\chi^{\ 3}\left[\left(1+K_v\right)f_{3v}\left(\chi,\upsilon,\phi\right)+K_h f_{3h}\left(\chi,\upsilon,\phi\right)\right]$$

$$= \dot{\theta}\gamma r_\chi^{\ 3}\begin{pmatrix}\dfrac{(1+K_v)}{6}\exp\left[\tan\phi(\upsilon-\chi)\right]\left(\sin(\upsilon-\chi)-\dfrac{L_1}{r_\chi}\sin\upsilon\right)\\[2mm]\left(\cos\chi-\dfrac{L_1}{r_\chi}+\exp\left[\tan\phi(\upsilon-\chi)\right]\cos\upsilon\right)+\\[2mm]\dfrac{K_h}{6}\exp\left[\tan\phi(\upsilon-\chi)\right]\left(\sin(\upsilon-\chi)-\dfrac{L_1}{r_\chi}\sin\upsilon\right)\\[2mm]\left(\sin\chi+\exp\left[\tan\phi(\upsilon-\chi)\right]\sin\upsilon\right)\end{pmatrix} \tag{6.27}$$

for block P-C-F:

$$\dot{W}_4 = \dot{\theta}\gamma r_\chi^{\ 3}\left[\left(1+K_v\right)f_{4v}\left(\chi,\upsilon,\phi\right)+K_h f_{4h}\left(\chi,\upsilon,\phi\right)\right]$$

$$= \dot{\theta}\gamma r_\chi^{\ 3}\begin{bmatrix}(1+K_v)\dfrac{\exp\left[3\tan\phi(\zeta-\chi)\right]\left(3tan\phi\cos\zeta+\sin\zeta\right)-3tan\phi\cos\chi-\sin\chi}{3\left(1+9tan^2\phi\right)}+\\[3mm]K_h\dfrac{\exp\left[3\tan\phi(\zeta-\chi)\right]\left(3tan\phi\sin\zeta-\cos\zeta\right)-3tan\phi\sin\chi+\cos\chi}{3\left(1+9tan^2\phi\right)}\end{bmatrix} \tag{6.28}$$

for block P-B-F:

$$\dot{W}_5 = \dot{\theta}\gamma r_\chi^{\ 3}\left[\left(1+K_v\right)f_{5v}\left(\chi,\upsilon,\phi\right)+K_h f_{5h}\left(\chi,\upsilon,\phi\right)\right]$$

$$= \dot{\theta}\gamma r_\chi^{\ 3}\left[\left(1+K_v\right)\dfrac{L_2}{6r_\chi}\sin\chi\left(2\cos\chi-\dfrac{L_2}{r_\chi}\right)+K_h\ \dfrac{L_2}{3r_\chi}\sin^2\chi\right] \tag{6.29}$$

for block P-C-B:

$$\dot{W}_6 = \dot{\theta}\gamma r_\chi^3 \left[\left(1+K_v\right) f_{6v}\left(\chi,\upsilon,\phi\right) + K_h f_{6h}\left(\chi,\upsilon,\phi\right) \right]$$

$$= \dot{\theta}\gamma r_\chi^3 \left[\begin{array}{l} \dfrac{\left(1+K_v\right)}{3}\exp\left[2\tan\phi(\zeta-\chi)\right]\cos^2\zeta\left(\exp\left[\tan\phi(\zeta-\chi)\right]\sin\zeta - \sin\chi\right) + \\[2mm] \dfrac{K_h}{6}\exp\left[\tan\phi(\zeta-\chi)\right]\cos\zeta\left(\exp\left[2\tan\phi(\zeta-\chi)\right]\sin^2\zeta - \sin^2\chi\right) \end{array} \right] \quad (6.30)$$

substituting Eq. (*6.6*) and Eq. (*6.24*) with their components into Eq. (*6.5*), the following expression is obtained:

$$c\dot{\theta}r_\chi^2\left(f_{B-C} + f_{C-D}\right) + K_t r_\chi^2 \dot{\theta}\left(g_2 + g_3\right)$$
$$= \dot{\theta}\gamma r_\chi^3 \left[\begin{array}{l} \left(1+K_v\right)\left(f_{1v} - f_{2v} - f_{3v} - f_{4v} + f_{5v} + f_{6v}\right) \\[1mm] + K_h\left(f_{1h} - f_{2h} - f_{3h} - f_{4h} + f_{5h} + f_{6h}\right) \end{array} \right] \quad (6.31)$$

Now, let us introduce the ratio of vertical to horizontal acceleration, λ as $\lambda = K_v/K_h$. Consistently with Figure 6.1, the $+$ sign indicates vertical downward acceleration, while the $-$ sign indicates vertical upward acceleration. An upper bound on the coefficient of yield acceleration, K_y, is obtained by solving Eq. (*6.31*) with respect to K_h:

$$K_y = \frac{\left[\dfrac{c}{\gamma H}\left(f_{B-C} + f_{C-D}\right) + \dfrac{K_t}{\gamma H}\left(g_2 + g_3\right)\right] - \dfrac{r_\chi}{H}\left(f_{1v} - f_{2v} - f_{3v} - f_{4v} + f_{5v} + f_{6v}\right)}{\dfrac{r_\chi}{H}\left[\begin{array}{l} \lambda\left(f_{1v} - f_{2v} - f_{3v} - f_{4v} + f_{5v} + f_{6v}\right) \\[1mm] + \left(f_{1h} - f_{2h} - f_{3h} - f_{4h} + f_{5h} + f_{6h}\right) \end{array} \right]} \quad (6.32)$$

$$K_y = f_y\left(\chi,\upsilon,\zeta,\phi,\frac{c}{\gamma H},\frac{K_t}{\gamma H},\beta,\lambda,t\right)$$

The global minimum of $f_y\left(\chi,\upsilon,\zeta,\phi,c/\gamma H,\beta,\lambda,t\right)$ over the three geometrical variables χ,υ,ζ provides the least upper bound on the coefficient of yield acceleration assuming that the most unfavourable crack for the slope is present. Results obtained using Eq. (*6.32*) are presented in Figure 6.3 and Figure 6.4 for geosynthetic-reinforced

and unreinforced cases respectively, providing the two terms needed to find the proposed stepwise yield acceleration for soil slopes with either zero tensile strength (*i.e.* $t = 0$) or half the maximum unconfined tensile strength of the Mohr-Coulomb criterion (*i.e.* $t = 0.5$). The solid lines in Figure 6.3 and Figure 6.4 refer to slopes that are initially intact but they can exhibit cracks forming as part of the incipient failure mechanism, while the dashed lines are for slopes with earthquake induced cracks (*i.e.* the formed crack is treated here as an open crack).

The stepwise yield acceleration, proposed in this chapter, can be found using these two lines (*i.e.* solid and dashed), where for a given soil slope properties, two values of yield acceleration are obtained. The one obtained from the solid line represents the starting value of the yield acceleration, which steps down to the value obtained from the dashed line as soon as exceeded for the first time by the applied acceleration, given by the earthquake record. It can be seen that the two lines (solid and dashed) in Figure 6.4 are close to each other, that is because the depth of the formed crack within reinforced soil is relatively shallow, especially for gentle slopes. The definition of the stepwise yield acceleration is detailed by an illustrative example later in this chapter. It also should be noted that failure passes below the slope toe was not permitted during the calculations for these charts. This type of failure might occur for gentle slope with low angle of shearing resistance (You & Michalowski, 1999).

6.4 Calculations of the Seismic Displacement

The maximum horizontal displacement of the slope face occurs at the slope toe (Chang et al., 1984). This displacement is denoted here as δu_x (see Figure 6.5). Based on

Newmark's method, the rate of δu_x can be calculated as follow (You & Michalowski, 1999):

$$\delta u_x = r_\upsilon \sin\upsilon \delta\theta = r_\upsilon \sin\upsilon \int\limits_{\delta t}\int\limits_{\delta t} \ddot{\theta}\, dt\, dt = C\int\limits_{\delta t}\int\limits_{\delta t}\left(K_i - K_y\right)g\, dt\, dt \tag{6.33}$$

where $\delta\theta$ is the angular displacement $\ddot{\theta}$ is the angular acceleration K_i is the applied horizontal coefficient of acceleration at step i, and C is a dimensionless coefficient that relates the displacement of the slope toe to the integral of the earthquake acceleration record above the level of yield acceleration. Performing the calculations, this coefficient can be expressed as:

$$C = \frac{\gamma r_\chi^4 \exp\left[\tan\phi(\upsilon - \chi)\right]\sin\upsilon \begin{bmatrix} \lambda\left(f_{1v} - f_{2v} - f_{3v} - f_{4v} + f_{5v} + f_{6v}\right) + \\ \left(f_{1h} - f_{2h} - f_{3h} - f_{4h} + f_{5h} + f_{6h}\right) \end{bmatrix}}{Gl^2} \tag{6.34}$$

with G being the weight of the potential sliding mass and l is the distance from point P to the centre of gravity of that mass. The calculations for G and l are listed in Appendix C. To this end, the seismic induced displacements can be calculated using Eq. (*6.33*) by assigning an earthquake record and calculating the yield acceleration for the slope of interest.
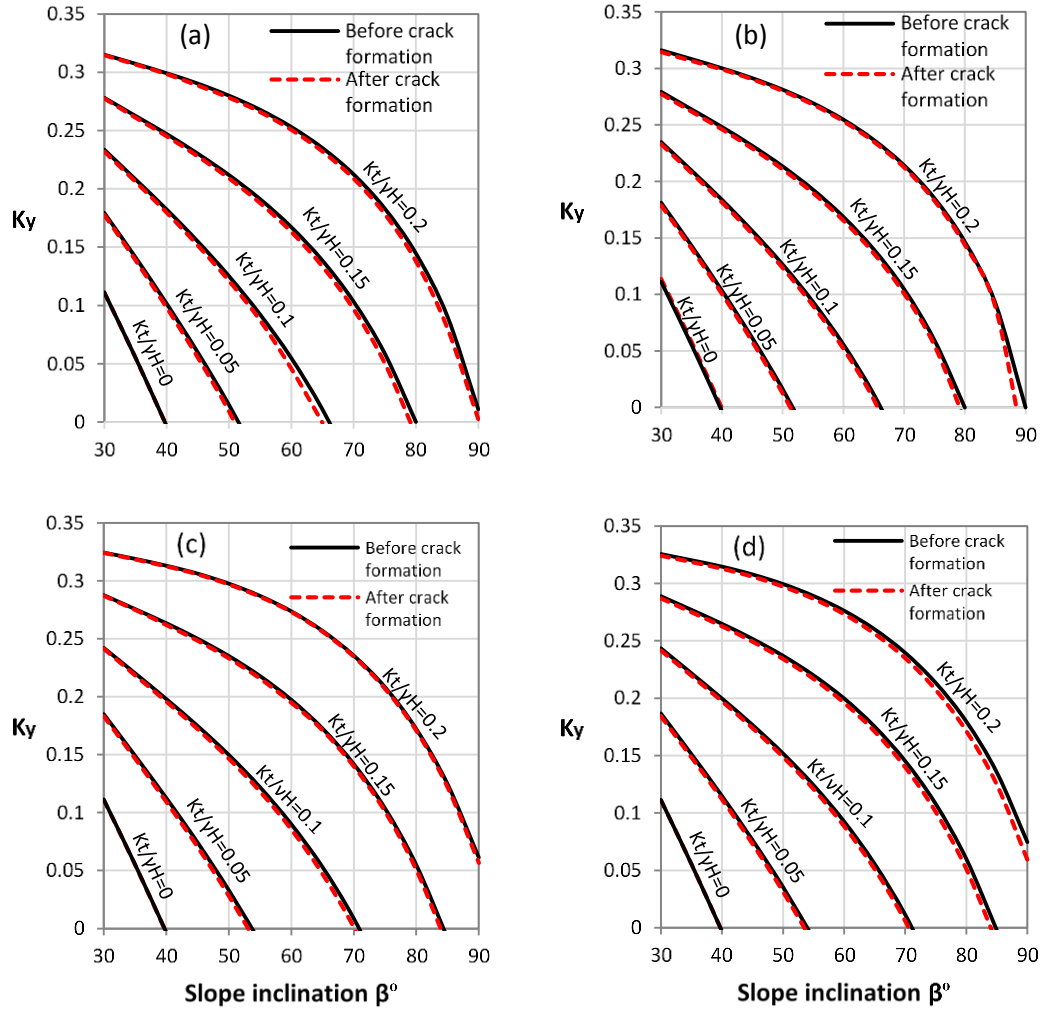
Figure 6.3 Yield horizontal acceleration for $\phi = 20°$, $c/\gamma H = 0.05$ and $\lambda = 0$. (a and b) for uniform distribution of reinforcement and (c and d) for linearly increasing distribution. Left hand side charts are for soil slopes with zero tensile strength while the right hand side are for soil slopes with limited tensile strength (i.e. half of Mohr-Coulomb's tensile strength).
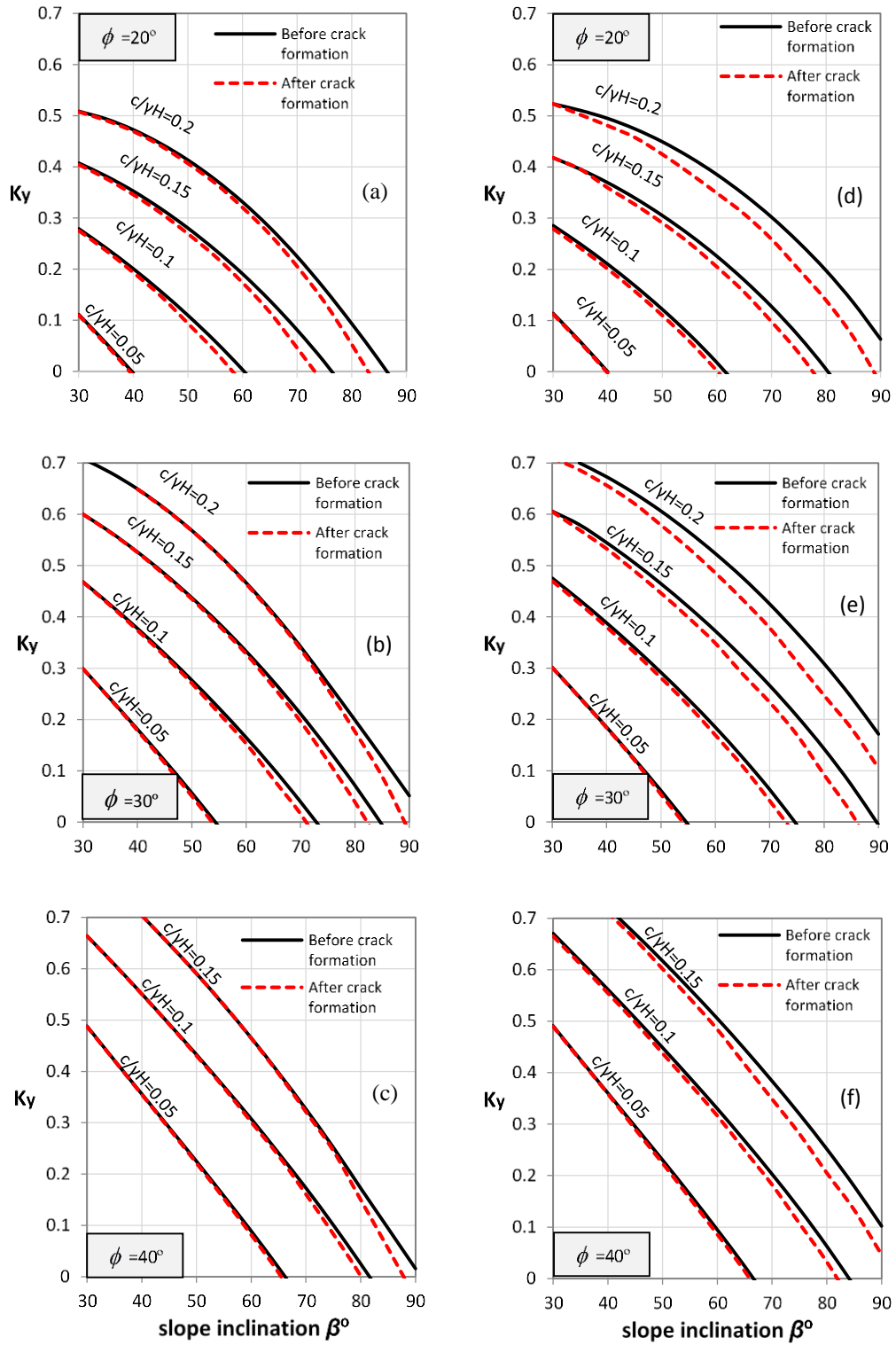
Figure 6.4 Yield horizontal acceleration for uniform distribution of reinforcement with zero vertical acceleration. Left hand side charts (a), (b) and (c) are for soil slopes with zero tensile strength while (d), (e) and (f) are for soil slopes with limited tensile strength (i.e. half of Mohr-Coulomb's tensile strength).

127
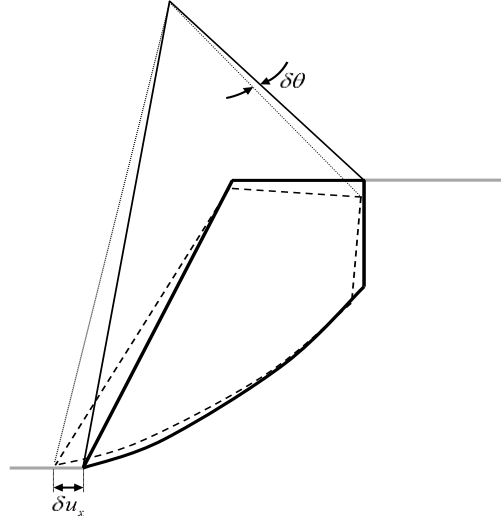
Figure 6.5 Illustration of the horizontal displacement at the slope toe and the angular displacement $\delta\theta$.

6.5   Illustrative Examples

First, unreinforced soil slope with $\beta = 70°$, $\phi = 20°$ $\lambda = 0$ and $c/\gamma H = 0.15$ and second,

geosynthetic-reinforced soil slope with $\beta = 75°$, $\phi = 20°$, $c/\gamma H = 0.1$, $\lambda = 0$, and

$K_t/\gamma H = 0.1$. Both subjected to the Northridge earthquake (1994), whose main

characteristics are listed in table 1. Four cases are analysed: case (I) soil slope with

full tensile strength, (*i.e.* $t = 1$), therefore not subject to tension cracks, case (II) soil

slope of limited tensile strength, in this case $t = 0.5$, case (III) soil slope of zero tensile

strength, (*i.e.* $t = 0$), and case (IV) soil slope subjected to the most adverse pre-existing

crack.

For unreinforced case, and according to the procedure mentioned earlier in this chapter, the stepwise yield acceleration for soil with limited or zero tensile strength is illustrated in Figure 6.6a. It can be noticed that the yield acceleration for a soil slope with limited tensile strength is reduced significantly when it is exceeded for the first time by the applied acceleration. This is because the crack formed as part of the failure at that instance, is then treated as a pre-existing one. Consequently, this could increase the estimated displacement as shown in Figure 6.6b.

As the displacement corresponding to a slope with the most detrimental pre-existing crack seems over conservative, at the same time, assuming an intact slope that remains intact during the earthquake may underestimate the displacement. However, assuming limited tensile strength for the soil slope can be adopted to bridge the gap between the conservatism, corresponding to a slope with the most detrimental pre-existing crack, and the underestimation of the displacement when ignoring the crack formation (*i.e.* intact slope). Figure 6.6c provides an insight as to the way the limited tensile strength could change the crack properties and the orientation of the failure mechanism.

For geosynthetic-reinforced case, Figure 6.7 compares yield acceleration, displacement and failure mechanism between slope with UD of reinforcement, and with LID of reinforcement. It is noticed that slope with LID has better performance than the same slope with UD. The yield acceleration seems less affected by the presence of crack, whether earthquake-induced or pre-existing crack. Consequently, the total horizontal displacement of the slope reinforced with LID less than UD's one.
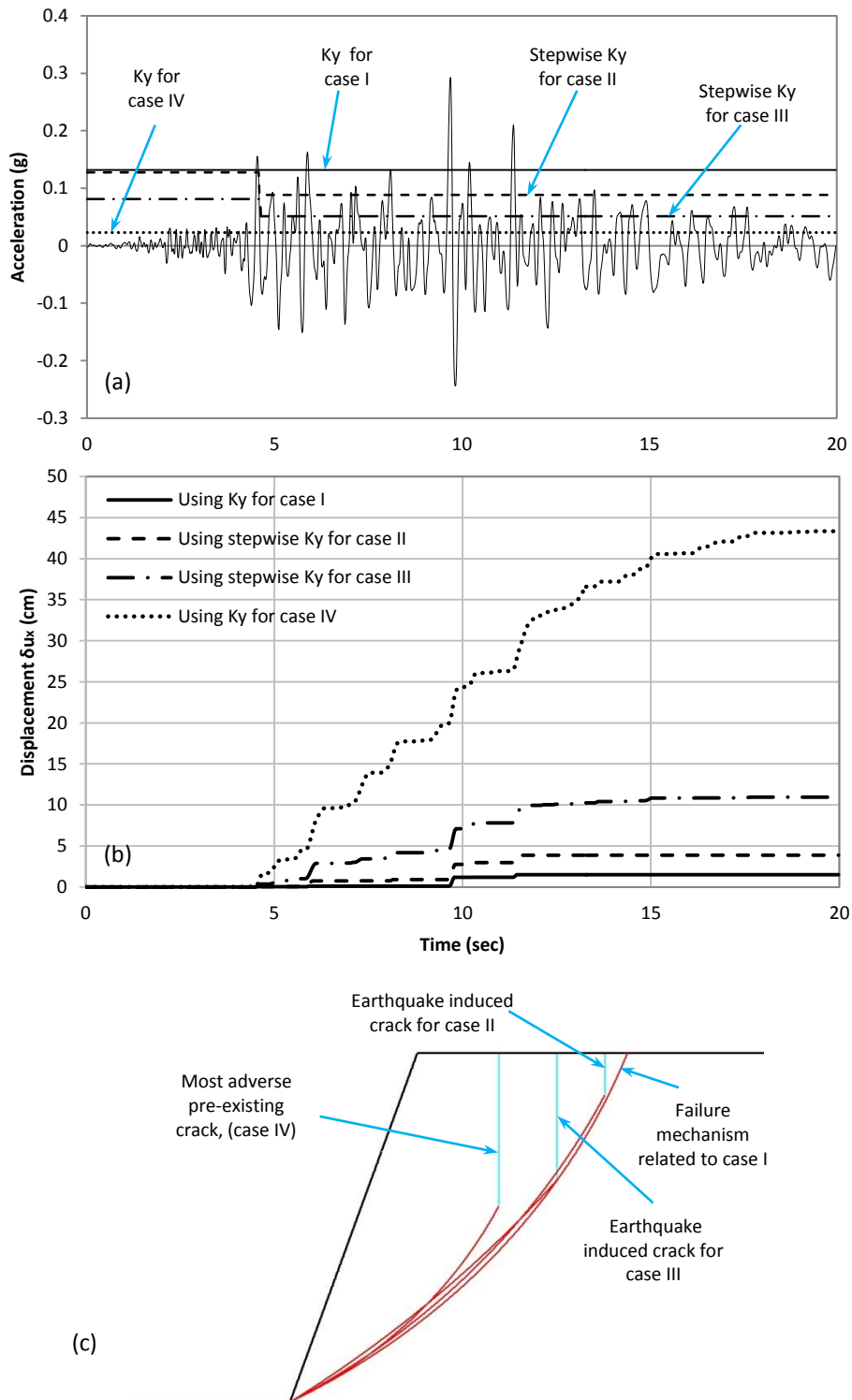
Figure 6.6 Slope with $\beta = 70°, \phi = 20°$ *and* $c/\gamma H = 0.15$ *. (a) Illustration of the calculated yield for the four cases considered employing the Northridge earthquake (1994) as seismic input. (b) Accumulated horizontal displacement at the slope toe, for the four cases considered. (c) Failure mechanisms associated with the calculated yield accelerations.*
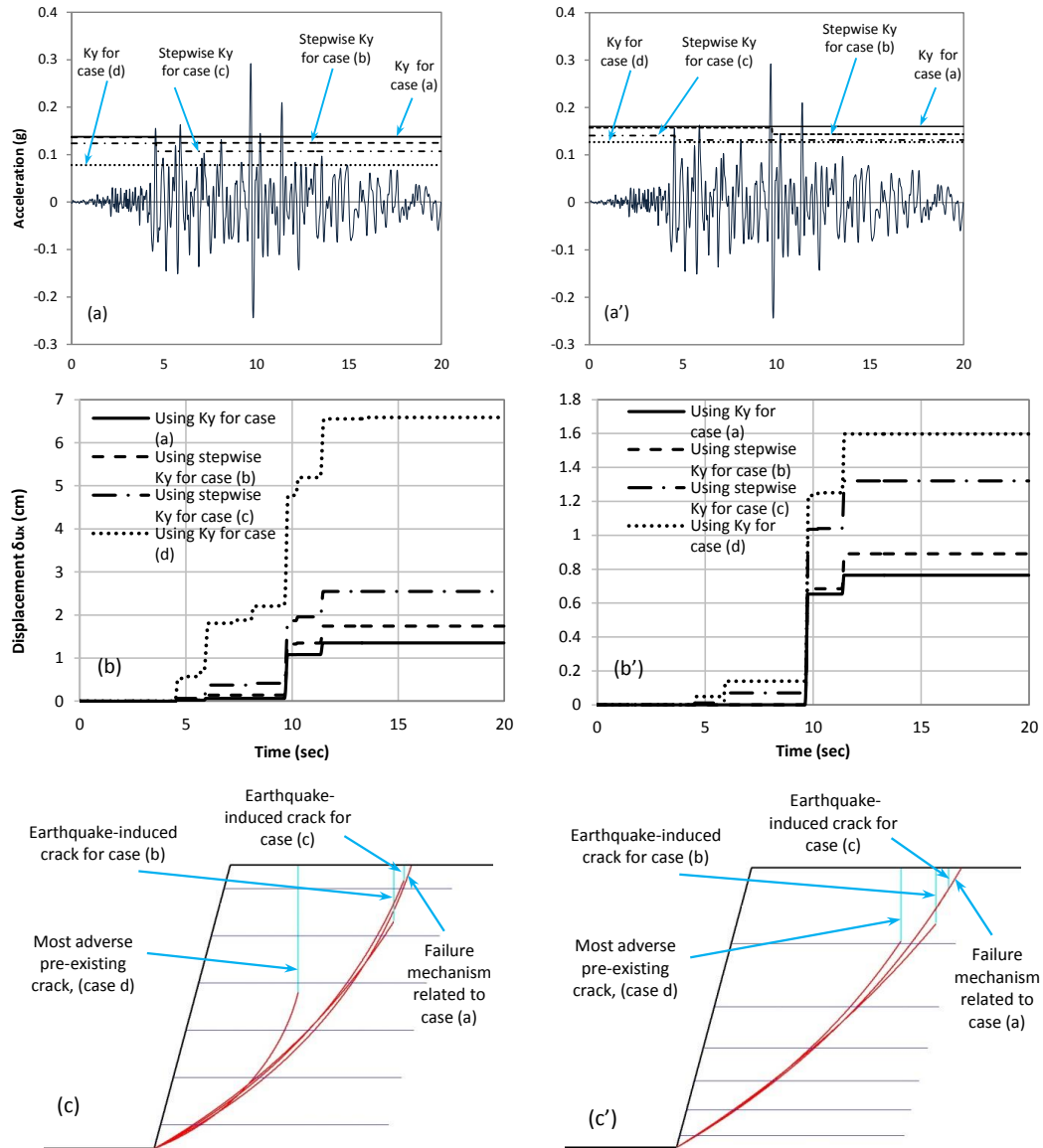
Figure 6.7 Yield accelerations, horizontal displacement (δux) and failure mechanisms for a slope with $\beta = 75°$, $\phi = 20°$ and $c / \gamma H = 0.1$ and $K_t / \gamma H = 0.1$. Left hand side is for uniform distribution of reinforcement while the right hand side is for linearly increasing distribution of reinforcement. (a and a') Yield accelerations corresponding to the four cases explained earlier employing Northridge earthquake (1994). (b and b') Comparison of the accumulated horizontal displacement of the slope toe. (c and c') Failure mechanisms related to the yield accelerations illustrated in (a and a').

Table 6.1 Main characteristics of the earthquakes considered in the example case.

Date	17/1/1994
Station	24283 Moorpark - Fire Sta.
Magnitude	6.7
Direction	180º
Peak acceleration (g)	0.292
Epicentre distance (km)	23

6.6   Conclusions

The upper bound theorem of limit analysis together with the pseudo static approach were employed to evaluate the displacements of cohesive frictional slopes subject to the formation of tension cracks. The formation of earthquake-induced tension cracks and their effect on the displacements were considered. The assumption of the stepwise yield acceleration can be used to reasonably bridge the gap between the conservatism corresponding to a slope with the most detrimental pre-existing crack, and the underestimation of the displacement when ignoring the crack formation throughout the analysis. Four cases were considered here: intact slopes of the highest unconfined tensile strength, intact slopes of limited tensile strength, intact slopes with no tensile strength, and slopes subject to cracks pre-existing the seismic event. Charts providing the values needed to calculate the stepwise yield acceleration are presented. It is noticed that slope with LID has better performance than the same slope with UD. The yield acceleration seems less affected by the presence of crack, whether earthquake-induced or pre-existing crack. Consequently, the total horizontal displacement of the slope reinforced with LID less than UD's one.

Chapter 7: Geosynthetics Layout Optimization for Reinforced Soil Slopes Subject to Cracks[5]

SUMMARY

The upper bound theorem of limit analysis is employed to investigate the effect of pre-existing cracks on the design length and distribution of geosynthetic layers in reinforced soil slopes. Two reinforcement layouts are used: uniform and linearly increasing distribution along the slope height. Compound failure mode involving pull-out in some layers and tension failure (rupture) in others are considered. Results show that slopes with pre-existing cracks require longer reinforcement layers than intact ones. It emerges that for both intact and fissured slopes, a linearly increasing distribution of reinforcement yields better results than a uniform one.

7.1 Introduction

The use of geosynthetics has been proven by many researchers to be a cost-effective method to stabilize soil structures, *e.g.* (Richard A. Jewell, 1991; D. Leshchinsky et al., 1995; Michalowski, 2002). The design guidelines for reinforced earth structures conservatively assume cohesion-less soil, see *e.g.* (Berg et al., 2009). However, fine-grained soils exhibiting non-negligible cohesion might be used as fill material. On one

---

[5] This chapter has been published in the *Procedings of the 12th International Symbosium on Landslides*, Napoli, Italy, (see Abd and Utili 2016)

hand, cohesion contributes to slope stability, but at the same time, cracks can develop in cohesive soils decreasing the beneficial effect of cohesion on slope stability. Cracks develop in cohesive slopes for different reasons, such as exceedance of the ground tensile strength (Rafael Baker, 1981), occurrence of differential settlements, desiccation and freezing (Hales & Roering, 2007). For unreinforced c-ϕ (cohesive-frictional) slopes, it has been shown that the presence of cracks can significantly reduce the stability of a slope subjected to seismic action (Abd, 2015a; Utili & Abd, 2016) as well as slopes under static conditions (Rafael Baker, 1981; Michalowski, 2013; Utili, 2013; G. Zhang, Wang, Qian, Zhang, & Qian, 2012). For geosynthetic reinforced slopes, the presence of cracks requires increased reinforcement as presented in previous chapters and leads to increased seismic displacements (Abd, 2015b).

Here, cracks are treated as no-tension non-cohesive perfectly smooth (no friction) interfaces; therefore, no energy is ever dissipated along a crack and the angle θ is 0°< θ < 180°. (Michalowski, 2013) has provided a limit analysis upper bound formulation for vertical cracks that are absent prior to the formation of the failure mechanism but instead form simultaneously with the onset of the failure mechanism in an initially intact slope because of the soil tensile strength being exceeded at the same time as the log-spiral surface D-C is formed (see Figure 7.1). However, cracks generated as part of the failure mechanism taking place are always less detrimental (critical) to slope stability than cracks pre-existing the formation of the slope failure mechanism, because they require energy to be dissipated for their formation which instead is not the case for pre-existing cracks (Michalowski, 2013). Therefore, in this chapter, only the presence of (more critical) pre-existing cracks is considered. Also, it will be

assumed that the most adverse scenario in terms of presence of cracks in the slope takes place, *i.e.* the most adverse possible crack for the stability of the slope will be assumed to exist. This conservative assumption reflects the fact that often neither the position nor the depth of the cracks present in the slope are known.

Figure 7.1 Log-spiral failure mechanism for reinforced slope with pre-existing crack and linearly decreasing length of reinforcement.

The length of geosynthetics layers can be calculated according to (Gao et al., 2016; H. I. Ling & Leshchinsky, 1998; Michalowski, 1997, 1998). All these studies assume cohesion-less soil and reinforcement of equal length. In this chapter, however, cohesive soil is examined and the possibility of a linearly decreasing length of reinforcement along the slope height is considered, in the search for a more economical design.

Geosynthetics layers within reinforced slopes are subject to three main possible failure modes (Michalowski, 1997): reinforcement rupture, pull out failure, and direct

sliding. Reinforcement rupture occurs when the tensile stress within geosynthetic layer exceeds its tensile strength. Pull-out failure happens when the effective length of reinforcement behind the slip surface (see L_e in Figure 7.1) is insufficient to resist the axial stresses acting within the reinforcement layer. Finally, direct sliding occurs when the reinforced mass slides along the lowest layer of geosynthetic reinforcement (not considered in this study). In this chapter, rupture failure is assumed to calculate the required reinforcement, while a combined (rupture and pull-out) failure is assumed to assess the effect of the cracks on the design length of reinforcement.

7.2 Length of reinforcement

The effect of pre-existing (*i.e.* open) cracks and cracks that form as part of the failure mechanism on the length of reinforcement layers is investigated. To calculate the minimum length of the reinforcement layers, a combined failure mode consisting of pull-out in some layers and rupture (tensile failure) in others, needs to be considered. The normalised length of reinforcement, L_r / H, is calculated following the procedure set by (Michalowski, 1997) extended to the case of $c - \phi$ soil slopes and accounting for the presence of cracks. Assuming all layers are of the same length, it turns out to be:

$$\frac{L_r}{H} = \begin{bmatrix} \dfrac{L_{ei}}{H} - \left(\cos\upsilon + \sin\upsilon\cot\beta\right)\dfrac{r_\chi}{H}\exp[\tan\phi\left(\upsilon - \chi\right)] + \\ \left(\cos\theta_i + \sin\theta_i\cot\beta\right)\dfrac{r_\chi}{H}\exp\left[\tan\phi\left(\theta_i - \chi\right)\right] + \dfrac{L_{si}}{H} - \dfrac{L_{ci}}{H} \end{bmatrix} \qquad (7.1)$$

with L_{ei}/H being the effective (*i.e.* anchorage) length of reinforcement (see Figure 7.1) yet to be calculated, θ_i being the angle related to the intersection between the failure surface and the layer *i,* and L_{si} the length of reinforcement to be saved (see Figure 7.1). L_{si} is calculated as:

$$\frac{L_{si}}{H} = \frac{(z_i - z_1)}{H}(\cot \beta - \cot \beta') \tag{7.2}$$

with z_1 = depth of the uppermost reinforcement layer measured from slope crest, β = slope inclination angle, β' = angle defining how the length of reinforcement decreases with depth.

L_{ci} being part of the length of reinforcement as illustrated in Figure 7.1a. Trigonometry dictates that for a reinforcement layer crossing the crack:

$$\frac{L_{ci}}{H} = \frac{r_\chi}{H}\exp\left[\tan \phi(\theta_i - \chi)\right]\cos \theta_i - \exp\left[\tan \phi(\zeta - \chi)\right]\cos \zeta \tag{7.3}$$

whereas for any reinforcement layer below the crack tip $L_{ci} = 0$. L_{ei}/H is determined from the following equation (Michalowski, 1997):

$$\frac{K_t}{\gamma H} = \frac{\left[\begin{array}{c}\left(\dfrac{r_\chi}{H}\right)^2(f_1 - f_2 - f_3 - f_4 + f_5 + f_6 + f_w) - \left(\dfrac{r_\chi}{H}\right)\dfrac{c}{\gamma H}(g_1 + g_2) - \\[2ex] 2f_b \tan \phi \sum_{i=1}^{j}\dfrac{z_i^*}{H}\dfrac{L_{ei}}{H}\left(\sin \chi + \dfrac{z_i}{r_\chi}\right)\end{array}\right]}{\dfrac{1}{n}\sum_{i=j+1}^{n}\left(\sin \chi + \dfrac{z_i}{r_\chi}\right)} \tag{7.4}$$

with $K_t / \gamma H$ determined from the semi-analytical method expounded in the previous chapter, and recalled in Eq. (7.5) below, and; j being the number of layers pulled out; z_i^* being the overburden depth of reinforcement layer i which for gentle slopes it can be less that the depth z_i of the reinforcement layer below the slope crest, f_b the bond coefficient between soil and reinforcement and n, the number of reinforcement layers.

$$\frac{K_t}{\gamma H} = \frac{\left(f_1 - f_2 - f_3 - f_4 + f_5 + f_6 + f_w\right)}{\dfrac{H}{r_\chi}\left(g_3 + g_4\right)} - \frac{c}{\gamma H}\left(\frac{g_1 + g_2}{g_3 + g_4}\right)$$
$$= f\left(\chi, \upsilon, \zeta, \beta, \gamma_w / \gamma, \phi, c / \gamma H, t\right)$$

(7.5)

7.2.1 Reinforcement layers of equal length

An optimization procedure is carried out to find the maximum value of L_r over the variables $\left(\chi, \upsilon, \zeta\right)$ for an example slope with $n = 6$. f_b was taken as 0.6 according to the latest report from the U.S. Federal Highway Administration (Berg et al., 2009). The results, presented in Figure 4.10, show that in case of the most adverse pre-existing crack being present the largest anchorage length is required and the higher the soil tensile strength the shorter the required reinforcement length (*i.e.* the case of $t = 1$ requires less anchorage length than $t = 0$). This is true for both reinforcement distributions considered. This finding is not surprising recalling from previous sections of the chapter the fact that the case of the most adverse pre-existing crack being present is the most critical one for slope stability and the higher the soil tensile strength is the less a slope is prone to tension cracking.

(a)

(b)
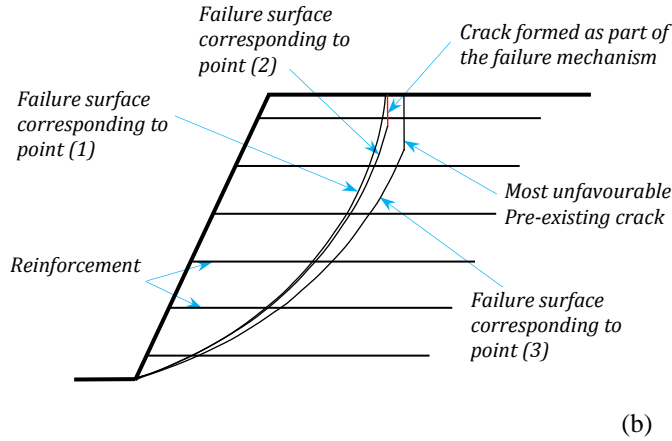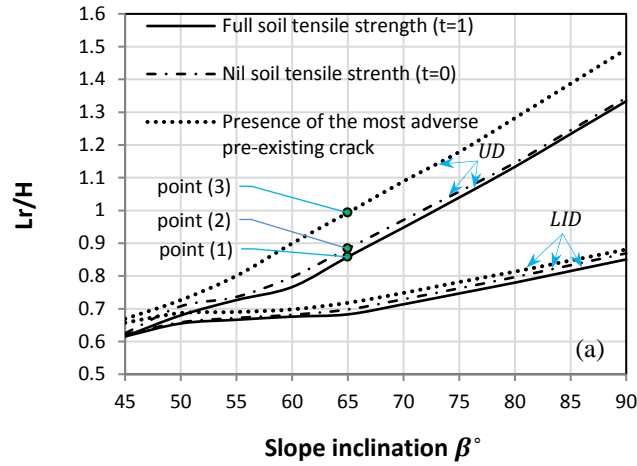
Figure 7.2 (a) Length of reinforcement versus slope inclination for a slope with $\phi = 20°$, $c / \gamma H = 0.05$ and $r_u = 0$. (b) Failure mechanisms for a slope with $\beta = 65°$ and uniform distribution of reinforcement: 1) case of intact slope not subject to crack formation (high tensile strength); 2) case of intact slope subject to crack formation (limited tensile strength); and 3) case of slope with a pre-existing crack.

7.2.2 Reinforcement layers of varied length

Let us now consider a linearly decreasing length of reinforcement along the slope height. The length of the upper layer is assumed to be the same as that found in the case of uniform length of reinforcement (*i.e.* the case in which all layers have the same length). The length of reinforcement layers that obtained earlier (see the

previous section) is assigned for the first upper most layer and kept constant, then the minimum angle β' (see Figure 7.1) reducing the length of all subsequent layers is sought accounting for all possible failure mechanisms (*i.e.*, pull-out and/or rupture). For example, the failure mechanism may involve the first layer(s) to be pulled out or by passed by the failure mechanism while the rest of the layers fail in tension. The results are illustrated in Figure 7.3: it emerges that the adoption of a uniform distribution of reinforcement leads to larger savings on the length of reinforcement than the case of linearly increasing reinforcement distribution.
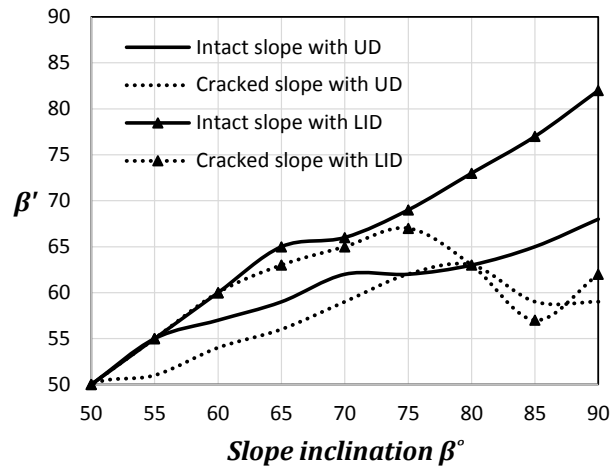
Figure 7.3 Slope inclination angle β versus β' for φ=20˚, c/γH=0.05, comparing intact slopes and slopes subjected to the most adverse pre-existing crack. UD and LID mean uniform distribution and linearly increasing distribution of reinforcement respectively.

7.3 Conclusions

The effect of the design length and distribution of geosynthetics on the stability of reinforced soil slopes exhibiting cracks which either pre-existing the onset of the slope failure mechanism or forming as part of the failure mechanism was investigated. The results here presented are preliminary and further study is required to check the lengths

of reinforcement here determined against failure for direct sliding which has not been considered in the study. The results show that the presence of cracks leads to larger lengths of reinforcement, and for steep slopes. The linearly decreasing length with depth can be implemented regardless of the presence of cracks providing more economical design. Moreover, comparing a uniform distribution of reinforcement with a linearly increasing distribution in case of fissured slopes, it is found that longer reinforcement layers are required when a uniform distribution is adopted.

Chapter 8: Optimal Shape Profiles for the Design of Geosynthetic-Reinforced Slopes[6]

SUMMARY

Currently geosynthetic-reinforced slopes are designed as straight profiles and a maximum of three tiers (and benches) is employed for multi-tiered walls. In this study, a numerical procedure based on the limit analysis upper bound method together with optimisation genetic algorithm is proposed to determine multi-linear profiles of optimal shapes for geosynthetic-reinforced slopes. Optimal shapes are here defined as those associated to the least possible amount of reinforcement required to keep the slope stable. The method provides an optimal profile for a prescribed average slope inclination, backfill strength properties and desired number of layers to be used. Two configurations for reinforcement layout are considered: uniform distribution and linearly increasing distribution with depth.

Second the potential saving from the use of the optimal profiles are investigated first for static then for seismic conditions with seismic action being accounted by employing pseudo-static forces. Results show saving on the level of reinforcement of up to 50% on the traditional straight profiles and 37% on concave circular profiles recently proposed by (Vahedifard et al., 2016a) for the same average slope inclination,

---

i.e. the same slope height and distance from toe to crest. Several stability charts illustrating the savings on the required amount of reinforcement are provided for the benefit of designers. Also it is shown that less volume of excavation is required when the optimal profiles are adopted.

8.1 Introduction

Currently georeinfroced slopes are designed according to a straight profile in elevation. However, in nature slope profiles exhibit all sorts of different shapes, ranging from concave to convex or partly convex and partly concave, see Figure 8.1. The literature on the mechanical stability of non-straight slope profiles is very limited: A.W. Jenike and B.C. Yen (1962) presented slope stability analyses in axial symmetry based on the slip-line theory formulated by Sokolovskiĭ (1960). Hoek and Bray (1981) argued that concave slopes in rock are more stable than convex slopes but they did not produce any systematic investigation to underpin their claim.

Figure 8.1 Photo taken north of Iraq shows the natural concave-convex profile.

With regard to geosynthetic reinforced slopes, recent research on multi-tiered reinforced walls seem to indicate that reinforced slopes of non-straight profile can be more stable than the traditional straight ones (Dov Leshchinsky & Han, 2004; Liu et al., 2014; G.-Q. Yang et al., 2014), but the geometric configuration considered are limited to a maximum of four walls (Stuedlein et al., 2010) and more importantly the studies do not compare the mechanical performance of non-straight profiles with the performance of straight profiles of the same average inclination so no firm conclusions can be drawn. In case of unreinforced slopes instead, better performance of concave profiles over straight profiles of the same average inclination has been systematically proved by (Utili & Nova, 2007) for concave profiles of log-spiral shape for cohesive frictional geomaterials. Then, (Jeldes et al., 2014; Vahedifard et al., 2016b)) considered concave profiles whose shape is derived from Sokolovski's theory of slip-lines and (Vahedifard et al., 2016b) concave circular profiles both showing superior properties to straight profiles in terms of mechanical stability. In (Vahedifard et al., 2016a) the performance of non straight (circular) concave profiles is systematically compared to the performance of reinforced slopes of the same average inclination made of frictional backfills. They show that circular concave profiles are always better from a stability point of view and conclude that saving of up to 30% on the required tensile strength of the reinforcement can be achieved. Unlike previous studies in this study, the search for the optimal profile will not be restricted to a particular category of shapes, *i.e.* circular or log-spiral or from Sokolovski's slip lines, but any possible shape will be considered to achieve the most economical possible design. The theoretical formulation adopted and the optimisation numerical algorithms employed are described in detail in (Utili & Wu, 2017).

8.2 Problem formulation

Aim of the formulation is to find the minimum required strength/amount of reinforcement for a load-free cohesion-less soil structure with horizontal upper surface and resting on a firm foundation. Two reinforcement layouts are included: uniform and linearly increasing distribution with depth, as illustrated in Figure 8.2. The tensile strength and amount of geosynthetic reinforcement is encapsulated as K_t which can be written as:

$$K_t = \frac{nT}{H} \tag{8.1}$$

with n the number of reinforcement layers, T the strength of a single layer at yielding point and H the height of the soil structure.
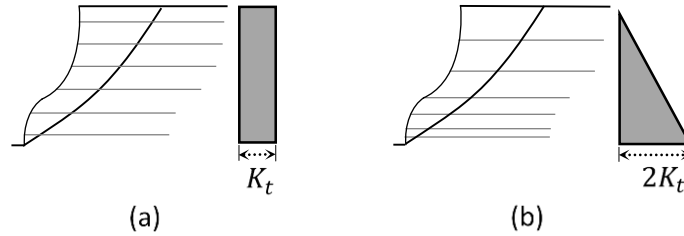
Figure 8.2 Geosynthetic-reinforcement layouts. (a) Uniformly distribution (UD), and (b) Linearly increasing distribution (LID) with depth.

A generic profile is discretized into *m+1* segments using *m* points with each point P_i has a constant height measured from the slope toe equal to *(i).H/ (m+1)* where *H* is the height of the soil structure. For each point P_i (see Figure 8.3), the x-coordinate x_i is allowed to vary between pre-defined lower and upper limits as shown in Figure 8.4. The crest and toe points are specified. By fixing these two points, the

average slope inclination $\beta = arctan\dfrac{H}{L}$ is prescribed. No other geometrical constraint

on the slope profile is imposed. Another constraint is applied to avoid highly unlikely

profiles (*e.g.* profiles with overhanging parts). Given the possible configurations of

these points, numerous profiles can be generated. By increasing *m* the discretization

of the slope profile becomes more refined. In order to seek the optimal profile, under

the constraint of fixed crest and toe, by changing x_i on each horizontal line, slopes

with different shapes are to be examined. Among all candidate profiles, the optimal

one provides the highest stability, which corresponds to the minimum amount of

reinforcement to maintain the slope stable.

Figure 8.3 Failure mechanism for multi-linear face profile.

According to the limit analysis upper bound theorem, the minimum amount of

reinforcement to keep the slope stable can be found by equating the external energy

rate done by the soil weight and external loads to the internal dissipation rate due to reinforcement strength. The potential failing part $(Q - P_0 - P_1 - P_2 ... P_{m+1})$ (see Figure 8.3) is assumed to rotate around point O in a log-spiral failure surface, which has the following equation:

$$r = r_\chi \exp\left[\tan\phi\left(\theta - \chi\right)\right] \tag{8.2}$$

where θ and χ are the angles made by r and r_χ respectively with the horizontal axis, r is the distance between the spiral centre, point O, and a generic point on the log-spiral slip surface, and r_χ is the length of the chord $O - R$. It should be noted that the log-spiral failure mechanism might no longer be the most critical failure mechanism for the current problem. However, this is beyond the scope of this study.
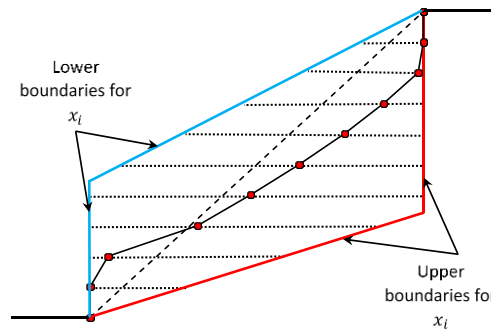
Figure 8.4 Illustration of the lower and upper boundaries used for horizontal distance x_i which measured from the structure's toe.

The (best) lower bound to the required reinforcement can be derived from the following energy balance equation:

$$\dot{D} = \dot{W} \tag{8.3}$$

where $\dot{D}$ and $\dot{W}$ are the internal energy dissipation rate and the external work rate respectively. The only component for $\dot{D}$ is $\dot{D}r_{(P_0 - Q)}$ being the energy rates dissipated along the log-spiral part $P_0 - Q$ by the reinforcement (see Figure 8.3). This energy rate can be calculated by integrating the product of the infinitesimal increment of reinforcement strain rate with the reinforcement tensile strength, T, averaged over the slope height. The following expression is obtained (Zhao, 1996):

$$\begin{aligned}\dot{D}r_{(P_0 - Q)} &= \frac{1}{2} K_t \dot{\theta} r_\chi^2 \left[exp \left[2 \tan \phi (\upsilon - \chi) \right] sin^2 \upsilon \right] \\ &= K_t \dot{\theta} r_\chi^2 f_r (\chi, \upsilon, \phi) \end{aligned} \tag{8.4}$$

where $\dot{\theta}$ is the angular velocity of the sliding part, υ is the angle made by r_υ with a horizontal reference.

The rate of external work $\dot{W}_{ext}$ for the sliding part $(Q - P_0 - P_1 - P_2 \ldots P_{m+1})$ is calculated as the work of block $O - Q - P_0$ minus the work of block $O - Q - P_{m+1}$ minus the algebraic summation of the work of blocks $\sum_{i=1}^{m+1} (O - P_{i-1} - P_i)$.

To account for the seismic action, in addition to the weight force, a horizontal pseudo-static force is added, $F_{PSh} = MK_h g = \gamma K_h A$, with M being the mass of the wedge, K_h the coefficient of horizontal seismic acceleration and g the gravitational acceleration. The calculation of the expressions for $\dot{W}_{ext}$ for each block is provided in (Utili & Abd, 2016) except for blocks $\sum_{i=1}^{m+1} (O - P_{i-1} - P_i)$. Here the final expression is recalled:

$$\dot{W}_{ext} = \dot{\theta} r_\chi^3 \left[\begin{array}{c} \left(f_{1v} - f_{2v} - f_{3v} - f_{4v} + f_{5v} + f_{6v} \right) + \\ K_h \left(f_{1h} - f_{2h} - f_{3h} - f_{4h} + f_{5h} + f_{6h} \right) \end{array} \right] \tag{8.5}$$

with $f_{1v}, f_{2v}, \ldots, f_{6v}$ and $f_{1h}, f_{2h}, \ldots, f_{6h}$ are functions accounting for the external work

done by the vertical (*i.e.* soil weight) and horizontal (*i.e.* seismic) forces respectively.

The final expressions can be found in Appendix A of (Utili & Abd, 2016) except for

f_{3v} and f_{3h}. As it can be seen in Figure 8.3, the work done by the block

$\left(O - P_0 - P_1 - P_2 \ldots P_{m+1} \right)$ can be obtained from the summation of the work done by the

blocks $\sum_{i=1}^{m+1} \left(O - P_{i-1} - P_i \right)$, this can be expressed as follow:

$$\dot{W}_{3v} = \dot{\theta} \gamma r_\chi^3 \sum_{i=1}^{m+1} \frac{C_i \cos \theta_i + C_{i-1} \cos \theta_{i-1}}{3} \left(\frac{A_i}{r_\chi^3} \right) = \dot{\theta} \gamma r_\chi^3 f_{3v} \left(\chi, \upsilon, \beta, m, x_i \right) \tag{8.6}$$

$$\dot{W}_{3h} = \dot{\theta} \gamma r_\chi^3 \sum_{i=1}^{m+1} \frac{C_i \sin \theta_i + C_{i-1} \sin \theta_{i-1}}{3} \left(\frac{A_i}{r_\chi^3} \right) = \dot{\theta} \gamma r_\chi^3 f_{3h} \left(\chi, \upsilon, \beta, m, x_i \right) \tag{8.7}$$

with *m*: number of points used to discretize the profile, C_i is the length of the chord

OP_i (see Figure 8.3) and can be expressed as:

$$C_i = \sqrt{ \left(r_\chi \exp \left[\tan \phi (\upsilon - \chi) \right] \sin \upsilon - \frac{i}{m+1} H \right)^2 + \left(r_\chi \exp \left[\tan \phi (\upsilon - \chi) \right] \cos \upsilon + x_i \right)^2 } \tag{8.8}$$

$$\theta_i = \frac{r_\chi \exp \left[\tan \phi (\upsilon - \chi) \right] \cos \upsilon + x_i}{C_i} \tag{8.9}$$

A_i: Area of the segment $O - P_{i-1} - P_i$ can be expressed as:

149

$$A_i = \frac{1}{2}\left[C_i.C_{i-1}.\sin\left(\theta_{i-1} - \theta_i\right) \right]$$ (8.10)

Substitution of the various energy rate contributions calculated into the energy balance Eq. (*8.3*), provides the "fitness" function to be optimized which leads to determine the required reinforcement $K_t / \gamma H$:

$$\frac{K_t}{\gamma H} = \frac{\left[\begin{array}{c} \left(f_{1v} - f_{2v} - f_{3v} - f_{4v} + f_{5v} + f_{6v} \right) \\ +K_h \left(f_{1h} - f_{2h} - f_{3h} - f_{4h} + f_{5h} + f_{6h} \right) \end{array} \right]}{\dfrac{H}{r_\chi}\left(f_r \right)}$$ (8.11)

$$\frac{K_t}{\gamma H} = f\left(\chi, \upsilon, \beta, \phi, K_h, m, x_i \right)$$

The minimum of the right hand side of Eq. (*8.11*) provides lower bound to the required reinforcement for a given profile shape.

For the current problem, it is also necessary to check the possibility of failure mechanism passing above the structure's toe because the failing mass for the failure mechanism passing above the toe is no longer similar in shape to the one passing through the toe. Hence, a constrained is applied such that the obtained "optimal" profile has no above the toe failure more critical than the toe one. It should be noted that it is very likely to have some above the toe failure mechanisms require exactly the same amount/tensile strength of reinforcement to the one corresponding to the toe failure. The required reinforcement for every possible failure surface $P_i - Q_i$ (see Figure 8.5) are compared to the required reinforcement corresponding to the failure mechanism passing through the toe point P_o. This constraint can be expressed as:

$$\left(\frac{K'_t}{\gamma h_i} \right) \cdot \frac{h_i}{H} \leq \frac{K_t}{\gamma H} \tag{8.12}$$

with $K' = \dfrac{n'T}{h_i}$, n' : number of reinforcement layers involved in the failure, and h_i :

the depth of the point i measured from the crest point P_{m+1} (see Figure 8.5).
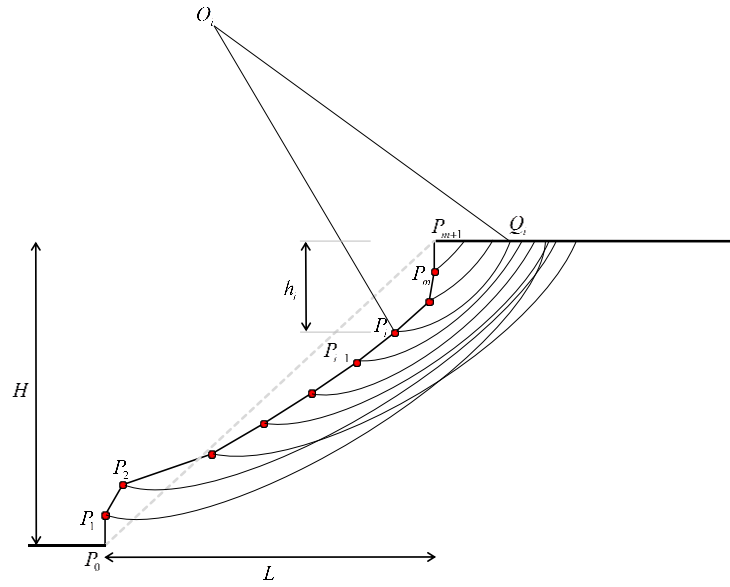
Figure 8.5 . Failure mechanisms passing above the structure's toe.

8.3   Optimisation algorithms

Genetic algorithms (GA) are optimization tools based on the evolution theory of natural selection that can solve both constrained and unconstrained problems. Genetic algorithms have become increasingly popular in the geotechnical community in the last two decades (Andrab, Hekmat, & Yusop, 2017). With regard to slope stability GA are mainly used to find the critical failure surface in soil slopes (*e.g.* (Goh, 1999; Sengupta & Upadhyay, 2009; Sun, Li, & Liu, 2008; Zolfaghari, Heath, & McCombie,

2005). (Utili & Wu, 2017) used genetic algorithm and pattern search, another optimization tool, to find the optimal profiles for slopes made of frictional cohesive geomaterials.

Genetic algorithm simply defines a population size; randomly choose individuals to be parents to form children for the next generation then applying crossover and mutation to produce subsequent generations until the fittest individual is found, Figure 8.6 presents a simplified flowchart of the algorithm.
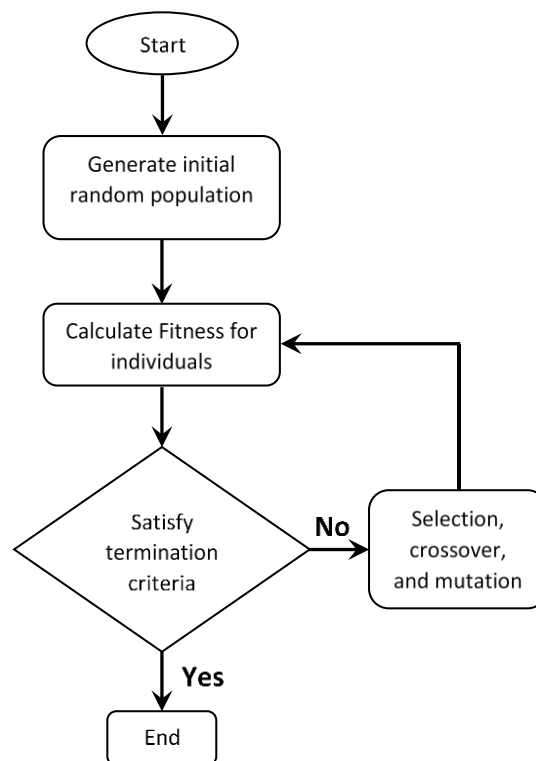
Figure 8.6 Simplified flowchart for genetic algorithm.

8.4   Results

Results of the obtained multi-linear profile and the corresponding required reinforcement are presented for a range of toe-crest line inclination β, discretising the height of the reinforced soil structures into 11 segments (*i.e.* 10 points). The results are obtained for soil structures reinforced with either uniform distribution (UD) or linearly increasing distribution (LID) of reinforcement. It should be noted that secondary reinforcement are assumed sufficient to prevent local failure at the face. In other words, to avoid shallow collapse between any of the two consecutive main reinforcement layers, secondary reinforcement has been reported by (Michalowski, 2000).

The difference in required reinforcement among planar, concave, and the current multi-linear profile is presented in Figure 8.7. It can be seen that using multi-linear profile instead of the conventional planar can make significant savings (*e.g.* up to 50%) on the required reinforcement. The dashed line in Figure 8.7a represents the results obtained from (Vahedifard et al., 2016a) for concave (*i.e.* circular arc) profile for $\phi = 30°$ and $40°$. It emerges that the current multi-linear profile is clearly better than the concave profile. For example, if $\beta = 50°$, $\phi = 40°$ concave profile can decrease the required reinforcement by 22.1% while the current multi-linear profile can decrease it by 50%. This means that for static case, the current multi-linear profile can decrease the required reinforcement obtained for concave profile by up to 36%.
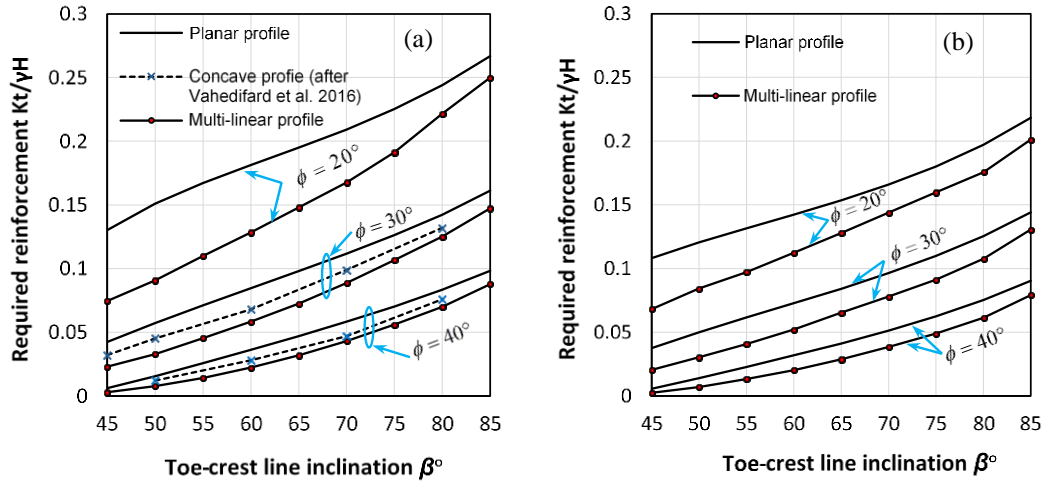
Figure 8.7 Difference in required reinforcement among planar, multi-linear and concave profile. (a) For uniform distribution of reinforcement. (b) For linearly increasing distribution of reinforcement.

The multi-linear profile is more effective (*i.e.* requires relatively less reinforcement) than the planar profile especially for gentle inclination and high angle of internal friction. This might be because gentle slopes allow more flexibility to shape the multi-linear profile besides gentle slope with high ϕ already require very little reinforcement that can be redundant when applying the multi-linear profile.

The shape of obtained multi-linear profile are presented in Figure 8.8, and Figure 8.9. It can be seen that the obtained profiles are smooth which can contribute to the aesthetic of the structure when completed. Also, it can be noticed that the obtained profiles are generally concave-convex rather than pure concave. This make sense because the active stress represented by the potential driving mass is minimized while the passive pressure generated by the convex near the structure's toe is maximized, bearing in mind the applied constraints.

The higher the angle of internal friction ϕ the less the degree of curvature and the more the similarity between profiles obtained from (UD) and (LID). However, profiles with LID seem to be less dependent on the passive pressure that comes from the

convex near the structure's toe because it has more reinforcement localized there providing the required support.

It can be seen that profiles with $\phi = 20°$ have higher curvature for the upper part of the slope, especially for uniform distribution of reinforcement. This can be attributed to fact that soil with low friction angle requires more reinforcement, which in turn provides lateral support leading to a steeper upper part of the structure.
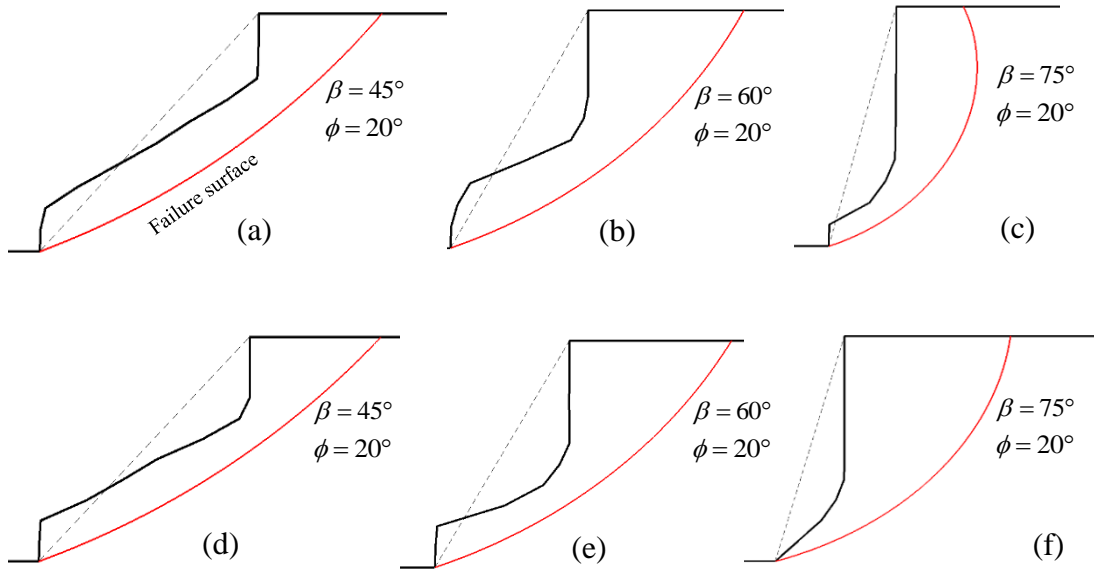
Figure 8.8 The obtained multi-linear profiles using 10 points (i.e. 11 segments) with the corresponding critical failure surfaces for $\phi = 20°$. (a), (b), and (c) are for uniform distribution of reinforcement with $\beta = 45°, 60°,$ and $75°$ respectively. similarly for (d), (e), and (f) but for linearly increasing distribution.
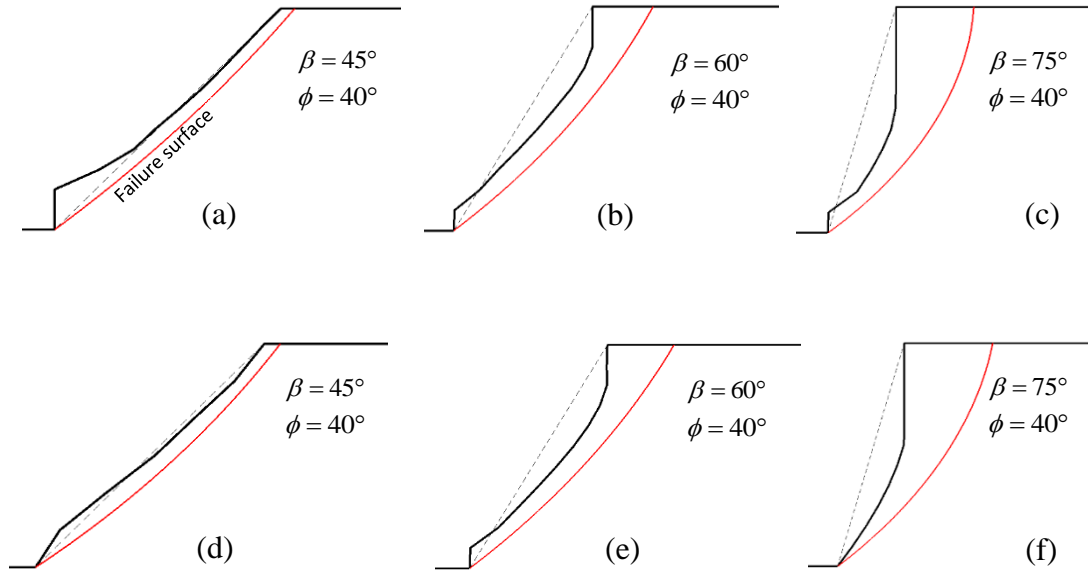
Figure 8.9 The obtained multi-linear profiles using 10 points (i.e. 11 segments) with the corresponding critical failure surfaces for $\phi = 40°$. (a), (b), and (c) are for uniform distribution of reinforcement with $\beta = 45°, 60°$, and $75°$ respectively. Similarly for (d), (e), and (f) but for linearly increasing distribution.

By calculating the failing area corresponding to multi-linear and planar profile, it can be concluded that potential failing volume associated with the multi-linear profile (see Figure 8.8 and Figure 8.9) is generally less than that for planar (apart from the case of $\beta = 45°$ and $\phi = 40°$). This might implie shorter embedding length of reinforcement layers and consequently less excavation works during construction. However, the length of the reinforcement for multi-linear profiles is beyond the scope of this study. The reason behind the unusual failure surface in Figure 8.8c is that the centre of rotation (*i.e.* point O) lies below the structure's crest. Consequently, the contribution of the reinforcement layers that lie above the centre of rotation is neglected, as they cannot sustain compressive stresses (Michalowski, 1997).

The normalised coordinates for the obtained profiles are listed in Appendix (F) as for uniform and linearly increasing distribution of reinforcement respectively.

Geotechnical designers can use these profiles as a benchmark to perform further numerical investigation depending on the problem at hand.

8.5 Seismic acceleration

Pseudo-static approach is employed here to model the effect of seismicity on the required reinforcement corresponding to either the multi-linear profile obtained earlier for static case or corresponding to a tailored profile obtained for the given seismic level. Figure 8.10 compares the required reinforcement between planar, and multi-linear profiles for different values of the horizontal seismic coefficient K_h and two values of toe-crest line inclination β. The figure also compares the required reinforcement between uniform and linearly increasing distribution of reinforcement. It can be easily seen from Figure 8.10a that the higher the level of horizontal acceleration the more the savings in required reinforcement when the seismic-tailored multi-linear profile is used. It also can be seen that the multi-linear profile corresponding to static case performs steadily when increasing the horizontal seismic acceleration by keeping the same difference in the required reinforcement from that of the conventional planar profile. Similar trend can be seen for soil structures with linearly increasing distribution of reinforcement Figure 8.10b but for less overall required reinforcement.
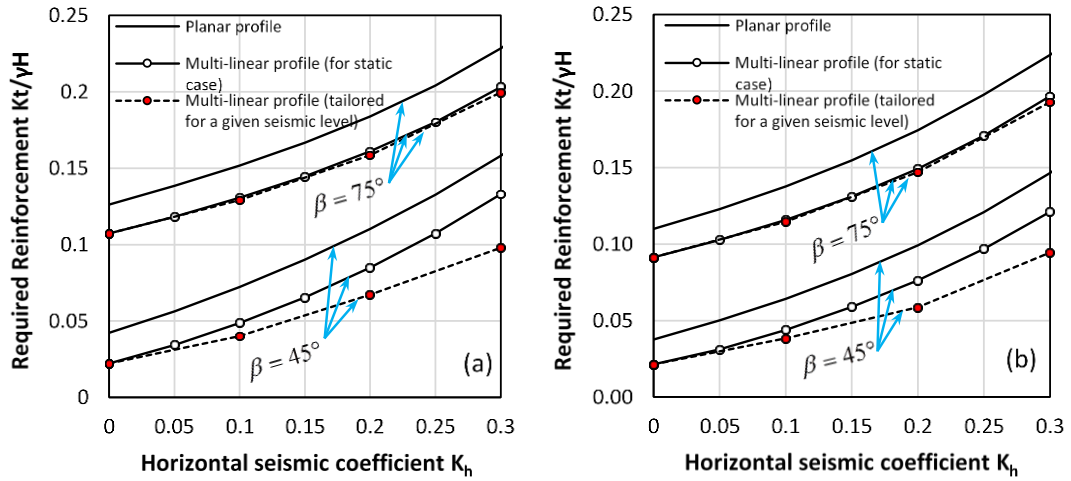
Figure 8.10 Planar versus multi-linear profile when subjected to pseudo static horizontal acceleration, for $\phi = 30°$. (a) For uniform distribution of reinforcement and (b) for linearly increasing distribution.

Results of the concave (*i.e.* circular arc) profile (Vahedifard et al., 2016a) that tailored for a given level of seismic action is compared in terms of the required reinforcement with the current multi-linear profile obtained for either static case and then subjected to seismic action or tailored specifically for a given seismic acceleration, see Figure 8.11. It can be seen that the multi-linear profile for static case and the one tailored for a given seismic level can decrease the required reinforcement obtained using circular-concave profile by up to 26% and 37% respectively. It should be noted that the value of $K_h = 0.5$ is extremely high, but for the sake of comparison it is included here.
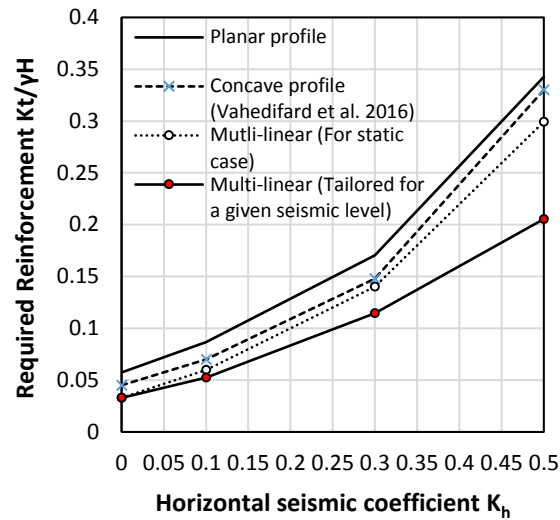
Figure 8.11 Multi-linear profile versus concave profile when subject to pseudo static horizontal acceleration, for and uniform distribution of reinforcement.

8.6 Conclusions

The potential for savings from the adoption of non-straight profiles for georeinforced slopes under both static and seismic conditions is investigated. Results show saving on the level of reinforcement of up to 50% on the traditional straight profiles and 37% on concave circular profiles recently proposed by (Vahedifard et al., 2016a) for the same average slope inclination, *i.e.* the same slope height and distance from toe to crest. Several stability charts illustrating the savings on the required amount of reinforcement are provided for the benefit of designers. Also tables containing the normalised coordinates for multi-linear profiles are provided.

   In the presence of seismic action, the non-straight profile optimised under static (gravity) load and the one obtained for a given level of seismicity are both found better than the straight profile as they can decrease the required reinforcement obtained from concave profile by up to 14.5% and 37% respectively. Profiles of optimal performance

for a prescribed level of seismic action are found to be particularly effective for the case of gentle profiles and high seismic excitation. Optimisation under seismic action is recommended for average inclination less than $60°$ (*i.e.* $\beta < 60°$) otherwise, the optimal profile obtained for the static case performs similarly.

The optimal non-straight slope profiles proposed here provide an ideal optimum but construction constraints may present the realisation of such optimum. However, the value of these profiles and more in general of a formulation allowing to calculate the optimal profiles for any given number of geosynthetic layers or tier wall as input is to provide a benchmark case against which the performance of various less optimal solutions can be measured. Finally it is worth noting that the optimal profiles not only require less reinforcement in comparison with straight profiles but it can improve the aesthetic of the structure too.

Chapter 9: Conclusions and Recommendations

9.1 Conclusions

This thesis has covered several points, among them: 1) Investigating the effect of pre-existing and forming cracks on the stability and displacement of unreinforced and geosynthetically-reinforced soil slopes subject to seismic action.2) Presenting a new semi-analytical method for the design of geosynthetic-reinforcement in cohesive backfills 3) Introducing the "step-wise" yield acceleration to account for cracks during estimating the earthquake-induced displacement. 3) Coming up with linearly decreasing length of reinforcement that can reduce the earth works during slope construction. Finally, 4) Enhancing the current methods for engineered slopes by obtaining the "optimal" shape of profile for geosynthetic-reinforced soil structure subject to seismic action.

From the analysis of unreinforced soil slopes that subject to seismic action, it can be concluded that the presence of cracks can reduce stability and yield acceleration by up to 30% in comparison with the case of intact slope. The amount of reduction depends on both the geometrical characteristics of the slope and the ground strength parameters: the reduction is higher for steep slopes of low friction angle ϕ subject to high accelerations, whereas for gentle slopes of high angle of shearing resistance ϕ subject to moderate earthquakes it is negligible. Vertical seismic acceleration is found to be as important as the horizontal one. Upward vertical acceleration can be detrimental and maps showing in which case this can happen is provided.

A new semi-analytical method for the design of geosynthetic-reinforcement in cohesive backfills was presented. The method, derived using the kinematic approach of limit analysis, provides the amount of required reinforcement as a function of slope inclination and of three soil strength parameters: angle of shearing resistance, cohesion, and tensile strength. and that cracks are often significantly detrimental to slope stability so they cannot be overlooked in the design calculations of the reinforcement. Also the method takes into account the presence of cracks which are a very common occurrence in cohesive soils. Cracks cannot be overlooked since may have a significant detrimental effect on the stability of the slopes. Lower bounds on the required level of reinforcement were determined and presented in the form of design charts. Various hydraulic scenarios were investigated as well.

It is shown that: I) the presence of cohesion allows achieving a less conservative design so that significant savings on the overall level of reinforcement can be made; II) there are several situations where the presence of cracks reduces significantly the stability of the reinforced slopes so that in general they cannot be neglected in the stability analysis performed to design the amount of reinforcement required; III) there are situations where the tensile strength of the ground, which rules the depth of the tension cracks forming in the reinforced slope, has a significant influence on slope stability, for instance with high levels of cohesion and angle of shearing resistance.

Design charts were presented which provide lower bounds on the required level of geosynthetic reinforcement as a function of slope inclination, soil strength parameters (angle of shearing resistance, cohesion, and tensile strength) and level of seismic pseudostatic acceleration.

The main findings emerging from these design charts are that i) seismic action affects gentler slopes to a much greater extent than steep slopes so that even for high levels of cohesions the reinforcement required for stability may be significantly higher; ii) seismic action tends to reduce the influence of pre-existing cracks on slope stability since the performance of slopes subject to strong earthquakes tends to be dominated by the intensity of the seismic acceleration rather than the presence or absence of cracks ; iii) the effect of seismic action is larger on LID reinforced slopes than on UD reinforced ones.

The assumption of the stepwise yield acceleration can be used to reasonably bridge the gap between the conservatism corresponding to a slope with the most detrimental pre-existing crack, and the underestimation of the displacement when ignoring the crack formation throughout the analysis. Charts providing the values needed to calculate the stepwise yield acceleration are presented. It is noticed that slope with LID has better performance than the same slope with UD. The yield acceleration seems less affected by the presence of crack, whether earthquake-induced or pre-existing crack. Consequently, the total horizontal displacement of the slope reinforced with LID less than UD's one.

The effect of the design length and distribution of geosynthetics on the stability of reinforced soil slopes exhibiting cracks which either pre-existing the onset of the slope failure mechanism or forming as part of the failure mechanism, was investigated. The results show that the presence of cracks leads to larger lengths of reinforcement, and for steep slopes, this amount of the extra required reinforcement length is independent of slope inclination. The linearly decreasing length with depth can be implemented

regardless the presence of cracks providing more economical design. Moreover, comparing a uniform distribution of reinforcement with a linearly increasing distribution in case of fissured slopes, it is found that longer reinforcement layers are required when a uniform distribution is adopted.

Finally, the upper bound theorem of limit analysis along with genetic algorithm (GA) are used to seek the optimal multi-linear profile for geosynthetic-reinforced soil structures using log-spiral failure mechanism. Results of the proposed method show that the obtained profile can decrease the required reinforcement by up to 37% and 50% in comparison with the concave and conventional planar profiles respectively. As expected, the required reinforcement of soil structures with multi-linear profile and linearly increasing distribution of reinforcement is found to be less than that of the corresponding uniform distribution of reinforcement. Tables contain the normalised coordinates for multi-linear profiles are provided. Geotechnical designers can use these profiles as a benchmark to conduct further numerical investigation. To sum up, multi-linear profile can be used to increase the stability of reinforced structure under static and pseudo static loading. The obtained multi-linear profile is compared with circular concave profiles and found to be more effective as it requires less reinforcement. Seismically customised profiles are recommended for toe-crest line inclination less than 60° (*i.e.* $\beta < 60°$) otherwise, the corresponding multi-linear profile obtained for static case would perform similarly. The application of multi linear profile could reduce the volume of excavation works during construction, and finally, it can add aesthetic touch to the structures when completed.

9.2   Recommendations

Here, a list of suggestions for future research is presented:

1- Conduct experimental work to validate further the new semi-analytical and numerical methodologies presented in chapters 3, 4 and 8. This work is likely to involve tests in geotechnical centrifuge, shaking table and 1g tests on down-scaled models.

2- Another future direction of research would be to perform 3D LA upper bound analyses accounting for the effect of cracks fissured unreinforced and geosynthetic-reinforced slopes subject to seismic action. However, it is worth recalling that the 2D upper bounds provided in the thesis are the most critical values since according to the theory plane strain failure mechanisms tend to be more critical than 3D ones.

3- There are several experimental studies in the literature about the load distribution among reinforcement layers. However, they only cover few parameters such as slope geometry, type of soil, and reinforcement layout. Genetic algorithm can be used to investigate all the possible configurations so that the optimal profile is found as the optimal against the most critical condition.

4- The study on the optimal profiles of reinforced slopes could be extended to investigate the performance of the obtained profiles under various environmental loads and erosive processes.

Bibliography

AASHTO. (2012). *Bridge design specifications, American Association of State Highway and Transportation Officials*. Washington DC, USA.

Abd, A. H. (2015a). *Earthquake-induced displacement of cohesive-frictional slopes subject to cracks.* Paper presented at the IOP Conference Series: Earth and Environmental Science.

Abd, A. H. (2015b). *Seismic displacement of geosynthetic-reinforced slopes subject to cracks.* Paper presented at the IOP Conference Series: Earth and Environmental Science.

Abd, A. H., & Utili, S. (2016). *Geosynthetics layout optimization for reinforced soil slopes subject to cracks.* Paper presented at the Landslides and Engineered Slopes. Experience, Theory and Practice: Proceedings of the 12th International Symposium on Landslides (Napoli, Italy, 12-19 June 2016).

Abd, A. H., & Utili, S. (2017a). Design of geosynthetic-reinforced slopes in cohesive backfills. *Geotextiles and Geomembranes, https://doi.org/10.1016/j.geotexmem.2017.08.004*.

Abd, A. H., & Utili, S. (2017b). Geosynthetic-Reinforced Slopes in Cohesive Soils Subject to Seismic Action. *Procedia Engineering, 189*, 898-907.

Abd, A. H., & Utili, S. (2017c). Profiles of optimal shape for geosynthetic-reinforced soil slopes. *Geotechnical and Geoenvironmental Engineering, under review*.

Allen, T. M., & Bathurst, R. J. (2015). Improved simplified method for prediction of loads in reinforced soil walls. *Journal of Geotechnical and Geoenvironmental Engineering, 141*(11), 04015049.

Allsop W., K. A., Morris M., Buijs F., Hassan R., Young M., Doorn N., der Meer J., Van Gelder P., Dyer M., Redaelli M., Utili S., Visser P., Bettess R., Lesniewska D., and Horst W. (2007). *Failure mechanisms for flood defence structures*. Retrieved from

Anderheggen, E., & Knöpfel, H. (1972). Finite element limit analysis using linear programming. *International journal of solids and structures, 8*(12), 1413-1431.

Anderson, D. G., Geoffrey, R. M., Ignatius, P. L., & (Joe), W. J. N. (2008). *Seismic analysis and design of retaining walls, buried structures, slopes, and embankments* (Vol. 611): Transportation Research Board.

Andrab, S. G., Hekmat, A., & Yusop, Z. B. (2017). Evolutionary Computations (GA and PSO) in Geotechnical Engineering. *Computational Water, Energy, and Environmental Engineering, 6*(2), 154.

Antao, A. N., Guerra, N. M. d. C., Matos Fernandes, M., & Cardoso, A. S. (2008). Influence of tension cut-off on the stability of anchored concrete soldier-pile walls in clay. *Canadian geotechnical journal, 45*(7), 1036-1044.

Ausilio, E., Conte, E., & Dente, G. (2000). Seismic stability analysis of reinforced slopes. *Soil Dynamics and Earthquake Engineering, 19*(3), 159-172.

Baker, R. (1981). Tensile strength, tension cracks, and stability of slopes. *Soils and foundations, 21*(2), 1-17.

Baker, R. (2003). Sufficient conditions for existence of physically significant solutions in limiting equilibrium slope stability analysis. *International journal of solids and structures, 40*(13), 3717-3735.

Bibliography

Berg, R. R., Christopher, B. R., & Samtani, N. C. (2009). *Design of Mechanically Stabilized Earth Walls and Reinforced Soil Slopes–Volume I*. Retrieved from

Bishop, A. W., & Morgenstern, N. R. (1960). Stability coefficients for earth slopes. *Geotechnique, 10*(4), 129-153.

Bishop, A. W., Webb, D. L., & Lewin, P. I. (1965). Undisturbed samples of London Clay from the Ashford Common shaft: strength–effective stress relationships. *Geotechnique, 15*(1), 1-31.

Boon, C. W., Houlsby, G. T., & Utili, S. (2012). A new algorithm for contact detection between convex polygonal and polyhedral particles in the discrete element method. *Computers and Geotechnics, 44*, 73-82.

Boon, C. W., Houlsby, G. T., & Utili, S. (2013). A new contact detection algorithm for three-dimensional non-spherical particles. *Powder technology, 248*, 94-102.

Boon, C. W., Houlsby, G. T., & Utili, S. (2014). New insights into the 1963 Vajont slide using 2D and 3D distinct-element method analyses. *Geotechnique, 64*(10), 800-816.

Cao, J., & Zaman, M. M. (1999). Analytical method for analysis of slope stability. *International Journal for Numerical and Analytical Methods in Geomechanics, 23*(5), 439-449.

Chang, C.-J., Chen, W. F., & Yao, J. T. P. (1984). Seismic displacements in slopes by limit analysis. *Journal of Geotechnical Engineering, 110*(7), 860-874.

Chen, W. F. (1975). *Limit analysis and soil plasticity*. Amsterdam, Netherlands.: Elsevier.

Chen, W. F., & Liu, X. L. (1990). *Limit analysis in soil mechanics*. Amsterdam, Netherlands.: Elsevier.

Conte, E., Silvestri, F., & Troncone, A. (2010). Stability analysis of slopes in soils with strain-softening behaviour. *Computers and Geotechnics, 37*(5), 710-722.

Crespellani, T., Madiai, C., & Vannucchi, G. (1998). Earthquake destructiveness potential factor and slope stability. *Geotechnique, 48*(3).

Crosta, G. B., Utili, S., De Blasio, F. V., & Castellanza, R. (2014). Reassessing rock mass properties and slope instability triggering conditions in Valles Marineris, Mars. *Earth and Planetary Science Letters, 388*, 329-342.

Dawson, E. M., Roth, W. H., & Drescher, A. (1999). Slope stability analysis by strength reduction. *Geotechnique, 49*(6), 835-840.

de Buhan, P., Mangiavacchi, R., Nova, R., Pellegrini, G., & Salençon, J. (1989). Yield design of reinforced earth walls by a homogenization method. *Geotechnique, 39*(2), 189-201.

Drescher, A., & Detournay, E. (1993). Limit load in translational failure mechanisms for associative and non-associative materials. *Geotechnique, 43*(3), 443-456.

Dyer, M., Utili, S., & Zielinski, M. (2009). *Field survey of desiccation fissuring of flood embankments*. Paper presented at the Proceedings of the Institution of Civil Engineers-Water Management.

EEA. (2010). *Mapping the impacts of natural hazards and technological accidents in Europe An overview of the last decade*. Retrieved from Technical report No 13/2010.:

Environment_Agency. (2006). *Condition assessment manual, managing flood risk*.

Bibliography

Document reference 116_03_SD01. Retrieved from

Eurogeosurvey. (2010). *Annual report. Available at http://www.eurogeosurveys.org/about-us/our-products/*. Retrieved from

Fellenius, W. (1927). *Erdstatische Berechnungenmit Reibung*

und Kohasion. Ernst, Berlin.

Fourie, A. B., & Fabian, K. J. (1987). Laboratory determination of clay-geotextile interaction. *Geotextiles and Geomembranes, 6*(4), 275-294.

Gao, Y., Yang, S., Zhang, F., & Leshchinsky, B. (2016). Three-dimensional reinforced slopes: Evaluation of required reinforcement strength and embedment length using limit analysis. *Geotextiles and Geomembranes, 44*(2), 133-142.

Gao, Y., Zhang, F., Lei, G. H., Li, D., Wu, Y., & Zhang, N. (2013). Stability charts for 3D failures of homogeneous slopes. *Journal of Geotechnical and Geoenvironmental Engineering, 139*(9), 1528-1538.

Goh, A. T. C. (1999). Genetic algorithm search for critical slip surface in multiple-wedge stability analysis. *Canadian geotechnical journal, 36*(2), 382-391.

Hales, T. C., & Roering, J. J. (2007). Climatic controls on frost cracking and implications for the evolution of bedrock landscapes. *Journal of Geophysical Research: Earth Surface, 112*(F2).

Hoek, E., & Bray, J. D. (1981). *Rock slope engineering*: CRC Press.

Hu, Y., Zhang, G., Zhang, J.-M., & Lee, C. F. (2010). Centrifuge modeling of geotextile-reinforced cohesive slopes. *Geotextiles and Geomembranes, 28*(1), 12-22.

Ingold, T. S. (1981). A laboratory simulation of reinforced clay walls. *Geotechnique, 31*(3), 399-412.

Ingold, T. S., & Miller, K. S. (1983). Drained axisymmetric loading of reinforced clay. *Journal of Geotechnical Engineering, 109*(7), 883-898.

Janbu, N. (1954). *Application of composite slip surfaces for stability analyses*. Paper presented at the European Conf. on Stability of Earth Slopes, Stockholm, Sweden.

Jeldes, I. A., Drumm, E. C., & Yoder, D. C. (2014). Design of stable concave slopes for reduced sediment delivery. *Journal of Geotechnical and Geoenvironmental Engineering, 141*(2), 04014093.

Jenike, A. W., & Yen, B. C. (1962). *Slope Stability in Axial Symmetry*.

Jenike, A. W., & Yen, B. C. (1962). *Slope stability in axial symmetry*. Paper presented at the Fifth Symposium on Rock Mechanics, Univeristy of Minnesota, USA.

Jewell, R. A. (1991). Application of revised design charts for steep reinforced slopes. *Geotextiles and Geomembranes, 10*(3), 203-233.

Jewell, R. A. (1996). *Soil reinforcement with geotextiles*. London, UK. : CIRIA and Thomas Telford.

Jiang, M., Zhu, F., Liu, F., & Utili, S. (2014). A bond contact model for methane hydrate-bearing sediments with interparticle cementation. *International Journal for Numerical and Analytical Methods in Geomechanics, 38*(17), 1823-1854.

Jibson, R. W. (2011). Methods for assessing the stability of slopes during earthquakes—A retrospective. *Engineering Geology, 122*(1), 43-50.

Konrad, J. M., & Ayad, R. (1997). A idealized framework for the analysis of cohesive soils undergoing desiccation. *Canadian geotechnical journal, 34*(4), 477-488.

Leshchinsky, D., & Boedeker, R. H. (1989). Geosynthetic reinforced soil structures. *Journal of Geotechnical Engineering, 115*(10), 1459-1478.

Leshchinsky, D., & Han, J. (2004). Geosynthetic reinforced multitiered walls. *Journal of Geotechnical and Geoenvironmental Engineering, 130*(12), 1225-1235.

Leshchinsky, D., Ling, H., & Hanks, G. (1995). Unified design approach to geosynthetic reinforced slopes and segmental walls. *Geosynthetics International, 2*(5), 845-881.

Leshchinsky, D., & Reinschmidt, A. J. (1985). Stability of membrane reinforced slopes. *Journal of Geotechnical Engineering, 111*(11), 1285-1300.

Ling, H. I., & Leshchinsky, D. (1998). Effects of vertical acceleration on seismic design of geosynthetic-reinforced soil structures. *Geotechnique, 48*(3), 347-373.

Ling, H. I., Leshchinsky, D., & Chou, N. N. S. (2001). Post-earthquake investigation on several geosynthetic-reinforced soil retaining walls and slopes during the Ji-Ji earthquake of Taiwan. *Soil Dynamics and Earthquake Engineering, 21*(4), 297-313.

Ling, H. I., Leshchinsky, D., & Mohri, Y. (1997). Soil slopes under combined horizontal and vertical seismic accelerations. *Earthquake engineering & structural dynamics, 26*(12), 1231-1241.

Ling, H. I., & Tatsuoka, F. (1994). Performance of anisotropic geosynthetic-reinforced cohesive soil mass. *Journal of Geotechnical Engineering, 120*(7), 1166-1184.

Little, A. L., & Price, V. E. (1958). The use of an electronic computer for slope stability analysis. *Geotechnique, 8*(3), 113–120

Liu, H., Yang, G., & Ling, H. I. (2014). Seismic response of multi-tiered reinforced soil retaining walls. *Soil Dynamics and Earthquake Engineering, 61*, 1-12.

Loukidis, D., Bandini, P., & Salgado, R. (2003). Stability of seismically loaded slopes using limit analysis. *Geotechnique, 53*(5), 463-480.

Makrodimopoulos, A., & Martin, C. M. (2007). Upper bound limit analysis using simplex strain elements and second-order cone programming. *International Journal for Numerical and Analytical Methods in Geomechanics, 31*(6), 835-865.

Manzari, M. T., & Nour, M. A. (2000). Significance of soil dilatancy in slope stability analysis. *Journal of Geotechnical and Geoenvironmental Engineering, 126*(1), 75-80.

Michalowski, R. L. (1997). Stability of uniformly reinforced slopes. *Journal of Geotechnical and Geoenvironmental Engineering, 123*(6), 546-556. doi:10.1061/(asce)1090-0241(1997)123:6(546)

Michalowski, R. L. (1998). Soil reinforcement for seismic design of geotechnical structures. *Computers and Geotechnics, 23*(1-2), 1-17. doi:10.1016/s0266-352x(98)00016-0

Michalowski, R. L. (2000). Secondary reinforcement for slopes. *Journal of Geotechnical and Geoenvironmental Engineering, 126*(12), 1166-1173.

Michalowski, R. L. (2002). Stability charts for uniform slopes. *Journal of Geotechnical and Geoenvironmental Engineering, 128*(4), 351-355.

Michalowski, R. L. (2013). Stability assessment of slopes with cracks using limit analysis. *Canadian geotechnical journal, 50*(10), 1011-1021.

Michalowski, R. L., & Zhao, A. (1995). Continuum versus structural approach to stability of reinforced soil. *Journal of Geotechnical Engineering, 121*(2), 152-162.

Mitchell, J. K. (1995). Reinforced Soil Structures with Poorly Draining Backfills Part II: Case Histories and Applications. *Geosynthetics International, 2*(1), 265-307.

Mononobe, H. (1929). *On the determination of earth pressures during earthquakes*. Paper presented at the world Engrg, Congr. , Tokyo, Japan.

Morgenstern, N. R., & Price, V. E. (1965). The analysis of the stability of general slip surfaces.

Munich_Re. (2012). Topics Geo: natural catastrophes 2011 analyses, assessment, position. from Geo risk Research NatCatService.

Nadukuru, S. S., & Michalowski, R. L. (2013). Three-dimensional displacement analysis of slopes subjected to seismic loads. *Canadian geotechnical journal, 50*(6), 650-661.

Newmark, N. M. (1965). Effects of earthquakes on dams and embankments. *Geotechnique, 15*(2), 139-160.

Noorzad, R., & Mirmoradi, S. H. (2010). Laboratory evaluation of the behavior of a geotextile reinforced clay. *Geotextiles and Geomembranes, 28*(4), 386-392.

Noorzad, R., & Omidvar, M. (2010). Seismic displacement analysis of embankment dams with reinforced cohesive shell. *Soil Dynamics and Earthquake Engineering, 30*(11), 1149-1157.

Okabe, S. (1924). General theory of earth pressure and seismic stability of retaining wall and dam. *J. Japan Soc. Civ Engrs, Tokyo, Japan, 12*.

OptumG2. (2014). OptumG2: www.optumce.com. Retrieved from www.optumce.com

Pastor, J. (1978). Limit analysis: numerical determination of complete

statical solutions. Application to the vertical cut. *J. Me´canique Applique´e (in French). 2*(2), 167–196.

Porbaha, A., & Goodings, D. J. (1996). Centrifuge modeling of geotextile-reinforced steep clay slopes. *Canadian geotechnical journal, 33*(5), 696-704.

Portelinha, F. H. M., Bueno, B. S., & Zornberg, J. G. (2013). Performance of nonwoven geotextile-reinforced walls under wetting conditions: laboratory and field investigations. *Geosynthetics International, 20*(2), 90-104.

Portelinha, F. H. M., Zornberg, J. G., & Pimentel, V. (2014). Field performance of retaining walls reinforced with woven and nonwoven geotextiles. *Geosynthetics International, 21*(4), 270-284.

Potts, D. M., Kovacevic, N., & Vaughan, P. R. (2009). Delayed collapse of cut slopes in stiff clay *Selected papers on geotechnical engineering by PR Vaughan* (pp. 362-391): Thomas Telford Publishing.

Potts, D. M., & Zdravkovic, L. (1999). *Finite elements analysis in geotechnical engineering: theory*: Thomas Telford.

Potts, D. M., & Zdravkovic, L. (2001). *Finite element analysis in geotechnical engineering: application* (Vol. 2): Thomas Telford.

SafeLand. (2012). *Living with landslide risk in Europe; Assessment, effects of global change, and risk management strategies*. Retrieved from Summary report, available at www.safeland-fp7.eu/:

Sawicki, A. (1983). Plastic limit behavior of reinforced earth. *Journal of Geotechnical Engineering, 109*(7), 1000-1005.

Sawicki, A., & Lesniewska, D. (1989). Limit analysis of cohesive slopes reinforced with geotextiles. *Computers and Geotechnics, 7*(1-2), 53-66.

Sawicki, A., & Leśniewska, D. (1991). Stability of fabric reinforced cohesive soil slopes. *Geotextiles and Geomembranes, 10*(2), 125-146.

Schuster, R. L., & Kockelman, W. J. (1996). *LANDSLIDES: INVESTIGATION AND MITIGATION. CHAPTER 5-PRINCIPLES OF LANDSLIDE HAZARD REDUCTION*.

Sengupta, A., & Upadhyay, A. (2009). Locating the critical failure surface in a slope stability analysis by genetic algorithm. *Applied Soft Computing, 9*(1), 387-392.

Shukha, R., & Baker, R. (2008). Design implications of the vertical pseudo-static coefficient in slope analysis. *Computers and Geotechnics, 35*(1), 86-96.

Sloan, S. W. (1989). Upper bound limit analysis using finite elements and linear programming. *International Journal for Numerical and Analytical Methods in Geomechanics, 13*(3), 263-282.

Sokolovskiĭ, V. V. (1960). *Statics of soil media*. London: Butterworths Scientific Publications.

Spencer, E. (1967). A method of analysis of the stability of embankments assuming parallel inter-slice forces. *Geotechnique, 17*(1), 11-26.

Spencer, E. (1968). Effect of tension on the stability of embankments. *Journal of Soil Mechanics & Foundations Div*.

Stuedlein, A. W., Bailey, M., Lindquist, D., Sankey, J., & Neely, W. J. (2010). Design and performance of a 46-m-high MSE wall. *Journal of Geotechnical and Geoenvironmental Engineering, 136*(6), 786-796.

Sukmak, K., Sukmak, P., Horpibulsuk, S., Han, J., Shen, S.-L., & Arulrajah, A. (2015). Effect of fine content on the pullout resistance mechanism of bearing reinforcement embedded in cohesive–frictional soils. *Geotextiles and Geomembranes, 43*(2), 107-117.

Sun, J., Li, J., & Liu, Q. (2008). Search for critical slip surface in slope stability analysis by spline-based GA method. *Journal of Geotechnical and Geoenvironmental Engineering, 134*(2), 252-256.

Tang, C.-S., Cui, Y.-J., Tang, A.-M., & Shi, B. (2009). Experiment evidence on the temperature dependence of desiccation cracking behavior of clayey soils. *Engineering Geology, 114*(3-4), 261-266.

Bibliography

Taylor, D. W. (1948). *Fundamentals of soil mechanics* (Vol. New York, USA.): John Wiley & Sons.

Terzaghi, K. (1943). *Theory of consolidation*: Wiley Online Library.

Terzaghi, K. (1950). *Mechanisms of Landslides*. Boulder, CO (USA): Engineering Geology (Berkeley) Volume, Geological Society of America, .

Utili, S. (2005). An analytical relationship for weathering induced slope retrogression: a benchmark. *RIG (Italian Geotechnical Journal), 39*(2), 9-30.

Utili, S. (2013). Investigation by limit analysis on the stability of slopes with cracks. *Geotechnique, 63*(2), 140-154.

Utili, S., & Abd, A. H. (2016). On the stability of fissured slopes subject to seismic action. *International Journal for Numerical and Analytical Methods in Geomechanics, 40*(5), 785-806. doi:10.1002/nag.2498

Utili, S., Castellanza, R., Galli, A., & Sentenac, P. (2015). Novel approach for health monitoring of earthen embankments. *Journal of Geotechnical and Geoenvironmental Engineering, 141*(3), 04014111.

Utili, S., & Crosta, G. B. (2011). Modeling the evolution of natural cliffs subject to weathering: 1. Limit analysis approach. *Journal of Geophysical Research: Earth Surface, 116*(F1).

Utili, S., & Nova, R. (2007). On the optimal profile of a slope. *Soils and foundations, 47*(4), 717-729.

Utili, S., & Nova, R. (2008). DEM analysis of bonded granular geomaterials. *International Journal for Numerical and Analytical Methods in Geomechanics, 32*(17), 1997-2031.

Utili, S., & Wu, W. (2017). Optimal profile shape for soil slopes. *Journal of Geotechnical and Geoenvironmental Engineering, under reivew*.

Vahedifard, F., Leshchinsky, B. A., Sehat, S., & Leshchinsky, D. (2014). Impact of cohesion on seismic design of geosynthetic-reinforced earth structures. *Journal of Geotechnical and Geoenvironmental Engineering, 140*(6), 04014016.

Vahedifard, F., Shahrokhabadi, S., & Leshchinsky, D. (2016a). Geosynthetic-reinforced soil structures with concave facing profile. *Geotextiles and Geomembranes, 44*(3), 358-365.

Vahedifard, F., Shahrokhabadi, S., & Leshchinsky, D. (2016b). Optimal profile for concave slopes under static and seismic conditions. *Canadian geotechnical journal, 53*(9), 1522-1532.

Vanicek, I., & Vanicek, M. (2008). *Earth structures: in transport, water and environmental engineering* (Vol. 4): Springer Science & Business Media.

Viswanadham, B. V. S., & Mahajan, R. R. (2007). Centrifuge model tests on geotextile-reinforced slopes. *Geosynthetics International, 14*(6), 365-379.

Wang, L., Zhang, G., & Zhang, J.-M. (2011). Centrifuge model tests of geotextile-reinforced soil embankments during an earthquake. *Geotextiles and Geomembranes, 29*(3), 222-232.

Yang, G.-Q., Liu, H., Zhou, Y.-T., & Xiong, B.-L. (2014). Post-construction performance of a two-tiered geogrid reinforced soil wall backfilled with soil-rock mixture. *Geotextiles and Geomembranes, 42*(2), 91-97.

Yang, K. H., Zornberg, J. G., Liu, C. N., & Lin, H. D. (2012). Stress distribution and development within geosynthetic-reinforced soil slopes. *Geosynthetics International, 19*(1), 62-78.

Yang, X.-g., & Chi, S.-c. (2014). Seismic stability of earth-rock dams using finite element limit analysis. *Soil Dynamics and Earthquake Engineering, 64*, 1-10.

You, L., & Michalowski, R. L. (1999). Displacement charts for slopes subjected to seismic loads. *Computers and Geotechnics, 25*(1), 45-55.

Zhang, F., Leshchinsky, D., Gao, Y., & Leshchinsky, B. (2014). Required unfactored strength of geosynthetics in reinforced 3D slopes. *Geotextiles and Geomembranes, 42*(6), 576-585.

Zhang, G., Wang, R., Qian, J., Zhang, J.-M., & Qian, J. (2012). Effect study of cracks on behavior of soil slope under rainfall conditions. *Soils and foundations, 52*(4), 634-643.

Zhao, A. (1996). Limit analysis of geosynthetic-reinforced soil slopes. *Geosynthetics International, 3*(6), 721-740.

Zheng, H., Liu, D. F., & Li, C. (2005). Slope stability analysis based on elasto-plastic finite element method. *International Journal for Numerical Methods in Engineering, 64*(14), 1871-1888.

Zienkiewicz O.C., Humpheson C., & Lewis RW. (1975). Associated and non-associated visco-plasticity and plasticity in soil mechanics. *Geotechnique, 25*(4), 671-689.

Zienkiewicz, O. C., & Taylor, R. L. (2005). *The finite element method: solid mechanics* (2nd ed. Vol. 1 and 2): Butterworth-heinemann.

Zolfaghari, A. R., Heath, A. C., & McCombie, P. F. (2005). Simple genetic algorithm search for critical non-circular failure surface in slope stability analysis. *Computers and Geotechnics, 32*(3), 139-152.

Zornberg, J. G., & Arriaga, F. (2003). Strain distribution within geosynthetic-reinforced slopes. *Journal of Geotechnical and Geoenvironmental Engineering, 129*(1), 32-45.

Zornberg, J. G., & Mitchell, J. K. (1994). Reinforced soil structures with poorly draining backfills. Part I: Reinforcement interactions and functions. *Geosynthetics International, 1*(2), 103-147.

Zornberg, J. G., Sitar, N., & Mitchell, J. K. (1998). Performance of geosynthetic reinforced slopes at failure. *Journal of Geotechnical and Geoenvironmental Engineering, 124*(8), 670-683.

Appendix A

Table A.1 Stability number $\gamma H / c$ for different values of horizontal acceleration and $K_v / K_h = 0$.

K_h	$\beta°$	Angle of shearing resistance $\phi°$				
		20	25	30	35	40
0	40	19.21862	30.49934	57.33376	165.1141	241.25
	45	15.28391	21.97215	34.55451	64.41562	184.0293
	50	12.6501	17.06628	24.32426	37.94947	70.19797
	55	10.72062	13.82772	18.50155	26.16767	40.52332
	60	9.212862	11.48608	14.69653	19.51605	27.40269
	65	7.974787	9.677732	11.9706	15.20153	20.04001
	70	6.915384	8.206805	9.880773	12.12864	15.28723
	75	5.973302	6.954292	8.186404	9.778181	11.90816
	80	5.097961	5.834455	6.734445	7.859755	9.30668
	85	4.223692	4.755381	5.38861	6.157108	7.110998
	90	2.901954	3.192025	3.525185	3.913376	4.481378
0.1	40	13.26825	18.8787	29.17833	52.57406	136.28
	45	11.25902	15.07934	21.25508	32.56642	58.18624
	50	9.749614	12.5062	16.60096	23.20517	35.26662
	55	8.544286	10.60673	13.4897	17.76212	24.63304
	60	7.53591	9.114089	11.22059	14.15765	18.49708
	65	6.659684	7.882636	9.456122	11.55026	14.4604
	70	5.872113	6.823714	8.011423	9.534297	11.55326
	75	5.139068	5.875704	6.771305	7.884293	9.304545
	80	4.42415	4.983231	5.646905	6.448989	7.439203
	85	3.709231	4.090759	4.711434	5.013685	5.805354
	90	2.994312	3.198286	3.727424	3.578381	4.307242
0.2	40	9.754395	13.01412	18.2117	27.54606	47.98322
	45	8.630443	11.04133	14.58487	20.22308	30.31972
	50	7.707033	9.549053	12.10168	15.8452	21.78384
	55	6.91502	8.351273	10.25414	12.88456	16.72996
	60	6.211838	7.344663	8.792777	10.70587	13.34118
	65	5.568458	6.465727	7.579224	8.997636	10.86388
	70	4.961967	5.670294	6.527068	7.585583	8.92716
	75	4.36878	4.92026	5.571955	6.355431	7.316665
	80	3.878797	4.319526	4.83066	5.432456	5.706171
	85	3.388815	3.718792	4.089365	4.509481	4.56824
	90	2.898833	3.118057	3.348071	3.586506	3.654224
0.3	40	7.455683	9.549624	12.60165	17.41281	25.92009
	45	6.789319	8.42204	10.66866	13.93902	19.08058
	50	6.197845	7.493382	9.199284	11.54265	14.94398
	55	5.657307	6.695403	8.015179	9.749116	12.12315
	60	5.150798	5.985497	7.016229	8.322686	10.03226
	65	4.664405	5.333652	6.139541	7.130546	8.380125
	70	4.183455	4.714171	5.338779	6.086402	6.999152
	75	3.685599	4.095861	4.568027	5.042258	5.764624
	80	3.187743	3.477552	3.807555	3.998114	4.645224
	85	2.689888	2.859243	3.104541	2.953978	3.754617
	90	2.192032	2.240933	2.531047	1.909826	2.946548

Table A.2 Stability number $\gamma H / c$ for different values of horizontal acceleration and $K_v / K_h = 0.5$.

K_h	$\beta°$	Angle of shearing resistance $\phi°$				
		20	25	30	35	40
0	**40**	19.21862	30.49934	57.33376	165.1141	--
	45	15.28391	21.97215	34.55451	64.41562	184.0293
	50	12.6501	17.06628	24.32426	37.94947	70.19797
	55	10.72062	13.82772	18.50155	26.16767	40.52332
	60	9.212862	11.48608	14.69653	19.51605	27.40269
	65	7.974787	9.677732	11.9706	15.20153	20.04001
	70	6.915384	8.206805	9.880773	12.12864	15.28723
	75	5.973302	6.954292	8.186404	9.778181	11.90816
	80	5.097961	5.834455	6.734445	7.859755	9.30668
	85	4.223692	4.755381	5.38861	6.157108	7.110998
	90	2.901954	3.192025	3.525185	3.913376	4.481378
0.1	**40**	12.8398	18.34097	28.52938	52.04656	132.8018
	45	10.86878	14.59606	20.65521	31.85161	57.62027
	50	9.395049	12.07541	16.07253	22.55592	34.50183
	55	8.222574	10.22319	13.02799	17.20121	23.95039
	60	7.244641	8.772763	10.8172	13.67635	17.91741
	65	6.39702	7.579641	9.104108	11.13791	13.97268
	70	5.636956	6.556288	7.705585	9.18208	11.14445
	75	4.931097	5.642327	6.508273	7.586265	8.964671
	80	4.244531	4.784327	5.425913	6.20253	7.163043
	85	3.509711	3.896872	4.545645	4.818795	5.5645
	90	2.77489	3.009417	3.545631	3.43506	4.145587
0.2	**40**	9.345778	12.5887	17.86762	27.65752	50.37088
	45	8.216266	10.58524	14.11962	19.85753	30.47202
	50	7.301712	9.096089	11.61012	15.35112	21.40955
	55	6.527068	7.917312	9.775281	12.37196	16.22389
	60	5.846349	6.937866	8.343126	10.21582	12.82415
	65	5.229145	6.090938	7.166856	8.547372	10.3799
	70	4.652296	5.331352	6.157123	7.183723	8.494651
	75	4.093407	4.622042	5.249855	6.008966	6.946649
	80	3.577828	3.988765	4.466746	5.030967	5.708579
	85	3.062249	3.355488	3.683636	4.052968	4.470508
	90	2.54667	2.722212	2.900527	3.074969	3.232438
0.3	**40**	7.176542	9.320804	12.54414	17.8548	27.90121
	45	6.469042	8.11111	10.42354	13.89459	19.59542
	50	5.859422	7.145386	8.870581	11.29505	14.9243
	55	5.315456	6.336445	7.654056	9.41754	11.88711
	60	4.81631	5.631993	6.652143	7.9649	9.714547
	65	4.345817	4.99741	5.790852	6.779425	8.045391
	70	3.889379	4.405744	5.01982	5.763612	6.684537
	75	3.427538	3.828369	4.294383	4.844229	5.504161
	80	2.952382	3.250993	3.568945	3.924845	4.4513
	85	2.477226	2.673617	2.843508	3.005462	3.56456
	90	2.00207	2.096241	2.345045	2.086078	2.718702

Table A.3 Stability number $\gamma H / c$ for different values of horizontal acceleration and $K_v / K_h = -0.5$.

K_h	$\beta°$	Angle of shearing resistance $\phi°$				
		20	25	30	35	40
0	**40**	19.21862	30.49934	57.33376	165.1141	-
	45	15.28391	21.97215	34.55451	64.41562	184.0293
	50	12.6501	17.06628	24.32426	37.94947	70.19797
	55	10.72062	13.82772	18.50155	26.16767	40.52332
	60	9.212862	11.48608	14.69653	19.51605	27.40269
	65	7.974787	9.677732	11.9706	15.20153	20.04001
	70	6.915384	8.206805	9.880773	12.12864	15.28723
	75	5.973302	6.954292	8.186404	9.778181	11.90816
	80	5.097961	5.834455	6.734445	7.859755	9.30668
	85	4.223692	4.755381	5.38861	6.157108	7.110998
	90	2.901954	3.192025	3.525185	3.913376	4.481378
0.1	**40**	13.7246	19.4454	29.84992	53.08334	132.8178
	45	11.67746	15.59431	21.88915	33.30876	58.74403
	50	10.13136	12.96771	17.16388	23.8895	36.06119
	55	8.891597	11.01964	13.98459	18.35893	25.35307
	60	7.851268	9.482797	11.65468	14.67262	19.11431
	65	6.944504	8.210232	9.835942	11.99345	14.98239
	70	6.127329	7.113428	8.34218	9.913752	11.9921
	75	5.364924	6.128774	7.055826	8.206051	9.670293
	80	4.619311	5.198872	5.885931	6.715297	7.73702
	85	3.81808	4.26897	4.716037	5.224544	5.803746
	90	3.066848	3.339068	3.546142	3.73379	3.870472
0.2	**40**	10.18195	13.44051	18.51788	27.32444	45.46605
	45	9.074433	11.5179	15.05052	20.54343	30.04183
	50	8.148514	10.03374	12.61367	16.33523	22.10433
	55	7.342	8.822593	10.76485	13.41548	17.22717
	60	6.617563	7.791177	9.279426	11.22542	13.87284
	65	5.947242	6.880227	8.029568	9.481637	11.37251
	70	5.308827	6.046442	6.933579	8.021188	9.38708
	75	4.676724	5.251035	5.925652	6.730843	7.710944
	80	4.044621	4.455627	4.859017	5.440499	6.034808
	85	3.412519	3.66022	3.807059	4.150154	4.358673
	90	2.780416	2.864812	2.755101	2.85981	2.682537
0.3	**40**	7.691206	9.700195	12.52512	16.76795	23.75449
	45	7.088293	8.686588	10.8258	13.83252	18.33591
	50	6.531667	7.818615	9.475678	11.6902	14.7952
	55	6.006845	7.048095	8.348065	10.01862	12.2447
	60	5.501058	6.343889	7.368636	8.642916	10.2748
	65	5.003003	5.680845	6.485424	7.459201	8.663078
	70	4.496674	5.033538	5.656787	6.391353	7.271979
	75	3.971572	4.388401	4.853255	5.323505	5.880879
	80	3.446471	3.743264	4.049722	4.255657	4.48978
	85	2.92137	3.098127	3.24619	3.187809	3.098681
	90	2.396268	2.45299	2.442658	2.119961	1.707582

Table A.4 Stability number $\gamma H / c$ for different values of horizontal acceleration and $K_v / K_h = 1$.

K_h	$\beta°$	Angle of shearing resistance $\phi°$				
		20	25	30	35	40
0	**40**	19.21862	30.49934	57.33376	165.1141	-
	45	15.28391	21.97215	34.55451	64.41562	184.0293
	50	12.6501	17.06628	24.32426	37.94947	70.19797
	55	10.72062	13.82772	18.50155	26.16767	40.52332
	60	9.212862	11.48608	14.69653	19.51605	27.40269
	65	7.974787	9.677732	11.9706	15.20153	20.04001
	70	6.915384	8.206805	9.880773	12.12864	15.28723
	75	5.973302	6.954292	8.186404	9.778181	11.90816
	80	5.097961	5.834455	6.734445	7.859755	9.30668
	85	4.223692	4.755381	5.38861	6.157108	7.110998
	90	2.901954	3.192025	3.525185	3.913376	4.481378
0.1	**40**	12.43692	17.83052	27.90225	51.5054	142.9898
	45	10.5039	14.14166	20.08654	31.16081	57.04626
	50	9.065084	11.67284	15.57549	21.93953	33.76237
	55	7.923767	9.865981	12.596	16.67247	23.30265
	60	6.974727	8.455913	10.44156	13.2258	17.37133
	65	6.154158	7.298605	8.77713	10.75317	13.51523
	70	5.419646	6.308793	7.421909	8.854317	10.7624
	75	4.739083	5.426421	6.264498	7.309253	8.648045
	80	4.078595	4.600371	5.221146	5.973711	6.905902
	85	3.418107	3.774322	4.177793	4.63817	5.163759
	90	2.757618	2.948272	3.134441	3.302629	3.421616
0.2	**40**	8.959617	12.1735	17.50194	27.68582	52.67131
	45	7.831891	10.15341	13.66097	19.46672	30.5253
	50	6.930781	8.675547	11.14359	14.86455	21.0035
	55	6.175443	7.51959	9.329509	11.88367	15.7236
	60	5.517296	6.568205	7.930051	9.758155	12.32882
	65	4.924943	5.752444	6.790888	8.131571	9.924549
	70	4.375507	5.026424	5.821373	6.815219	8.091996
	75	3.847315	4.353623	4.957467	5.691253	6.60299
	80	3.309156	3.691762	4.13763	4.665049	5.300413
	85	2.770997	3.029902	3.317793	3.638845	3.997836
	90	2.232838	2.368041	2.497955	2.61264	2.69526
0.3	**40**	6.884714	9.054008	12.4044	18.14297	29.72696
	45	6.152232	7.786673	10.13482	13.75583	19.94223
	50	5.535421	6.800948	8.524306	10.99597	14.79651
	55	4.995553	5.991867	7.293777	9.063214	11.59186
	60	4.508057	5.299379	6.299369	7.602723	9.366982
	65	4.055311	4.684905	5.458755	6.433462	7.697412
	70	3.622053	4.12046	4.717985	5.448503	6.363519
	75	3.191561	3.579425	4.033393	4.574403	5.230621
	80	2.761069	3.038391	3.3488	3.700304	4.097724
	85	2.330577	2.497357	2.664208	2.826204	2.964826
	90	1.900085	1.956322	1.979616	1.952105	1.831928

Table A.5 Stability number $\gamma H / c$ for different values of horizontal acceleration and $K_v / K_h = -1$.

K_h	$\beta°$	Angle of shearing resistance $\phi°$				
		20	**25**	**30**	**35**	**40**
0	40	19.21862	30.49934	57.33376	165.1141	-
	45	15.28391	21.97215	34.55451	64.41562	184.0293
	50	12.6501	17.06628	24.32426	37.94947	70.19797
	55	10.72062	13.82772	18.50155	26.16767	40.52332
	60	9.212862	11.48608	14.69653	19.51605	27.40269
	65	7.974787	9.677732	11.9706	15.20153	20.04001
	70	6.915384	8.206805	9.880773	12.12864	15.28723
	75	5.973302	6.954292	8.186404	9.778181	11.90816
	80	5.097961	5.834455	6.734445	7.859755	9.30668
	85	4.223692	4.755381	5.38861	6.157108	7.110998
	90	2.901954	3.192025	3.525185	3.913376	4.481378
0.1	40	14.2109	20.04292	30.54149	53.56603	129.2311
	45	12.12658	16.1423	22.55379	34.07092	59.24721
	50	10.54252	13.46246	17.76262	24.60791	36.87386
	55	9.267337	11.46394	14.51446	18.99436	26.10895
	60	8.193041	9.880814	12.12118	15.22419	19.76719
	65	7.253724	8.565536	10.24598	12.46977	15.53996
	70	6.40501	7.42776	8.699873	10.32305	12.46344
	75	5.610883	6.403805	7.364187	8.553374	10.0641
	80	4.831398	5.43307	6.144975	7.002606	8.057049
	85	3.992679	4.462336	4.925763	5.451838	6.049998
	90	3.153959	3.491601	3.706552	3.901071	4.042947
0.2	40	10.61937	13.85188	18.75827	26.94644	42.78066
	45	9.543714	12.00489	15.49674	20.78665	29.5912
	50	8.623904	10.54395	13.13347	16.79928	22.33494
	55	7.809173	9.329339	11.29945	13.95001	17.68991
	60	7.065699	8.277757	9.79958	11.76605	14.40134
	65	6.368754	7.335512	8.516802	9.994616	11.89504
	70	5.696016	6.46178	7.375526	8.485988	9.866086
	75	5.019991	5.614674	6.309551	7.12975	8.120159
	80	4.343965	4.767567	5.243575	5.773512	6.54562
	85	3.667939	3.920461	4.17761	4.417275	5.2054
	90	3.104237	3.073355	3.111624	3.061037	4.1054
0.3	40	7.812575	9.69275	12.2231	15.82056	21.31349
	45	7.307534	8.835712	10.81139	13.47519	17.25654
	50	6.813921	8.06289	9.626243	11.64808	14.36856
	55	6.325642	7.346924	8.590876	10.14643	12.1525
	60	5.836263	6.667227	7.656413	8.857606	10.35296
	65	5.335345	6.004129	6.782951	7.704578	8.816336
	70	4.80608	5.332854	5.909489	6.55155	7.422454
	75	4.276816	4.661579	5.036028	5.398522	6.023664
	80	3.747552	3.990304	4.162566	4.245494	4.627328
	85	3.218287	3.319029	3.289104	3.092466	3.230992
	90	-	-	-	-	-

Appendix B

The rate of external work for the sliding wedge E-B-C-D, $\dot{W}_{ext}$, is calculated from the following summation:

$$\dot{W}_{ext} = \dot{W}_1 - \dot{W}_2 - \dot{W}_3 - \left(\dot{W}_4 - \dot{W}_5 - \dot{W}_6 \right) \tag{B.1}$$

Where $\dot{W}_1, \dot{W}_2, \dot{W}_3, \dot{W}_4, \dot{W}_5$ and $\dot{W}_6$ are the external work rates, done by soil weight as well as seismic action, corresponding to blocks P-D-F, P-E-F, P-D-E, P-C-F, P-B-F and P-C-B respectively (see Figure 3.1) and their final expression are listed as follow:

$$
\begin{aligned}
\dot{W}_1 &= \dot{\theta} \gamma r_\chi^3 \left[\left(1 + K_v\right) f_{1v} + K_h f_{1h} \right] \\
&= \dot{\theta} \gamma r_\chi^3 \left[\begin{array}{l} \left(1 + K_v\right) \dfrac{\exp\left[3\tan\phi(\upsilon - \chi)\right]\left(3\tan\phi\cos\upsilon + \sin\upsilon\right) - 3\tan\phi\cos\chi - \sin\chi}{3\left(1 + 9\tan^2\phi\right)} + \\[2ex] K_h \dfrac{\exp\left[3\tan\phi(\upsilon - \chi)\right]\left(3\tan\phi\sin\upsilon + \cos\upsilon\right) - 3\tan\phi\sin\chi - \cos\chi}{3\left(1 + 9\tan^2\phi\right)} \end{array} \right]
\end{aligned} \tag{B.2}
$$

with $\dot{\theta}$ being the rate of angular displacement of the failing wedge E-B-C-D.

$$
\begin{aligned}
\dot{W}_2 &= \dot{\theta} \gamma r_\chi^3 \left[\left(1 + K_v\right) f_{2v} + K_h f_{2h} \right] \\
&= \dot{\theta} \gamma r_\chi^3 \left[\left(1 + K_v\right) \dfrac{l_1}{6r_\chi} \sin\chi \left(2\cos\chi - \dfrac{l_1}{r_\chi} \right) + K_h \dfrac{l_1}{3r_\chi} \sin^2\chi \right]
\end{aligned} \tag{B.3}
$$

$$\dot{W}_3 = \dot{\theta}\gamma r_\chi^3 \left[(1+K_v) f_{3v} + K_h f_{3h} \right]$$

$$= \dot{\theta}\gamma r_\chi^3 \begin{bmatrix} \dfrac{(1+K_v)}{6}\exp\left[\tan\phi(\upsilon-\chi)\right]\left(\sin(\upsilon-\chi)-\dfrac{l_1}{r_\chi}\sin\upsilon\right) \\[2ex] \left(\cos\chi - \dfrac{l_1}{r_\chi} + \exp\left[\tan\phi(\upsilon-\chi)\right]\cos\upsilon\right) \\[2ex] + \dfrac{K_h}{6}\exp\left[\tan\phi(\upsilon-\chi)\right]\left(\sin(\upsilon-\chi)-\dfrac{l_1}{r_\chi}\sin\upsilon\right) \\[2ex] \left(\sin\chi + \exp\left[\tan\phi(\upsilon-\chi)\right]\sin\upsilon\right) \end{bmatrix} \quad \text{(B.4)}$$

$$\dot{W}_4 = \dot{\theta}\gamma r_\chi^3 \left[(1+K_v) f_{4v} + K_h f_{4h} \right]$$

$$= \dot{\theta}\gamma r_\chi^3 \begin{bmatrix} (1+K_v)\dfrac{\exp\left[3\tan\phi(\xi-\chi)\right](3\tan\phi\cos\xi+\sin\xi)-3\tan\phi\cos\chi-\sin\chi}{3(1+9\tan^2\phi)} + \\[3ex] K_h \dfrac{\exp\left[3\tan\phi(\xi-\chi)\right](3\tan\phi\sin\xi+\cos\xi)-3\tan\phi\sin\chi-\cos\chi}{3(1+9\tan^2\phi)} \end{bmatrix} \quad \text{(B.5)}$$

$$\dot{W}_5 = \dot{\theta}\gamma r_\chi^3 \left[(1+K_v) f_{5v} + K_h f_{5h} \right]$$

$$= \dot{\theta}\gamma r_\chi^3 \left[(1+K_v)\dfrac{l_2}{6r_\chi}\sin\chi\left(2\cos\chi-\dfrac{l_2}{r_\chi}\right) + K_h\dfrac{l_2}{3r_\chi}\sin^2\chi \right] \quad \text{(B.6)}$$

$$\dot{W}_6 = \dot{\theta}\gamma r_\chi^3 \left[(1+K_v) f_{6v} + K_h f_{6h} \right]$$

$$= \dot{\theta}\gamma r_\chi^3 \begin{bmatrix} \dfrac{(1+K_v)}{3}\exp\left[2\tan\phi(\xi-\chi)\right]\cos^2\xi\left(\exp\left[\tan\phi(\xi-\chi)\right]\sin\xi-\sin\chi\right) + \\[3ex] \dfrac{K_h}{6}\exp\left[\tan\phi(\xi-\chi)\right]\cos\xi\left(\exp\left[2\tan\phi(\xi-\chi)\right]\sin^2\xi-\sin^2\chi\right) \end{bmatrix} \quad \text{(B.7)}$$

Appendix C

Calculation for the weight of the sliding mass B-C-E-D and its arm length, mentioned in Chapter 3, called G and l, respectively.

$$G = \gamma A \tag{C.1}$$

$$A = A_1 - A_2 - A_3 - A_4 + A_5 + A_6 \tag{C.2}$$

$$A_1 = \frac{r_\chi^2}{2} \left[\frac{\exp\left[2\tan\phi(\upsilon - \chi)\right] - 1}{2\tan\phi} \right] \tag{C.3}$$

$$A_2 = \frac{1}{2} r_\chi L_1 \sin\chi \tag{C.4}$$

$$A_3 = \frac{1}{2} r_\chi H \left[\frac{\exp\left[\tan\phi(\upsilon - \chi)\right]\sin(\beta + \upsilon)}{\sin\beta} \right] \tag{C.5}$$

$$A_4 = \frac{r_\chi^2}{2} \left[\frac{\exp\left[2\tan\phi(\zeta - \chi)\right] - 1}{2\tan\phi} \right] \tag{C.6}$$

$$A_5 = \frac{1}{2} r_\chi L_2 \sin\chi \tag{C.7}$$

$$A_6 = \frac{1}{2} \delta r_\zeta \cos\zeta = \frac{1}{2} r_\chi \delta \left[\exp\left[\tan\phi(\zeta - \chi)\right]\cos\zeta \right] \tag{C.8}$$

The arm length of the weight, l, is given by:

$$l = \frac{\sqrt{\left(\gamma r_\chi^3 \left(f_{1v} - f_{2v} - f_{3v} - f_{4v} + f_{5v} + f_{6v}\right)\right)^2 + \left(\gamma r_\chi^3 \left(f_{1h} - f_{2h} - f_{3h} - f_{4h} + f_{5h} + f_{6h}\right)\right)^2}}{G} \tag{C.9}$$

Appendix D

For linearly increasing distribution (LID), the expression for the energy dissipated by the geosynthetics along the log-spiral part C-D can be expressed as follow:

$$\dot{D}_{r(C-D)} = \frac{2K_t \dot{\theta} r_\chi^2}{\dfrac{H}{r_\chi}} \left[\begin{array}{c} (1/3)\exp\left[3\tan\phi(\upsilon-\chi)\right]\sin^3\upsilon \\ -\exp\left[3\tan\phi(\zeta-\chi)\right]\sin^3\zeta \\ -\dfrac{\sin\chi}{2}\left(\begin{array}{c} \exp\left[2\tan\phi(\upsilon-\chi)\right]\sin^2\upsilon \\ -\exp\left[2\tan\phi(\zeta-\chi)\right]\sin^2\zeta \end{array} \right) \end{array} \right] \tag{D.1}$$

$$\dot{D}_{r(C-D)} = K_t \dot{\theta} r_\chi^2 g_2\left(\chi,\upsilon,\zeta,\phi\right) \tag{D.2}$$

Analogously, the energy dissipated by geosynthetics along the crack B-C can be written:

$$\dot{D}_{r(B-C)} = 2K_t \dot{\theta} r_\chi^2 \left[\begin{array}{c} \dfrac{\exp\left[2\tan\phi(\zeta-\chi)\right]\cos^2\zeta}{\exp\left[\tan\phi(\upsilon-\chi)\right]\sin\upsilon-\sin\chi} \\ \displaystyle\int_\mu^\zeta \left(\begin{array}{c} \left(\exp\left[\tan\phi(\theta-\chi)\right]\sin\theta-\sin\chi\right) \\ \tan\theta\sec^2\theta d\theta \end{array} \right) \end{array} \right] \tag{D.3}$$

$$\dot{D}_{r(B-C)} = K_t \dot{\theta} r_\chi^2 g_4\left(\chi,\upsilon,\zeta,\phi\right) \tag{D.4}$$

Appendix E

Calculations for the external work rate function due to pore water pressure.

$$\dot{W}_w = \gamma \dot{\theta} r_x^3 f_w (\chi, \upsilon, \zeta, \phi) \tag{E.1}$$

$$f_w (\chi, \upsilon, \zeta, \phi) = \frac{r_u}{r_x^3} \left(\int_{\theta_w}^{\zeta} z_c r_c^2 \tan \theta d\theta + \int_{\zeta}^{\theta_1} z_1 r^2 \tan \phi d\theta + \int_{\theta_1}^{\upsilon} z_2 r^2 \tan \phi d\theta \right) \tag{E.2}$$

where z_c z_1 and z_2 are illustrated in Figure E.1, and their mathematical expressions

can be found geometrically as follow:

$$z_c = r_\chi \left(\exp \left[\tan \phi (\zeta - \chi) \right] \cos \zeta \tan \theta - \sin \chi \right) \tag{E.3}$$

$$z_1 = r_\chi \left(\exp \left[\tan \phi (\theta - \chi) \right] \sin \theta - \sin \chi \right) \tag{E.4}$$

$$z_2 = r_\chi \left(\exp \left[\tan \phi (\theta - \chi) \right] \sin \theta - \left[\begin{matrix} \exp \left[\tan \phi (\theta_1 - \chi) \right] \cos \theta_1 - \\ \exp \left[\tan \phi (\theta - \chi) \right] \cos \theta \end{matrix} \right] \tan \beta - \sin \chi \right) \tag{E.5}$$

the angle θ_1 can be found from this equation:

$$\exp \left[\tan \phi (\theta_1 - \chi) \right] \cos \theta_1 - \cos \chi + \frac{l_1}{r_\chi} = 0 \tag{E.6}$$
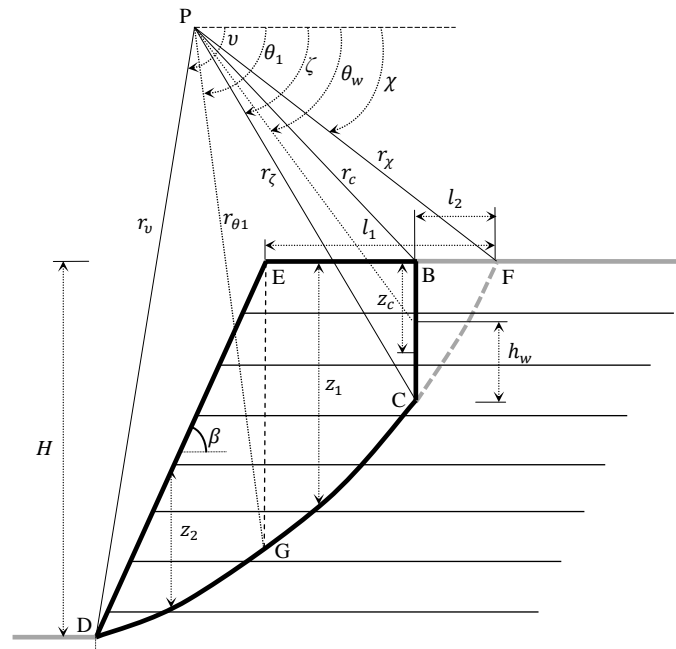
Figure E.1 Illustration of the geometrical parameters used for the calculation of the work due to pore water pressures.

Appendix F

Table F.1 Normalised coordinates x_i / L and y_i / H (see Figure 8.3) of the multi-linear profile and the corresponding required reinforcement for $K_h = 0$, cohesion-less soil, and uniform distribution of reinforcement. The toe point P_0 has the coordinates (0,0) and the crest point P_{11} has (1,1).

$\beta°$	$\phi°$	$K_t/\gamma H$	y_i/H (Normalised height of the point P_i measured from the toe)									
			0.09	0.18	0.27	0.36	0.45	0.55	0.64	0.73	0.82	0.91
			x_i/H (Normalised horizontal distance of the point P_i measured from the toe)									
			P_1	P_2	P_3	P_4	P_5	P_6	P_7	P_8	P_9	P_{10}
45	20	0.075648	0.0020	0.0252	0.1750	0.3550	0.5327	0.6843	0.8551	0.9940	0.9997	0.9998
	30	0.022193	0.0005	0.1182	0.2547	0.3822	0.5123	0.6264	0.7475	0.8586	0.9590	0.9947
	40	0.002864	0.0000	0.0004	0.1999	0.3503	0.4447	0.5502	0.6501	0.7396	0.8253	0.9100
50	20	0.090828	0.0033	0.0285	0.2379	0.4397	0.6124	0.8197	0.9581	0.9998	0.9999	0.9999
	30	0.032881	0.0015	0.1026	0.2768	0.4153	0.5519	0.6867	0.8215	0.9338	0.9968	0.9999
	40	0.007625	0.0034	0.1724	0.2435	0.3752	0.4965	0.5935	0.7068	0.8084	0.9052	0.9812
55	20	0.109859	0.0033	0.0353	0.1690	0.4607	0.7557	0.8803	0.9802	0.9928	0.9985	0.9993
	30	0.045326	0.0011	0.1032	0.3116	0.4635	0.6035	0.7796	0.8938	0.9803	0.9982	0.9982
	40	0.014172	0.0045	0.1644	0.2944	0.4069	0.5373	0.6558	0.7697	0.8765	0.9619	0.9999
60	20	0.128288	0.0054	0.0505	0.1439	0.5262	0.8764	0.9706	0.9999	0.9999	0.9999	1.0000
	30	0.058226	0.0040	0.1551	0.3291	0.5483	0.7315	0.8682	0.9658	0.9991	0.9993	0.9996
	40	0.02219	0.0054	0.1878	0.3222	0.4687	0.6053	0.7301	0.8505	0.9440	0.9999	1.0000
65	20	0.148059	0.0067	0.0291	0.2829	0.8061	0.9413	0.9995	0.9996	0.9999	0.9998	1.0000
	30	0.072403	0.0064	0.2460	0.4760	0.6755	0.8325	0.9476	0.9997	0.9998	0.9988	0.9992
	40	0.03177	0.0068	0.2358	0.3966	0.5353	0.7009	0.8280	0.9304	0.9999	0.9999	1.0000
70	20	0.167701	0.0086	0.0801	0.7184	0.9009	0.9995	0.9999	0.9999	0.9999	0.9999	1.0000
	30	0.088565	0.0085	0.3333	0.4999	0.6666	0.8333	0.9995	0.9995	0.9999	0.9999	1.0000
	40	0.042992	0.0050	0.3182	0.5012	0.6653	0.8064	0.9224	0.9977	0.9991	0.9991	1.0000
75	20	0.191783	0.0103	0.6036	0.8419	0.9799	0.9890	0.9911	0.9948	0.9972	0.9996	1.0000
	30	0.106601	0.0115	0.5333	0.7529	0.9119	0.9907	0.9932	0.9933	0.9992	0.9997	0.9997
	40	0.056061	0.0104	0.4271	0.6229	0.7907	0.9235	0.9897	0.9997	0.9997	0.9994	0.9994
80	20	0.221727	0.4698	0.7962	0.9525	0.9790	0.9824	0.9843	0.9946	0.9977	0.9988	1.0000
	30	0.12507	0.3691	0.6564	0.8885	0.9831	0.9880	0.9969	0.9962	0.9982	0.9989	1.0000
	40	0.069986	0.2843	0.5417	0.764	0.9409	0.9860	0.9869	0.9889	0.9996	0.9996	1.0000
85	20	0.249993	0.6074	0.9456	0.9566	0.9664	0.9752	0.9756	0.9883	0.9942	0.9966	0.9961
	30	0.147369	0.4999	0.9148	0.9645	0.9664	0.9812	0.9843	0.9932	0.9974	0.9983	0.9977
	40	0.087855	0.4283	0.7918	0.9678	0.9840	0.9843	0.9864	0.9885	0.9891	0.9912	0.9961

Table F.2 Normalised coordinates x_i/L and y_i/H (see Figure 8.3) of the multi-linear profile and the corresponding required reinforcement for $K_h = 0$, cohesion-less soil, and linearly increasing distribution of reinforcement. The toe point P_0 has the coordinates (0,0) and the crest point P_{11} has (1,1).

$\beta°$	$\phi°$	$K_i/\gamma H$	y_i/H (Normalised height of the point P_i measured from the toe)									
			0.09	0.18	0.27	0.36	0.45	0.55	0.64	0.73	0.82	0.91
			x_i/H (Normalised horizontal distance of the point P_i measured from the toe)									
			P_1	P_2	P_3	P_4	P_5	P_6	P_7	P_8	P_9	P_{10}
45	20	0.068093	0.0031	0.0091	0.2271	0.3985	0.5595	0.7781	0.9517	0.9999	1.0000	1.0000
	30	0.020486	0.0031	0.1324	0.2642	0.4041	0.5101	0.6558	0.747	0.8824	0.9654	0.9942
	40	0.002525	0.0565	0.1177	0.2389	0.3503	0.4647	0.5702	0.6601	0.7546	0.8553	0.9299
50	20	0.082921	0.0034	0.0341	0.2395	0.4251	0.7075	0.9181	0.9868	0.9999	1.0000	1.0000
	30	0.030297	0.0038	0.0748	0.1773	0.4428	0.5862	0.7227	0.8561	0.9478	0.9999	0.9999
	40	0.007086	0.0033	0.1594	0.2798	0.3780	0.4983	0.6066	0.7124	0.8159	0.9118	0.9815
55	20	0.098253	0.0029	0.0379	0.2448	0.6462	0.8288	0.9595	0.9893	0.9967	0.9967	1.0000
	30	0.040836	0.0019	0.1943	0.3370	0.4667	0.6791	0.8169	0.9188	0.985	1.0000	1.0000
	40	0.013323	0.0003	0.1743	0.3050	0.4186	0.5495	0.6669	0.7806	0.8823	0.9581	0.9867
60	20	0.112429	0.0050	0.0173	0.5172	0.8074	0.928	0.9996	0.9999	0.9999	0.9999	1.0000
	30	0.052176	0.0053	0.2369	0.4388	0.6193	0.7719	0.8867	0.9675	1.0000	1.0000	1.0000
	40	0.020327	0.0044	0.2078	0.3516	0.4931	0.6284	0.7531	0.8607	0.9449	0.9965	0.9956
65	20	0.127992	0.0000	0.3718	0.6913	0.8788	0.9794	0.9998	1.0000	1.0000	1.0000	1.0000
	30	0.065492	0.0066	0.3332	0.5000	0.6667	0.8333	0.9526	1.0000	1.0000	1.0000	1.0000
	40	0.028752	0.0067	0.2724	0.4343	0.5837	0.7206	0.8371	0.9299	0.9948	1.0000	1.0000
70	20	0.143884	0.0069	0.6036	0.8044	0.9423	0.9995	0.9997	0.9996	0.9999	0.9999	0.9999
	30	0.078072	0.0084	0.4578	0.6491	0.8049	0.9244	0.9996	0.9996	0.9996	1.0000	1.0000
	40	0.038545	0.0080	0.3589	0.5285	0.6806	0.8107	0.9158	0.9930	0.9997	0.9998	0.9998
75	20	0.159751	0.3330	0.6663	0.8789	0.9964	0.9982	0.9994	0.9999	0.9995	0.9998	1.0000
	30	0.091306	0.2854	0.5268	0.726	0.8841	0.9997	0.9993	1.0000	1.0000	1.0000	1.0000
	40	0.04903	0.2255	0.4311	0.6138	0.7704	0.8984	0.9962	0.9997	0.9998	0.9998	0.9999
80	20	0.175604	0.4292	0.7465	0.9786	0.9979	0.9985	0.9982	0.9997	0.9999	0.9999	0.9999
	30	0.106976	0.3326	0.6102	0.8355	0.9996	0.9995	0.9996	0.9999	0.9999	0.9999	0.9999
	40	0.061469	0.2718	0.5127	0.7193	0.8917	0.9999	0.9998	0.9997	0.9998	0.9999	0.9999
85	20	0.201316	0.4990	0.9905	0.9919	0.9952	0.9947	0.9972	0.9972	0.9983	0.9979	0.9995
	30	0.130626	0.3331	0.6664	0.9968	0.9989	0.9986	0.9996	0.9997	0.9999	0.9999	0.9999
	40	0.079198	0.3926	0.7286	0.9975	0.9969	0.9987	0.9996	0.9998	0.9999	0.9999	0.9999

Appendix G: Program Scripts (Matlab R2016a)

G.1 Scripts used in Chapter 3: Fissured slopes subject to earthquake

```matlab
% Main program
% -------------------------------------------------------------------
clear

% Input data
% -------------------------------------------------------------------
% slope inclination [deg]
beta_grad_high=65;
beta_grad_low=65;
deltabeta_grad=1;
% friction angle [deg]
phi_grad=20
%-------------------------------------------------------------------
% seismic coefficients
K_h=0.0;
lambda=0;      % ratio of Kv/Kh


%-------------------------------------------------------------------
% guess values
x_guess_grad_ini=40
y_guess_grad_ini=91
z_guess_grad_ini=55
x_delta_grad=4;
y_delta_grad=4;
z_delta_grad=4;

% unit weights
gamma=20;
gamma_w=10;
gammarat=gamma_w/gamma;

% derived variables
n1=fix((beta_grad_high-beta_grad_low)/deltabeta_grad)+1 %round the decimal number to
lower integer

beta_grad=beta_grad_low:deltabeta_grad:beta_grad_high
b=tan(phi_grad/180*pi);
K_v=K_h*lambda;
% determination of angles in radians
beta=beta_grad/180*pi;

X0=[x_guess_grad_ini/180*pi;y_guess_grad_ini/180*pi;z_guess_grad_ini/180*pi];
Xdelta=[x_delta_grad/180*pi,y_delta_grad/180*pi,z_delta_grad/180*pi];

for i=1:n1
    if flag==1
        %
    else
        [X,M_]=funxyz_seismic(X0,Xdelta,b,beta(i),K_h,lambda);
    end
    if M_==-1
        string='minimum not found'
        break
    elseif M_==-2
        string='found minimum is not absolute'
        break
    end
    M(i)=M_
    x(i)=X(1);
    y(i)=X(2);
```

```
    z(i)=X(3);
    X0=X;

    d_norm=(exp(b*(z(i)-x(i)))*sin(z(i))-sin(x(i)))/(exp(b*(y(i)-x(i)))*sin(y(i))-
sin(x(i)));
    Lrx=sin(y(i)-x(i))/sin(y(i))-
sin(y(i)+beta(i))/(sin(y(i))*sin(beta(i)))*(exp(b*(y(i)-x(i)))*sin(y(i))-sin(x(i)));
    lrx=-exp(b*(z(i)-x(i)))*cos(z(i))+cos(x(i));
    rx_norm=1/(exp(b*(y(i)-x(i)))*sin(y(i))-sin(x(i)));
    hx_norm(i)=(Lrx-lrx)*rx_norm;
    Xcir=-rx_norm.*exp(b.*(y(i)-x(i))).*cos(y(i));
    Ycir=rx_norm.*exp(b.*(y(i)-x(i))).*sin(y(i));


    % normalized area of failure af/h^2

area1_norm=rx_norm^2*(exp(2*b*(y(i)-x(i)))-1)/(4*b);
area2_norm=1/2*rx_norm^2*sin(x(i))*(-exp(b*(y(i)-x(i)))*cos(y(i))+cos(x(i)));
area3_norm=1/2*rx_norm*exp(b*(y(i)-x(i)))*cos(y(i));
area4_norm=cot (beta(i))/2;
area5_norm=rx_norm^2*(exp(2*b*(z(i)-x(i)))-1)/(4*b);
area6_norm=1/2*rx_norm^2*sin(x(i))*(cos(x(i))-exp(b*(z(i)-x(i)))*cos(z(i)));
area7_norm=1/2*rx_norm^2*(exp(b*(z(i)-x(i)))*sin(z(i))-sin(x(i)))*exp(b*(z(i)-
x(i)))*cos(z(i));
af(i)=area1_norm-area2_norm-area3_norm-area4_norm-area5_norm+area6_norm+area7_norm;


end

c_norm=1./M;
x_grad=x.*180./pi;
y_grad=y.*180./pi;
z_grad=z.*180./pi;

%Plotting
H_ini=1;
plot_line(H_ini,beta,'k')
axis equal
plot_line(H_ini,phi,'g')
% Spiral plotting
for j=1:n1
    plot_spiral_tenscrack
end
hold off


figure(1)
hold on
plot(phi_grad,c_norm,'LineStyle','-','LineWidth',1,'Color','k');
% lambda=1 dashed; lambda=0.5 solid; lambda=0 dashed-dotted
xlabel('\phi_m [deg]');
ylabel('N_m');

figure(2)
hold on
plot(phi_grad,d_norm,'LineStyle','-','LineWidth',1,'Color','k');
xlabel('\phi_m [deg]');
ylabel('\delta/H');

figure(3)
hold on
plot(phi_grad,lrx,'LineWidth',1,'Color','g');
xlabel('\phi_m [deg]');
ylabel('horizontal distance of crack from slope crest');
plot(phi_grad,Lrx,'LineWidth',1,'Color','r');
plot(phi_grad,hx_norm,'LineWidth',1,'Color','k');
hold off
------


function [X,M_] = funxyz(X0,Xdelta,b,beta,K_h,lambda);
```

```
K_v=lambda*K_h;
x_guess=X0(1);
y_guess=X0(2);
z_guess=X0(3);
x_delta=Xdelta(1);
y_delta=Xdelta(2);
z_delta=Xdelta(3);
x_range=(-x_delta+x_guess):(0.1/180*pi):(x_delta+x_guess);
y_range=(-y_delta+y_guess):(0.1/180*pi):(y_delta+y_guess);
z_range=(-z_delta+z_guess):(0.1/180*pi):(z_delta+z_guess);
x_range_grad=x_range*180/pi;
y_range_grad=y_range*180/pi;
z_range_grad=z_range*180/pi;

m=size(x_range);
n3=m(2);
m=size(y_range);
n4=m(2);
m=size(z_range);
n5=m(2);
for k=1:n3
    for l=1:n4
        for j=1:n5
            if (x_range(k)>y_range(l)-10e-6) | (x_range(k)>z_range(j)-10e-6) |
(z_range(j)>y_range(l)-10e-6)
                funM(k,l,j)=NaN;
            else
                fHrx=exp(b*(y_range(l)-x_range(k)))*sin(y_range(l))-sin(x_range(k));
                fd=exp(2*b*(z_range(j)-x_range(k)))*(exp(2*b*(y_range(l)-
z_range(j)))-1)/(2*b);
                f1_v=(exp(3*b*(y_range(l)-
x_range(k)))*(sin(y_range(l))+3*b*cos(y_range(l)))-3*b*cos(x_range(k))-
sin(x_range(k)))/(3*(1+9*b^2));
                fLrx=sin(y_range(l)-x_range(k))/sin(y_range(l))-
sin(y_range(l)+beta)/(sin(y_range(l))*sin(beta))*(exp(b*(y_range(l)-
x_range(k)))*sin(y_range(l))-sin(x_range(k)));
                f2_v=1/6*fLrx*sin(x_range(k))*(2*cos(x_range(k))-fLrx);
                f3_v=1/6*exp(b*(y_range(l)-x_range(k)))*(sin(y_range(l)-x_range(k))-
fLrx*sin(y_range(l)))*(cos(x_range(k))-fLrx+cos(y_range(l))*exp(b*(y_range(l)-
x_range(k))));
                f4_v=(exp(3*b*(z_range(j)-
x_range(k)))*(sin(z_range(j))+3*b*cos(z_range(j)))-3*b*cos(x_range(k))-
sin(x_range(k)))/(3*(1+9*b^2));
                f5_v=1/6*sin(x_range(k))*((cos(x_range(k)))^2-exp(2*b*(z_range(j)-
x_range(k)))*(cos(z_range(j)))^2);
                f6_v=1/3*exp(2*b*(z_range(j)-
x_range(k)))*(cos(z_range(j)))^2*(sin(z_range(j))*exp(b*(z_range(j)-x_range(k)))-
sin(x_range(k)));
                flrx=cos(x_range(k))-exp(b*(z_range(j)-x_range(k)))*cos(z_range(j));
                f1_h=(exp(3*b*(y_range(l)-x_range(k)))*(-
cos(y_range(l))+3*b*sin(y_range(l)))-
3*b*sin(x_range(k))+cos(x_range(k)))/(3*(1+9*b^2));
                f2_h=1/3*fLrx*(sin(x_range(k)))^2;
                f3_h=1/6*exp(b*(y_range(l)-x_range(k)))*(sin(y_range(l)-x_range(k))-
fLrx*sin(y_range(l)))*(exp(b*(y_range(l)-
x_range(k)))*sin(y_range(l))+sin(x_range(k)));
                f4_h=(exp(3*b*(z_range(j)-x_range(k)))*(3*b*sin(z_range(j))-
cos(z_range(j)))-3*b*sin(x_range(k))+cos(x_range(k)))/(3*(1+9*b^2));
                f5_h=1/3*flrx*(sin(x_range(k)))^2;
                f6_h=1/6*exp(b*(z_range(j)-
x_range(k)))*cos(z_range(j))*(exp(2*b*(z_range(j)-x_range(k)))*sin(z_range(j))^2-
sin(x_range(k))^2);
                % no need for function p4 since most critical mechanism
                % never involves a crack from the slope face
                funM(k,l,j)=(fHrx*fd)/((f1_v-f2_v-f3_v-f4_v+f5_v+f6_v)*(1+K_v)+(f1_h-
f2_h-f3_h-f4_h+f5_h+f6_h)*K_h);
            end
            if (funM(k,l,j) < 1.0) | (funM(k,l,j) > 10e8)
                funM(k,l,j)=NaN;
            end
        end
    end
```

```
        end
end
i=1;
for k=2:(n3-1)
    for l=2:(n4-1)
        for j=2:(n5-1)
            if (funM(k,l,j)<Inf)
                if (funM(k-1,l,j)>funM(k,l,j)) && (funM(k+1,l,j)>funM(k,l,j)) &&
(funM(k,l-1,j)>funM(k,l,j)) && (funM(k,l+1,j)>funM(k,l,j)) && (funM(k,l,j-
1)>funM(k,l,j)) && (funM(k,l,j+1)>funM(k,l,j)) &&(funM(k-1,l-1,j)>funM(k,l,j)) &&
(funM(k-1,l+1,j)>funM(k,l,j)) && (funM(k+1,l-1,j)>funM(k,l,j)) &&
(funM(k+1,l+1,j)>funM(k,l,j)) &&(funM(k-1,l,j-1)>funM(k,l,j)) && (funM(k-
1,l,j+1)>funM(k,l,j)) && (funM(k+1,l,j-1)>funM(k,l,j)) &&
(funM(k+1,l,j+1)>funM(k,l,j)) &&(funM(k,l-1,j-1)>funM(k,l,j)) && (funM(k,l-
1,j+1)>funM(k,l,j)) && (funM(k,l+1,j-1)>funM(k,l,j)) && (funM(k,l+1,j+1)>funM(k,l,j))
&& (funM(k-1,l-1,j-1)>funM(k,l,j)) && (funM(k+1,l+1,j+1)>funM(k,l,j))
                    potminima(i)=funM(k,l,j);
                    potx(i)=k;
                    poty(i)=l;
                    potz(i)=j;
                    i=i+1;
                end
            end
        end
    end
end
[M_,II]=min(potminima);
% test to check that the found minimum is an absolute minimum in the
% assigned domain
test=min(min(min(funM)));
if M_==test
    k=potx(II);
    l=poty(II);
    j=potz(II);
    X(1)=x_range(k);
    X(2)=y_range(l);
    X(3)=z_range(j);
else
    M_=-1;
    X(1)=NaN;
    X(2)=NaN;
    X(3)=NaN;
end
```

G.2 Scripts used in Chapter 4 and 5: Reinforcement for cohesive backfills

```
% Main program
% -----------------------------------------------------------------------
clear
clc
% Input data
% -----------------------------------------------------------------------
% c/gamma.H : cogh is the normalized cohesion
cogh=0.0%:0.01:0.1;
%n1=max(size(cogh));

% Kh horizontal seismic coefficient
Kh=0:0.05:0.3;
n1=max(size(Kh));

% friction angle [deg]
```

```
phi_grad=30;
phi=phi_grad/180*pi;
b=tan(phi);

%  slope inclination [deg]
beta_grad=45:5:45;
beta=beta_grad/180*pi;
%n1=max(size(beta_grad));

% imaginary slope inclination for the below the toe failure
beta_prime_grad=beta_grad;
beta_prime=beta_prime_grad*pi/180;

% pore pressure coefficient ru
ru=0.0;
% reinforcement layout RL, for uniform Rl=1 and for LID, RL=2
RL=1;
N=6 ; % number of layers (for plotting only)
% unit weights
gamma=20;
gamma_w=10;
gammarat=gamma_w/gamma;
% Crack scenario: (for nil tensile strength of soil, t=0), (for half of Mohr-Coulomb
% unconfined tensile strength t=0.5), (for  whole Mohr-Coulomb unconfined tensile
strength t=1)
% and (for pre-existing crack, t=-1), for intact slope i.e. no crack t=2
t=2;


% range of the angles
x_range_grad=-40:1:80;
y_range_grad=60:1:120;
z_range_grad=0:1:80;

x_range=x_range_grad*pi/180;
y_range=y_range_grad*pi/180;
z_range=z_range_grad*pi/180;

n3=max(size(x_range));
n4=max(size(y_range));
n5=max(size(z_range));



d=0;
for i=1:n1
    for k=1:n3
        for l=1:n4
            for j=1:n5
                if (x_range(k)>y_range(l)-10e-6) || (x_range(k)>z_range(j)-10e-6) ||
(z_range(j)>y_range(l)-10e-6)
                    K_req_(k,l,j)=NaN;
                    Z(k,l,j)=NaN;
                    F(k,l,j)=NaN;
                else

[X,Kreq_,Flag]=funxyz_n(x_range(k),y_range(l),z_range(j),b,beta,cogh,Kh(i),t,ru,gamma
rat,RL);

                    K_req_(k,l,j)=Kreq_;
                    Z(k,l,j)=X;
                    F(k,l,j)=Flag;
                end
            end
        end
    end

    [Kreq(i), I]=max(K_req_(:))
    [I2,I3,I4] = ind2sub(size(K_req_),I);

    ZZ=Z(:);
    z_(i)=ZZ(I);
```

191

```matlab
    FF=F(:);
    flag(i)=FF(I);

    beta_prime_=beta_prime;
    x_(i)=x_range(I2);
    y_(i)=y_range(I3);
    %z_(i)=z_range(I4);
    if   (I2==n3)
        d=d+1
        kreq=NaN;
        string='Increase x_range'
    elseif (I2==1)
        d=d+1
        kreq=NaN;
        string='Decrease x_range'
    elseif (I3==n4)
        d=d+1
        kreq=NaN;
        string='Increase y_range'
    elseif (I3==1)
        d=d+1
        kreq=NaN;
        string='Decrease y_range'
    end
    if flag(i)>0
        string='Active constraint'
    end

end

K_req=Kreq;
flag_=flag;
betaprime_grad=beta_prime_*180/pi;
x_grad=x_.*180./pi;
y_grad=y_.*180./pi;
z_grad=z_.*180./pi;
betaprime=beta_prime_;
dd=d;

d_norm=(exp(b*(z_-x_)).*sin(z_)-sin(x_))./(exp(b.*(y_-x_)).*sin(y_)-sin(x_));
Lrx=-exp(b.*(y_-
x_)).*sin(betaprime+y_)./sin(betaprime)+sin(betaprime+x_)./sin(betaprime);
lrx=-exp(b.*(z_-x_)).*cos(z_)+cos(x_);
rx_norm=1./(exp(b.*(y_-x_)).*sin(y_)-sin(x_));
hx_norm=(Lrx-lrx).*rx_norm;
Xcir=-rx_norm.*exp(b.*(y_-x_)).*cos(y_);
Ycir=rx_norm.*exp(b.*(y_-x_)).*sin(y_);

figure(2)
hold on
% Plotting
H_ini=1;
% Spiral plotting
for j=1:i
    plot_line(H_ini,beta,'k')
    axis equal
    plot_line_toe(H_ini,0,'k')
    plot_crack(H_ini,beta,'g',d_norm(j),hx_norm(i))
    plot_line_slopesurface(H_ini,beta,'k')
    plot_line_reinforcement(H_ini,beta,N,RL,'b')
    plot_spiral_tenscrack_betaprime
    plot_line_white(H_ini,beta,'w')
end
hold off

if RL==1
    string='using Uniform Distribution of reinforcement'
else
    string='using Linearly Increasing Distribution of reinforcement'
end
------
```

```matlab
function [X,Kreq_,Flag] =
funxyz_n(x_range,y_range,z_range,b,beta,cogh,Kh,t,ru,gammarat,RL)

x=x_range;
y=y_range;
z=z_range;

beta_prime=beta;

Hrx=(exp(b*(y-x)))*sin(y)-sin(x);  %  H/rx
phi=atan(b);

c_d=(1/Hrx)*exp(b*(z-x))*sin(z)-sin(x);% current depth of the crack
if ru==0
    m_d=3.83*cogh*tan(pi/4+phi/2) ; %maximum dry crack depth
else
    m_d=(2*cogh*tan(pi/4+phi/2))/(1-ru);   %maximum wet crack depth
end
if c_d > m_d
    F=1;
    if cogh==0
        z=x;
    else
        x0=x;
        % fun=@(th_1)exp(b*(th_1-x_range(k)))*cos(th_1)-cos(x_range(k))+fLrx;
        options = optimset('TolX',1e-10);
        [z, ~, ~, output] = fzero(@(z)exp(b*(z-x))*sin(z)-sin(x)-m_d,x0,options);
    end
else
    z=z_range;
    F=0;
end


% calculations of the dissipated enrgey function for the crack formation
tan_theta_c=sin(x)/((exp(b*(z-x)))*cos(z));
theta_c=atan(tan_theta_c);
if t==2
    z=x;
    gc=0;

elseif t==0
    ft=0;
    int_ft=0;
    int_fc = integral(@(theta) (1-sin(theta))./(cos(theta)).^3,theta_c,z);
    fc=2*cos(phi)/(1-sin(phi));
    gc=(sin(x)/tan_theta_c)^2*(fc/2*int_fc+ft/(1-sin(phi))*int_ft);
elseif t==0.5
    int_fc = integral(@(theta) (1-sin(theta))./(cos(theta)).^3,theta_c,z);
    int_ft = integral(@(theta) (sin(theta)-sin(phi))./(cos(theta)).^3,theta_c,z);
    fc=2*cos(phi)/(1-sin(phi));
    ft=cos(phi)/(1+sin(phi));
    gc=(sin(x)/tan_theta_c)^2*(fc/2*int_fc+ft/(1-sin(phi))*int_ft);
elseif t==1
    int_fc = integral(@(theta) (1-sin(theta))./(cos(theta)).^3,theta_c,z);
    int_ft = integral(@(theta) (sin(theta)-sin(phi))./(cos(theta)).^3,theta_c,z);
    fc=2*cos(phi)/(1-sin(phi));
    ft=2*cos(phi)/(1+sin(phi));
    gc=(sin(x)/tan_theta_c)^2*(fc/2*int_fc+ft/(1-sin(phi))*int_ft);
else
    gc=0;
end

g1=((exp(2*b*(z-x)))*(exp(2*b*(y-z))-1))/(2*b);


if RL==1
    %  for uniformly distributed mode:
    if  x<0
        g23=(exp(2*b*(y-x))*(sin(y))^2)/2;
    else
        g23=(exp(2*b*(y-x))*(sin(y))^2-(sin(x))^2)/2;
```

```
        end
else
    %  for linearly increasing density mode:
    if   x<0
        g23=(2/Hrx)*((1/3)*(exp(3*b*(y-x))*(sin(y))^3)-(sin(x)/2)*(exp(2*b*(y-
x))*(sin(y))^2));
    else
        g23=(2/Hrx)*((1/3)*(exp(3*b*(y-x))*(sin(y))^3-(sin(x))^3)-
(sin(x)/2)*(exp(2*b*(y-x))*(sin(y))^2-(sin(x))^2));
    end
end

f1=(exp(3*b*(y-x))*(sin(y)+3*b*cos(y))-3*b*cos(x)-sin(x))/(3*(1+9*b^2));
Lrx=-exp(b*(y-
x))*sin(beta_prime+y)/sin(beta_prime)+sin(beta_prime+x)/sin(beta_prime);
f2=1/6*Lrx*sin(x)*(2*cos(x)-Lrx);
f3=1/6*exp(b*(y-x))*(sin(y-x)-Lrx*sin(y))*(cos(x)-Lrx+cos(y)*exp(b*(y-x)));
%f4=1/2*Hrx^2*(cot(beta_prime)-cot(beta))*(cos(x)-Lrx-
1/3*Hrx*(cot(beta_prime)+cot(beta))) ;% for below the toe failure
p1=(exp(3*b*(z-x))*(sin(z)+3*b*cos(z))-3*b*cos(x)-sin(x))/(3*(1+9*b^2));
p2=1/6*sin(x)*((cos(x))^2-exp(2*b*(z-x))*(cos(z))^2);
p3=1/3*exp(2*b*(z-x))*(cos(z))^2*(sin(z)*exp(b*(z-x))-sin(x));
lrx=cos(x)-exp(b*(z-x))*cos(z);
f1_h=(exp(3*b*(y-x))*(-cos(y)+3*b*sin(y))-3*b*sin(x)+cos(x))/(3*(1+9*b^2));
f2_h=1/3*Lrx*(sin(x))^2;
f3_h=1/6*exp(b*(y-x))*(sin(y-x)-Lrx*sin(y))*(exp(b*(y-x))*sin(y)+sin(x));
p1_h=(exp(3*b*(z-x))*(3*b*sin(z)-cos(z))-3*b*sin(x)+cos(x))/(3*(1+9*b^2));
p2_h=1/3*lrx*(sin(x))^2;
p3_h=1/6*exp(b*(z-x))*cos(z)*(exp(2*b*(z-x))*sin(z)^2-sin(x)^2);

% Calculation of external work rate done by pore pressure along the log-spiral part
using ru
if ru==0
    pu=0;
else
    % first: calculation of the angle Th_1 (the angle made by the line between point
P and the point of vertical projection of the crest point on the log-spiral surface
    x0=0.5;
    % fun=@(th_1)exp(b*(th_1-x_range(k)))*cos(th_1)-cos(x_range(k))+fLrx;
    options = optimset('TolX',1e-10);
    [Th_1, ~, ~, output] = fzero(@(Th_1)exp(b*(Th_1-x))*cos(Th_1)-
cos(x)+Lrx,x0,options);
    if (Th_1>y-10e-6)  || (Th_1<x)
        funK=NaN;
    end
    if beta_prime<beta
        x1=y; %(Th_1+y)/2;
        options = optimset('TolX',1e-10);
        [Th_2, ~, ~, output2] = fzero(@(Th_2)exp(b*(Th_2-x))*cos(Th_2)-
cos(x)+Lrx+Hrx*cot(beta),x1,options);
        if (Th_2>y-10e-6)  || (Th_2<Th_1)
            funK=NaN;
        end
        u_3=@(Th)(exp(b.*(Th-x)).*sin(Th)-exp(b.*(y-x))*sin(y)).*b.*(exp(2.*b.*(Th-
x)));
        u3=integral(u_3,Th_2,y);
    else
        u3=0;
    end
    % second: calculation of the angle th_w (which is the angle betwen the hoizontal
and the chord between the point p and the water level within the crack.
    d_ = exp(b*(z-x))*sin(z)-sin(x);  % the depth of the crack

    th_w=atan((exp(b*(z-x))*sin(z)-ru*(1/gammarat)*d_)/(exp(b*(z-x))*cos(z)));

    % third calculations of uc, u1 and u2
    u_c=@(Th)(exp(b.*(z-x)).*cos(z).*tan(Th)-sin(x)).*tan(Th).*(exp(2.*b.*(z-
x)).*(cos(z)).^2)./(cos(Th)).^2;
    u_1=@(Th)(exp(b.*(Th-x)).*sin(Th)-sin(x)).*b.*(exp(2.*b.*(Th-x)));
    u_2=@(Th)(exp(b.*(Th-x)).*sin(Th)-(exp(b.*(Th_1-x)).*cos(Th_1)-exp(b.*(Th-
x)).*cos(Th)).*tan(beta)-sin(x)).*b.*(exp(2.*b.*(Th-x)));
```

```
    % forth: integration of uc, u1 and u2
    uc=integral(u_c,th_w,z);
    u1=integral(u_1,z,Th_1);
    u2=integral(u_2,Th_1,y);
    pu=ru*(uc+u1+u2+u3);
end

if ((exp(b*(z-x))*cos(z))>= (exp(b*(y-x))*cos(y)+Hrx*cot(beta))) %tension crack is
from the slope crest
    funK=(((f1-f2-f3-p1+p2+p3)+Kh*(f1_h-f2_h-f3_h-p1_h+p2_h+p3_h))/(Hrx*g23))-
cogh*((g1+gc)/g23);
else
    funK=(((f1-f2-f3-p1+p2+p3)+Kh*(f1_h-f2_h-f3_h-p1_h+p2_h+p3_h))/(Hrx*g23))-
cogh*((g1+gc)/g23);
end
if Lrx< 0
    funK=-2;
end
% end
if  funK>3 || funK<-1
    Kreq_=NaN;
else
    Kreq_=funK;
end
X=z;

Flag=F;
end
```

G.3 Scripts used in Chapter 6: Earthquake-induced displacement

```
% Main program
% -----------------------------------------------------------------------
clear
clc
% Input data
% -----------------------------------------------------------------------
% friction angle [deg]
phi_grad=20;
phi=phi_grad/180*pi;
b=tan(phi);

%  slope inclination [deg]
beta_grad=60;
beta=beta_grad/180*pi;
n1=max(size(beta_grad));
% imaginary slope inclination for the below the toe failure
beta_prime_grad=beta_grad
beta_prime=beta_prime_grad*pi/180;

% c/gamma*H cogh
cogh=0;

% lambda=Kv/Kh ratio
lambda=0;

acc=load('Northridge Moorpark.txt'); % importing earthquake acceleration data.
z1=acc';
c1=z1(:);
L=c1';
K=L(1:1000);
d=size(K);
m1=d(2)
t_interval= 0.02; % the time interval (sec), given with the earthquake data.
t=0:t_interval:(m1-1)*(t_interval);
Kmax=max(K);
% soil tensile strength (for tension cut-off, T=0), (for limited tensile
% strength T=0.5) and (for pre-existing crack, T=1),and (for intact, T=1.5)
```

195

```
T=1.5;

% pore pressure coefficient ru
ru=0;

gamma=20;
gamma_w=10;
gammarat=gamma_w/gamma;

% range of the angles
x_range_grad=0:1:80;
y_range_grad=50:1:130;
z_range_grad=0:1:80;

x_range=x_range_grad*pi/180;
y_range=y_range_grad*pi/180;
z_range=z_range_grad*pi/180;

n3=max(size(x_range));
n4=max(size(y_range));
n5=max(size(z_range));
c=0;
d=0;
for i=1:n1
    beta_prime_grad=(beta_grad):(-2):(beta_grad-0);
    beta_prime=beta_prime_grad*pi/180;
    n2=max(size(beta_prime));
    for h=1:n2
        for k=1:n3
            for l=1:n4
                for j=1:n5
                    if (x_range(k)>y_range(l)-10e-6) || (x_range(k)>z_range(j)-10e-6)
|| (z_range(j)>y_range(l)-10e-6)|| (z_range(j)<0)
                        M_(k,l,j)=NaN;
                    elseif (h>1) && (y_range(l)*180/pi)< (90+phi_grad)
                        M_(k,l,j)=NaN;
                    else

[N]=funxyz(x_range(k),y_range(l),z_range(j),b,beta,beta_prime(h),cogh,ru,gammarat,T(i
),lambda);

                        M_(k,l,j)=N;
                    end
                end
            end
        end
    end

    [Ya(i), I]=min(M_(:))
    [I2,I3,I4] = ind2sub(size(M_),I);

    beta_prime_=beta_prime;
    x(i)=x_range(I2);
    y(i)=y_range(I3);
    z(i)=z_range(I4);

    if (I2==n3) |(I2==1)
        d=d+1
        Ya(i)=NaN;
        string='increase x_range'
    elseif (I3==n4) |(I3==1)
        d=d+1
        Ya(i)=NaN;
        string='increase y_range'
    elseif (I4==n5) |(I4==1)
        d=d+1
        Ya(i)=NaN;
        string='increase z_range'
    end

end
```

```
for i=1:n1
    % Calculation of the yield acceleration considering pre-existing crack instead of
the formed one.
    if T(i)==1.5
        Ya_p(i)=Ya(i);
        x_range=x(i);
        y_range=y(i);
        z_range=x(i);
    else
        T(i)=1; % that means pre-existing crack
        x_range=x(i);
        y_range=y(i);
        z_range=z(i);

[N]=funxyz(x_range,y_range,z_range,b,beta,beta_prime,cogh,ru,gammarat,T(i),lambda);
        Ya_p(i)=N
    end


    %calculation of the dimensionless coefficient C (following Michalowski 99),
useful parameters:
    Lrx(i)=sin(y(i)-x(i))./sin(y(i))-(exp(b.*(y(i)-x(i))).*sin(y(i))-
sin(x(i))).*sin(y(i)+beta)./(sin(y(i)).*sin(beta));
    lrx(i)=-exp(b.*(z(i)-x(i))).*cos(z(i))+cos(x(i));
    rx_norm(i)=1./(exp(b.*(y(i)-x(i))).*sin(y(i))-sin(x(i)));
    hx_norm(i)=(Lrx(i)-lrx(i)).*rx_norm(i);
    fHrx(i)= (exp(b.*(y(i)-x(i)))).*sin(y(i))-sin(x(i));  % H/rx
    delta(i)=exp(b.*(z(i)-x(i))).*sin(z(i))-sin(x(i));   % crack depth/rx
    f1_v(i)=(exp(3.*b.*(y(i)-x(i))).*(sin(y(i))+3.*b.*cos(y(i)))-3.*b.*cos(x(i))-
sin(x(i)))./(3.*(1+9*b.^2));
    f2_v(i)=1./6.*Lrx(i).*sin(x(i)).*(2.*cos(x(i))-Lrx(i));
    f3_v(i)=1./6.*exp(b.*(y(i)-x(i))).*(sin(y(i)-x(i))-
Lrx(i).*sin(y(i))).*(cos(x(i))-Lrx(i)+cos(y(i)).*exp(b.*(y(i)-x(i))));
    f4_v(i)=(exp(3.*b.*(z(i)-x(i))).*(sin(z(i))+3.*b.*cos(z(i)))-3.*b.*cos(x(i))-
sin(x(i)))./(3.*(1+9.*b.^2));
    f5_v(i)=1./6.*sin(x(i)).*((cos(x(i))).^2-exp(2.*b.*(z(i)-x(i))).*(cos(z(i))).^2);
    f6_v(i)=1./3.*exp(2.*b.*(z(i)-x(i))).*(cos(z(i))).^2.*(sin(z(i)).*exp(b.*(z(i)-
x(i)))-sin(x(i)));
    f1_h(i)=(exp(3.*b.*(y(i)-x(i))).*(-cos(y(i))+3.*b.*sin(y(i)))-
3.*b.*sin(x(i))+cos(x(i)))./(3.*(1+9.*b.^2));
    f2_h(i)=1./3.*Lrx(i).*(sin(x(i))).^2;
    f3_h(i)=1./6.*exp(b.*(y(i)-x(i))).*(sin(y(i)-x(i))-
Lrx(i).*sin(y(i))).*(exp(b.*(y(i)-x(i))).*sin(y(i))+sin(x(i)));
    f4_h(i)=(exp(3.*b.*(z(i)-x(i))).*(3.*b.*sin(z(i))-cos(z(i)))-
3.*b.*sin(x(i))+cos(x(i)))./(3.*(1+9*b.^2));
    f5_h(i)=1./3.*lrx(i).*(sin(x(i))).^2;
    f6_h(i)=1./6.*exp(b.*(z(i)-x(i))).*cos(z(i)).*(exp(2.*b.*(z(i)-
x(i))).*sin(z(i)).^2-sin(x(i)).^2);
    % Calculation of (C)

    C_1(i)=(sin(y(i)).*exp(b.*(y(i)-x(i)))).*(lambda*(f1_v(i)-f2_v(i)-f3_v(i)-
f4_v(i)+f5_v(i)+f6_v(i))+(f1_h(i)-f2_h(i)-f3_h(i)-f4_h(i)+f5_h(i)+f6_h(i)));
    C_2(i)=(1/2).*((exp(2.*b.*(y(i)-x(i)))-1)./(2.*b)-Lrx(i).*sin(x(i))-
fHrx(i).*exp(b.*(y(i)-x(i))).*sin(beta+y(i))./(sin(beta))-(exp(2.*b.*(z(i)-x(i)))-
1)./(2.*b)+lrx(i).*sin(x(i))+delta(i).*(exp(b.*(z(i)-x(i))).*cos(z(i))));
    C_3(i)=(f1_v(i)-f2_v(i)-f3_v(i)-f4_v(i)+f5_v(i)+f6_v(i)).^2+(f1_h(i)-f2_h(i)-
f3_h(i)-f4_h(i)+f5_h(i)+f6_h(i)).^2;
    C_(i)=C_1(i).*C_2(i)/C_3(i);

    E=0;
    F=0;
    K(m1+1)=0;
    for jj=1:m1
        V(jj)=(((K(jj)-Ya(i))+(K(jj+1)-Ya(i)))./2).*100.*9.806.*(t_interval);
% where V is the velocity (cm/sec) (+ and -).
        e(jj)= V(jj)+E(jj);                                % to extract only
positive accumulated velocity where E(jj) is the previous velocity.
        if e(jj)<0
            e(jj)=0;
            D(jj)=F(jj);                                % F(jj) is the previous
displacment.
        else
```

```
            D(jj)=F(jj)+e(jj).*t_interval ;          % D is the accumulated block
displacement (cm) with respect to the ground surface (independent on the slope).
        end
        E(jj+1)=e(jj);
        F(jj+1)=D(jj);
    end
    Dx_f=C_(i).*D;    % the horizontal accumulated displacemnt (cm)due to the
formation of the crack.
    % finding the point at which the yield acceleration should drop (that is the
first time at which displacment occurs and completed).
    if Ya(i)<Kmax && Ya(i)> 0 && Ya_p(i)> 0

        for jj=1:m1
            if  ((e(jj)>0) && (e(jj+1)==0))
                dp(jj)=jj+1;
            end
        end
        vv=min(nonzeros(dp));
        D1=D(1:vv);   % dispalcement due to the initail yield acceleration.

        E(vv)=0;
        F(vv)=D(vv);
        for jj=vv:m1   % after the yield acceleration drop
            V(jj)=(((K(jj)-Ya_p(i))+(K(jj+1)-Ya_p(i)))./2).*100.*9.806.*(t_interval);
% where V is the velocity (cm/sec) (+ and -).
            e(jj)= V(jj)+E(jj);                               % to extract only
positive accumlated velocity where E(jj) is the previous velocity.
            if e(jj)<0
                e(jj)=0;
                Ds(jj)=F(jj);                                 % F(jj) is the
previous displacment.
            else
                Ds(jj)=F(jj)+e(jj).*t_interval ;        % D is the accumulated block
displacement (cm) with respect to the ground surface (independent on the slope).
            end
            E(jj+1)=e(jj);
            F(jj+1)=Ds(jj);
        end
        D2=Ds((vv):m1-1);

        DD=horzcat(D1,D2);

    else
        if Ya(i)>Kmax
            DD(1:m1)=0;
        else
            DD(1:m1)=NaN;
        end
    end

    K=K(1:m1);

    Dx_s=C_(i).*DD;    % Dx_int is the horizontal accumulated displacemnt (cm)
    Dmax(i)=(max(Dx_s));
    figure (3)
    hold on
    %     if i==n1
    %         plot (t,Dx_s,'k')
    %     elseif i==n1-1
    %         plot (t,Dx_s,'r')
    %     else
    %         plot (t,Dx_s,'b')
    %         plot (t,Dx_f,'g')
    %     end
    plot (t,Dx_s,'k')
    xlabel('time[sec]');
    ylabel('Displacement [cm]');
    title('Time-Displacement relationship')
    hold off
    if Ya(i)<Kmax && Ya(i)> 0 && Ya_p(i)> 0
        for jj=1:m1
            if jj<vv
```

```matlab
                Kys(jj)=Ya(i);
            else
                Kys(jj)=Ya_p(i) ;
            end
        end
    else
        Kys(1:m1)=Ya(i);
    end
    K=K(1:m1);
    figure (4)
    hold on
    plot (t,K);
    plot (t,Kys,'r');
    title('earthquake acc. with intact and cracked yield acc.')
    hold off

end
Dmax=Dmax';
Ky=Ya
Ky_p=Ya_p
C=C_;
betaprime_grad=beta_prime_*180/pi
x_grad=x.*180./pi
y_grad=y.*180./pi
z_grad=z.*180./pi
betaprime=beta_prime_;
cc=c
dd=d
z=x;
d_norm=(exp(b*(z-x)).*sin(z)-sin(x))./(exp(b.*(y-x)).*sin(y)-sin(x));
Lrx=-exp(b.*(y-
x)).*sin(betaprime+y)./sin(betaprime)+sin(betaprime+x)./sin(betaprime);
lrx=-exp(b.*(z-x)).*cos(z)+cos(x);
rx_norm=1./(exp(b.*(y-x)).*sin(y)-sin(x));
hx_norm=(Lrx-lrx).*rx_norm;
Xcir=-rx_norm.*exp(b.*(y-x)).*cos(y);
Ycir=rx_norm.*exp(b.*(y-x)).*sin(y);

% figure(1)
% hold on
% plot(T,Ky);
% xlabel('Tensile Strength');
% ylabel('Yield Acceleration');
% hold off

figure(2)
hold on
% Plotting
H_ini=1;
% Spiral plotting
for j=1:i
    plot_line(H_ini,beta,'k')
    axis equal
    plot_line_toe(H_ini,0,'k')
    plot_crack(H_ini,beta,'g',d_norm(j),hx_norm(j))
    plot_line_slopesurface(H_ini,beta,'k')
    plot_spiral_tenscrack_betaprime
end
hold off
------


function [N] =
funxyz(x_range,y_range,z_range,b,beta,beta_prime,cogh,ru,gammarat,T,lambda)

x=x_range;
y=y_range;
z=z_range;

phi=atan(b);
```

```
% calculations of the dissipated enrgey function for the crack formation
tan_theta_c=sin(x)/((exp(b*(z-x)))*cos(z));
theta_c=atan(tan_theta_c);
if T==1.5
    z=x;
    gc=0;
else
    if T==0
        ft=0;
        int_ft=0;
        int_fc = integral(@(theta) (1-sin(theta))./(cos(theta)).^3,theta_c,z);
        fc=2*cos(phi)/(1-sin(phi));
        gc=(sin(x)/tan_theta_c)^2*(fc/2*int_fc+ft/(1-sin(phi))*int_ft);
    elseif T==0.5
        int_fc = integral(@(theta) (1-sin(theta))./(cos(theta)).^3,theta_c,z);
        int_ft = integral(@(theta) (sin(theta)-sin(phi))./(cos(theta)).^3,theta_c,z);
        fc=2*cos(phi)/(1-sin(phi));
        ft=cos(phi)/(1+sin(phi));
        gc=(sin(x)/tan_theta_c)^2*(fc/2*int_fc+ft/(1-sin(phi))*int_ft);
    else
        gc=0;
    end
end

g=exp(b*(y-x))*sin(y)-sin(x);      % H/rx
g1=exp(2*b*(z-x))*(exp(2*b*(y-z))-1)/(2*b);               % function of the dissipated
energy
f1_v=(exp(3*b*(y-x))*(sin(y)+3*b*cos(y))-3*b*cos(x)-sin(x))/(3*(1+9*b^2));
Lrx=sin(y-x)/sin(y)-sin(y+beta)/(sin(y)*sin(beta))*(exp(b*(y-x))*sin(y)-sin(x));  %
L1/rx
f2_v=1/6*Lrx*sin(x)*(2*cos(x)-Lrx);
f3_v=1/6*exp(b*(y-x))*(sin(y-x)-Lrx*sin(y))*(cos(x)-Lrx+cos(y)*exp(b*(y-x)));
f4_v=(exp(3*b*(z-x))*(sin(z)+3*b*cos(z))-3*b*cos(x)-sin(x))/(3*(1+9*b^2));
f5_v=1/6*sin(x)*((cos(x))^2-exp(2*b*(z-x))*(cos(z))^2);
f6_v=1/3*exp(2*b*(z-x))*(cos(z))^2*(sin(z)*exp(b*(z-x))-sin(x));
lrx=cos(x)-exp(b*(z-x))*cos(z);        % L2/rx
f1_h=(exp(3*b*(y-x))*(-cos(y)+3*b*sin(y))-3*b*sin(x)+cos(x))/(3*(1+9*b^2));
f2_h=1/3*Lrx*(sin(x))^2;
f3_h=1/6*exp(b*(y-x))*(sin(y-x)-Lrx*sin(y))*(exp(b*(y-x))*sin(y)+sin(x));
f4_h=(exp(3*b*(z-x))*(3*b*sin(z)-cos(z))-3*b*sin(x)+cos(x))/(3*(1+9*b^2));
f5_h=1/3*lrx*(sin(x))^2;
f6_h=1/6*exp(b*(z-x))*cos(z)*(exp(2*b*(z-x))*sin(z)^2-sin(x)^2);
% Calculation of external work rate done by pore pressure along the log-spiral part
using ru
if ru==0
    pu=0;
else
    % first: calculation of the angle Th_1 (the angle made by the line between point
P and the point of vertical projection of the crest point on the log-spiral surface
    x0=0.5;
    % fun=@(th_1)exp(b*(th_1-x_range(k)))*cos(th_1)-cos(x_range(k))+fLrx;
    options = optimset('TolX',1e-10);
    [Th_1, ~, ~, output] = fzero(@(Th_1)exp(b*(Th_1-x))*cos(Th_1)-
cos(x)+Lrx,x0,options);
    if (Th_1>y-10e-6)  || (Th_1<x)
        Ky=NaN;
    end
    if beta_prime<beta
        x1=y; %(Th_1+y)/2;
        options = optimset('TolX',1e-10);
        [Th_2, ~, ~, output2] = fzero(@(Th_2)exp(b*(Th_2-x))*cos(Th_2)-
cos(x)+Lrx+g*cot(beta),x1,options);
        if (Th_2>y-10e-6)  || (Th_2<Th_1)
            Ky=NaN;
        end
        u_3=@(Th) (exp(b.*(Th-x)).*sin(Th)-exp(b.*(y-x))*sin(y)).*b.*(exp(2.*b.*(Th-
x)));
        u3=integral(u_3,Th_2,y);
    else
        u3=0;
    end
```

```
    % second: calculation of the angle th_w (which is the angle betwen the hoizontal
and the chord between the point p and the water level within the crack.
    d_ = exp(b*(z-x))*sin(z)-sin(x);  % the depth of the crack

    th_w=atan((exp(b*(z-x))*sin(z)-ru*(1/gammarat)*d_)/(exp(b*(z-x))*cos(z)));

    % third calculations of uc, u1 and u2
    u_c=@(Th)(exp(b.*(z-x)).*cos(z).*tan(Th)-sin(x)).*tan(Th).*(exp(2.*b.*(z-
x)).*(cos(z)).^2)./(cos(Th)).^2;
    u_1=@(Th)(exp(b.*(Th-x)).*sin(Th)-sin(x)).*b.*(exp(2.*b.*(Th-x)));
    u_2=@(Th)(exp(b.*(Th-x)).*sin(Th)-(exp(b.*(Th_1-x)).*cos(Th_1)-exp(b.*(Th-
x)).*cos(Th)).*tan(beta)-sin(x)).*b.*(exp(2.*b.*(Th-x)));

    % forth: integration of uc, u1 and u2
    uc=integral(u_c,th_w,z);
    u1=integral(u_1,z,Th_1);
    u2=integral(u_2,Th_1,y);
    pu=ru*(uc+u1+u2+u3);
end

Ky=(cogh*(g1+gc)-(f1_v-f2_v-f3_v-f4_v+f5_v+f6_v)/g)/(((f1_v-f2_v-f3_v-
f4_v+f5_v+f6_v)*lambda+(f1_h-f2_h-f3_h-f4_h+f5_h+f6_h))/g);

if Lrx-lrx < 0 || Ky>3 || Ky<-1
    Ky=NaN;
end
N=Ky;
end
```

G.4 Scripts used in Chapter 7: Length of reinforcement

```
% Main program
% ------------------------------------------------------------------------
clear
clc
% Input data
% ------------------------------------------------------------------------
% c/gamma.H : cogh is the normalized cohesion
cogh=0.05;

% friction angle [deg]
phi_grad=20;
phi=phi_grad/180*pi;
b=tan(phi);

%  slope inclination [deg]
beta_grad=40:5:90;
beta=beta_grad/180*pi;
n1=max(size(beta_grad));
% imaginary slope inclination for the below the toe failure
beta_prime_grad=beta_grad
beta_prime=beta_prime_grad*pi/180;

% pore pressure coefficient ru
ru=0;

% unit weights
gamma=20;
gamma_w=10;
gammarat=gamma_w/gamma;

% number of reinforcement layers N
N=6;
% bonding coefficient fb
fb=0.5;
% reinforcement layout RL, for uniform Rl=1 and for LID, RL=2
RL=1;
```

```matlab
% range of the angles
x_range_grad=-20:1:80;
y_range_grad=60:1:130;
z_range_grad=0:1:80;

x_range=x_range_grad*pi/180;
y_range=y_range_grad*pi/180;
z_range=z_range_grad*pi/180;

n3=max(size(x_range));
n4=max(size(y_range));
n5=max(size(z_range));
d=0;
c=0;
for i=1:n1
    beta_prime_grad=(beta_grad(i)):(-2):(beta_grad(i)-0);
    beta_prime=beta_prime_grad*pi/180;
    n2=max(size(beta_prime));
    for h=1:n2
        for k=1:n3
            for l=1:n4
                for j=1:n5
                    if (x_range(k)>y_range(l)-10e-6) | (x_range(k)>z_range(j)-10e-6)
| (z_range(j)>y_range(l)-10e-6)
                        K_req_(h,k,l,j)=NaN;
                    elseif (h>1) && (y_range(l)*180/pi)< (90+phi_grad)
                        K_req_(h,k,l,j)=NaN;
                    else

[X,Kreq_]=funxyz(x_range(k),y_range(l),z_range(j),b,beta(i),beta_prime(h),cogh,ru,gam
marat,RL);

                        K_req_(h,k,l,j)=Kreq_;
                    end
                end
            end
        end
    end
    [Kreq(i), I]=max(K_req_(:))
    [I1,I2,I3,I4] = ind2sub(size(K_req_),I);

    beta_prime_(i)=beta_prime(I1);
    x_(i)=x_range(I2);
    y_(i)=y_range(I3);
    z_(i)=z_range(I4);
    if I1==n2 && n2>1
        c=c+1
        string='larger beta_prime required'
    elseif (I2==n3) |(I2==1)
        d=d+1
        string='increase x_range'
    elseif (I3==n4) |(I3==1)
        d=d+1
        string='increase y_range'
    elseif (I4==n5) |(I4==1)
        d=d+1
        string='increase z_range'
    end
end

betaprime_grad=beta_prime_*180/pi;
x_grad=x_.*180./pi
y_grad=y_.*180./pi
z_grad=z_.*180./pi
betaprime=beta_prime_;
cc=c
dd=d

d_norm=(exp(b*(z_-x_)).*sin(z_)-sin(x_))./(exp(b.*(y_-x_)).*sin(y_)-sin(x_));
Lrx=-exp(b.*(y_-
x_)).*sin(betaprime+y_)./sin(betaprime)+sin(betaprime+x_)./sin(betaprime);
```

```
lrx=-exp(b.*(z_-x_)).*cos(z_)+cos(x_);
rx_norm=1./(exp(b.*(y_-x_)).*sin(y_)-sin(x_));
hx_norm=(Lrx-lrx).*rx_norm;
Xcir=-rx_norm.*exp(b.*(y_-x_)).*cos(y_);
Ycir=rx_norm.*exp(b.*(y_-x_)).*sin(y_);

% Calculation of the length of reinforcement

x_range_grad=40:2:60;
y_range_grad=55:2:80;
z_range_grad=40:2:60;

x_range=x_range_grad*pi/180;
y_range=y_range_grad*pi/180;
z_range=z_range_grad*pi/180;


n3=max(size(x_range));
n4=max(size(y_range));
n5=max(size(z_range));
cL=0;
dL=0;

for i=1:n1
    beta_prime_grad_L=(beta_grad(i)):(-2):(beta_grad(i)-0);
    beta_prime_L=beta_prime_grad_L*pi/180;
    n2=max(size(beta_prime_L));
    for h=1:n2
        for k=1:n3
            for l=1:n4
                for j=1:n5
                    if (x_range(k)>y_range(l)-10e-6) || (x_range(k)>z_range(j)-10e-6)
|| (z_range(j)>y_range(l)-10e-6)
                        L(h,k,l,j)=NaN;

                    elseif (h>1) && (y_range(l)*180/pi)< (90+phi_grad)
                        L(h,k,l,j)=NaN;
                    else

[L,X1]=funxyz_length(Kreq(i),x_range(k),y_range(l),z_range(j),b,beta(i),beta_prime_L(
h),ru,cogh,gammarat,fb,N,RL,x_(i));

                        L_(h,k,l,j)=L;
                        XX(h,k,l,j)=X1;
                    end
                end
            end
        end

        [LoH(i), I]=max(L_(:))
        [I1,I2,I3,I4] = ind2sub(size(L_),I);

        X=(XX(:));
        FM=X(I);   % this provides which scenario has happened.

        beta_prime_L(i)=beta_prime_L(I1);
        x_L(i)=x_range(I2);
        y_L(i)=y_range(I3);
        z_L(i)=z_range(I4);
        if I1==n2 && n2>1
            string='larger beta_prime required'
            cL=cL+1
        elseif (I2==n3) |(I2==1)
            dL=dL+1
            string='increase x_range'
        elseif (I3==n4) |(I3==1)
            dL=dL+1
            string='increase y_range'
        elseif (I4==n5) |(I4==1)
            dL=dL+1
            string='increase z_range'
        end
```

```matlab
    end
end
%parameters for the Length of reinforcement
beta_prime_grad=(beta_grad-28);
beta_prime=beta_prime_grad*pi/180;

for i=1:n1
    beta_prime_grad_L=(beta_grad(i)):(-1):(beta_grad(i)-0);
    beta_prime_L=beta_prime_grad_L*pi/180;
    n2=max(size(beta_prime));
    for h=1:n2
        for k=1:n3
            for l=1:n4
                for j=1:n5
                if (x_range(k)>y_range(l)-10e-6)
                    B(h,k,l,j)=NaN;

                elseif (h>1) && (y_range(l)*180/pi)< (90+phi_grad)
                    B(h,k,l,j)=NaN;
                else

[B]=fun_xyz_LD_length(Kreq,LoH,x_range(k),y_range(l),z_range(j),b,beta(i),beta_prime,
ru,gammarat,fb,N,RL,x_(i),cogh);
                    B_(h,k,l,j)=B;
                end
                end
            end
        end
        Beta(i)=max(B_(:))

    end
end

beta_prime=Beta*pi/180;
g=(exp(b*(y_L-x_L)))*sin(y_L)-sin(x_L);   %  H/rx


betaprime_grad_L=beta_prime_L*180/pi
x_grad_L=x_L.*180./pi
y_grad_L=y_L.*180./pi
z_grad_L=z_L.*180./pi
betaprime_L=beta_prime_L;
ccL=cL
ddL=dL
d_norm_L=(exp(b*(z_L-x_L)).*sin(z_L)-sin(x_L))./(exp(b.*(y_L-x_L)).*sin(y_L)-
sin(x_L));
Lrx_L=-exp(b.*(y_L-
x_L)).*sin(betaprime_L+y_L)./sin(betaprime_L)+sin(betaprime_L+x_L)./sin(betaprime_L);
lrx_L=-exp(b.*(z_L-x_L)).*cos(z_L)+cos(x_L);
rx_norm_L=1./(exp(b.*(y_L-x_L)).*sin(y_L)-sin(x_L));
hx_norm_L=(Lrx_L-lrx_L).*rx_norm_L;
Xcir_L=-rx_norm_L.*exp(b.*(y_L-x_L)).*cos(y_L);
Ycir_L=rx_norm_L.*exp(b.*(y_L-x_L)).*sin(y_L);


for i=1:N
        if RL==1
            Z(i)=(i-0.5)*g/N ;% where Z(i) the depth of the i layer measured from the
upper slope surface.
        else
            Z(i)=(2/3)*g*N*(sqrt((i/N)^3)-sqrt(((i-1)/N)^3));
        end
        L_prime(i)=((Z(i)-Z(1))*(cot(beta_prime)-cot(beta)));
        L(i)=LoH-L_prime(i);
end

figure(7)
hold on
H_ini=1;
% Spiral plotting
for j=1
    plot_line(H_ini,beta,'k')
```

```
        plot_crack(H_ini,beta(j),'r',d_norm_L,hx_norm_L)
        axis equal
        plot_line_L(H_ini,beta_prime,'g')
        %plot_line(H_ini,phi,'g')
        plot_line_toe(H_ini,0,'k')
        plot_line_slopesurface(H_ini,beta(j),'k')

        %plot_spiral_tenscrack_betaprime
        plot_spiral_tenscrack_betaprime_L
        plot_line_reinforcement(H_ini,beta,beta_prime,N,LoH,'b',RL,g)
end
hold off
if RL==1
     string='using Uniform Distribution of reinforcement'
else
    string='using Linearly Increasing Distribution of reinforcement'
end

% save all variables
str1=num2str(beta_grad);
str2=num2str(phi_grad);
str3=num2str(cogh*100);
str4=int2str(ru*100);
str5=num2str(RL);
filename=['Beta',str1,'Phi',str2,'cogh',str3,'ru',str4,'RL',str5,'.mat'];
save (filename)


-----


function [L,X1]=
funxyz_length(Kreq,x_range,y_range,z_range,b,beta,beta_prime_L,ru,cogh,gammarat,fb,N,
RL,x_)

x=x_range;
y=y_range;
z=z_range;
    g=(exp(b*(y-x)))*sin(y)-sin(x);  %  H/rx
    g1=((exp(2*b*(z-x)))*(exp(2*b*(y-z))-1))/(2*b);
    f1=(exp(3*b*(y-x))*(sin(y)+3*b*cos(y))-3*b*cos(x)-sin(x))/(3*(1+9*b^2));
    Lrx=-exp(b*(y-
x))*sin(beta_prime_L+y)/sin(beta_prime_L)+sin(beta_prime_L+x)/sin(beta_prime_L);
    f2=1/6*Lrx*sin(x)*(2*cos(x)-Lrx);
    f3=1/6*exp(b*(y-x))*(sin(y-x)-Lrx*sin(y))*(cos(x)-Lrx+cos(y)*exp(b*(y-x)));
    f4=1/2*g^2*(cot(beta_prime_L)-cot(beta))*(cos(x)-Lrx-
1/3*g*(cot(beta_prime_L)+cot(beta))) ;% for below the toe failure
    p1=(exp(3*b*(z-x))*(sin(z)+3*b*cos(z))-3*b*cos(x)-sin(x))/(3*(1+9*b^2));
    p2=1/6*sin(x)*((cos(x))^2-exp(2*b*(z-x))*(cos(z))^2);
    p3=1/3*exp(2*b*(z-x))*(cos(z))^2*(sin(z)*exp(b*(z-x))-sin(x));


    %  calculation of the angle Th_1 (the angle made by the line between point P and
the point of vertical projection of the crest point on the log-spiral surface
    % it is out of the loop becuase it is needed later for the calculations of length
of rienforcement.
    x0=(x+y)/2;
    options = optimset('TolX',1e-10);
    [Th_1, ~, ~, output] = fzero(@(Th_1)exp(b*(Th_1-x))*cos(Th_1)-
cos(x)+Lrx,x0,options);

    % calculation of the angle Th_2
    if beta_prime_L<beta
        x1=y; %(Th_1+y)/2;
        options = optimset('TolX',1e-10);
        [Th_2, ~, ~, output1] = fzero(@(Th_2)exp(b*(Th_2-x))*cos(Th_2)-
cos(x)+Lrx+g*cot(beta),x1,options);
    end

    if (Th_1>y-10e-6)  || (Th_1<x)
        string='Th_1 not found';
        L=NaN;
```

```
            X1=NaN;
            X2=NaN;
        elseif (beta_prime_L<beta) && ((Th_2>y-10e-10) || (Th_2<Th_1))
            string='Th_2 not found';
            L=NaN;
            X1=NaN;
            X2=NaN;
        else
            % Calculation of external work rate done by pore pressure along the log-
spiral part using ru
            if ru==0
                pu=0;
            else
                if beta_prime_L<beta
                    u_3=@(Th)(exp(b.*(Th-x)).*sin(Th)-exp(b.*(y-
x))*sin(y)).*b.*(exp(2.*b.*(Th-x)));
                    u3=integral(u_3,Th_2,y);
                else
                    u3=0;
                end

                % second: calculation of the angle th_w (which is the angle betwen the
hoizontal and the chord between the point p and the water level within the crack.
                d_= exp(b*(z-x))*sin(z)-sin(x);  % the depth of the crack

                th_w=atan((exp(b*(z-x))*sin(z)-ru*(1/gammarat)*d_)/(exp(b*(z-
x))*cos(z)));

                % third calculations of uc, u1 and u2
                u_c=@(Th)(exp(b.*(z-x)).*cos(z).*tan(Th)-sin(x)).*tan(Th).*(exp(2.*b.*(z-
x)).*(cos(z)).^2)./(cos(Th)).^2;
                u_1=@(Th)(exp(b.*(Th-x)).*sin(Th)-sin(x)).*b.*(exp(2.*b.*(Th-x)));
                u_2=@(Th)(exp(b.*(Th-x)).*sin(Th)-(exp(b.*(Th_1-x)).*cos(Th_1)-
exp(b.*(Th-x)).*cos(Th)).*tan(beta)-sin(x)).*b.*(exp(2.*b.*(Th-x)));

                % forth: integration of uc, u1 and u2
                uc=integral(u_c,th_w,z);
                u1=integral(u_1,z,Th_1);
                u2=integral(u_2,Th_1,y);
                pu=ru*(uc+u1+u2+u3);
            end

            for i=1:N
                if RL==1
                    Z(i)=(i-0.5)*g/N; % where Z(i) the depth of the i layer measured from
the upper slope surface.
                else
                    Z(i)=(2/3)*g*N*(sqrt((i/N)^3)-sqrt(((i-1)/N)^3));
                end
                % Calculating the angle Th_i (intersection of failure surface with the
layer in question.
                x2=x+y/2;
                options = optimset('TolX',1e-10);
                [Th_i, ~, ~, output2] = fzero(@(Th_i)exp(b*(Th_i-x))*sin(Th_i)-sin(x)-
Z(i),x2,options);

                if (Th_i>y-10e-6)  || (Th_i<x)
                    string='Th_i not found';
                    Th_i=NaN;
                    Kreq=NaN;
                end
                if Th_i<z
                    le1(i)=(1/g)*((cos(y)+sin(y)*cot(beta))*exp(b*(y-x))-
(cos(Th_i)+sin(Th_i)*cot(beta))*exp(b*(Th_i-x))-exp(b*(Th_i-x))*cos(Th_i)+exp(b*(z-
x))*cos(z));
                else
                    le1(i)=(1/g)*((cos(y)+sin(y)*cot(beta))*exp(b*(y-x))-
(cos(Th_i)+sin(Th_i)*cot(beta))*exp(b*(Th_i-x)));
                end
```

```
            if Th_i<=Th_1 % that is the case when the failure surface intersects the
reinforcement under the slope upper slope surface (the horizontal line).

                Z_(i)=(1/g)*(exp(b*(Th_i-x))*sin(Th_i)-sin(x)); % where Z_(i) is the
depth of the i layer measured either from slope face or from the upper slope surface.
            else
                % if beta_prime_L==beta
                Th_2=y;
                % end
                Z_(i)=(1/g)*(exp(b.*(Th_i-x)).*sin(Th_i)-exp(b.*(y-
x)).*sin(y)+(exp(b.*(Th_i-x)).* cos(Th_i)-exp(b.*(Th_2-x)).*cos(Th_2)).*tan(beta));
            end

            le(i)=Kreq./(N*2*Z_(i)*fb*b*(1-ru));
            LL(i)=le(i)+(cos(Th_i)+sin(Th_i)*cot(beta))*(1/g)*exp(b.*(Th_i-x))-
(cos(y)+sin(y)*cot(beta))*(1/g)*exp(b.*(y-x));

            if (x<0) && ((sin(x)+Z(1))<0) || (x_<0) && ((sin(x_)+Z(1))<0)
                Z(1)=0;
            end
        end
        if Kreq<10
            x3=0.5;
            options = optimset('TolX',1e-4);
            %---------------------------------- if one layer only is pulled-out -
-------------------------------------.
        %(1)% if the first layer is pulled-out and the rest fail in tension
        if  (sin(x_)+Z(1)>0) && (sin(x)+Z(1)>0)
            [L1, ~, ~, output3] = fzero(@(L1)(-Kreq+((1/g)^2*(f1-f2-f3-f4-
p1+p2+p3+pu)-(1/g)*g1*cogh-2*fb*b*(1-
ru)*(Z_(1)*(le1(1)+L1)*(sin(x)+Z(1))))/((1/N)*(sin(x)+Z(2)+sin(x)+Z(3)+sin(x)+Z(4)+si
n(x)+Z(5)+sin(x)+Z(6)))),x3,options);
            if (L1<0) || (L1>10) || ((le1(1)+L1)<0)
                L1=NaN;
            elseif L1>LL(1)
                L1=LL(1);
            end
        else
            L1=NaN;
        end

        %(2)% if the first layer is bypassed and the second layer is pulled-out while
the rest fail in tension
        [L2, ~, ~, output4] = fzero(@(L2)(-Kreq+((1/g)^2*(f1-f2-f3-f4-p1+p2+p3+pu)-
(1/g)*g1*cogh-2*fb*b*(1-
ru)*(Z_(2)*(le1(2)+L2)*(sin(x)+Z(2))))/((1/N)*(sin(x)+Z(3)+sin(x)+Z(4)+sin(x)+Z(5)+si
n(x)+Z(6)))),x3,options);
            if (L2<0)|| (L2>10)|| ((le1(1)+L2)>0) || ((le1(2)+L2)<0)
                L2=NaN;
            elseif L2>LL(2)
                L2=LL(2);
            end
        %(3)% if 1&2 are bypassed and the third layer is pulled-out while the rest
fail in tension
        [L3, ~, ~, output5] = fzero(@(L3)(-Kreq+((1/g)^2*(f1-f2-f3-f4-p1+p2+p3+pu)-
(1/g)*g1*cogh-2*fb*b*(1-
ru)*(Z_(3)*(le1(3)+L3)*(sin(x)+Z(3))))/((1/N)*(sin(x)+Z(4)+sin(x)+Z(5)+sin(x)+Z(6))))
,x3,options);
            if (L3<0)|| (L3>10)|| ((le1(1)+L3)>0)|| ((le1(2)+L3)>0) || ((le1(3)+L3)<0)
                L3=NaN;
            elseif L3>LL(3)
                L3=LL(3);
            end
        %(4)% if 1,2&3 are bypassed and the fourth layer is pulled-out while the rest
fail in tension
        [L4, ~, ~, output6] = fzero(@(L4)(-Kreq+((1/g)^2*(f1-f2-f3-f4-p1+p2+p3+pu)-
(1/g)*g1*cogh-2*fb*b*(1-
ru)*(Z_(4)*(le1(4)+L4)*(sin(x)+Z(4))))/((1/N)*(sin(x)+Z(5)+sin(x)+Z(6)))),x3,options)
;
            if (L4<0)|| (L4>10)|| ((le1(1)+L4)>0)|| ((le1(2)+L4)>0)||((le1(3)+L4)>0) ||
((le1(4)+L4)<0)
                L4=NaN;
```

```
        elseif L4>LL(4)
            L4=LL(4);
        end
        %(5)% if 1,2,3&4 are bypassed and the fifth layer is pulled-out while the
sixth fails in tension
        [L5, ~, ~, output7] = fzero(@(L5)(-Kreq+((1/g)^2*(f1-f2-f3-f4-p1+p2+p3+pu)-
(1/g)*g1*cogh-2*fb*b*(1-
ru)*(Z_(5)*(le1(5)+L5)*(sin(x)+Z(5))))/((1/N)*(sin(x)+Z(6)))),x3,options);
        if (L5<0)|| (L5>10)|| ((le1(1)+L5)>0)|| ((le1(2)+L5)>0)|| ((le1(3)+L5)>0)||
((le1(4)+L5)>0) || ((le1(5)+L5)<0)
            L5=NaN;
        elseif L5>LL(5)
            L5=LL(5);
        end
        %---------------------------------- if two layers only are pulled-out --
-----------------------------------.
        if (sin(x_)+Z(1)>0) && (sin(x)+Z(1)>0) % this to avoid getting relatively
long reinforcement, because all layers will depends on length of the topmost layer!
            %(6)% if 1&2 are pulled-out while the rest fail in tension
            [L6, ~, ~, output8] = fzero(@(L6)(-Kreq+((1/g)^2*(f1-f2-f3-f4-
p1+p2+p3+pu)-(1/g)*g1*cogh-2*fb*b*(1-
ru)*(Z_(1)*(le1(1)+L6)*(sin(x)+Z(1))+Z_(2)*(le1(2)+L6)*(sin(x)+Z(2))))/((1/N)*(sin(x)
+Z(3)+sin(x)+Z(4)+sin(x)+Z(5)+sin(x)+Z(6)))),x3,options);
                if (L6<0)|| (L6>10)|| ((le1(1)+L6)<0) || ((le1(2)+L6)<0)
                    L6=NaN;
                elseif L6>LL(1)
                    L6=LL(1);
                end
        else
            L6=NaN;
        end
        %(7)% if 1 is bypassed and 2&3 are pulled-out while the rest fail in tension
        [L7, ~, ~, output9] = fzero(@(L7)(-Kreq+((1/g)^2*(f1-f2-f3-f4-p1+p2+p3+pu)-
(1/g)*g1*cogh-2*fb*b*(1-
ru)*(Z_(2)*(le1(2)+L7)*(sin(x)+Z(2))+Z_(3)*(le1(3)+L7)*(sin(x)+Z(3))))/((1/N)*(sin(x)
+Z(4)+sin(x)+Z(5)+sin(x)+Z(6)))),x3,options);
        if (L7<0)|| (L7>10)|| ((le1(1)+L7)>0) || ((le1(2)+L7)<0)
            L7=NaN;
        elseif L7>LL(2)
            L7=LL(2);
        end

        %(8)% if 1&2 are bypassed and 3&4 are pulled-out while the rest fail in
tension
        [L8, ~, ~, output10] = fzero(@(L8)(-Kreq+((1/g)^2*(f1-f2-f3-f4-p1+p2+p3+pu)-
(1/g)*g1*cogh-2*fb*b*(1-
ru)*(Z_(3)*(le1(3)+L8)*(sin(x)+Z(3))+Z_(4)*(le1(4)+L8)*(sin(x)+Z(4))))/((1/N)*(sin(x)
+Z(5)+sin(x)+Z(6)))),x3,options);
        if (L8<0)|| (L8>10)|| ((le1(1)+L8)>0) || ((le1(2)+L8)>0)|| ((le1(3)+L8)<0)
            L8=NaN;
        elseif L8>LL(3)
            L8=LL(3);
        end
        %(9)% if 1,2&3 are bypassed and 4&5 are pulled-out while the 6th fails in
tension
        [L9, ~, ~, output11] = fzero(@(L9)(-Kreq+((1/g)^2*(f1-f2-f3-f4-p1+p2+p3+pu)-
(1/g)*g1*cogh-2*fb*b*(1-
ru)*(Z_(4)*(le1(4)+L9)*(sin(x)+Z(4))+Z_(5)*(le1(5)+L9)*(sin(x)+Z(5))))/((1/N)*(sin(x)
+Z(6)))),x3,options);
        if (L9<0)|| (L9>10)|| ((le1(1)+L9)>0) || ((le1(2)+L9)>0)|| ((le1(3)+L9)>0)||
((le1(4)+L9)<0)
            L9=NaN;
        elseif L9>LL(4)
            L9=LL(4);
        end
        %---------------------------------- if three layers are pulled-out -----
-----------------------------------.
        if (sin(x_)+Z(1)>0) && (sin(x)+Z(1)>0)
            %(10)% if 1,2&3 are pulled-out while the rest fail in tension
            [L10, ~, ~, output12] = fzero(@(L10)(-Kreq+((1/g)^2*(f1-f2-f3-f4-
p1+p2+p3+pu)-(1/g)*g1*cogh-2*fb*b*(1-
```

```
ru)*(Z_(1)*(le1(1)+L10)*(sin(x)+Z(1))+Z_(2)*(le1(2)+L10)*(sin(x)+Z(2))+Z_(3)*(le1(3)+
L10)*(sin(x)+Z(3))))/((1/N)*(sin(x)+Z(4)+sin(x)+Z(5)+sin(x)+Z(6)))),x3,options);
            if (L10<0)|| (L10>10)|| ((le1(1)+L10)<0) || ((le1(2)+L10)<0)||
((le1(3)+L10)<0)
                L10=NaN;
            elseif L10>LL(1)
                L10=LL(1);
            end
        else
            L10=NaN;
        end
        %(11)% if the 1st is bypassed and 2,3&4 are pulled-out while the rest fail in
tension
        [L11, ~, ~, output13] = fzero(@(L11)(-Kreq+((1/g)^2*(f1-f2-f3-f4-
p1+p2+p3+pu)-(1/g)*g1*cogh-2*fb*b*(1-
ru)*(Z_(2)*(le1(2)+L11)*(sin(x)+Z(2))+Z_(3)*(le1(3)+L11)*(sin(x)+Z(3))+Z_(4)*(le1(4)+
L11)*(sin(x)+Z(4))))/((1/N)*(sin(x)+Z(5)+sin(x)+Z(6)))),x3,options);
            if (L11<0)|| (L11>10)|| ((le1(1)+L11)>0) || ((le1(2)+L11)<0)||
((le1(3)+L11)<0)||((le1(4)+L11)<0)
                L11=NaN;
        elseif L11>LL(2)
                L11=LL(2);
            end
        %(12)% if the 1&2 are bypassed and 3,4&5 are pulled-out while the 6th fails
in tension
        [L12, ~, ~, output14] = fzero(@(L12)(-Kreq+((1/g)^2*(f1-f2-f3-f4-
p1+p2+p3+pu)-(1/g)*g1*cogh-2*fb*b*(1-
ru)*(Z_(3)*(le1(3)+L12)*(sin(x)+Z(3))+Z_(4)*(le1(4)+L12)*(sin(x)+Z(4))+Z_(5)*(le1(5)+
L12)*(sin(x)+Z(5))))/((1/N)*(sin(x)+Z(6)))),x3,options);
            if (L12<0)|| (L12>3)|| ((le1(1)+L12)>0) || ((le1(2)+L12)>0)||
((le1(3)+L12)<0)|| ((le1(4)+L12)<0)|| ((le1(5)+L12)<0)
                L12=NaN;
        elseif L12>LL(3)
                L12=LL(3);
            end
        if (sin(x_)+Z(1)>0) && (sin(x)+Z(1)>0)
            %(13)% if the 3&4 are bypassed and 1,2&5 are pulled-out while the 6th
fails in tension, this might be the case for gentle slope (i.e Beta less than 45).
            [L13, ~, ~, output15] = fzero(@(L13)(-Kreq+((1/g)^2*(f1-f2-f3-f4-
p1+p2+p3+pu)-(1/g)*g1*cogh-2*fb*b*(1-
ru)*(Z_(1)*(le1(1)+L13)*(sin(x)+Z(1))+Z_(2)*(le1(2)+L13)*(sin(x)+Z(2))+Z_(5)*(le1(5)+
L13)*(sin(x)+Z(5))))/((1/N)*(sin(x)+Z(6)))),x3,options);
                if (L13<0)|| (L13>10)|| ((le1(1)+L13)<0) || ((le1(2)+L13)<0)||
((le1(3)+L13)>0)|| ((le1(4)+L13)>0)|| ((le1(5)+L13)<0)
                    L13=NaN;
            elseif L13>LL(1)
                    L13=LL(1);
                end
            %(14)% if the 2&3 are bypassed and 1,4&5 are pulled-out while the 6th
fails in tension, this might be the case for gentle slope (i.e Beta less than 45).
            [L14, ~,~, output16] = fzero(@(L14)(-Kreq+((1/g)^2*(f1-f2-f3-f4-
p1+p2+p3+pu)-(1/g)*g1*cogh-2*fb*b*(1-
ru)*(Z_(1)*(le1(1)+L14)*(sin(x)+Z(1))+Z_(4)*(le1(4)+L14)*(sin(x)+Z(4))+Z_(5)*(le1(5)+
L14)*(sin(x)+Z(5))))/((1/N)*(sin(x)+Z(6)))),x3,options);
                if (L14<0)|| (L14>10)|| ((le1(1)+L14)<0) || ((le1(2)+L14)>0)||
((le1(3)+L14)>0)|| ((le1(4)+L14)<0)|| ((le1(5)+L14)<0)
                    L14=NaN;
            elseif L14>LL(1)
                    L14=LL(1);
                end

            %------------------------------------ if four layers are pulled-out --
-------------------------------------.
            %(15)% if 1,2,3&4 are pulled-out while the rest fail in tension
            [L15, ~,~, output17] = fzero(@(L15)(-Kreq+((1/g)^2*(f1-f2-f3-f4-
p1+p2+p3+pu)-(1/g)*g1*cogh-2*fb*b*(1-
ru)*(Z_(1)*(le1(1)+L15)*(sin(x)+Z(1))+Z_(2)*(le1(2)+L15)*(sin(x)+Z(2))+Z_(3)*(le1(3)+
L15)*(sin(x)+Z(3))+Z_(4)*(le1(4)+L15)*(sin(x)+Z(4))))/((1/N)*(sin(x)+Z(5)+sin(x)+Z(6)
))),x3,options);
                if (L15<0)|| (L15>10)|| ((le1(1)+L15)<0) || ((le1(2)+L15)<0)||
((le1(3)+L15)<0)|| ((le1(4)+L15)<0)
                    L15=NaN;
```

```
        elseif L15>LL(1)
            L15=LL(1);
        end
    else
        L13=NaN;
        L14=NaN;
        L15=NaN;
    end
    %(16)% if the 1st is bypassed and  2,3,4&5 are pulled-out while the 6th fails
in tension
    [L16, ~,~, output18] = fzero(@(L16)(-Kreq+((1/g)^2*(f1-f2-f3-f4-p1+p2+p3+pu)-
(1/g)*g1*cogh-2*fb*b*(1-
ru)*(Z_(1)*(le1(1)+L16)*(sin(x)+Z(1))+Z_(2)*(le1(2)+L16)*(sin(x)+Z(2))+Z_(3)*(le1(3)+
L16)*(sin(x)+Z(3))+Z_(4)*(le1(4)+L16)*(sin(x)+Z(4))))/((1/N)*(sin(x)+Z(5)+sin(x)+Z(6)
))),x3,options);
    if (L16<0)|| (L16>10)|| ((le1(1)+L16)>0) || ((le1(2)+L16)<0)||
((le1(3)+L16)<0)|| ((le1(4)+L16)<0)|| ((le1(4)+L16)<0)
        L16=NaN;
    elseif L16>LL(2)
        L16=LL(2);
    end
    %------------------------------------ Other cases to be considered  -----
-----------------------------------.

    %(17% if 3&4 are bypassed and 2&5 are pulled-out while the rest fail in
tension
    [L17, ~, ~, output21] = fzero(@(L17)(-Kreq+((1/g)^2*(f1-f2-f3-f4-
p1+p2+p3+pu)-(1/g)*g1*cogh-2*fb*b*(1-
ru)*(Z_(2)*(le1(2)+L17)*(sin(x)+Z(2))+Z_(5)*(le1(5)+L17)*(sin(x)+Z(5))))/((1/N)*(sin(
x)+Z(1)+sin(x)+Z(6)))),x3,options);
    if (L17<0)|| (L17>10)|| ((le1(1)+L17)<0) || ((le1(2)+L17)<0)||
((le1(3)+L17)>0)|| ((le1(4)+L17)>0)|| ((le1(5)+L17)<0)
        L17=NaN;
    elseif L17>LL(2)
        L17=LL(2);
    end
    %(18)% if 1,2&6 fail in tension, and 3&5 are pulled-out while the fourth is
bypassed
    [L18, ~, ~, output22] = fzero(@(L18)(-Kreq+((1/g)^2*(f1-f2-f3-f4-
p1+p2+p3+pu)-(1/g)*g1*cogh-2*fb*b*(1-
ru)*(Z_(3)*(le1(3)+L18)*(sin(x)+Z(3))+Z_(5)*(le1(5)+L18)*(sin(x)+Z(5))))/((1/N)*(sin(
x)+Z(1)+sin(x)+Z(2)+sin(x)+Z(6)))),x3,options);
    if (L18<0)|| (L18>10)|| ((le1(1)+L18)<0) || ((le1(2)+L18)<0)||
((le1(6)+L18)<0)|| ((le1(4)+L18)>0)||  ((le1(3)+L18)<0) || ((le1(5)+L18)<0)
        L18=NaN;
    elseif L18>LL(3)
        L18=LL(3);
    end

    L_=[L1 L2 L3 L4 L5 L6 L7 L8 L9 L10 L11 L12 L13 L14 L15 L16 L17 L18];
    [L,I]=max(L_);
    X1=I;
    else
        L=NaN;
        X1=NaN;

    end
end

end
```

G.5 Scripts used in Chapter 8: Optimal profile

```
% Main program: Genetic Algorithm
```

```matlab
% ------------------------------------------------------------------------
clear;
clc;
n_points =10;

beta_g=75;
phi_g=30;

ObjectiveFunction = @Fun_MC;      % objective function to maximize
% Number of variables
LB = zeros(1,n_points); % Lower bound
UB = ones(1,n_points);  % Upper bound

beta=beta_g/180*pi;
phi=phi_g/180*pi;

for j=1:n_points    % constraints on the upper and lower bounds to eliminate the zones
that are highly unlikely to be involved.
    Y(j)=j/n_points;
    if Y(j) <=0.4
        UB(j)=Y(j);

    else
        UB(j)=1;
    end
    if Y(j) <=0.3
        Temp(j)=Y(j)/0.3;

    else
        Temp(j)=1;
    end
    LB(j)=(1-Temp(j));
end
LB=fliplr(LB);
UB=(UB);
figure (12)
hold on
plot (-LB,-Y)
plot(-UB,-Y)
hold off

opts = gaoptimset('PopulationSize',500, 'StallGenLimit',100, 'Generations',2000,
'UseParallel', 'always');

ConstraintFunction = @ConstraintR;
[R,Fval,exitFlag,Output] =
ga(ObjectiveFunction,n_points,[],[],[],[],LB,UB,ConstraintFunction,opts);

N=-1/Fval;
L_array=[0 (1-fliplr(R)) 1];
H_array=zeros(1,n_points+2);
for i=1:(n_points+2)
    H_array(i)=(i-1)/(n_points+1)*tan(beta);
end

[N_,X]=Fun_MC2(R,n_points,beta,phi);  % to extract the values of x,y, and z.
N1=-1/N_;

x_grad=X(1)*180/pi;
y_grad=X(2)*180/pi;
z_grad=X(1)*180/pi;

betaprime=beta;
b=tan(phi);
x=X(1);
y=X(2);
z=X(1);

d_norm=(exp(b*(z-x)).*sin(z)-sin(x))./(exp(b.*(y-x)).*sin(y)-sin(x));
Lrx=-exp(b.*(y-
x)).*sin(betaprime+y)./sin(betaprime)+sin(betaprime+x)./sin(betaprime);
lrx=-exp(b.*(z-x)).*cos(z)+cos(x);
```

```matlab
rx_norm=tan(beta)./(exp(b.*(y-x)).*sin(y)-sin(x));
hx_norm=(Lrx-lrx).*rx_norm;
Xcir=-rx_norm.*exp(b.*(y-x)).*cos(y);
Ycir=rx_norm.*exp(b.*(y-x)).*sin(y);

figure(4)
hold on
L_array=[0 (1-fliplr(R)) 1];
H_array=zeros(1,n_points+2);
for i=1:(n_points+2)
    H_array(i)=(i-1)/(n_points+1)*tan(beta);
end
plot(L_array, H_array,'k','LineWidth',2)
H_ini=tan(beta);
% Spiral plotting
for j=1
    plot_line(H_ini,beta,'--k')
    axis equal
    plot_line_toe(H_ini,0,'k')
    plot_line_slopesurface(H_ini,beta,'k')
    plot_spiral_tenscrack_betaprime
    plot_spiral
    plot_crack(H_ini,beta,'k',d_norm,hx_norm)
end
hold off


filename = '10points,Kh=0.2,beta75,phi=30,LID.mat';
save(filename)
----------


% Constraint function

function [c, ceq] = ConstraintR(R)

n_points=10;
c=ones(1,n_points-1);
for i=1:(n_points-1)
    c(i)=R(i)-R(i+1);
end
c=c';
ceq = [];
--------


% function to be maximized
function N_=Fun_MC(R)

n_points=10;

% slope inclination [deg]
beta_grad=75;
% friction angle [deg]
phi_grad=30;

% c/gamma.H : cogh is the normalized cohesion
cogh=0.0;
% Kh horizontal seismic coefficient
Kh=0.2;
% reinforcement layout RL, for uniform Rl=1 and for LID, RL=2
RL=2;
% Crack scenario: (for nil tensile strength of soil, t=0), (for half of unconfined
% tensile strength t=0.5), (for  whole unconfined Mohr-Coulomb tensile strength t=1)
% and (for pre-existing crack, t=-1), for intact slope i.e. no crack t=2
t=2;

% derived variables in radian
beta=beta_grad/180*pi;
phi=phi_grad/180*pi;
```

```matlab
b=tan(phi);

% initial values
x_range_grad=-21:2:89;
y_range_grad=60:2:120;
z_range_grad=0:2:0;

x_range=x_range_grad/180*pi;
y_range=y_range_grad/180*pi;
z_range=z_range_grad/180*pi;

n1=max(size(x_range));
n2=max(size(y_range));
n3=max(size(z_range));

MatrixN=zeros(n1,n2,n3);
N_all=zeros(1,n_points+1);
X_all=zeros(3,n_points+1);

H_R=zeros(1,n_points+1);
for k=1:(n_points+1)
    H_R(k)=(n_points+1)/(n_points+2-k);
end

R_new=R;
beta_new=beta;

for loop=1:(n_points+1)
    for i=1:n1
        for j=1:n2
            for k=1:n3
                x=x_range(i);
                y=y_range(j);
                z=z_range(k);
                if (x>y-10e-6) %|| (x>z-10e-6) || (z>y-10e-6)
                    MatrixN(i,j,k)=NaN;
                else
                    MatrixN(i,j,k)=funXY_Crack(x,y,z,beta_new,b,(n_points+1-
loop),R_new,t,cogh,RL,Kh);
                end
            end
        end
    end

    [N_all(loop),BiI]=min(MatrixN(:));
    [x_f,y_f,z_f]=ind2sub(size(MatrixN),BiI);
    X_all(1,loop)=x_range(x_f);
    X_all(2,loop)=y_range(y_f);
    X_all(3,loop)=z_range(z_f);

    R_temp=R_new;
    if (n_points+1-loop)==0
        R_new=NaN;
        beta_new=NaN;
    else
        if (n_points-loop)==0
            R_new=NaN;
        else
            R_new=zeros(1,n_points-loop);
            for k=1:(n_points-loop)
                R_new(k)=R_temp(k)/R_temp(n_points+1-loop);
            end
        end
        beta_new=atan(tan(beta_new)*(n_points+1-loop)/(n_points+2-
loop)/R_temp(n_points+1-loop));
    end
end

N_all=H_R.*N_all;
[N_, toe]=min(N_all);
if toe==1
    flag=1;
```

```matlab
    for i=1:(n_points+1)
        if isnan(N_all(i))
            flag=0;
        end
    end
    if flag==0;
        N_=1;
    else
        X(1)=X_all(1,toe);
        X(2)=X_all(2,toe);
        X(3)=X_all(3,toe);
        N_=-N_;
    end
else
    N_=1;
end


-------


% function to calculate the required reinforcement
function N=funXY_Crack(x,y,z,beta,b,n_points,R,t,cogh,RL,Kh)
z=x;
flag=1;

H=exp(b*(y-x))*sin(y)-sin(x);
L=H/tan(beta);
Lrx=sin(x+beta)/sin(beta)-exp(b*(y-x))*sin(y+beta)/sin(beta);
rc=sqrt(sin(x)*sin(x)+(cos(x)-Lrx)^2);
sc=acos((cos(x)-Lrx)/rc);
ry=exp(b*(y-x));

H_points=zeros(1,n_points);
L_points=zeros(1,n_points);
ss=zeros(1,n_points);
rr=zeros(1,n_points);

for i=1:n_points
    H_points(i)=sin(x)+H*i/(n_points+1);
    L_points(i)=cos(x)-Lrx-R(i)*L;
    rr(i)=sqrt(H_points(i)*H_points(i)+L_points(i)*L_points(i));
    ss(i)=acos(L_points(i)/rr(i));
    if rr(i)>exp(b*(ss(i)-x))
        flag=0;
    end
    if ss(i)>y
        flag=0;
    end
end

if flag==1
    if t==2
        z=x;
        gc=0;

    elseif t==0
        ft=0;
        int_ft=0;
        int_fc = integral(@(theta) (1-sin(theta))./(cos(theta)).^3,theta_c,z);
        fc=2*cos(phi)/(1-sin(phi));
        gc=(sin(x)/tan_theta_c)^2*(fc/2*int_fc+ft/(1-sin(phi))*int_ft);
    elseif t==0.5
        int_fc = integral(@(theta) (1-sin(theta))./(cos(theta)).^3,theta_c,z);
        int_ft = integral(@(theta) (sin(theta)-sin(phi))./(cos(theta)).^3,theta_c,z);
        fc=2*cos(phi)/(1-sin(phi));
        ft=cos(phi)/(1+sin(phi));
        gc=(sin(x)/tan_theta_c)^2*(fc/2*int_fc+ft/(1-sin(phi))*int_ft);
    elseif t==1
        int_fc = integral(@(theta) (1-sin(theta))./(cos(theta)).^3,theta_c,z);
        int_ft = integral(@(theta) (sin(theta)-sin(phi))./(cos(theta)).^3,theta_c,z);
        fc=2*cos(phi)/(1-sin(phi));
```

```
            ft=2*cos(phi)/(1+sin(phi));
            gc=(sin(x)/tan_theta_c)^2*(fc/2*int_fc+ft/(1-sin(phi))*int_ft);
        else
            gc=0;
        end


        if RL==1
            %  for uniformly distributed mode:
            if  x<0
                g23=(exp(2*b*(y-x))*(sin(y))^2)/2;
            else
                g23=(exp(2*b*(y-x))*(sin(y))^2-(sin(x))^2)/2;
            end
        else
            %  for linearly increasing density mode:
            if  x<0
                g23=(2/H)*((1/3)*(exp(3*b*(y-x))*(sin(y))^3)-(sin(x)/2)*(exp(2*b*(y-
x))*(sin(y))^2));
            else
                g23=(2/H)*((1/3)*(exp(3*b*(y-x))*(sin(y))^3-(sin(x))^3)-
(sin(x)/2)*(exp(2*b*(y-x))*(sin(y))^2-(sin(x))^2));
            end
        end

        g1=((exp(2*b*(z-x)))*(exp(2*b*(y-z))-1))/(2*b);
        %g=exp(2*b*(z-x))*(exp(2*b*(y-z))-1)*(exp(b*(y-x))*sin(y)-sin(x))/(2*b);
        f1=(exp(3*b*(y-x))*(sin(y)+3*b*cos(y))-3*b*cos(x)-sin(x))/(3*(1+9*b^2));
        f2=1/6*Lrx*sin(x)*(2*cos(x)-Lrx);
        f3=0;

        if z==x
            p1=0;
            p2=0;
            p3=0;
        else
            p1=(exp(3*b*(z-x))*(sin(z)+3*b*cos(z))-3*b*cos(x)-sin(x))/(3*(1+9*b^2));
            p2=1/6*sin(x)*((cos(x))^2-exp(2*b*(z-x))*(cos(z))^2);
            p3=1/3*exp(2*b*(z-x))*(cos(z))^2*(sin(z)*exp(b*(z-x))-sin(x));
        end

        if Kh==0
            f1_h=0;
            f2_h=0;
            f3_h=0;
            p1_h=0;
            p2_h=0;
            p3_h=0;
        else
            lrx=cos(x)-exp(b*(z-x))*cos(z);
            f1_h=(exp(3*b*(y-x))*(-cos(y)+3*b*sin(y))-3*b*sin(x)+cos(x))/(3*(1+9*b^2));
            f2_h=1/3*Lrx*(sin(x))^2;

            p1_h=(exp(3*b*(z-x))*(3*b*sin(z)-cos(z))-3*b*sin(x)+cos(x))/(3*(1+9*b^2));
            p2_h=1/3*lrx*(sin(x))^2;
            p3_h=1/6*exp(b*(z-x))*cos(z)*(exp(2*b*(z-x))*sin(z)^2-sin(x)^2);
        end

        if n_points==0
            f3=fun3(rc,sc,ry,y);
            f3_h=fun3h(rc,sc,ry,y);
        end
        if n_points==1
            f3=fun3(rc,sc,rr(1),ss(1))+fun3(rr(1),ss(1),ry,y);
            f3_h=fun3h(rc,sc,rr(1),ss(1))+fun3h(rr(1),ss(1),ry,y);
        end
        if n_points>1
            f3=fun3(rc,sc,rr(1),ss(1));
            if Kh>0
                f3_h= fun3h(rc,sc,rr(1),ss(1));
            end
```

```matlab
        for i=1:(n_points-1)
            f3=f3+fun3(rr(i),ss(i),rr(i+1),ss(i+1));
            if Kh>0
                f3_h= f3_h+fun3h(rr(i),ss(i),rr(i+1),ss(i+1));
            end
        end
        f3=f3+fun3(rr(n_points),ss(n_points),ry,y);
        if Kh>0
            f3_h= f3_h+fun3h(rr(n_points),ss(n_points),ry,y);
        end
    end

    %g=exp(2*b*(z-x))*(exp(2*b*(y-z))-1)*(exp(b*(y-x))*sin(y)-sin(x))/(2*b);
    %N=g/(f1-f2-f3-p1+p2+p3);
    N=1/((((f1-f2-f3-p1+p2+p3)+Kh*(f1_h-f2_h-f3_h-p1_h+p2_h+p3_h))/(H*g23))-
cogh*((g1+gc)/g23));
    if N<-1 || N>500
        N=NaN;
    end
else
    N=NaN;
end
------


function F=fun3(r1,s1,r2,s2)

    x1=r1*cos(s1);
    y1=r1*sin(s1);
    x2=r2*cos(s2);
    y2=r2*sin(s2);
    S=1/2*abs(x1*y2-x2*y1);
    F=(x1+x2)/3*S;
```